Cationic Lytic Peptides as Drugs or Drug Carriers for Targeted Cancer Therapy

by

Sheng Lu

A thesis

presented to the University of Waterloo

in fulfillment of the

thesis requirement for the degree of

Doctor of Philosophy

in

Chemical Engineering

Waterloo, Ontario, Canada, 2014

AUTHOR'S DECLARATION

I hereby declare that I am the sole author of this thesis. This is a true copy of the thesis, including any required final revisions, as accepted by my examiners.

I understand that my thesis may be made electronically available to the public.

Abstract

Cationic lytic peptides (CLPs) have emerged as new anticancer agents with a new mode of action. This category of peptides is given the characteristics of overall positive charges and amphiphilicity, inducing cell death by disrupting integrity of cytoplasmic membranes or depolarizing mitochondrial membranes. Cationic lytic peptides show advantages to conventional chemotherapeutics in preferential killing of cancer cells and ability to avoid general mechanisms of multidrug resistance associated with cancer cells. The biocompatibility and the biodegradability of many CLPs are other advantages. These properties make CLPs promising therapeutics for cancer therapy.

Although significant progress has been achieved over the past decade, high activity and high specificity towards cancer cells, as well as enhanced stability in serum, are still needed for clinical usage of CLPs. To address these issues, this thesis focuses on three aspects: a) the molecular mechanism of the preferential activity of CLPs on different lipid membranes, which is the main cause for the CLP selective cytotoxicity; b) stimuli-responsive design in CLPs for self-guided delivery; c) utilization of CLPs as delivery vehicles for the hydrophobic anticancer drug ellipticine (EPT). The last aspect is to take advantage of CLP's capability to encapsulate hydrophobic compounds and deliver to cancerous cells. The studies include: (i) investigation of the CLP induced leakage on liposomes with various lipid compositions; (ii) characterization of the stimuli-responsive properties of the CLP and the properties of CLP-ellipticine complexes; (iii) evaluation of the selective cytotoxicity of the CLPs and CLP-ellipticine complexes on various cell lines; (iv) evaluation of the anticancer activity of CLPs *in vitro* and *in vivo*.

The peptide C6, an 18-mer arginine-rich peptide, was found to adopt an amphiphilic helical

conformation on 1-palmitoyl-2-oleoyl-3-sn-glycero-phosphocholine (POPC) membranes, and induce membrane leakage. The POPC liposome leakage and A549 cell death induced by C6 was shown in a concentration-dependent manner. The amount of C6 required to achieve a given level of membrane damage, as measured by efflux of fluorescent dye or cell mortality, increases linearly with lipid concentration or cell count. The hydrogen bonding between arginine residues of C6 and cholesterol-rich membrane was found to play an important role in the lytic activity of the peptide, as evidenced in both the leakage study and molecular dynamics analysis. The effect of hydrogen bonding was also observed in subsequent cytotoxicity studies performed on A549 (lung cancer cells with low cholesterol content), MCF-7 (breast cancer cells with high cholesterol content) and erythrocytes (abundant cholesterol in membranes). These results provide a new insight in tuning the activity of CLPs against cholesterol-rich membranes by modulation of hydrogen bonding.

The peptide C6 was shown to possess moderate selectivity towards cancerous cells *in vitro.* By comparing the IC_{50} values, C6 was ~2-fold more effective against A549 and MCF-7 cells than NIH-3T3 fibroblast cells. Intratumoral injection of C6 in an A549 nude mouse tumor model resulted in a marked reduction in tumor size. Except for being a therapeutic agent, C6 was found to be able to stabilize neutralEPT in aqueous solution. The cytotoxicity study showed that C6-EPT complexes were more efficient in inhibiting the growth of A549 cells than either C6 or EPT alone. At the IC_{50} of C6-EPT complexes, neither C6 nor EPT alone was toxic at their complex concentration, demonstrating the synergistic effect between C6 and delivered EPT. Neutral EPT showed comparable cytotoxicity towards A549 and NIH-3T3 cells; in contrast, C6-EPT complexes showed ~2-fold higher activity than C6 against A549 cells, and comparable cytotoxicity to C6 against NIH-3T3 cells. These results indicate that C6 could enhance the efficacy of EPT (synergistic effect) and selectively deliver EPT in accordance with its own selectivity. To explain the enhanced cytotoxicity of C6-EPT complexes and selectivity of C6-EPT complexes, a “CLP-assisted uptake” mechanism was proposed: the membrane lytic action of C6

could increase cell membrane permeability, facilitating the cellular uptake of EPT, resulting in the enhancement of cytotoxicity. As C6 is shown to be less active against NIH-3T3, less permeability is induced by C6 on NIH-3T3 cell membranes than A549 cell membranes, leading to different degrees of enhancement. This is the essence of the selective delivery.

Stimuli-responsive strategy is widely used in drug delivery systems to improve delivery efficiency and reduce side effect, but CLP with stimuli-responsive cytotoxicity has not been reported. C8, a stimuli-responsive cationic peptide, was designed based on our amino acid pairing principle (AAP). The C8 peptide sequence contained five types of amino acid residues, arginine, isoleucine, asparagine, histidine and tryptophan, which are alternatively arranged in the sequence. According to the properties of the side chain of the amino acids, positively charged arginine residues provide repulsive electrostatic forces, while isoleucine residues and asparagine residues provide attractive hydrophobic interactions and hydrogen bonding, respectively. The ionizable histidine residues could provide either hydrogen bonding or electrostatic repulsion depending on their protonation status. Controlled by the balance of intermolecular forces between repulsive and attractive interactions, the peptide can self-assemble into β-sheet rich nanofibers or disassemble into unstructured monomers. C8 was shown to be a triple-responsive self-assembling peptide: the pH affects protonation state of the three histidine residues, temperature affects hydrogen bonding and hydrophobic interactions, and the presence of urea interferes with the formation of hydrogen bonds. Cytotoxicity studies confirmed that the nanostructure formation of C8 could work as the "switch" to control the lytic activity: the nanostructured C8 is non-toxic while the disassembled C8 monomers are toxic. This work showed the potential of CLPs to deliver themselves for stimuli-triggered (self-guided) delivery.

The potential of C8-mediated EPT delivery system was also investigated. The C8 nanofibers were found to encapsulate neutral EPT in aqueous solution at pH 8.0, and disassemble at pH 4.0, releasing protonated EPT. In addition to the enhanced efficacy and selectivity found in C6-mediated system, C8-EPT complexes further showed pH-triggered cytotoxicity: the

nanostructured C8-EPT complexes/co-assemblies showed minimal cytotoxicity, and became cytotoxic after disassembling in acidic environment. The studies on C6- or C8- mediated EPT delivery systems demonstrate the potential of using CLPs as multifunctional carriers for hydrophobic drugs.

Acknowledgements

Foremost, I would like to express my sincere gratitude to my supervisor, Dr. Pu Chen, who has provided me continuous support, valuable advisory and critical guidance during my PhD study at the University of Waterloo. His guidance helped me overcome the difficulties met in my research, encouraged and inspired me in pursuing advanced research in nano-bioengineering. His scientific vision and enthusiasm continuously conveyed a spirit that teaches me to become a creative, open minded, optimistic and independent researcher. I greatly appreciate that he provided me the chance to work on this cutting-edge research field in his lab.

My next acknowledgements go to the following individuals who have contributed to the experiments, discussions and/or suggestions on my PhD research projects. Professor Heiko Heerklotz from Leslie Dan Faculty of Pharmacy, University of Toronto introduced a calcein-based liposome leakage assay to study the membrane activity and selectivity of lytic peptides; his students, Helen Fan and Trong Shen, have carried out many liposome leakage assays. They also provided valuable suggestions on experimental design and data analysis. Professor Mikko Karttunen and his postdoctoral research assistants, Amir Mohsen Pourmousa and Drew Bennett, provided molecular dynamics analysis. Professor Yongfang Yuan and her students, Rong Wang and Yan Wu, from No. 3 People's Hospital Affiliated to Shanghai Jiao Tong University School of Medicine have collaborated with us on *in vivo* studies. We have had frequent tele-conference calls to exchange ideas and discuss animal results. Mishi Savulescu from the Biology department has performed serveral cytometry experiments for me. Professor Guy Guillemette from the

Chemistry Department, University of Waterloo kindly allowed us to use his circular dichroism spectrometer.

I also want to extend my thanks to my current and previous group members as well as our lab managers: Tatianna Sheinin, Xiaoxia Han, Nita Modi and Doan The Nam Long for their great help and contributions in organizing the lab and consumable ordering. Dafeng Chu has kindly shared his valuable experience and thoughtful discussion to me, which benefited me a lot. Yong Ding, my colleague and best friend, provided me with lots of suggestions on my experimental design and data interpretation. Thank to all the help from my colleagues, Wen Xu, Ran Pan, Zizhen Wan, Danyang Zhao, Parisa Sadatmousavi, Ali Sheikholeslam, Baolin Cheng and Lei Zhang in biomedical research group and all the members in the energy research group of our lab. During my PhD study, I also received great help from undergraduate research assistants working in our lab: Jack Chen, Jason Li and Piaopiao Long. Their efforts are acknowledged.

Lastly, and also most importantly, I would like to thank my families and my girlfriend for their unlimited support and endless love. Also I thank my friends, especially, Lei Jia, a friend from undergraduate, for their enormous encouragement and help. Without them, I can achieved none of my progress.

This thesis, a product of my PhD study, is dedicated to all of them.

Table of Contents

AUTHOR'S DECLARATION ..... **ii**

Abstract ..... **iii**

Acknowledgements ..... **vii**

Table of Contents ..... **ix**

List of Figures ..... **xiv**

List of Tables ..... **xx**

Nomenclatures ..... **xxi**

Amino Acid Abbreviations ..... **xxiv**

Chapter 1 ..... **1**

Introduction **1**

1.1 Overview **1**

1.2 Objectives **7**

1.3 Outline of the thesis **7**

Chapter 2 ..... **9**

Literature Review **9**

2.1 Current advances in cationic lytic peptides as anticancer agents **9**

2.1.1 Naturally occurring AMPs for cancer treatment 10

2.1.2 Synthetic CLPs for cancer treatment 15

2.1.3 Membrane selectivity of CLPs 17

2.2 Current advances in anticancer drug delivery. **20**

2.2.1 Stimuli-responsive systems 23

2.2.2 Multi-responsive systems 29

2.2.3 Self-assembling peptide-mediated systems 30

2.2.4 Amino acid pairing (AAP) principle 33

Chapter 3 ..... **37**

Beyond Electrostatics: Tuning the Membrane Selectivity of a Cationic Lytic Peptide by Hydrogen Bonding **37**

3.1 Introduction **37**

3.2 Materials and methods **39**

3.2.1 Materials 39

3.2.2 Sample preparation 40

3.2.3 Circular dichroism spectroscopy 41

3.2.4 Steady-state fluorescence 41

3.2.5 Time-resolved fluorescence leakage assay 42

3.2.6 Estimation of cell surface 42

3.2.7 Partition coefficient estimated in cellular system 42

3.2.8 Determination of cholesterol level 43

3.2.9 Cell proliferation assay 44

3.2.10 Hemolysis assay 44

3.3 Results **45**

3.3.1 Physicochemical characterization of C6 and C6/POPC interactions 45

3.3.2 Time-resolved fluorescence leakage assay 47

3.3.3 Partitioning behaviour in liposome and cellular systems 49

3.3.4 Activity of C6 against cholesterol-rich membranes 51

3.3.5 Effect of phosphate ions on membrane activity of C6 52

3.3.6 Hemolytic activity of C6 55

3.4 Discussion **56**

3.5 Conclusion **64**

Chapter 4 ..... **65**

Antitumor Activity of an Amphiphilic Cationic Lytic Peptide and its Potential as Anticancer Drug Carrier for Enhanced and Selective Delivery **65**

4.1 Introduction **65**

4.2 Materials and methods **67**

4.2.1 Sample preparation 67

4.2.2 Cell culture 67

4.2.3 Cellular uptake of C6-EPT complexes 68

4.2.4 MTS assay....68
4.2.5 Annexin V assay....69
4.2.6 Lung carcinoma xenograft experiments....69
4.2.7 Statistical analysis....69
4.2.8 Ellipticine loading capacity....69
4.2.9 Dynamic laser scattering....70
4.2.10 Surface tension measurement....70
4.2.11 Atomic force microscopy....70
4.2.12 Fluorescence spectroscopy....71
4.2.13 Circular dichroism spectroscopy....71
4.3 Results and discussion....72
4.3.1 *In vitro* cytotoxicity evaluation....72
4.3.2 Inhibition of tumor growth in xenografts....73
4.3.3 Drug delivery potential of C6....74
4.3.4 CLP-assisted delivery.....77
4.4 Conclusion....83
Chapter 5....85
Stimuli-responsive Self-assembling Cationic Lytic Peptide and its Potential for Self-guided Delivery....85
5.1 Introduction....85
5.2 Materials and methods....87
5.2.1 Sample preparation....87
5.2.2 Fluorescence spectroscopy....87
5.2.3 Circular dichroism spectroscopy....88
5.2.4 Microscopy....88
5.2.5 Cell culture....89
5.2.6 MTS assay....89
5.2.7 Hemolysis study....90
5.3 Results and discussion....91
5.3.1 Peptide design....91
5.3.2 Self-assembly/disassembly of C8 in response to pH change....93
5.3.3 Temperature effect on reversible self-assembly/disassembly of C8....95
5.3.4 Effect of urea on self-assembly of C8....101

5.3.5 Estimation of force contributions 102
5.3.6 Nanostructure-dependent lytic action of C8 104
5.4 Conclusions 111
Chapter 6 112
pH-responsive Cationic Lytic Peptide for Synergistic, Selective and On-demand Delivery 112
6.1 Introduction 112
6.2 Materials and methods 114
6.2.1 Sample preparation 114
6.2.2 Cell culture 114
6.2.3 MTS assay 115
6.2.4 Statistical analysis 115
6.2.5 Annexin V assay 116
6.2.6 Atomic force microscopy 116
6.2.7 Fluorescence spectroscopy 116
6.2.8 Circular dichroism spectroscopy 116
6.2.9 Membrane leakage assay 117
6.2.10 Molecular dynamics simulations 118
6.3 Results 118
6.3.1 Selective cytotoxicity 118
6.3.2 Mechanism of cell death induced by C8 119
6.3.3 Selective and on-demand drug delivery 121
6.3.4 Membrane selectivity and lysis 127
6.4 Discussion 130
Chapter 7 133
Conclusions and Recommendations 133
8.1 Original contributions to research 133
8.1.1 Tuning the membrane selectivity of C6 by hydrogen bonding. 133
8.1.2 *In vitro* and *in vivo* anticancer activity of C6 and *in vitro* delivery of C6-EPT complexes. 134
8.1.3 Stimuli-responsiveness and nanostructure-dependent cytotoxicity of C8. 135

8.1.4 Co-assembly of ellipticine with C8 and pH-responsive, synergistic and selective delivery of C8-EPT complexes. 136
8.2 Recommendation 136
References 139

List of Figures

Figure 1.1 The proposed models of action for CLPs in bilayer membrane. Reprinted with permission from reference[9] © 2014 Elsevier. 2

Figure 2.1 Guandinium-phosphate complex stabilized by bidentate hydrogen bonds and electrostatic interaction. Reprinted with permission from reference [11] © 2014 ACS. 20

Figure 2.2 Timeline of the development of nanomedicines. Adapted with permission from reference [37] © 2014 NPG. 23

Figure 2.3 Schematic illustrations of the mechanisms for thermosensitive liposomal drug delivery systems. (a) The temperature-triggered unfolding of a leucine zipper peptide in the peptide-lipid hybrid systems. Reprinted with permission from reference [55] © 2014 ACS. (b) Drug-permeable pores created by the temperature-triggered generation of carbon dioxide bubbules. Reprinted with permission from reference [154] © 2014 ACS. 25

Figure 2.4 Schematic illustrations of the mechanisms for photosensitive drug delivery systems. (a) Azobezene-modified DNA-controlled reversible release system. Reprinted with permission from reference [155] © 2014 ACS. (b) Photosensitive thymine modified MSNPs. Reprinted with permission from reference [159] © 2014 ACS. (c) Photoswitching spiropyran-PEGylated lipid system. Reprinted with permission from reference [157] © 2014 ACS. 27

Figure 2.5 Schematic illustrations of the mechanisms for pH-triggered exposure of TAT peptide. (a) pH-degradable hydazone bond (Hz) allows the removal of the PEG_{2k}shield at low pH. Reprinted with permission from reference [163] © 2014 Elsevier. (b) Acid-induced pop-up of folded PEG chains. Reprinted with permission from reference [164] © 2014 Elsevier. 29

Figure 2.6 Schematic illustrations of (a) the nanoribbon formed by self-assembly of TβP and encapsulation of hydrophobic guest molecules. Reprinted with permission from reference [172] © 2014 Wiley. (b) Conformational change of $K^{P}_{160}(L_{0.3}/K_{0.7})_{40}$ coploypeptide, and release of entrapped Fura-2 dye from peptide vesicles. Reprinted with permission from reference [173] © 2014 NPG. 30

Figure 2.7 (a) Chemical structure of ionic-complementary peptide EAK16-II. (b) Schematic illustration of EAK 16-II self-assembly. Reprint with permission from reference [67] © 2014 Elsevier. 31

Figure 2.8 (a) The fluorescence spectra of EAK16-II-ellipticine complexes after 24 h stirring with 0.1 mg/ml ellipticine and various peptide concentrations. The fluorescence emission peak at ~520 nm indicates protonated ellipticine, and peak at ~468 nm indicates crystalline ellipticine. (b) SEM images of the EAK16-II-ellipticine complexes. Reprinted with permission from reference [70] © 2014 Wiley. 33

Figure 2.9 (a) AFM images of the self-assembled nanostructures of APP8 at various concentrations (2.2–87 μM). The scale bar is 250 nm. (b) A proposed self-assembly mechanism in relation to the CAC of APP8. (c) APP8 anti-parallel **β**-sheets that form with the assistance of paired interactions: hydrophobic amino acid pairing (involving **π**-**π** stacking), ionic pairing and hydrogen bonding pairing. (d) The cytotoxicity of the APP8-EPT complexes on serial dilutions. 1x refers to the complexes with 25 $\mu g/ml^{-1}$ (21.8 μM) APP8 and 10 $\mu g/mL^{-1}$ (40.6 μM) EPT in the final culture media. Reprinted with permission from reference [72] © 2014 Wiley. 36

Figure 3.1 (a) CD spectra of 80 μM C6 in N buffer (110 mM NaCl, 10 mM Tris, 0.5 mM EDTA at pH 7.4) incubated for 1 hour with and without 2 mM POPC LUVs. (b) Fluorescence spectra of tryptophan at 10 μM C6 incubated with varying POPC concentrations up to 20 μM. CD spectra of 80 μM C6 in (c) N buffer solution (110 mM NaCl, 10 mM Tris, 0.5 mM EDTA at pH 7.4) or in (d) P buffer solution (50 mM NaH_2PO_4, 60 mM NaCl, 10 mM Tris and 0.5 mM EDTA at pH7.4) with different incubation times. 46

Figure 3.2 (a) Fluorescence lifetime τ vs. peptide concentration C_p. τ_E and τ_F are entrapped and free lifetimes respectively, and letters indicate sample series with lipid concentrations (C_L) of 100 μM (A), 200 μM (B), 300 μM (C) and 400 μM (D). (b) Efflux as a function of C_p for the four series, with errors of ±10% efflux. (c) Equi-activity analysis: The peptide concentration required to induce a particular leakage value at a specific C_L. The line of best fit for each efflux value yields parameters in equation (1). (d) IC_{50} of C6 against A549 cells as a function of seeding density in the cell proliferation assay. The IC_{50} value for each cell density was averaged from at least three independent experiments. Error bars represent standard deviations ($n \geq 3$). 48

Figure 3.3 Efflux vs. C6 concentration profiles for POPC (100 μM) as well as for POPC and cholesterol liposomes in NaCl (N) and in phosphate (P) buffers. Vertical error bars are standard deviations obtained from at least three independent experiments. Horizontal error bars represent the instrumental error in the lipid concentration measurement..... 52

Figure 3.4 (a) A snapshot of simulation from above the membrane at 67 ns. The arginine residues in C6 peptide are shown in green with the rest residues shown in yellow, POPC molecules in red and cholesterol molecules in blue. The arginine residues are labeled with numbers to indicate the position of each arginine residue in C6 molecule. The N-terminus of C6 orients to right in the snapshot. (b) The occurrence of H-bonds between the guanidinium group of each arginine residue and POPC (black line) or CHOL (red line) molecules over time. The simulation shows that each guanidinium group can form a maximum of 7 H-bonds with neighbouring POPC molecules. All the arginine residues form H-bonds with neighbouring POPC molecules; while only arginine residues at position 1, 4, 11, 15 and 18 (refer to ARG1, ARG4, ARG11, ARG15, and ARG18) form ~ 1 H-bond with neighbouring CHOL molecules, respectively. A neighbouring molecule is defined whenever POPC head groups or cholesterol hydroxyl groups are not farther than 0.35 nm of any atom of C6 peptide..... 54

Figure 3.5 (a) Relative cholesterol levels of A549 cell line and MCF-7 cell line. *In vitro* cytotoxicity of C6 towards (b) A549 lung cancer cells, (c) MCF-7 breast cancer cells, and the hemolytic activity of C6 on (d) rabbit red blood cells. The results were averaged from at least three independent experiments. Error bars represent the standard deviation of multiple experiments..... 56
Figure 3.6 CD spectra of 80 μM C6 in N buffer solution (110 mM NaCl, 10 mM Tris, 0.5 mM EDTA at pH 7.4) or in P buffer solution (50 mM NaH_2PO_4, 60 mM NaCl, 10 mM Tris and 0.5 mM EDTA at pH7.4), with the presence of 2 mM POPC liposomes or 2 mM POPC/cholesterol (4:1) liposomes, after 1h incubation..... 60

Figure 4.1 *In vitro* cytotoxicity evaluation. (a) Cytotoxicity of C6 against A549 (lung carcinoma), MCF-7 (breast carcinoma) and NIH-3T3 (mouse fibroblast). (b) A549 cells were treated with water or C6 peptide for 18 h. The apoptotic stage of cells was determined by FITC-Annexin V and 7-AAD staining..... 73
Figure 4.2 Intratumor administration of C6 in BALB/c nude mice. (a) The tumor sizes and (b) The body weights of mice in untreated, saline or C6 treated groups. (c) The representative images of A549 tumor in untreated, saline or C6 treated groups. *p<0.05 versus untreated group..... 74
Figure 4.3 Physicochemical characterization of C6 and C6-EPT complexes. (a) Helical wheel of C6. (b) Critical aggregation concentration of C6 determined by equilibrium surface tension of C6. (c) Nanostructures of C6 or C6-EPT complexes determined by AFM. The scale bar is 200 nm. (d) Size distributions of C6 or C6-EPT complexes determined by DLS. (e) Secondary structures of C6 in aqueous solution or in C6-EPT complexes determined by CD. (f) Normalized fluorescence emission spectrum of C6-EPT complexes. 75
Figure 4.4 C6-mediated CLP-assisted cellular uptake of EPT. (a) Illustration for the CLP-assisted delivery mechanism. The formulation of C6-EPT complexes is based on the characterizations. (b) Cellular uptake of EPT delivered by C6 monitored using fluorescence microscope. EPT is shown in green, DAPI is shown in blue. 1X sample refers to complexes with with 125 μg/ml (53.6 μM) C6 and ~3.5 μg/ml (14.2 μM) EPT in the final culture media. The concentration of C6 sample was 125 μg/ml (53.6 μM). (c) Time study of cellular uptake of EPT from 1X C6-EPT complexes at 10 min, 20 min, 30 min and 40 min, respectively. 79
Figure 4.5 Evaluation of the cytotoxicity of (a) neutral EPT and C6-EPT complexes against (b,c) A549 (lung carcinoma) and (d,e) NIH-3T3 (mouse fibroblast). C6+ and C6-EPT+ refer to the samples diluted with 80 μg/ml (32.4 μM) C6 aqueous solution. X-axis represents the concentration of C6 in each sample, including C6 alone and C6-EPT complexes; the concentrations of EPT in C6-EPT complexes are shown in the brackets. The concentrations presented are mass concentrations (μg/ml) in the culture media. The viabilities were averaged from at least three independent experiments. Error bars are standard deviation (n>3). *p<0.05, **p<0.01 between the two samples..... 82

Scheme 5.1 Design of the model stimuli-responsive self-assembling CLP C8. (**a**) Helical wheel of C8. The charged amino acid residues are shown as light blue

triangles, uncharged hydrophilic amino acid residues are shown as red circles, and hydrophobic amino acid residues are shown as green diamonds. The amount of green decreases with the decreased hydrophobicity. (**b**) The mechanism of the intermolecular forces controlled self-assembly/disassembly of C8. The colors represent different types of forces provided by the side chains of amino acids. Depending on the protonation status of histidine residues, the overall intermolecular forces could become repulsive, leading to unstructured C8 monomers, or become attractive, leading to fibrous self-assemblies. 92

Figure 5.1 Characterization of the self-assembly and disassembly of C8. (a) circular dichroism spectra of C8 at pH 8.0 and at pH 4.0. (b) fluorescent emission of tryptophan residual of C8 at pH 8.0 and at pH 4.0. c-d, AFM images of C8 samples at pH 8.0 (c) and at pH 4.0 (d). The scale bar is 500 nm. 94

Figure 5.2 Secondary structures of C8 at various conditions. a-c, circular dichroism spectra of C8 at various pHs after incubation at 0 ^{0}C (a), 22 ^{0}C (b) and 37 ^{0}C (c), respectively..... 96

Figure 5.3 AFM images of C8 samples at various conditions. (a) C8 at pH 5.4 and at pH 5.8 incubated at 0 ^{0}C for 2 d and 10 d, respectively. (b) C8 at pH 5.0 and at pH 5.4 incubated at 22 ^{0}C for 2 d and 10 d, respectively. (c) C8 at pH 5.0 incubated at 37 ^{0}C for 6 h. The scale bar is 500 nm. 97

Figure 5.4 Imaging the self-assembling process of C8 by AFM.The sample at pH 8.0 incubated at 0 ^{0}C was imaged at 12 hours, 1day, 2 days and 4 days, respectively, after pH adjustment; 1 hour, 3 hours, 8 hours and 1day were chosen for the sample incubated at 22 ^{0}C; and 0.5 hour, 3 hours, 6 hours and 9 hours were chosen for the samples incubated at 37 ^{0}C. The scale bar is 500 nm. 99

Figure 5.5 Imaging the disassembling process of C8 by AFM. The sample at pH 8.0 incubated at 0 ^{0}C was imaged at 1 hour, 3 hours, 8 hours and 18 hours, respectively, after pH adjustment to pH 4.0; 1 hour, 3 hours, 8 hours and 20 hours were chosen for the sample incubated at 22 ^{0}C. The scale bar is 500 nm. 100

Figure 5.6 The morphology of C8 samples at pH 4.0 (a) after 1 d incubation at 37 ^{0}C and that at pH 3.0 (b) after 6 h incubation at 37 ^{0}C. Both samples are made from C8 sample at pH 8.0 with 1 d incubation at 37 ^{0}C. The scale bar is 500 nm. 101

Figure 5.7 Characterization of C8 with the presence of urea. (a**)** Circular dichroism spectra of C8 at pH 6.0 with the presence of 20 mM urea after 2 d incubation. The CD spectra of C8 (pH 6.0) without urea was taken from Figure 5.2.a. (b) AFM images ofthe sample after 2 d o f incubation and 10 d incubation, respectively. The scale bar is 500 nm..... 102

Figure 5.8 Evaluation of the cytotoxicity and hemolytic effect of nanostructured and unstructured C8 samples. a-e, viabilities of cancerous cell lines: A549 (a), U87MG (b), MCF-7 (c) and non-cancerous cell lines: NIH-3T3 (d), HUVEC (e) after 1 day treatment of C8 at pH 7.4 or C8 at pH 4.0. The data are averaged from at least three independent replicates. The standard deviations are shown as error bars. 106

Figure 5.10 The hemolysis induced by C8 at pH 7.4 and C8 at pH 4.0 on rabbit red blood cells, respectively. The data are averaged from three independent replicates. The standard deviations are shown as error bars. 108
Figure 5.11 Visualization of morphologies of A549 cells before and after incubation with nanostructured or unstructured C8. a-f, SEM images (a-c) and deflection images associated with corresponding reconstructed 3-D images (d-f) of non-treated A549 cells (a,d) and A549 cells after incubation with 20 μM C8 at pH 7.4 (b,e) or with 5 μM C8 at pH 4.0 (c,f) for 3 hours, respectively. 110

Figure 6.1 Cytotoxicity of C8 against A549 (lung carcinoma), MCF-7 (breast carcinoma) and NIH-3T3 (mouse fibroblast). The cells were incubated with C8 for 24 h. The data are averaged from at least three independent replicates. The error bars represent standard deviations. 119
Figure 6.2 The mechanism of cell death induced by C8. (a) The apoptotic stage of A549 cells treated with unstructured C8 determined by FITC-Annexin and 7-AAD labeling. (b) The morphology of A549 cells treated with unstructured C8. The images were produced using a EVOS ® FL Cell imaging system (AMG, Mill Creek, USA). 120
Figure 6.3 Characterization of C8-EPT co-assemblies and proposed co-assembly and delivery mechanism. a-c. the characterization of physicochemical properties of C8-EPT co-assemblies at pH 4 or pH 8 using AFM (a), fluorescence microscopy (b) and circular dichroism (c). The C8-EPT co-assemblies contain 500 μg/ml (214.6 μM) C8 and 50 μg/ml (203.3 μM) EPT, the C8 pH 8 sample is at the concentration of 500 μg/ml (214.6 μM). d) Schematic of the co-assembly of C8-EPT and the on-demand CLP-assisted delivery mechanism. 122
Figure 6.4 (a) Cytotoxicity of (left) EAK16-II-EPT co-assemblies (1X refers to 125 μg/ml EAK16-II (77.4 μM) and 25 μg/ml (51.8 μM) EPT) or (right) C8-EPT (pH 4) sample (1X refers to 125 μg/ml (53.6 μM) C8 and 12.5 μg/ml (50.8 μM) EPT) against A549 cells with 1h of incubation. The viabilities were averaged from at least three independent experiments, error bars are standard deviations. (b) Optical microscopy images of untreated A549 cells and A549 cells treated with C8-EPT (pH 4) sample for 2 min. 124
Figure 6.5 Evaluation of the cytotoxicity of EPT and C8-EPT co-assemblies against A549 (lung carcinoma) and NIH-3T3 (mouse fibroblast). Cytotoxicity of protonated EPT (a) and C8-EPT co-assemblies diluted with water (b,d) and unstructured C8 aqueous solution at concentration of 60 μg/ml (25.2 μM) (c,e). The samples with "+" represent that they are diluted with unstructured C8 aqueous solution. 1X refers to 12.5 μg/ml (50.8 μM) EPT, or 125 μg/ml (53.6 μM) C8, or the C8-EPT co-assemblies with 125 μg/ml (53.6 μM) C8 and 12.5 μg/ml (50.8 μM) EPT in the final culture media. The viabilities were averaged from at least three independent experiments, Error bars are standard deviation. *$p<0.05$, **$p<0.01$ between the two samples. 126
Figure 6.6 Membrane leakage induced by C8. (a) Leakage induced by C8 on pure POPC, POPC+20% cholesterol and *E. coli* extract lipid membranes. (b)Atomistic molecular dynamics simulations of C8 aggregation within different model membranes. Representations are: water, red; lipid tails, thin cyan; POPC

phosphorous, yellow; POPG phosphorous, blue; cholesterol oxygen, white; the peptides are in cartoon representation colored by residue type (charged and histidine, blue; hydrophobic white; polar, green). 128
Figure 6.7 (a) The top view of a pore in the POPC bilayer with neutral (left) and charged (right) C8 peptides. Water is not shown for clarity, and the peptide and lipids are in Van der Waals representation. The peptide is coloured white for hydrophobic residues, green for polar and blue for histidine and arginine. A calcein molecule in licorice representation is over laid on the pore to illustrate that the pore is large enough to leak calcein when C8's histidines are charged, but not when neutral. (b) Free energy profiles for moving a single C8 peptide from water to the center of the different membranes. These calculations were performed with the MARTINI coarse-grained model. The free energy troughs at the water-membrane interface show that monomers would bind to the lipid environment. 129

List of Tables

Table 2.1 Naturally occurring AMPs with anticancer activities. 10
Table 2.2 Non-ideal properties of drugs and their therapeutic implications. Adapted from reference [144]. 21
Table 2.3 Properties of the side chains of natural amino acids at physiological condition. Adapted from reference [72] 34
Table 2.4 Hydrogen bonding, ionic complementary and all pairing self-assembling peptides. Summarized from reference [72]. 35

Table 3.1 Partition coefficient K, R_e and C_p^{aq} obtained from the calcein leakage assay with C6 and POPC LUVs. 50
Table 3.2 Arginine-to-lysine ratio and hemolytic effect of selected naturally occurring CLPs 63

Nomenclatures

Acronym	Full name
7-AAD	7-aminoactinomycin D
A549	Non-small cell lung cancer cell line
AAP	Amino acid pairing
ADSA-P	Axisymmetric drop shape analysis-profile
AFM	Atomic force microscopy
AMPs	Antimicrobial peptides
ATCC	American type culture collection
CAC	Critical aggregation concentration
CD	Circular dichroism
CHOL	Cholesterol
CLPs	Cationic lytic peptides
CLVs	Calcein-loaded vesicles
CPT	Camptothecin
DAPI	4',6-diamidino-2-phenylindole
DDS	Drug delivery system
DLS	Dynamic laser scattering
DOPA	1,2-dioleoyl-sn-glycero-3-phosphate
DOPC	1,2-dioleoyl-sn-glycero-3-phosphocholine
DOPE	1,2-dioleoyl-sn-glycero-3-phosphoethanolamine
DOPG	1,2-dioleoyl-sn-glycero-3-phospho-(1'-rac-glycerol)
DSPE-PEG (2000)	1,2-distearoyl-sn-glycero-3-phosphoethanolamine-N-[amino(polyethylene glycol)-2000]
EDTA	Ethylenediaminetetraacetic acid
EPR	Enhanced permeability and retention
EPT	Ellipticine

FACS	Fluorescence-activated cell sorting
FBS	Fetal bovine serum
FDA	Food and drug administration
FITC	Fluorescein isothiocyanate
GSH	Glutathione
HUVEC	Human umbilical vein endothelial cells
LUVs	Large unilamellar vesicles
MMP2	Matrix metalloproteinase 2
MC	Merocyanine
MCF-7	Human breast cancer cell line
MD	Molecular dynamics
MDR	Multidrug resistance
MPEG	Methyl ether poly(ethylene glycol)
MSNPs	Mesoporous silica nanoparticles
MTS	3-(4,5-dimethylthiazol-2-yl)-5-(3-carboxymethoxyphenyl)-2-(4-sulfophenyl)-2H-tetrazolium
MTT	3-(4,5-Dimethylthiazol-2-yl)-2,5-diphenyltetrazolium bromide
NIH-3T3	Mouse embryonic fibroblast cell line
NIR	Near-infrared
PAE	Poly (β-amino ester)
PBS	Phosphate buffer saline
PE	Phosphatidylethanolamine
PEG	Polyethylene gloycol
PFP	Perfluoropentane
PG	Phosphatidylglycerol
POPC	1-palmitoyl-2-oleoyl-*sn*-glycero-3-phosphocholine
PS	Phosphatidylserine
PTX	Paclitaxel
RBCs	Red blood cells
SEM	Scanning electron microscopy
SP	Spiropyran
SPAnH	Poly [aniline-co-N-(1-one-butyric acid) aniline]
TCSPC	Time-correlated single photon counting

Tris	Tris(hydroxymethyl)methylamine
TSLs	Thermosensitive liposomes
U87MG	Human primary glioblastoma cell line
UV	Ultraviolet

Amino Acid Abbreviations

Amino acid name	Abbreviation	Side chain property*
Alanine	A	Hydrophobic
Arginine	R	Positively charged
Asparagine	N	Polar uncharged
Aspartic acid	D	Negatively charged
Cysteine	C	Polar uncharged
Glutamic acid	E	Negatively charged
Glutamine	Q	Polar uncharged
Glycine	G	Hydrophobic
Histidine	H	Positively charged
Isoleucine	I	Hydrophobic
Leucine	L	Hydrophobic
Lysine	K	Positively charged
Methionine	M	Hydrophobic
Phenylalanine	F	Hydrophobic
Proline	P	Hydrophobic
Serine	S	Polar uncharged
Threonine	T	Polar uncharged
Tryptophan	W	Hydrophobic
Tyrosine	Y	Hydrophobic
Valine	V	Hydrophobic

*** The charge properties are determined at physiological pH**

Chapter 1

Introduction

1.1 Overview

To date, surgery, radiotherapy and chemotherapy are the major means to treat cancer in clinics [1, 2]. Surgery and radiotherapy are often successful for localized primary tumor treatment, whereby chemotherapy is the usual choice for metastatic tumor treatment. The use of conventional chemotherapeutic agents is often limited by poor solubility and the deleterious side effects to normal tissue cells [3, 4]. Moreover, cancer cells always generate multidrug resistance (MDR), normally arising from an over-expression of the membrane bound P-glycoprotein. The P-glycoprotein pumps the conventional anticancer drugs out of the cell cytoplasm, resulting in reduced therapeutic efficacy [5]. To address these issues relating to conventional chemotherapeutic agents, current research efforts are focusing on developing: (i) a new class of anticancer agents and (ii) efficient drug delivery systems for conventional anticancer drugs.

Cationic lytic peptides (CLPs) are one of the promising drug candidates under investigation for cancer treatment. As a class of anticancer agents, CLPs offer two important advantages over conventional chemotherapeutic agents: selective cytotoxicity towards cancerous cells and ability to combat MDR [6, 7]. This class of peptides were first discovered in a diverse range of natural sources, including microbes, insects, plants, animals and humans [8], and were initially recognized as antimicrobial peptides (AMPs) because of their broad spectrum of antimicrobial activities [9]. In addition to antimicrobial activity, some of these peptides exhibit cytotoxicity towards various types of cancer cells [7]. These peptides are generally positively charged (i.e., their net charges vary from +2 to +9 at pH 7), and have an amphiphilic structure which is

considered to be a key factor influencing their membrane lytic activity [6]. Most CLPs are unstructured in aqueous solutions, but adopt a bioactive α-helical conformation [10] or β-sheet/hairpin structures [11, 12] when they contact the surface of membrane mimics or biological membranes. The amphiphilicity enables the insertion of CLPs into phospholipid bilayers, disrupting the membrane integrity, causing the leakage of the intracellular contents and lysis of the cells. Thus, in this context, these peptides are referred to as "cationic lytic peptides". There are several membrane-disruption models that have been proposed to explain the membrane actions of CLPs. Some of the most accepted models used to illustrate the process of membrane permeabilization include the carpet model [13, 14], barrel-stave model [15, 16], toroidal model [17] and detergent-like membrane-lytic model [18] (Figure 1.1).

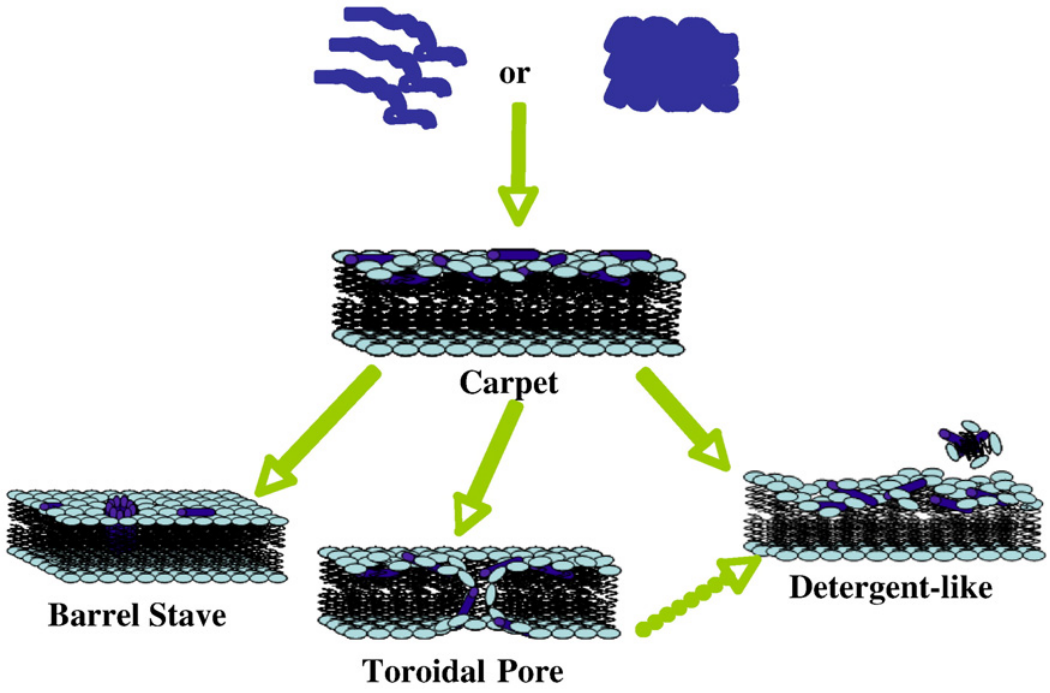

Figure 1.1 The proposed models of action for CLPs in bilayer membrane. Reprinted with permission from reference [6] © 2014 Elsevier.

These cationic peptides are believed to preferentially bind to negatively charged cell membranes due to electrostatic interactions. As a number of cancer cells possess negatively

charged surfaces due to over-exposure of phosphatidylserine [19, 20] and high levels of aberrant O-glycosylated mucins [21, 22], CLPs could target this trait and selectively lyse cancerous cells [12, 23, 24]. CLPs kill cells via direct membrane lysis, which should avoid the general mechanisms of MDR. Thus, CLPs also show the ability to combat multidrug resistant cancer cells [25, 26]. Although CLPs have shown promises through *in vitro* studies, enzymatic degradation in serum becomes the major obstacle for their *in vivo* application [7, 27]. One approach to preserve the activity of CLPs *in vivo* involves the utilization of all-D-amino acid in the peptide design [27, 28]. To understand the mode of actions of CLPs, the effects of peptide length and charge density [29], overall hydrophobicity [30], and bulky amino acids [31] on the interaction between CLPs and phospholipid membranes (including zwitterionic, anionic and cholesterol-rich membranes) have been investigated. This established understanding provides important implications for designing CLPs with enhanced efficacy and specificity towards cancerous cells. Other alternatives involve conjugating CLPs with tumor-homing peptides [32] or antibodies [33], and nanotechnology-based delivery strategies [34, 35]. These approaches will be reviewed in the following sections.

In the past several decades, nanotechnology has offered numerous possibilities to improve bioactivity and prolong bioavailability of conventional chemotherapies for cancer therapy [36, 37]. A broad range of nanoparticle-based drug delivery systems has been developed to achieve cancer specific delivery of therapeutic agents via improved pharmacokinetics and pharmacodynamics, and ligand-mediated targeting. The basic principle of these delivery systems is to provide a protective, hydrophobic interior that can solubilize hydrophobic anticancer drugs in aqueous solutions. Furthermore, nanoparticles with proper size range (between ~10 nm and 100 nm) could have prolonged circulation time by avoiding renal clearance or reticuloendothelial system (RES) clearance, and enhanced passive accumulation by extravasation to tumor neovasculatures, a phenomenon known as the enhanced permeability and retention (EPR) effect [37, 38]. Moreover, surface properties of nanoparticles also play an important role in avoiding the

adsorption of proteins that are recognized by RES cells; coating drug surfaces with hydrophilic polymers, such as polyethylene glycol (PEG), has been a predominant strategy to reduce protein adsorption and elongate the blood circulation of the drug [39]. There have been several FDA approved polymer-drug conjugates in the market. For instance, Oncaspar® is PEGylated L-asparaginase, which was approved in 1994 for acute lymphoblastic leukemia treatment [40]. The nanoparticle surfaces can also be decorated by targeting ligands, which allow the accumulation of nanoparticles at surfaces of cancer cells that overexpress tumor-associated receptors and enhance the cellular uptake of nanoparticles by receptor-mediated endocytosis [41].

Currently, smart stimuli-responsive (or on-demand) delivery systems have received tremendous attention in the field of tumor specific drug delivery research [36, 42]. The design of stimuli-responsive system involves multi-disciplinary principles, which require a bond cleavage or molecular/supermolecular conformational changes in response to endogenous or exogenous stimuli, leading to the tailored release of a delivered cargo at the desired sites. The endogenous stimuli involve changes in pH [43, 44], elevated levels of glutathione (GSH) [45, 46] and enzymes [47-50]. The externally applied stimuli can be light [51-53], ultrasound [54-56], heat [57, 58] or magnetic fields [59, 60]. Although these targeted- or stimuli-responsive drug delivery systems have shown promising results in *in vitro* and *in vivo* studies, very few of them have reached clinical stages. Challenges remain in translating concepts to applications, such as inefficient delivery, biocompatibility and biodegradability of materials [42].

Peptide-based drug delivery systems have drawn much attention due to their versatility in design [61-65], bio-functionalities [41], and potential advances in biocompatibility and non-toxic degradation product [66]. Our lab for many years has investigated the potential use of a class of ionic-complementary, self-assembling peptides as anticancer drug carriers. These peptides contain alternatively arranged negatively charged glutamic acid (E) residues and positively charged lysine (K) residues, resulting in ionic complementarity, which leads to stable β-sheet-rich self-assembled structures [67, 68]. Additionally, the presence of hydrophobic residues, such as

alanine (A) or phenylalanine (F), allows the peptides to encapsulate hydrophobic molecules [69, 70]. EAK16-II, one of the ionic complementary peptides, has shown promise in both *in vitro* and *in vivo* delivery of hydrophobic anticancer drug ellipticine (EPT) by exhibiting significantly higher anticancer efficacy when compared to the free drug [71, 72]. Encouraged by these results, an amino acid pairing (AAP) principle has been proposed for designing self-assembling peptides with side chain complementarity. This design principle is primarily guided by three types of side chain interactions: hydrophobic, hydrogen bonding and electrostatic. The side chain complementarity could lead to paired interactions, meanwhile the choice of amino acids should also achieve certain physiochemical stability to maximize the paired affinity and minimize free energy [73]. One of the CLPs studied in this research project is designed based on the AAP principle.

This research project focuses on exploring the potential of CLPs in anticancer treatment, involving acting as anticancer agents or anticancer drug carriers. An arginine-rich CLP, C6 (Ac-RLLRLLLRLWRRL-LRLLR-NH_2), was used to study the hydrogen bonding effect on the lytic activity of CLP towards membranes with or without cholesterol. The membrane selectivity of C6 was studied by monitoring the leakage induced by peptides on phospholipid membranes with different compositions. Molecular dynamics (MD) simulations were performed to provide molecular level insight. The cytotoxicity of peptides against two cancerous cell lines, A549 lung cancer cells and MCF-7 breast cancer cells, and NIH-3T3 fibroblast cell line, as well as their hemolytic activity, were evaluated to show the impact of membrane selectivity on the lytic activity of C6 towards different cell lines.. To incorporate the advantages of stimuli-responsive system into CLPs, a stimuli-responsive self-assembling CLP C8 (Ac-WHIINNIIHHIINNIIRR-NH_2) was designed based on the AAP principle. The side chains of arginine (R) residues could provide repulsive electrostatic forces, while the side chains of isoleucine (I) residues and asparagine (N) residues provided attractive hydrophobic interactions and hydrogen bonding, respectively. The Tryptophan (W) residue could provide hydrogen bonding, hydrophobic

interaction and π-π stacking. The ionizable histidine (H) residues could provide either hydrogen bonding or electrostatic repulsion depending on their protonation status. The balance between attractive forces and repulsive forces was tunable in response to applied stimuli, such as heat and changes in pH, resulting in transitions between β-sheet-rich nanofibers and unstructured monomers. The cytotoxicity of C8 was found to correlate with the formation of nanofibers. The impact of other stimuli (temperature and the presence of urea) on the reversible self-assembly of C8 was characterized using atomic force microscopy (AFM) and circular dichroism (CD).

The amphiphilic nature of C6 and C8 allowed them to interact and encapsulate hydrophobic drugs, showing the possibility as drug carriers. This research project also investigated the complexation and *in vitro* delivery of hydrophobic anticancer drugs using CLPs. The interesting aspect was that the delivery vehicles were also drugs. Ellipticine was used as the delivery cargo for several reasons. First, EPT is a hydrophobic molecule. Second, the fluorescent properties of EPT have been fully studied [74], which made it easy to characterize its molecular state. Third, an effective delivery system is required urgently to reduce the adverse effects encountered during early clinical trials of its derivatives [75, 76]. The physicochemical properties of peptide-EPT complexes were characterized by various techniques, including fluorescence spectroscopy, CD, dynamic laser scattering (DLS) and AFM. Cytotoxicity studies have shown an enhanced therapeutic efficacy of delivered EPT with C6 and that the C6-EPT complexes selectively killed cancerous cells. These observations were explained by a proposed "CLP-assisted uptake" mechanism. Furthermore, utilizing the stimuli-responsive properties, the C8-EPT delivery system showed a potential for on-demand delivery: nanostructure formed C8-EPT co-assembly showed minimal cytotoxicity; while C8-EPT co-assembly disassembled in acidic environment, releasing the encapsulated EPT and C8 peptide monomers, which exhibited enhanced and selective cytotoxicity as that found in C6-EPT system. Taken together, the results reported in the works provide a new strategy to design CLPs for the purpose of stimuli-responsive delivery and therapy, as well as a new concept to use CLPs as drug carriers for multifunctional delivery (including

enhanced, selective and on-demand delivery). The fully characterized stimuli-responsive properties of C8 and the information on molecular mechanism of membrane selectivity of CLPs would be helpful to develop CLPs or CLP-mediated drug delivery systems with desired stimuli-responsive properties and improved tumor specificity.

1.2 Objectives

The goals of this research project involve three aspects: 1) investigating the potential of incorporating CLPs with stimuli-responsive properties on both nanostructure and lytic activity; 2) investigating the potential of CLP-mediated drug delivery systems for multifunctional delivery; and 3) investigating the molecular mechanism of CLP membrane activity. The specific objectives of the research project are listed below:

a. Study of molecular mechanism by which CLPs interact with membrane of membrane selectivity of CLPs; the knowledge will aid the design of CLPs to improve the cancer specificity of CLPs or CLP-based drug delivery systems.
b. Characterization of the stimuli-responsive self-assembling properties of C8 in response to changes in pH, temperature and the presence of urea; these properties provide essential information to design CLPs with desired stimuli-responsiveness.
c. Investigation of the nanostructure-dependent cytotoxicity of C8
d. Investigation on the potential of CLP-mediated drug delivery system for multifunctional (enhanced, selective, on-demand) delivery.

1.3 Outline of the thesis

This thesis consists of seven chapters. The scope of each chapter is listed as follows:

Chapter 1 gives an overview of the thesis. It includes a brief introduction to problems in conventional chemotherapy for cancer treatment, CLPs and the progress in their anticancer application, and the recent advances in the development of drug delivery systems. The objectives and the scope of the thesis are also given in this chapter.

Chapter 2 provides a review of current advances in the development of CLPs, stimuli-responsive drug delivery systems, and self-assembling peptide-mediated drug delivery systems.

Chapter 3 introduces an arginine-rich lytic peptide C6. The membrane lytic behavior of C6 is characterized with liposome vesicles and mammalian cells. Of particular interest is that inhibition of hydrogen bonding between C6 and phospholipid membranes reduces the leakage on cholesterol-rich membranes. This effect is also seen in cytotoxicity studies.

Chapter 4 reports the *in vivo* anticancer activity of C6 by intratumoral administration. The potential use of C6 as ellipticine carriers is also investigated. The C6-mediated drug delivery system shows selectivity towards cancerous cells, along with synergism between C6 and the delivered drug.

Chapter 5 introduces a novel stimuli-responsive cationic lytic peptide C8. The peptide is found to self-assemble into β-sheet rich nanofibers and disassemble into unstructured monomers in response to changes in pH. The nanostructure-controlled lytic activity of C8 is also demonstrated.

Chapter 6 investigates the enhanced, selective and on-demand delivery of ellipticine mediated by C8. The membrane selectivity of C8 is also discussed.

Chapter 7 presents the conclusions of studies of the thesis, contributions of this research project and recommendations for future work.

Chapter 2

Literature Review

2.1 Current advances in cationic lytic peptides as anticancer agents

As early as the first half of the 20th century, many polypeptides isolated from various sources, including bacteria, insects, invertebrates and vertebrates, have shown antimicrobial activities [77]. Although these naturally occurring antimicrobial peptides (AMPs) are highly heterogeneous in their amino acid sequences, they still share some features in common, such as amphiphilic nature and positive charges. These characteristics allow them to selectively bind to anionic phospholipids or other negatively charged components on the outer surface of bacterial membranes via electrostatic interaction, followed by insertion into membrane bilayers to form pores [6, 77]. Most AMPs possess a broad spectrum of antimicrobial activity against Gram-positive and Gram-negative bacteria, along with ability to combat antibiotic-resistance developed by bacteria, which make AMPs a promising class of antimicrobial agents [77-79].

In addition to antimicrobial activity, some cationic antimicrobial peptides were also shown to have anticancer activities. Sharing the same mode of action, AMPs disrupt the integrity of cell membranes and lyse cells via necrosis [80, 81], or induce apoptotic death by depolarizing mitochondrial membranes [23, 24, 81]. They can selectively kill cancerous cells [24, 82] and combat MDR generated by cancerous cells [25, 83]. Although naturally occurring AMPs have advantages of selective killing of cancerous cells and combating MDR when compared to conventional chemotherapeutics, they are still facing issues such as serum stability, hemolytic

activity and insufficient tumor specificity that cause failures in *in vivo* studies[6]. Synthetic cationic lytic peptides provide multiple alternatives to improve upon those deficiencies. The strategies involve introducing D-amino acids in peptide sequences, conjugating CLPs to targeting moieties or rendering CLPs nanostructures. The detailed cases are briefly reviewed in the following sections.

2.1.1 Naturally occurring AMPs for cancer treatment

In this section, studies on naturally occurring AMPs and their derivatives as anticancer agents are reviewed. The most studied AMPs are listed in Table 2.1.

Table 2.1 Naturally occurring AMPs with anticancer activities.

Peptide	Source	Amino acid sequence*
Cecropin A	Hyalophora cecropia (insect)	**K**W**K**LF**KK**IE**K**VGQNI**R**DGII**K**AGPAVAVVGQATQIA**K**
Cecropin B	Hyalophora cecropia (insect)	**K**W**K**VF**KK**IE**K**MG**R**NI**R**NGIV**K**AGPAIAVLGEA**K**AL
Melittin	Bee venom	GIGAVL**K**VLTTGLPALISWI**KRKR**QQ
Tachyplesin I	Horseshoe crab	**K**WCF**R**VCY**R**GICY**RR**C**R**
Magainins 2	Frog (amphibian)	GIG**K**FLHSA**KK**FG**K**AFVGEIMNS
Gaegurins 5	Frog (amphibian)	FLGALF**K**VAS**K**VLPSV**K**CAIT**KK**C
Bovine Lactoferricin	Mammalian lactoferrin	F**K**C**RR**WQW**R**M**KK**LGAPSITCV**RR**AF
LL-37	Human cathelicidin	LLGDFF**RK**S**K**E**K**IG**K**EF**KR**IVQ**R**I**K**DFL**R**NLVPRTES
BMAP-28	Bovine cathelicidin	GGL**R**SLG**RK**IL**R**AW**KK**YGPIIVPII**RI**

* bold letters indicates cationic amino acids

Cecropin A and cecropin B are the most studied antimicrobial peptides in the cecropin-family, which are isolated from insects. Both of the peptides possess a secondary structure of two α helices, of which the N-terminal helix is amphiphilic while the C-terminal helix is relatively

hydrophobic [84, 85]. Cecropin A and cecropin B were proven to be effective at lysing different human cancer cells, while they were not harmful to normal tissue cells at the same concentrations [83, 86, 87]. Moreover, a synergistic effect was found when combining treatments of cecropin A with the chemotherapeutic agents 5-fluorouracil and cytarabine on CCRF-SB leukemia cells [87]. Srisailam *et al.* compared the lytic activities of two cecropin B analogues (cecropin B1 and cecropin B3) against several human leukemia cell lines [88]. The analogues were designed by multiple amino acid substitutions in the cecropin B sequence. Cecropin B3, which possesses two hydrophobic α-helices, was found to lose its pore-forming ability; in contrast, cecropin B1, consisting of two amphiphilic α-helices, lysed the cancer cells successfully with minor cytotoxicity against normal fibroblasts. These results may indicate the importance of an amphiphilic N-terminal α-helix in initiating the binding of cecropin B to anionic cancer cell membranes.

Melittin is an AMP extracted from European honeybee venom. Melittin has a hydrophobic N-terminal portion and a positively charged C-terminal portion. Studies have indicated that the melittin monomer was not effective towards destabilizing lipid bilayer membrane, while a melittin dimer perturbed the integrity of a 1,2-dioleoyl-sn-glycero-3-phosphocholine (DOPC) membrane successfully [89]. Membrane disruption caused by melittin is suggested to be the consequence of self-association of melittin monomers via the barrel-stave mechanism [90]. Interestingly, besides membrane destabilization, melittin could transiently activate phospholipase D, which may activate an uncharacterized signal transduction pathway enhancing cell lysis [91]. However, melittin was found to be cytotoxic to both cancerous and healthy cells [92-94]. Due to its lack of selectivity for malignant cells, research efforts have been focused on targeting melittin to tumor vasculature and/or cancerous cells via attachment to moieties that recognize over expressed surface structures on cancer cells. Holle *et al.* reported an attempt to utilize matrix metalloproteinase-2, which is over expressed by tumor vascular endothelium and cancer cells [95]. The strategy was based on the cleavage of a melittin-avidin conjugate by matrix

metalloproteinase-2 at the targeted sites, reactivating the lytic function of melittin [96]. The melittin-avidin conjugate proved to be cytotoxic against DU145 prostate cancer cells and SKOV3 ovarian cancer cells. Normal fibroblast cells, which possess less matrix metalloproteinase-2, were barely affected by the melittin-avidin conjugate. Russell *et al*. reported an alternative strategy by conjugating monoclonal antibodies with a melittin like peptide for tumor targeting [97]. An improved survival of mice bearing subcutaneous human prostate cancer xenografts was observed after being treated by this immunoconjugate.

Tachyplesin I is another well studied AMP, which is isolated from hemocytes of horeshoe crabs. Tachyplesin I contains two anti-parallel β-sheets with all six positively charged residues exposed on the peptide surface, resulting in an enhanced structural amphiphilicity [98]. There are two disulfide bonds that facilitate the stabilization of the peptide configuration. Moreover, the disulfide bonds are believed to protect tachyplesin I against proteolytic degradation [99]. Unlike other anticancer AMPs, tachyplesin I was found to kill TSU prostate cancer cells by binding to hyaluronan that over-expressed on the cell surface, followed by activating the classic complement pathway and inducing complement-mediated cell death to the cancer cells coated with tachyplesin I [100]. Since hyaluronan is also largely expressed on the endothelial cell surface involved in tumor neovascularization [101], tachyplesin I induced complement-mediated lysis might be utilized to inhibit tumor angiogenesis. Chen *et al*. synthesized RGD-tachyplesin I for targeting to integrins on the surface of endothelial cells and TSU prostate cancer cells [102]. The results indicated that the cell death was induced by destruction of the cell membranes and caspase-dependent apoptosis. The activation of the apoptotic pathway is probably due to the disruption of mitochondrial membranes by the positively charged RGD-tachyplesin I internalized by cancer cells. Although the *in vivo* study showed that RGD-tachyplesin I successfully inhibited the growth of B16 melanoma cells in mice [102], it was found to interact with neutral lipid at high concentrations, resulting in increased hemolytic activity [103]. Interestingly, a non-lytic killing mechanism was also observed in tachyplesin I treated SMMC-7721 hepatoma cells, involving

morphological alteration, decreased expression of the *c-myc* oncogene and tumor associated antigen, and increased expression of the tumor suppressor gene $p21^{WAP/CIP1}$ [104].

Magainins are a class of AMPs isolated from skin secretions of the African clawed frog [105]. Among them, magainin 2 shows selective cytotoxicity towards cancerous cells [26, 28, 106]. To improve the anticancer efficacy, analogues of magainins were developed by multiple amino acid substitutions. Magainin A and magainin G, which were designed to have enhanced α-helical structure, are more potent on hematopoietic and solid tumor cell lines, while show low or non-hemolytic effect at effective concentrations [26]. Moreover, they are also effective against drug-resistant tumor cell lines. MSI-136, another magainin analogue, and its all-D-amino acid counterpart, MSI-238, were found to be more potent than magainin 2 in *in vivo* study [28]. Gaegurins are also found in skin secretions of amphibians. They are random-coils in aqueous solution, but adopt amphiphilic α-helical conformations when in contact with membranes, inducing pore-formation via barrel-stave and/or carpet mode [14]. Among the gaegurins family, gaegurin 5, as well as its analogues, show broad and selective cytotoxicity towards various types of tumor cells [107].

Lactoferricin is a product of acid-pepsin hydrolysis of mammalian lactoferrin that possess anti-microbial properties [108]. Bovine lactoferricin (LfcinB) isolated from cow's milk is reported to have higher anti-bacterial potency than human lactoferricin [109]. LfcinB is suggested to form a distorted β-sheet conformation placing the positively charged amino acid residues on one face and most hydrophobic amino acid residues on the other [110]. LfcinB was proven to be cytotoxic against various types of neoplastic cells originating from humans and mice through *in vitro* studies [24, 80, 111, 112], at concentrations that are not harmful to healthy cells, including untransformed lymphocytes, fibroblasts, endothelial cells and erythrocytes [24, 113]. The lactoferricin-mediated cancer cell killing involves both necrosis and apoptosis. Initially, LfcinB binds to the cell membranes and forms transmembrane pores, causing the loss of plasma membrane integrity. Subsequently, peptides enter the cytoplasmic compartment through the pores

and attach to negatively charged mitochondrial membranes, inducing a collapse of the mitochondrial membrane potential and activation of caspase-dependent apoptosis [80, 114]. LfcinB treated mouse fibrosarcoma cells and human neurboblastoma cells were mainly killed via necrosis due to membrane lysis, whereas leukemia and breast cancer cells exposed to LfcinB died via an apoptotic way involving the generation of reactive oxygen species, dissipation of mitochondrial membrane potential, and activation of caspase-3 and caspase-9 [24]. This is possibly because that the LfcinB-mediated membrane damage in the aforementioned case was repairable and the internalized LfcinB induced the apoptotic cell death. Although the presence of high concentrations of serum reduces the activity of LFcinB [115], LfcinB is effective in inhibiting tumor growth *in vivo* [80, 116]. A study has also shown that LfcinB exhibited a structure induced antiangiogenic activity [117]. Nevertheless, the exact contributions of the lytic and antiangiogenic effect of LfcinB to the suppression of tumor growth still require investigation.

Among the cathelicidin-related antimicrobial peptides, LL-37 is the only one derived from human sources. It is reported that LL-37 is unstructured in pure water, while its helical structure can be stabilized either by increasing the peptide concentration or by adding salts [10]. The formation of the helical oligomer is believed to help LL-37 escape enzymatic proteolysis [82]. Although LL-37 successfully shows antitumor activities against a gastric cancer xenograft [118], the fact that LL-37 exhibits a significant hemolytic effect [82] and lacks the ability to specifically target to cancer cells [119] limits its development as a therapeutic drug. Interestingly, a recent study shows that LL-37 was strongly expressed in malignant melanoma and, instead of inhibiting the growth of melanoma cells, promoted melanoma cell proliferation and migration [120].

There is another class of AMPs that are derived from bovine cathelicidin. Typically, these peptides consist of a cationic N-terminal portion forming an amphiphilic α-helix and a hydrophobic C-terminal portion. BMAP-28 is a member of the cathelicidin-related AMPs. The anticancer activities of BMAP-28 have been demonstrated on various leukemia cell lines [121]. Cells exposed to the BMAP peptides went through a membrane permeabilization with an influx

of Ca^{2+}, followed by an apoptotic DNA fragmentation. A continuous study further revealed that BMAP-28 created a permeable transition pore in mitochondrial membranes of U937 and K562 human leukemia cell lines, resulting in a drop in mitochondrial membrane potential that lead to a cytochrome *c* release and apoptotic death [122]. BMAP-28 was not effective against non-proliferating lymphocytes [121], showing their inability to eliminate dormant cancerous cells. Along with their severe hemolytic activity at concentrations above 30 μM [123], the application of BMAP-28 was limited as an anticancer agent.

2.1.2 Synthetic CLPs for cancer treatment

The amphiphilic α-helical structure of CLPs is thought to play an important role in AMP-mediated transmembrane pore forming. Studies on the synthetic analogues of naturally occurring AMPs designed by amino acid substitutions revealed that enhanced amphiphilicity could promote the antimicrobial activity of AMPs as well as their cytotoxicity [124]. To better understand the structure-activity relationship, synthetic peptides have drawn considerable interest because the flexibility of sequence design allows different degrees of amphiphilicity and helicity. Some of the *de novo* designed lytic peptides have received much attention [125, 126]. One of the most popular synthetic peptides is $(KLAKLAK)_2$ comprised of 14 amino acids. The $(KLAKLAK)_2$ peptide exhibits selectivity between killing bacteria and killing eukaryotic cells [126].

Due to the fact that diastereomeric peptides are capable of resisting proteolytic degradation while maintaining their original lytic activities [127, 128], incorporating D-amino acids is widely applied in synthetic lytic peptides. A study showed that an amphiphilic peptide D-K_6L_9, modified from L-K_6L_9 (LKLLKKLLKKLLKLL-NH_2) by selectively substituting 5 L-amino acids with D-amino acids, exhibited specific *in vitro* cytotoxicity against prostate cancer cells with low hemolytic activity [27]. Interestingly, it was also found that L-K_6L_9 exhibited severe hemolytic activity, which may imply another advantage of D-amino acids as building blocks for synthetic

peptides. Surprisingly, the intratumoral treatment with D-K_6L_9 almost inhibited the growth of 22RV1 prostate cancer xenografts completely. In contrast, L-K_6L_9 lost its function in serum, barely showing antitumor activity. Subsequent studies conducted involved the systemic injection of D-K_6L_9 to 22RV1 xenograft-bearing mice, showing suppressed growth of tumors and possible vascular targeting and antiangiogenesis activity of D-K_6L_9 [81]. The study also demonstrated necrotic cell death, accompanied with depolarization of the cytoplasmic membrane induced by D-K_6L_9.

To further enhance tumor specificity of CLPs, targeting strategies have also been applied to enhance the selective cytotoxicity towards cancerous cells. Ellerby *et al.* coupled a homing domain (CNGRC or RGD-4C) with an all-D-form $(KLAKLAK)_2$ peptide aiming at facilitating the recognition by targeted cells and internalization of peptides [32]. The designed peptide showed selective cytotoxicity to angiogenic endothelial cells, such as tumor vasculature, and as a consequence inhibited tumor progression with no obvious side effects. In another approach, anti-CD19 and anti-CD33 antibodies were selected as targeting moieties to conjugate with D-$(KLAKLAK)_2$ [32]. The antibody-peptide conjugates showed high selectivity towards cells expressing suitable surface recognition structures. Anti-CD19 conjugated peptide was also found to be effective against fresh chronic lymphocytic leukemia cells from patients. Rapid internalization of $(KLAKLAK)_2$ was attempted by fusing the pro-apoptotic domain with a protein transduction domain, PTD-5 [129]. This peptide (DP-1) triggered rapid apoptosis in cell lines isolated from murine fibrosarcoma and human head and neck tumors. Furthermore, *in vivo* test of DP-1 by intratumoral injections showed effective inhibition of MCA205 tumor caused by DP-1, while no apparent side effects were observed. Zhong *et al.* adopted a membrane type 1-matrix metalloproteinase (MT1-MMP) sensitive linker to cyclize a CLP (LRLALKLALKALKAALKL), inducing spatial constrain on the formation of amphiphilic conformation [130]. The MDA-MB-435 cell line is known to overexpress MT1-MMP, while MCF-7 does not. The cyclized CLP showed higher cytotoxicity towards MDA-MB-435 than that towards MCF-7, showing the

possibility of targeting the tumor-associated enzyme. A recent study utilized negative charges on cancerous cell membranes to neutralize positive charges on CLPs, allowing CLP to adopt an active β-turn conformation [12]. The peptide showed selective killing of cancerous cells and low hemolytic effect.

Taking advantage of the high-aspect-ratio of nanostructures, Standley *et al.* incorporated $(KLAKLAK)_2$ peptide with a β-sheet promoting sequence and a hydrophobic alkyl tail to form nanofibers [131], for the purpose of overcoming poor cell penetration and fast *in vivo* degradation. This peptide, which is termed KLAK PA (peptide amphiphile), showed enhanced cellular uptake and cytotoxicity when compare to $(KLAKLAK)_2$ peptide. Subsequent *in vivo* study showed that KLAK PA successfully suppressed the growth of MDA-MB-231 human breast cancer orthotopic tumors in mice [34], which supports that the nanostructure formation could provide proteolytic resistance and elongate the circulation time. Agemy *et al.* conjugated all-D-form $(KLAKLAK)_2$ with a targeting sequence CGKRK, and coupled this peptide to iron oxide "nanoworms" (NW) to peptide ($CGKRK_D[KLAKLAK]_2$-NWs) for a targeted delivery [132]. Interestingly, after coupling to the NW, the system showed a significant cytotoxicity enhancement *in vitro*. Moreover, intravenously injected $CGKRK_D[KLAKLAK]_2$-NWs were found to accumulate in tumor vessels of glioblastoma-bearing mice and were able to eradicate most tumors. Lee *et al.* used a pH-responsive polysaccharidic ionic complex to deliver an all-D-form $(KLAKLAK)_2$ to an acidic tumor microenvironment [35]. This strategy also provides an alternative to reduce the side effect of CLPs.

2.1.3 Membrane selectivity of CLPs

In this section, the current progress on the studies of CLPs membrane activity and selectivity will be reviewed. The outer leaflet of bacteria membrane is rich in anionic phospholipids, such as phosphatidylglycerol (PG) and cardiolipin [133]; cancerous cells over

express phosphatidylserine (PS) and have elevated levels of aberrant O-glycosylated mucins on their membrane surfaces. These traits contribute to negative charges on cell membrane surfaces, which are considered to be the reason for the selectivity of CLPs towards bacteria or cancer cells via electrostatic interaction. The high amount of cholesterol presents in eukaryotic cell membranes increases the membrane cohesion and stiffness by condensing the phospholipid bilayers [134], which is thought to hinder the insertion of CLPs into membranes. A recent study evaluated the activities of melittin analogues, which were designed by multiple amino acid substitutions at 10 selected positions on melittin sequence, on membranes with various compositions [135]. Some of the melittin analogues showed better pore-forming ability on cholesterol-rich membranes or on negatively charged membranes, while there are cases showing no pronounced preference on negatively charged, cholesterol-rich or zwitterionic membranes [135]. These findings imply that there is still more to discover on the mechanism of CLP membrane selectivity.

In order to stabilize the pores on membranes, CLPs should be able to span the thickness of the membrane bilayers. Hence, the length of CLPs could be one factor that affects the pore-forming ability. Ringstad *et al.* investigated the membrane lytic activities of $(AKKARA)_n$ (n=1-4) and $(ARKAAKKA)_n$ (n=1-3) peptides [29]. These peptides existed as random coils in both buffer and the presence of phospholipid bilayers. Hence, the effect of changes in secondary structure can be excluded. The peptide-induced leakage was studied on either a zwitterionic membrane (DOPC/cholesterol) or an anionic membrane (DOPC/DOPA/cholesterol), showing that peptides with increased length induced enhanced leakage on both membranes; longer peptides also exhibited stronger antimicrobial activities. The author attributed increased membrane adsorption of long peptides to the enhanced activities. In the same work, the author also investigated the effect of electrostatic interaction. They reduced the peptide charge density by substituting arginine and lysine by histidine or added NaCl to screen the surface charges of peptide and phospholipid membranes. In both cases, the peptides showed decreased membrane lytic and

antimicrobial activities, indicating the importance of electrostatic interaction in membrane lytic activity of CLPs. However, too much peptide charge will limit the adsorption of CLPs due to electrostatic repulsion among peptides [136], and decreases antimicrobial activity [137]. Increasing the negative charges on membrane is another alternative to enhance electrostatic interaction between peptides and membranes, leading to increased peptide adsorption. However, negative charges may hinder the insertion of peptides by arresting them electrostatically close to the interface of the phospholipid bilayer [138]. Furthermore, there are studies that showed polyanionic glycosaminoglycans expressed on the cell surfaces or in biological fluids inhibited the lytic activities of CLPs [139, 140].

Ringstad *et al.* found that increasing the hydrophobicity of CLPs enhanced adsorption on phospholipid membranes as well as membrane lytic activity [30]. However, this enhancement accompanies a reduced membrane selectivity. Cornut *et al* reported that CLPs with high hydrophobicity to charge ratio showed strong lytic activity towards both bacteria and eukaryotic cells [141]. To increase the hydrophobicity of CLPs, attachment of a hydrophobic block made of hydrophobic amino acids can be used. For example, GKH17 (GKHKNKGKKNGKHNGWK) showed an increased lytic activity on anionic cholesterol-free (DOPE/DOPG) membranes after being end-tagged with one, three and five tryptophan residues (GKH17-W, GKH17-WWW and GKH17-WWWWW) [31]. However, as cholesterol condenses phospholipid membranes, it is energy costly for the bulky tryptophan-tags to insert into the compact cholesterol-rich membranes; as a consequence, GKH17 with an end-tag of five tryptophan residues induced less leakage on DOPC/cholesterol membranes than on DOPC membranes [31].

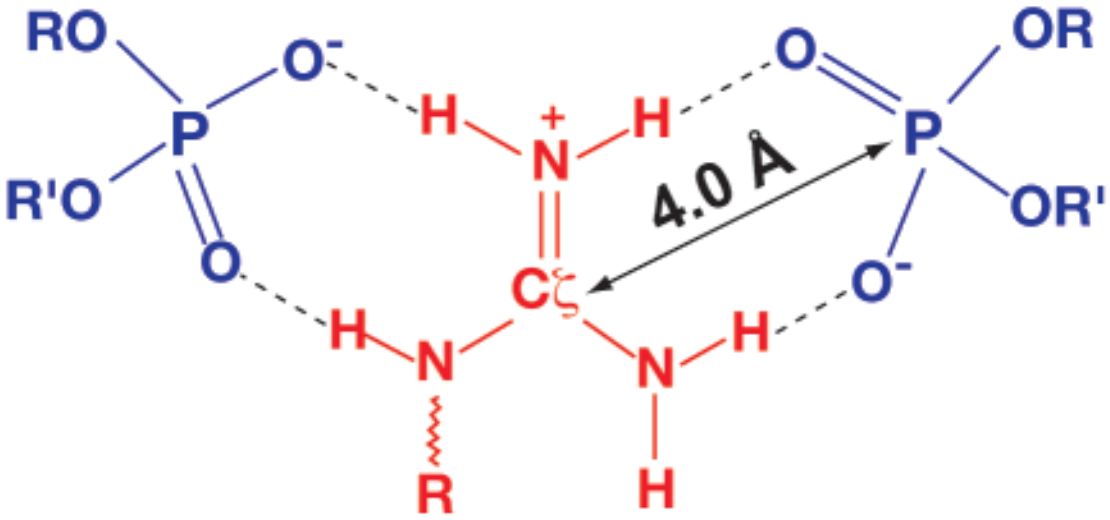

Figure 2.1 Guandinium-phosphate complex stabilized by bidentate hydrogen bonds and electrostatic interaction. Reprinted with permission from reference [11] © 2014 ACS.

It was also found that the guanidinium group of arginine can complex with the phosphate head groups of phospholipids via both electrostatic interaction and bidenate hydrogen bonds (Figure 2.1) [11]. The bonded polar groups form lipophilic ion-pairs, and hence, facilitate the entry of arginine residuals into non-polar lipid membrane cores [142, 143]. As a consequence, arginine-rich CLPs are more efficient in penetrating cell membranes than corresponding lysine-rich CLPs [142].

2.2 Current advances in anticancer drug delivery.

The "free" traditional hydrophobic anticancer drugs suffer from poor solubility, poor pharmacokinetics and adverse side effects, which cause most of the failures at clinical stage [144]. Since Richard Feynman raised the concept of nanodrug delivery devices in his talk "There's Plenty of Room at the Bottom" in 1959, a tremendous number of nanoscaled drug delivery systems have been developed to address these issues by improving the solubility, altering the pharmacokinetics (PK) and biodistribution of the delivered drugs [37]. Several of the

nanomedicines have already been approved by FDA. Table 2.2 summarizes the problems of free drugs and the improvements made by drug delivery systems. Figure 2.2 is a timeline of major events and discoveries during the development of nanomedicines.

Table 2.2 Non-ideal properties of drugs and their therapeutic implications. Adapted from reference [145].

Problem	Implication	Effect of drug delivery system (DDS)
Poor solubility	A convenient pharmaceutical format is difficult to achieve, as hydrophobic drugs may precipitate in aqueous media. Toxicities are associated with the use of excipients such as Cremphor® EL (the solubilizer for paclitaxel in Taxol).	DDS such as lipid micelles or liposomes provide both hydrophilic and hydrophobic environments, enhancing drug solubility.
Tissue damage on extravasation	Inadvertent extravasation of cytotoxic drugs leads to tissue damage, e.g., tissue necrosis with free doxorubicin.	Regulated drug release from the DDS can reduce or eliminate tissue damage on accidental extravasation.
Rapid breakdown of the drug *in vivo*	Loss of activity of the drug follows administration, e.g., loss of activity of Camptothecins at physiological pH.	DDS protects the drug from premature degradation and functions as a sustained release system. Lower doses of drug are required.
Unfavorable pharmacokinetics	Drug is cleared too rapidly by the kidney. For example, requiring high doses or continuous infusion.	DDS can substantially alter the PK of the drug and reduce clearance. Rapid renal clearance of small molecules is avoided.
Poor biodistribution	Drugs that have widespread distribution in the body can affect normal tissues, resulting in dose limiting side effects, such as the cardiac toxicity of doxorubicin.	The particulate nature of DDS lowers the volume of distribution and helps to reduce side effects in sensitive, Non-target tissues.
Lack of selectivity for target tissues	Distribution of the drug to normal tissues leads to side effects that restrict the amount of drug that can be administered. Low concentrations of drugs in target tissues will result in suboptimal therapeutic effects.	DDS can increase drug concentrations in diseased tissues such as tumors by the EPR effect. Ligand-mediated targeting of the DDS can further improve drug specificity.

The size and surface properties of the therapeutic nanoparticles play a key role in their pharmacodynamic behavior, biodistribution and cell internalization. Nanoparticles in the size range of 10-100 nm can avoid rapid clearance by the kidneys or through extravasation [146], while they are still small enough to accumulate in tumor tissue via enhanced permeability and retention effect [37]. The surfaces of nanoparticles need charges (negative or positive) to prevent self-aggregation. Yet the charges should be low enough to inhibit the non-specific interactions between the nanoparticles and proteins *in vivo*, and avoid the macrophage scavenging [39]. Coating the nanoparticles with hydrophilic polymers, such as polyethylene gloycol (PEG), also minimizes the non-specific interactions via steric stabilization, resulting in elongated body circulation [147]. The adding of targeting ligands provides specific interactions between nanoparticles and cell surfaces via ligand-receptor recognition, enhancing cellular uptake of nanoparticles into cancer cells and accumulation in tumor [41].

Stimuli-responsive systems received tremendous attentions in recent research for drug delivery owing to their tailored release profiles with excellent spatial, temporal and dosage control [42]. Self-assembling peptides are also emerging as a promising class of biomaterials for drug delivery application due to bio-functionality, design flexibility and potential biocompatibility [71, 148]. In this section, I reviewed several recent stimuli-responsive or self-assembling peptide-mediated systems to indicate the current advance in the development of drug delivery systems.

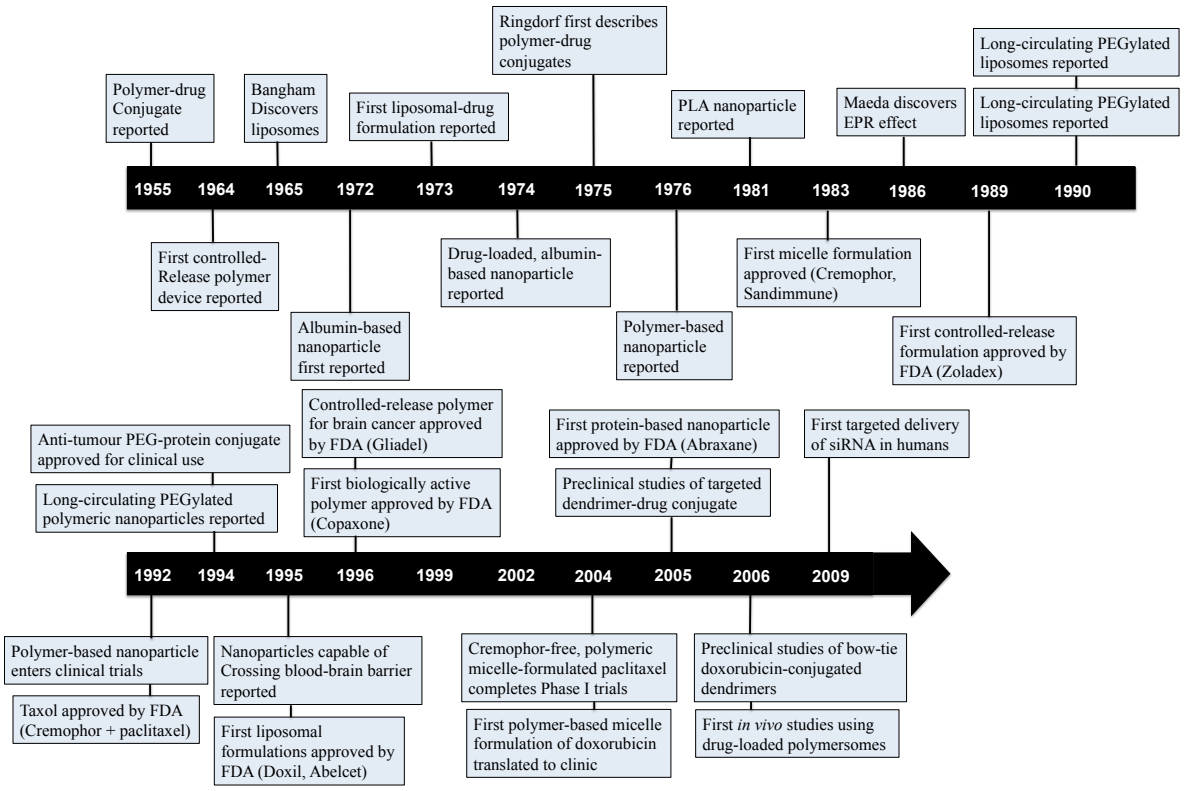

Figure 2.2 Timeline of the development of nanomedicines. Adapted with permission from reference [37] © 2014 NPG.

2.2.1 Stimuli-responsive systems

The concept of stimuli-responsive drug delivery was first suggested by Yatvin, M.B. in the late 1970s [149]. The stimuli-responsive delivery is an efficient delivery strategy, which in principle allows controlled release of drug at desired disease sites. In the past decade, owing to progress in material science, a great number of stimuli-responsive materials have been developed for anticancer drug delivery. These delicate systems can react to various stimuli, which are generally categorized into exogenous applied stimuli and endogenous stimuli.

Exogenous stimuli-responsive systems

Thermo-sensitive systems

The first stimuli-responsive drug carrier, a liposome-based thermo-sensitive system, was

introduced by Yatvin [149]. This system utilized liquid-crystalline transition of liposome at elevated temperature to trigger the release of encapsulated contents. Since then, several types of thermo-sensitive liposomes (TSLs) have been studied [150-152]. The TSL-based doxorubicin delivery system, ThermoDox (Celsion Corporation), has reached phase II trials for the treatment of breast cancer and colorectal liver metastasis, and phase III trials for the treatment of hepatocellular carcinoma [153], showing the potential of TSLs systems in clinical usage. For cancer treatment, ideal thermosensitive drug carriers should retain their cargo at body temperature (~37 ^{o}C), and release the loaded drug rapidly at a locally heated tumor site (~40-42 ^{o}C). Recently, Al-Ahmady *et al.* introduced leucine zipper peptide-lipid hybrid vesicles [57], which combine the advantages of traditional TSLs with the dissociative, unfolding properties of a temperature-sensitive peptide to optimize drug release at 42 ^{o}C (Figure 2.3.a). Chen *et al.* developed a promising bubble-generating liposomal system for rapid local drug release [154]. These liposomes encapsulated ammonium bicarbonate, which decomposed at mild hyperthermia (~42 ^{o}C), generating carbon dioxide bubbles. The carbon dioxide bubbles created permeable defects in the lipid bilayer, leading to the release of encapsulated drug (Figure 2.3.b).

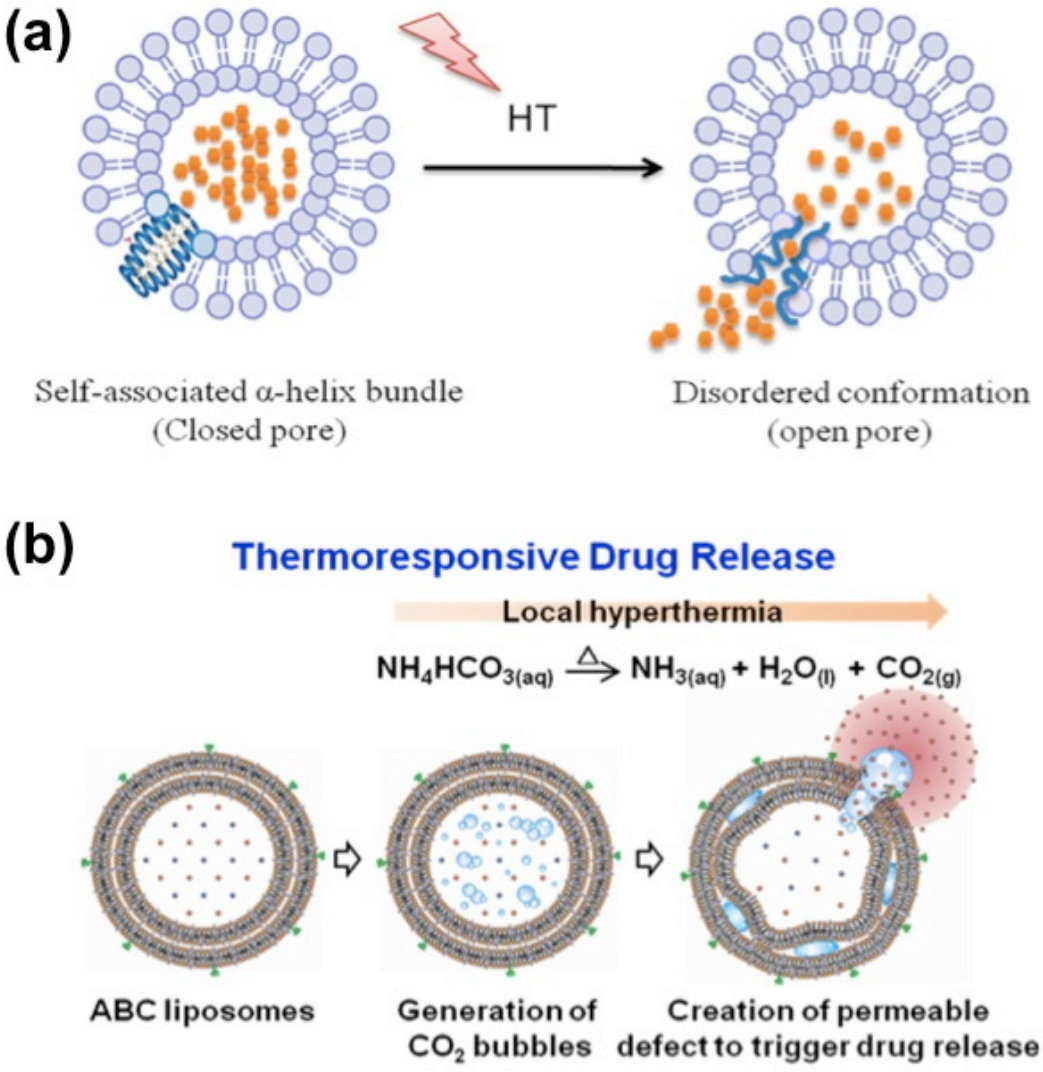

Figure 2.3 Schematic illustrations of the mechanisms for thermosensitive liposomal drug delivery systems. (a) The temperature-triggered unfolding of a leucine zipper peptide in the peptide-lipid hybrid systems. Reprinted with permission from reference [57] © 2014 ACS. (b) Drug-permeable pores created by the temperature-triggered generation of carbon dioxide bubbules. Reprinted with permission from reference [154] © 2014 ACS.

Light-sensitive systems

There are various strategies to induce light-trigged drug release. Azobenzene groups and their derivatives undergo a reversible isomerization on irradiation of ultraviolet or visible region. This property has been utilized to control the uncapping/capping of molecular pore gates of mesoporous silica nanoparticles (MSNPs), enabling photoregulated drug release (Figure 2.4.a)

[155, 156]. Furthermore, Tong *et al.* took advantage of the photoisomerization between Spiropyran (SP) and merocyanine (MC), inducing ultraviolet light-triggered size shrinkage in spiropyran-PEGylated lipid nanoparticles for better tissue penetration (Figure 2.4.c) [157]. Further *in vivo* studies confirmed the shrinkage enhanced tumor penetration [158]. Alternatively, He *et al.* used a photodimerization-cleavage cycle of thymine as a switch for MSNP opening and closing (Figure 2.4.b) [159]. Comparing to ultraviolet light sources, near-infrared (NIR) is more favorable to clinical applications owing to deeper tissue penetration, lower scattering properties and minimal harm to tissues. Recently, Carter *et al.* reported a liposomal system containing 10 mol% porphyrin–phospholipid for NIR-triggered drug release [53]. Systemic administration of the system showed enhanced deposition of loaded doxorubicin in response to NIR irradiation.

Ultrasound and magnetically responsive systems

Ultrasound can trigger the release of drugs from various types of nanocarriers by inducing thermal and/or mechanical effects and transiently increase cell membrane permeability, leading to enhanced cellular uptake [160]. Ultrasound triggered conversion from nanoemulsions into microbubbles is also a prevailing strategy for ultrasound-responsive systems. Rapoport *et al.* encapsulated paclitaxel (PTX)-loaded perfluoropentane (PFP) nanoemulsions using poly(ethylene oxide)-co-poly(L-lactide) (PEG-PLLA) micelles for ultrasound-trigger drug release [55]. Under therapeutic ultrasound, PFP microbubbles were generated through acoustic droplet vaporization, promoting release and/or cellular uptake of the encapsulated PTX in tumor tissue. Magnetic guidance also provides a means to improve drug accumulation in tumor tissues. Plassat *et al.* developed a PEG-coated liposomal system with superparamagnetic nanocrystals of maghemite (γ-Fe_2O_3) encapsulated for selective delivery of the steroid anti-estrogen RU 58668 [60]. The results showed that the magnetic force essentially accumulated the liposomes nearby the cancer cells, promoting cellular uptake and anti-estrogentic activity. Hua *et al.* also demonstrated a poly[aniline-co-N-(1-one-butyric acid) aniline] (SPAnH) coated magnetic system enhanced the

concentration and retention of the bound drug in tumor site [161].

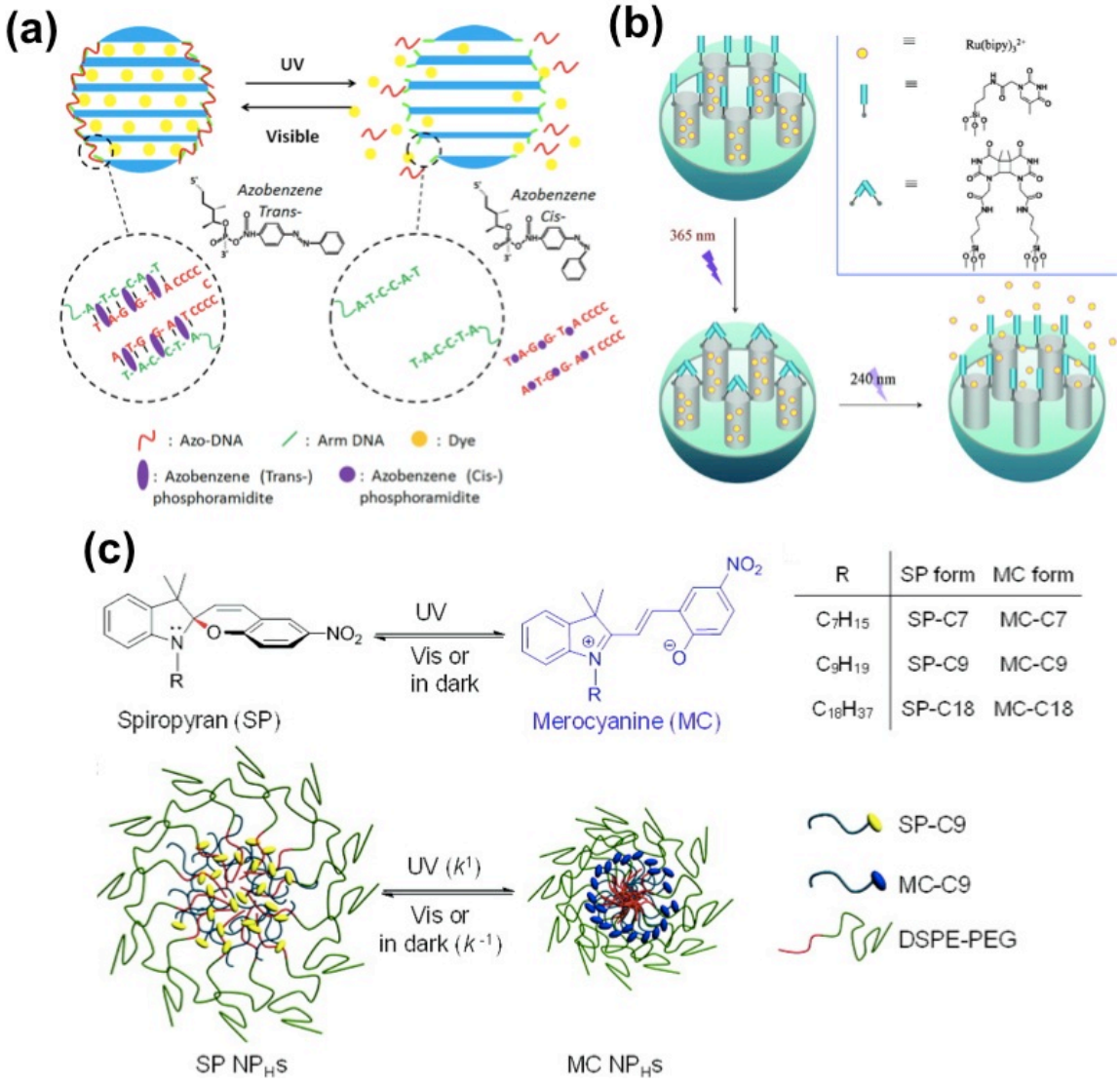

Figure 2.4 Schematic illustrations of the mechanisms for photosensitive drug delivery systems. (a) Azobezene-modified DNA-controlled reversible release system. Reprinted with permission from reference [155] © 2014 ACS. (b) Photosensitive thymine modified MSNPs. Reprinted with permission from reference [159] © 2014 ACS. (c) Photoswitching spiropyran-PEGylated lipid system. Reprinted with permission from reference [157] © 2014 ACS.

Endogenous stimuli-responsive systems

pH-sensitive systems

The irregular angiogenesis in fast-growing tumors causes abnormal metabolism, leading to a slightly acidic extracellular tumor pH (6.5-7.2) [162]. This trait is widely used by pH-sensitive drug delivery systems to target tumor microenvironments. The major strategies for constructing pH-sensitive systems involve the use of ionizable groups that undergo pH-responsive conformational and/or solubility changes, and the cleavage of pH-sensitive bonds. Min *et al.* introduecd a methyl ether poly(ethylene glycol)-block-poly(β-amino ester) (MPEG-PAE) micelle system for camptothecin (CPT) delivery [44]. The ionization of tertiary diamine moieties of MPEG-PAE caused a sudden disassembly at pH 6.4-6.8, releasing entrapped CPT. Cell penetrating moieties are commonly used to decorate the surface of nanocarriers for enhanced cell internalization. Koren *et al*. conjugated PEG chains via an acid-sensitive hydrazone bond to sheild TAT peptide (transactivating regulatory protein sequence) decorated liposomes [163]. The hydrolyzation of the bonds at lowered pH allowed exposure of the TAT sequence for improved cell internalization (Figure 2.5.a). Alternatively, Lee *et al.* ultilized the protonation of polyhistidine at acidic tumor extracellular pH to extend copolymer chain, facilitating exposure of terminal TAT sequences (Figure 2.5.b) [164]. An *et al.* developed a transmembrane peptide which either adsorbed to membrane or inserted into membrane in response to changes in pH [165]. They linked a hydrophobic toxin, phalloidin, with the peptide to facilitate the cell internalization in a pH-dependent manner.

Redox-sensitive systems

Disulphide bonds are sensitive to glutathione (GSH). Taking advantage of dramatic variation in intracellular and extracellular GSH concentrations [166], single disulphide bonds connecting two polymer blocks [167] or disulphide cross links [168] can be used to trigger the intracelluar release of drug. Matrix metalloproteinase 2 (MMP2) is known to be overexpressed in the tumour microenvironment [42]. Zhu *et al.* reported MMP2-sensitive systems using a synthetic peptide linker (GPLGIAGQ) to trigger the deshielding of long PEG chains, improving the exposure of

TAT peptide for enhanced cell internalization [48, 49].

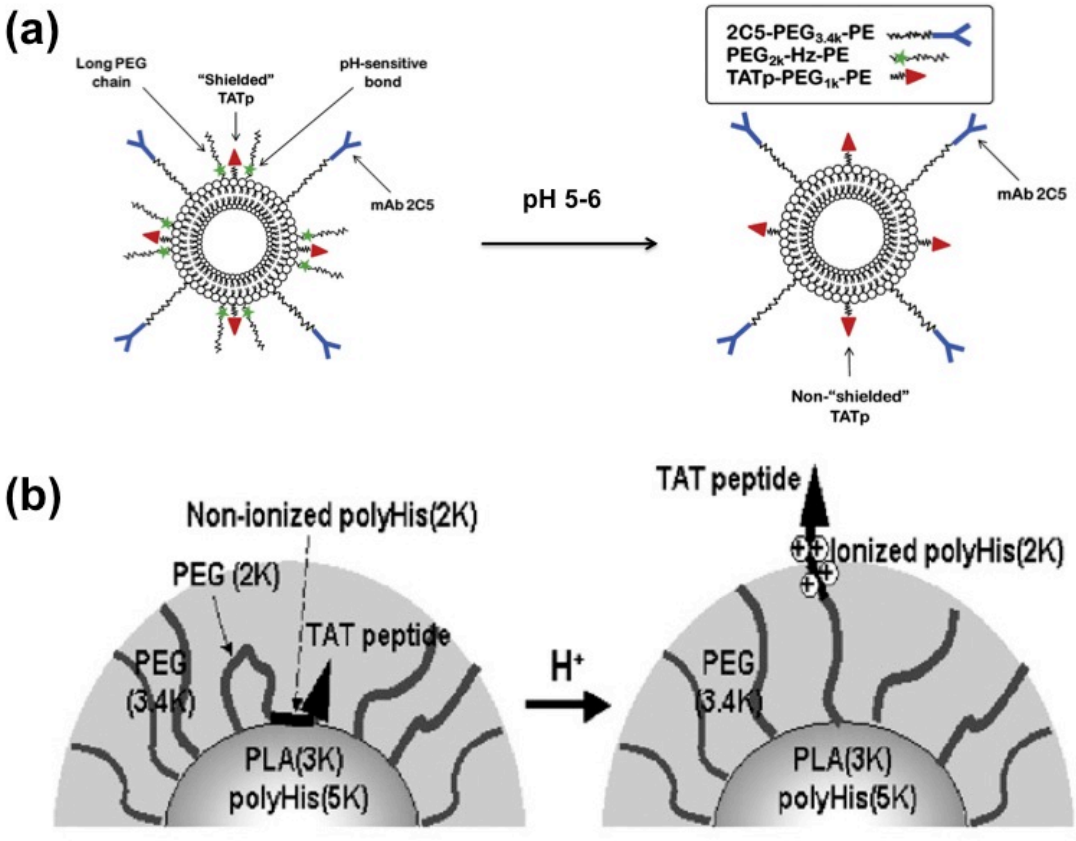

Figure 2.5 Schematic illustrations of the mechanisms for pH-triggered exposure of TAT peptide. (a) pH-degradable hydazone bond (Hz) allows the removal of the PEG_{2k}shield at low pH. Reprinted with permission from reference [163] © 2014 Elsevier. (b) Acid-induced pop-up of folded PEG chains. Reprinted with permission from reference [164] © 2014 Elsevier.

2.2.2 Multi-responsive systems

Drug delivery systems that respond to more than one stimulus have been developed to further improve the delivery efficiency. For example, a pH-sensitive polypeptidic micelle system with a redox-sensitive crosslinked interlayer disassemble in a reductant-rich environment, resulting in improved release and therapeutic efficacy of loaded doxorubicin *in vivo* [169]. Polymeric vesicle systems can undergo size changes in response to ultrasound and acidic-

stimulus, leading to fast drug release. A biodegradable polymeric nanocapsule system that shows triple-responsiveness to ultrasound, pH and GSH has also been reported [46].

2.2.3 Self-assembling peptide-mediated systems

Self-assembling peptides are emerging as promising nano-biomaterials in the field of drug delivery because of their favorable properties such as biocompatibility, less-immunogenicity and the ability to be biodegraded to non-toxic amino acids. The unique propensities of many peptides for cell penetration and bio-recognition [170, 171] also make them promising to overcome some major problems in drug delivery, such as delivery efficiency and targeting.

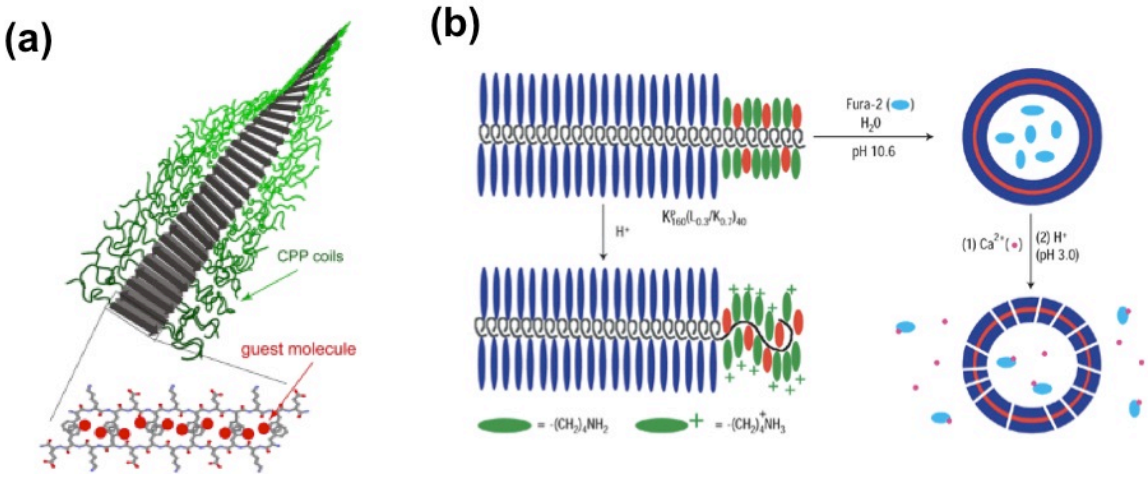

Figure 2.6 Schematic illustrations of (a) the nanoribbon formed by self-assembly of TβP and encapsulation of hydrophobic guest molecules. Reprinted with permission from reference [172] © 2014 Wiley. (b) Conformational change of $K^P_{160}(L_{0.3}/K_{0.7})_{40}$ coploypeptide, and release of entrapped Fura-2 dye from peptide vesicles. Reprinted with permission from reference [173] © 2014 NPG.

Lim *et al.* designed a TβP peptide consisting of three blocks: a TAT cell penetrating block (GRKKRRQRRRPPQ), a linker (GSGG), and a β-sheet forming block (FKFEFKFEFKFE) (Figure 2.6.a) [172]. The peptide could self-assemble into β-sheet nanoribbons, creating

hydrophobic interior to carry guest molecules. The exterior cell penetrating motifs facilitated internalization of the nanoribbons into cells and release of drug into the cytoplasm. Holowka *et al.* developed a group of K_xL_y diblock copolypeptides for vesicle formation [62]. Further modification on the leucine-rich block (substituting leucine with lysine) induced pH-responsive conformational change, leading to destablization of the vesiclar assembly and leakage (Figure 2.6.b) [173]. Another arginine-rich analogue showed the potential of intracellular delivery *in vitro* [174].

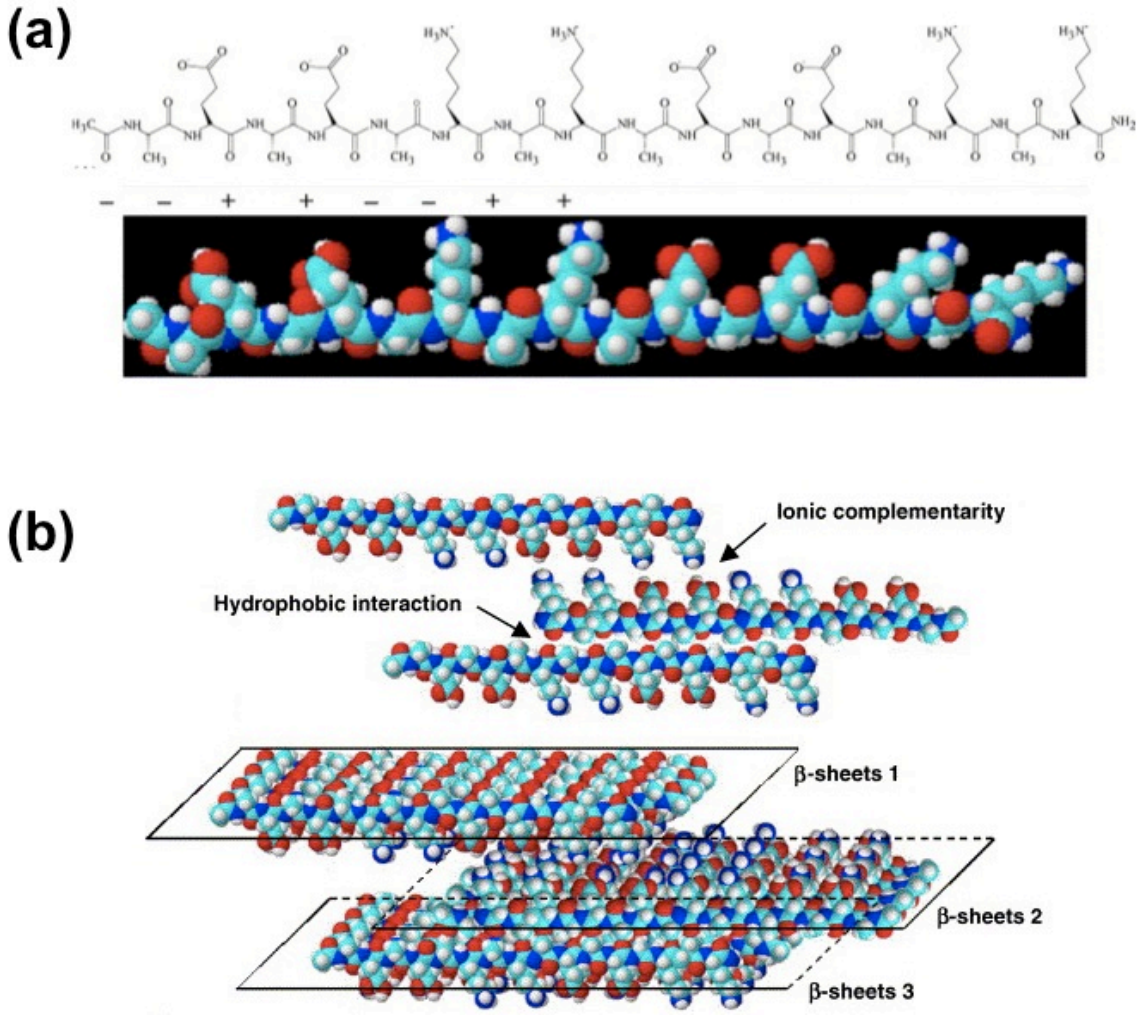

Figure 2.7 (a) Chemical structure of ionic-complementary peptide EAK16-II. (b) Schematic illustration of EAK 16-II self-assembly. Reprint with permission from reference [68] © 2014 Elsevier.

Ionic complementary peptides are a special class of self-assembling peptides. These peptides feature a unique amphiphilic structure consisting of alternating hydrophobic and hydrophilic amino acids in the sequence. The positive and negative charges are alternatively arranged, resulting in a complementary ionic structure. The first ionic complementary peptide, EAK16-II, was discovered from a yeast Z-DNA binding protein by Zhang *et al*. [175]. EAK16-II (AEAEAKAKAEAEAKAK) is composed of 16 amino acids alternating pairs of negatively charged glutamic acids and positively charged lysine, separated by a hydrophobic alanine (Figure 2.7.a). It self-assembles into β-sheet rich nanofibers through hydrogphobic interaction, backbone hydrogen bonding and ionic-complementarity, exhibiting separated hydrophobic and hydrophilic faces (Figure 2.7.b) [68]. The amphiphilic nature and good biocompatibility with cultured mammalian cells [176] make EAK16-II a promising biomaterial to construct nanocarriers for hydrophobic drugs.

To investigate the potential use of EAK16-II as a hydrophobic drug carrier, pioneering work was done by Keyes-Baig *et al.* using pyrene as a model hydrophobic compound [70]. The EAK16-II peptide was found to stabilize crystalline pyrene in aqueous solution with high loading efficiency. Fung *et al.* found that EAK16-II could stabilize hydrophobic anticancer drug ellipticine at two molecular states (protonated or crystalline) depending on the combinations of EAK16-II and ellipticine (EPT) concentrations (Figure 2.8.a-b) [71]. The compositions of EAK16-II-ellipticine complexes were found to affect their anticancer efficacy *in vitro*. Subsequent studies used two EAK16-II analogues, EAK16-IV (AEAEAEAEAK-AKAKAK, changed charge distribution) and EFK16-II (FEFEFKFKFEFEFKFK, increased hydrophobicity), to study the effect of charge distribution and hydrophobicity on the complexation and *in vitro* delivery of ellipticine [69]. Similar as EAK16-II, EAK16-IV was found to stabilize protonated or crystalline ellipticine depending on the peptide concentration; on the other hand, EFK16-II could stabilize neutral ellipticine and ellipticine crystalline in aqueous solution. Cytotoxicity studies

showed that the charge distribution of the EAK peptide did not affect the anticancer efficacy of the complexes *in vitro*; in contrast, the increased hydrophobicity enhanced the stability of EFK16-II-ellipticine complexes upon dilution.

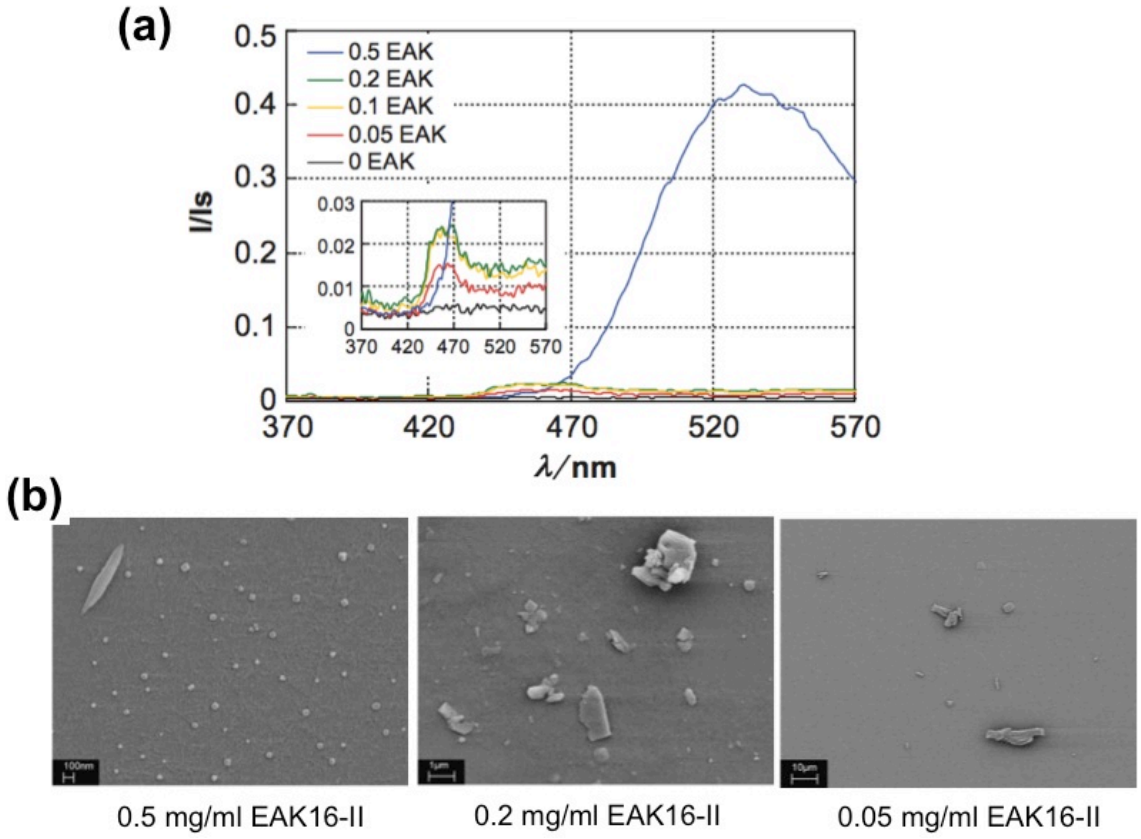

Figure 2.8 (a) The fluorescence spectra of EAK16-II-ellipticine complexes after 24 h stirring with 0.1 mg/ml ellipticine and various peptide concentrations. The fluorescence emission peak at ~520 nm indicates protonated ellipticine, and peak at ~468 nm indicates crystalline ellipticine. (b) SEM images of the EAK16-II-ellipticine complexes. Reprinted with permission from reference [71] © 2014 Wiley.

2.2.4 Amino acid pairing (AAP) principle

Amino acid pairing (AAP) is a systematic design principle for complementary self-assembling peptides, developed in Dr. Chen's research group [73]. The amino acid side chains of the 20 naturally existing amino acids provide major intermolecular interactions involving

electrostatic interaction, hydrogen bonding and hydrophobic interaction, driving the process of self-assembly. To form hydrogen bonding, a hydrogen donor and a hydrogen acceptor are required. Two amino acids that can form hydrogen bonding via their side chains are seen as a hydrogen pair (e.g., asparagine-serine pair). Two amino acids with oppositely charged side chains form an ionic pair (e.g., glutamic acid-lysine pair). The hydrophobic amino acid pairing utilizes non-polar side chains with similar structures (e.g. alkyl chains or aromatic structures) to facilitate self-assembly [73]. Table 2.3 lists the amino acids and their corresponding interactions provided by side chains at physiological condition. The AAP principle suggests alternatively arranged paired interactions for better matching and achieving certain stereo-chemical and physicochemical stability, and minimum free energy [73]. Table 2.4 lists examples of different AAP self-assembling peptide systems: HBPP peptide series are designed based on hydrogen bonding pairs; EAK16-II is ionic-complementary peptide; APP8 peptide contains all types of pairs.

Table 2.3 Properties of the side chains of natural amino acids at physiological condition. Adapted from reference [73].

	Amino acids
Hydrogen donor	S, T, C, N, H, Q, W, R, Y, K
Hydrogen acceptor	S, T, C, N, M, D, Q, W, R, E, H[a)], Y
Positively charged	H[b)], K, R
Negatively charged	D, E

[a)] uncharged H at pH>6; [b)] protonated H at pH<6.

The all-pairing self-assembling peptide (APP8) is a special amino acid pairing self-assembling peptide. This peptide consists of glutamine and asparagine to form hydrogen bonding

pair, glutamic acid and lysine to form ionic pair, and phenylalanine to provide hydrophobic interaction assisted by π-π stacking via aromatic rings to stabilize the self-assembled structure. The paired interactions facilitate an anti-parallel β-sheet formation as illustrated in Figure 2.9.c. Those β-sheets further self-assemble into fibrous structures in a concentration dependent manner. The critical aggregation concentration (CAC) of this peptide is ~10 μM. As shown in Figure 2.9.a-b, the peptide nanofibers form bundles beyond this concentration.

Table 2.4 Hydrogen bonding, ionic complementary and all pairing self-assembling peptides. Summarized from reference [73].

Peptides	Primary amino acid sequences	Secondary structures*	Self-assembly
HBPP-1	QN	r.c	Needle-like aggregates
HBPP-2	QNQN	r.c	Fibers
HBPP-3	QQNN	r.c	Amorpohous aggregates
HBPP-4	NS	n.a	Fibers
HBPP-5	NSNS	n.a	Fibers
HBPP-6	NNSS	n.a	Fibers
HBPP-7	NSNSNSNS	β-sheet	Fibers
EAK16-II	AEAEARARAEAEARAR	β-sheet	Fibers
APP8	FEFQFNFK	β-sheet	Fibers

*r.c: random coil; n.a: not available.

Besides providing paired interactions, the hydrophobic nature of phenylalanine provides hydrophobic region to encapsulate hydrophobic compounds. The charged amino acids and polar amino acids increase overall hydrophilicity of peptide. Further study has shown the potential of APP8 as EPT carrier [73]. The cytotoxicity of APP8-EPT complexes was tested on two cancer cell lines, A549 and MCF-7. The APP8-EPT complexes maintained good anticancer efficacy upon serial dilution in water (Figure 2.9.d).

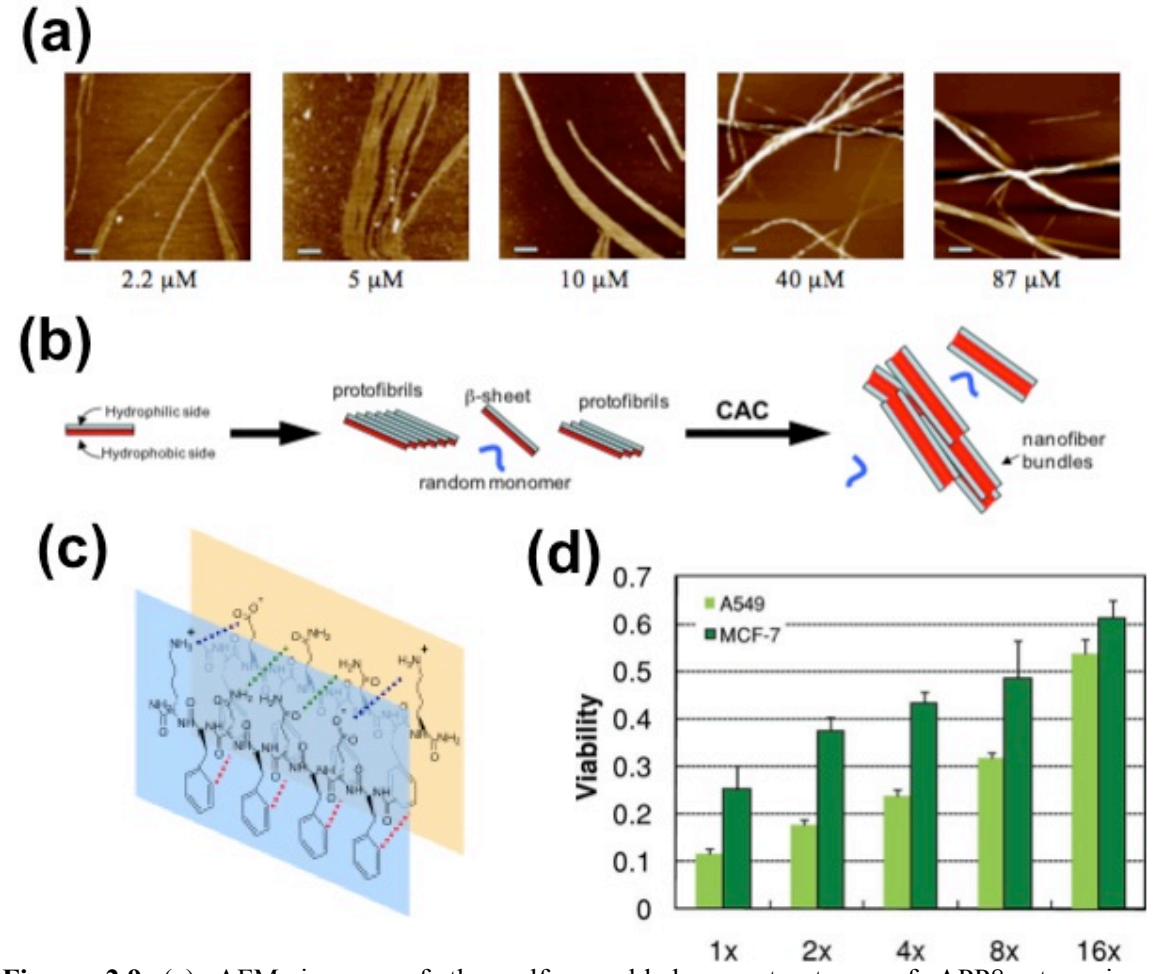

Figure 2.9 (a) AFM images of the self-assembled nanostructures of APP8 at various concentrations (2.2–87 μM). The scale bar is 250 nm. (b) A proposed self-assembly mechanism in relation to the CAC of APP8. (c) APP8 anti-parallel **β**-sheets that form with the assistance of paired interactions: hydrophobic amino acid pairing (involving **π-π** stacking), ionic pairing and hydrogen bonding pairing. (d) The cytotoxicity of the APP8-EPT complexes on serial dilutions. 1x refers to the complexes with 25 $\mu g/ml^{-1}$ (21.8 μM) APP8 and 10 $\mu g/mL^{-1}$ (40.6 μM) EPT in the final culture media. Reprinted with permission from reference [73] © 2014 Wiley.

Chapter 3*

Beyond Electrostatics: Tuning the Membrane Selectivity of a Cationic Lytic Peptide by Hydrogen Bonding

3.1 Introduction

Cationic lytic peptides (CLPs) have received increasing recognition as anti-tumor agents due to their activity against tumours [25, 27, 177] and their ability to avoid multidrug resistance (MDR) occurring in cancer cells [26, 80]. Although the mechanisms of action of CLPs are not completely understood, most CLPs are believed to lyse cells by permeabilizing their cell membrane [6, 178]. Several models have been proposed to describe the mode of membrane disruption including barrel-stave [15], toroidal pore [17], detergent-like mode of action [18], and molecular electroporation[179]. Many of the CLPs that demonstrate membrane activity are unstructured in aqueous solution. However, when they come into contact with the membrane, most of the CLPs will adopt an amphiphilic helical structure with a hydrophilic face and a hydrophobic face [9, 10, 126]. The hydrophilic face is largely cationic that allows the peptide to adsorb to the targeted membrane surface via electrostatic interactions and hydrogen bonding, while the hydrophobic face facilitates the insertion of peptide into the hydrophobic domain of the lipid bilayer.

* This chapter is based on a manuscript "S. Lu, T. Shen, M. Pourmousa, D. Zhao, P. Long, H. Fan, M. Karttunen, P. Chen, Beyond Electrostatics: Tuning the Membrane Selectivity of a Cationic Lytic Peptide by Hydrogen Bonding". T. Shen and H. Fan are collaborators from University of Toronto, M. Pourmousa and M. Karttunen are collaborators from University of Waterloo.
Author contribution: S.L. conceived the idea and designed experiments; T.S. performed liposome leakage studies; M.P. performed MD simulations; S.L. performed *in vitro* characterization experiments; S.L. and P.L. performed the cytotoxicity studies; D.Z. performed hemolysis studies; S.L., H.F., M.P. analyzed the data; S.L. and H.F. wrote the manuscript; P.C. and M.K. edited the manuscript.

CLPs are classically known to be antimicrobial agents due to their electrostatic interactions with negatively charged bacterial membranes [180]. However, it has been shown that when the amphiphilic CLP has a large fraction of hydrophobic residues, it becomes active against mammalian cells [181]. Unlike normal mammalian cell membranes which contain mostly zwitterionic lipids, cancer cell membranes typically contain elevated levels of negatively charged components such as phosphatidylserine (PS) [19, 182] and O-glycosylated mucins which are high molecular weight glycoproteins with negatively charged saccharides [21, 22]. The electrostatic attraction between CLPs and negatively charged cancer cell membranes is the standard explanation for the cancer specificity of CLPs, although the overall mechanism is not understood [6, 12, 27].

Cholesterol is an essential structural component of eukaryotic cell membranes and is abundant in the outer leaflet of red blood cell membranes [183, 184]. Cholesterol regulates membrane fluidity and permeability and thus interferes with the membrane disrupting efficacy of CLPs [185]. Previous studies in synthetic lipid systems have shown that the presence of cholesterol decreases the efficacy of CLPs [186-188]. However, interestingly, a recent study on high-throughput screening of melittin-like peptides showed that some variants of melittin have improved potency on cholesterol containing lipid vesicles [135]. This finding suggests that besides the preference of negatively charged phospholipids due to electrostatic interactions, cholesterol can also contribute to the membrane selectivity of CLPs although the reason for the improved efficacy against cholesterol-rich vesicles was not discussed.

We previously reported a study on peptide-siRNA co-assembly involving an arginine-rich peptide with a sequence of (n-RLLRLLLRLWRRLLRLLR-c) [189], or C6 in short. In the present work, we study the activity of C6 against artificial membranes with the well-established calcein leakage assay. Membrane leakage is evaluated by time-resolved fluorescence spectroscopy in an assay previously published by Patel et al. [190]. In contrast to the classic calcein leakage assay, the fluorescent lifetimes of the self-quenching dye can be determined from

time-resolved fluorescence decay profiles. The efflux value is determined from the relative contribution of lifetimes of the free dye and the entrapped dye inside vesicles to the overall decay curve, rather than from total fluorescence intensities. The time-resolved fluorescence assay offers information on how the peptide disrupts the membrane, which can be classified into two broad categories: all-or-none leakage or graded leakage [190]. All-or-none leakage typically involves the formation of stable pores or asymmetry-induced membrane ruptures, where the disruption in the membrane allows all of the contents of the vesicle to equilibrate with the bulk solution environment. Graded leakage typically involves transient disordering in the membrane that allows only a small amount of the vesicle contents to leak out at a time.

In the current study, we compared the performance of C6 in vesicles and in cells by examining its water-membrane partition coefficients in the two systems. Two cancer cell lines as well as red blood cells were tested in the *in vitro* assays. We also investigated the impact of cholesterol and arginine residues on the efficacy of the peptide against cholesterol-rich zwitterionic membranes.

3.2 Materials and methods

3.2.1 Materials

The peptide C6 (Mw 2470 g/mol, purity > 95%) was purchased from CanPeptide Inc. (Montreal, Canada), which followed solid phase peptide synthesis method on Rink amide MBHA resin (AAPPTec, Kentucky, USA) manually, with Fmoc (fluorenylmethyloxycarbonyl) chemistry. Briefly described: the deprotection of Fmoc (AAPPTec, Kentucky, USA) was accomplished by the treatment with 20% Piperidine (≥99.5%, Sigma Aldrich, Oakville, Canada) in DMF (N,N-dimethylformamide) (≥99.8%, Sigma Aldrich, Oakville, Canada), followed by coupling with activated carboxyl functional group of the next amino acid. During the synthesis, the coupling process was monitored with Kaiser Test. Before the synthesized peptides were

cleaved from resin with 95% TFA (trifluroacetic acid) (Sigma Aldrich, Oakville, Canada), the acetylation of N-terminal was carried out applying acetate anhydride (Sigma Aldrich, Oakville, Canada). The crude peptides were purified in Waters LC200 preparative system (Waters, Massachusettes, USA) equipped with Phenomenex Gemini C18 column (Phenomenex, California, USA).

Calcein, cholesterol, Tris(hydroxymethyl)aminomethane (Tris) hydrochloride, ethylenediaminetetraacetic acid (EDTA), Triton X-100, chloroform (≥99.5%) and methanol (≥99.8%) and MTT-based *In Vitro* Toxicology Assay Kit were obtained from Sigma Aldrich (Oakville, Canada); 1-palmitoyl-2-oleoyl-3-sn-glycero-phosphocholine (POPC) and 1,2-distearoyl-sn-glycero-3-phosphoethanolamine-N-[amino(poly-ethyleneglycol)-2000] (DSPE-PEG2000) were obtained from Avanti Polar Lipids (Alabaster, USA); phosphate colorimetric assay kit was purchased from BioVision (Milpitas, USA); A549 cells (non-small cell lung cancer) and MCF-7 cells (breast cancer) were obtained from ATCC (Manassas, USA); the culture media F-12 (Kaighn's modification) and MEM Eagles with Earle's Balanced Salts were obtained from HyClone Laboratories (Mississauga, Canada); fetal bovine serum (FBS) and trypsin-ETDA were obtained from Invitrogen (Burlington, Canada); phosphate buffer saline (PBS) and penicillin/streptomycin (10000 U) were obtained from MP Biomedicals (Montreal, Canada). Fresh rabbit ear venous blood (2-year old female New Zealand White rabbit, 4.5 kg) was obtained from Central Animal Facility (Waterloo, Canada).

3.2.2 Sample preparation

For the leakage assays, freshly made aqueous solutions of 600 mM C6 were diluted in either 10 mM Tris, 110 mM NaCl, and 0.5 mM EDTA at pH 7.4 (N buffer) or 10 mM Tris, 50 mM NaH_2PO_4, 60 mM NaCl and 0.5 mM EDTA at pH 7.4 (P buffer). For all other experiments C6 was directly dissolved in either N buffer or P buffer. Two membrane compositions were

investigated: POPC and POPC with ~20 mol% cholesterol. The lipid in chloroform was dried under nitrogen and then vacuum to form a film, which was hydrated in N buffer followed by eight freeze-and-thaw cycles. The resulting multi-lamellar vesicles were extruded at least fifteen times through 100 nm pore size filters (Waters, Ontario, Canada) to obtain large unilamellar vesicles (LUVs).

3.2.3 Circular dichroism spectroscopy

The secondary structures of the peptide in buffer alone and in the presence of POPC membranes were determined with a J-810 spectropolarimeter (Jasco Europe, Cremella, Italy). The spectra were recorded from 250 nm to 200 nm at 25°C. To determine the secondary structure of C6 in solution, 80 μM peptide in N buffer or P buffer was measured in a 1mm long quartz cell (Hellma, Concord, Canada) at various time points, respectively. For experiments with LUVs, 80 μM C6 was incubated with 2 mM POPC for 1 hour before spectra acquisition. The raw CD ellipticity (millidegrees) was presented. The spectra were averaged from three replicates.

3.2.4 Steady-state fluorescence

A Type QM4-SE Fluorometer (PTI, London, Canada) with a continuous xenon lamp source was used to monitor the intrinsic fluorescence of tryptophan in C6. Solutions of 10 μM C6 were incubated with POPC LUVs at concentrations ranging from 2.5 to 20 μM for 1 hour (in N buffer), then scanned at an excitation wavelength of 280 nm and emission wavelength range of 310 to 400 nm, with slit widths of 0.5 mm and 2 mm, respectively. Fluorescence spectrum of N buffer was used as blank.

3.2.5 Time-resolved fluorescence leakage assay

LUVs of POPC or POPC and ~20 mol% cholesterol were prepared by extrusion as previously described, except with a hydrating buffer consisting of 70 mM calcein, 10 mM Tris and 0.5 mM EDTA at pH 7.4. Calcein was then removed from outside the liposomes by exchanging the external buffer for N buffer (containing 135mM NaCl) on a PD-10 De-salting Column (GE healthcare, New Jersey, USA). The lipid concentration was then determined by a phosphate assay kit. The calcein-loaded vesicles (CLVs) were added to varying concentrations of C6 (in N buffer or P buffer) in polystyrene cuvettes (Fisher scientific, Ottawa, Canada). After 1 hour of incubation on a rotatory shaker, the samples were assayed in a Horiba JobinYvon FluoroLog 3 (Edison, NJ, USA) equipped with time-correlated single photon counting (TCSPC) for time-resolved fluorescence. The excitation source was a 467 nm, 1 MHz laser diode and emission was measured at 515 nm for 180 seconds. The resulting decay profiles were then saved with the instrument response function for further analysis as previously described [190]. The leakage profiles obtained from at least three independent experiments were then averaged to obtain the final results.

3.2.6 Estimation of cell surface

The images of A549 cells were obtained using an EVOS ® FL Cell Imaging System (AMG, Mill Creek, USA). The surface area of each single cell was estimated by counting the pixels that the cell occupied in the image. Matlab 2008 (MathWorks, Natick, USA) was used to analyze the images. The surface area of a single A549 cell was averaged from the surface area of 133 cells, which was calculated to be $2076 \pm 714\ \mu m^2$.

3.2.7 Partition coefficient estimated in cellular system

The peptide to lipid ratio for membrane-bound peptide in a cellular system can be calculated

by dividing the concentration of membrane-bound peptide ($C_{\text{membrane-bound peptide}}$) to number of cells ratio (obtained from the linear trend line equation shown in Figure3.2.d) by the concentration of lipids that one single cell can contribute (C_a). Considering the bilayer structure of cell membranes, a factor of 2 should multiply the average cell surface area. Hence, the concentration of lipids contributed by a single A549 cell can be estimated by the following equation,

$$C_a = \frac{2\times\ average\ cell\ surface\ area}{N_A \times lipid\ head\ area \times volume\ of\ culture\ media(200\ \mu l)} \quad \text{Eq. 3.1}$$

As 2076 μm^2 was adopted as the average cell surface area and 0.65 nm^2 was adopted as the lipid head area, C_a was calculated to be 5.3×10^{-5} μM. Since A549 cells split in around 22 hours, the number of A549 cells could double after 1 day of incubation. Hence, the lipid concentration contributed by A549 cells should also double, and the membrane-bound peptide to lipid ratio (R_e) for the cellular system can be calculated as

$$R_e = \frac{(C_{\text{membrane-bound peptide}})\ \text{to number of cells ratio}}{2 \times C_a} = 14.2 \quad \text{Eq. 3.2}$$

The aqueous concentration of free C6 was known to be 10.35 μM, so the partition coefficient was calculated to be $1.4 \times10^6\ M^{-1}$. This is a rough estimation due to factors, such as a) the presence of other components in the membrane and b) the vertical dimension of the cell membrane surface is not counted in microscopy images. Hence, the calculated number may still have an error in the range of 50%.

3.2.8 Determination of cholesterol level

The cholesterol levels of A549 cell line and MCF-7 cell line were quantified using an Amplex® Red Cholesterol Assay Kit (Invitrogen, Burlington, Canada). The cholesterol was extracted by mixing 200 μl culture media containing 5×10^6 A549 cells or MCF-7 cells with 400 μl chloroform-methanol (v/v 2:1) in1.5 ml microcentrifuge tubes. The tubes were vortexed and incubated for 1 day. Afterwards, the tubes were centrifuged for 10 min at 14000 rpm to separate

the aqueous phase and organic phase. The organic phase was transferred to a clean tube and dried under nitrogen (prepurified). The dried cholesterol/lipids mixture was then dissolved in 250 µl reaction buffer provided in the kit, following with 10 min sonication. The cholesterol/lipids buffer solution was mixed with the reagents following the protocol provided by the company. The kit reacted with cholesterol and produced fluorescent resorufin, which was excited at 560 nm. The fluorescence intensity at 587 nm was averaged from 584 to 590 nm. A 10 µg/ml cholesterol sample was adopted as reference to standardize the fluorescence intensities from each independent experiment. The relative cholesterol levels of cell lines were obtained by dividing the fluorescence intensities of samples by the fluorescence intensity of the cholesterol standard sample. The relative cholesterol level of the standard sample was set as 1.

3.2.9 Cell proliferation assay

The *in vitro* cytotoxicity of C6 was evaluated in both buffers using the MTT assay. A549 cells were cultured in F12K media containing 10% FBS and 1% penicillin/streptomycin. They were then seeded into 96-well plates at 5000 cells/well, 10000 cells/well and 20000 cells/well followed by a 24 hour incubation. MCF-7 cells were cultured in MEM media containing 10% FBS and 1% penicillin/streptomycin. They were seeded at 20000 cells/well and incubated for 24 h. The cells were then incubated with C6 for 1 hour before adding MTT. A detailed description of the MTT assay can be found in literature [71].

3.2.10 Hemolysis assay

The hemolysis assay was performed *in vitro* by using fresh rabbit ear venous blood. The venous blood was collected in K2EDTA anticoagulant tubes (BD medical, Mississauga, Canada), centrifuged at 1500 rpm for 15 min and washed three times with PBS buffer. After washing, the red blood cells (RBCs) were isolated and suspended in N buffer or P buffer to obtain a 5%

hematocrit solution. Varying concentrations of C6 were incubated with 1% RBCs at 37°C for 2 hours. RBCs mixed with 1% Triton X-100 and the corresponding buffer were used as positive and negative controls to obtain 100% and 0% hemolysis, respectively. The samples were centrifuged at 3000 rpm for 5 min and the supernatants were collected in a 96-well plate. The released hemoglobin was monitored at 540 nm using a FLUOstar microplate reader (BMG Labtech, Ortenberg, Germany). The percentages of hemolysis were then determined with the following equation:

$$Hemolysis\ \% = \frac{Abs(sample) - Abs(-)}{Abs(+) - Abs(-)} \times 100\%$$

where Abs(sample), Abs(+) and Abs(-) denote the absorbances of C6-treated, Triton-treated and buffer-treated RBCs, respectively. The animal studies followed the protocols approved by the University of Waterloo Office of Research Ethics and the Animal Care Committee.

3.3 Results

3.3.1 Physicochemical characterization of C6 and C6/POPC interactions

As reported in our previous study, C6 mainly adopted a random coil conformation in aqueous solution, in accordance with what is found for classic antimicrobial peptides [181, 189]. We then characterized the secondary structure of C6 in N buffer. The CD spectrum of C6 in N buffer (Figure 3.1.a) exhibited a minima at 208 and 222 nm which indicated that C6 took on an α-helical conformation in N buffer. The difference in peptide conformation in water versus in buffer may be due to the presence of salt which screens the positively charged arginine residues, resulting in reduced electrostatic repulsion between them thus stabilizing the helical structure. The kinetics of secondary structure formation in C6 was also studied (Figure 3.1.c), which suggested that the α-helical conformation of C6 was fairly stable in N buffer.

Most membrane-active cationic peptides fold into an amphiphilic structure when associated

with lipid membranes, which facilitates peptide insertion [79]. The general form of the CD spectrum of C6 was conserved when C6 was incubated with POPC vesicles, but the ratio of the ellipticity minima at 208 nm and 222 nm increased (Figure 3.1.a). The spectrum also became more negative between 208 nm and 222 nm, which may result from the formation of β-sheets/turns [191]. These changes suggested that C6 changed conformation upon associating with the membrane.

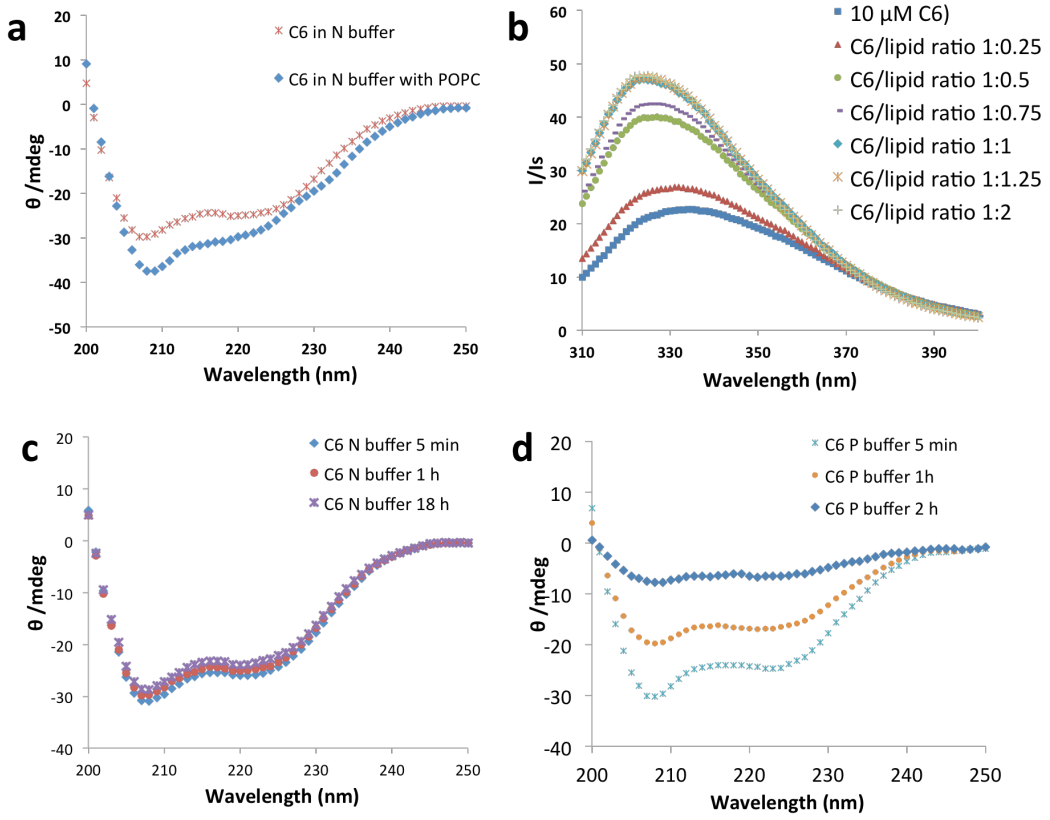

Figure 3.1 (a) CD spectra of 80 μM C6 in N buffer (110 mM NaCl, 10 mM Tris, 0.5 mM EDTA at pH 7.4) incubated for 1 hour with and without 2 mM POPC LUVs. (b) Fluorescence spectra of tryptophan at 10 μM C6 incubated with varying POPC concentrations up to 20 μM. CD spectra of 80 μM C6 in (c) N buffer solution (110 mM NaCl, 10 mM Tris, 0.5 mM EDTA at pH 7.4) or in (d) P buffer solution (50 mM NaH_2PO_4, 60 mM NaCl, 10 mM Tris and 0.5 mM EDTA at pH7.4) with different incubation times.

To further confirm the association between C6 and POPC membranes, the intrinsic

fluorescence of the single tryptophan residue located in the centre of the C6 sequence was monitored by incubating the peptide with varying concentrations of POPC vesicles. Hydrophobic interactions between the acyl chains of POPC and the tryptophan of C6 would be expected to cause blue shifts in the fluorescence spectra. This was indeed observed for peptide to lipid ratios of up to 4:1, as shown in Figure 3.1.b where the tryptophan emission peak shifted from ~335 to ~323 nm. The blue shift from above 330 nm to below 330 nm indicated a transfer of the tryptophan residue from a polar to an apolar environment as a result of the membrane association of C6 [192]. The blue shift was accompanied by approximately a two-fold increase in fluorescence intensity at the highest lipid concentration studied (1:2 peptide:lipid molar ratio). The fluorescence spectra showed no further changes above equi-molar ratios of C6 and POPC.

3.3.2 Time-resolved fluorescence leakage assay

Both CD and steady-state fluorescence spectra suggest that C6 binds or inserts into POPC membranes. To evaluate the extent of membrane permeabilization caused by C6, time-resolved fluorescence leakage assays were carried out with POPC LUVs in the presence of N buffer. The N buffer contained 135 mM NaCl instead of the 110 mM used in other experiments for it to be iso-osmotic with the buffer in the liposome interior. Calcein, a self-quenching fluorescent dye was loaded into the vesicles. Bi-exponential functions were fitted to the fluorescence decay traces with one component for entrapped calcein and the other for free calcein in bulk solution: well-entrapped calcein yields a lifetime τ_E of about 0.4 ns while greatly diluted calcein (< 5 μM) in bulk solution has a lifetime τ_F of 4 ns. Calcein efflux or leakage values resulting from C6 addition were then calculated based on the pre-exponential factors for the two different lifetime components [190].

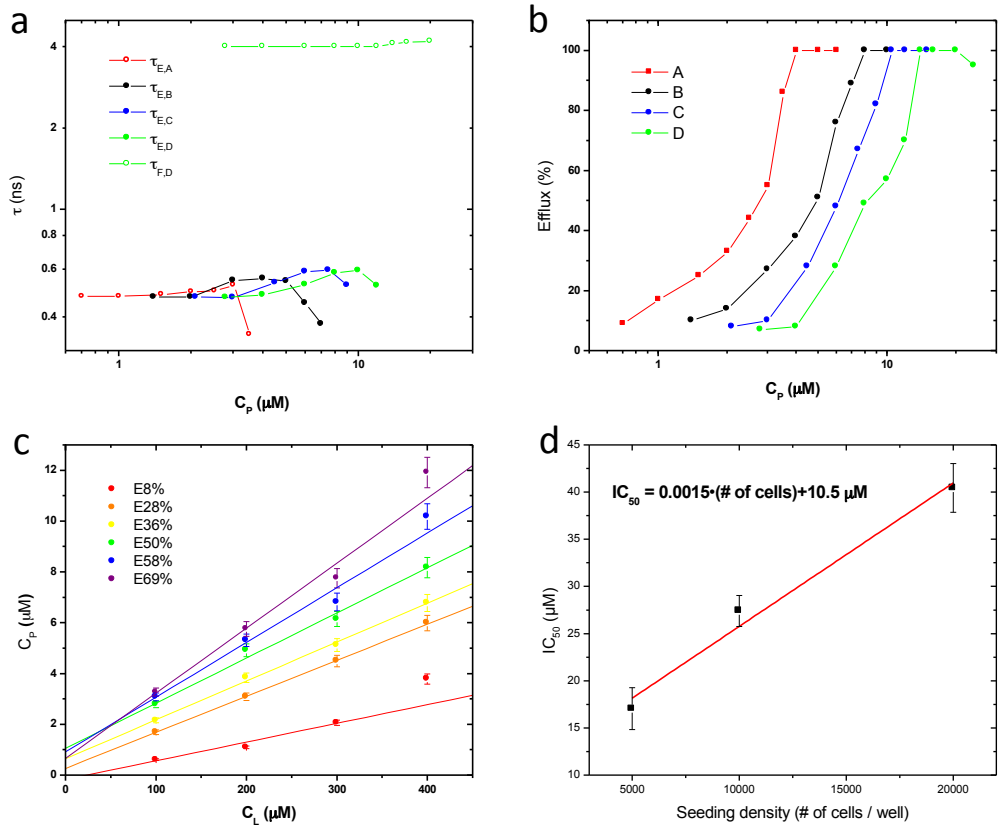

Figure 3.2 (a) Fluorescence lifetime τ vs. peptide concentration C_p. τ_E and τ_F are entrapped and free lifetimes respectively, and letters indicate sample series with lipid concentrations (C_L) of 100 μM (A), 200 μM (B), 300 μM (C) and 400 μM (D). (b) Efflux as a function of C_p for the four series, with errors of ±10% efflux. (c) Equi-activity analysis: The peptide concentration required to induce a particular leakage value at a specific C_L. The line of best fit for each efflux value yields parameters in equation (1). (d) IC_{50} of C6 against A549 cells as a function of seeding density in the cell proliferation assay. The IC_{50} value for each cell density was averaged from at least three independent experiments. Error bars represent standard deviations ($n \geq 3$).

The leakage assay with POPC consisted of four series of samples with increasing lipid concentrations (C_L): 100 μM, 200 μM, 300 μM and 400 μM. As shown in Figure 3.2.a, τ_E for all four series remains largely unchanged with increasing C6 concentrations. This indicates that a vesicle in the solution is either intact (0.4 ns lifetime), or have all of its calcein equilibrated with bulk solution (4 ns lifetime). Therefore the mechanism of C6-induced leakage is all-or-none, which is associated with membrane defects that last on the order of milliseconds, allowing all of the entrapped calcein to equilibrate. The calculated efflux values for the four series are plotted

against peptide concentration in Figure 3.2.b. The results show that for 100–400 μM POPC, C6 induces significant membrane disruption at low micromolar concentrations—a typical active range for CLPs. Also, more C6 is needed to induce the same leakage level at higher lipid concentrations, indicating that membrane permeabilization is unequivocally associated with C6-membrane interactions.

3.3.3 Partitioning behaviour in liposome and cellular systems

To further investigate the partitioning-dependent membrane activity of C6, peptide concentrations that cause specific efflux values were plotted against their corresponding lipid concentrations in an equi-activity analysis (Figure 3.2.c). To induce the same amount of leakage, the required concentration of C6 increases linearly with increasing lipid concentration as described by

$$C_p = R_e C_L + C_p^{aq} \qquad \text{Eq. 3.3}$$

where the slope R_e is the peptide to lipid ratio in the membrane and C_p^{aq} is the concentration of free peptide in aqueous solution. The R_e and C_p^{aq} for each arbitrarily chosen efflux value were obtained from linear fits and are summarized in Table 3.1. It was observed that with increasing efflux values, higher amounts of peptide were found in both aqueous solution and in the membrane environment, although the differences in aqueous concentrations were not statistically significant. Since the lifetime of the entrapped component of calcein remained largely unchanged at 0.4 ns in Figure 3.2.a as a result of all-or-none leakage caused by C6 in POPC vesicles, higher peptide concentrations were expected to cause more vesicles to sustain C6-induced defects that would result in complete calcein efflux. The increase in the fraction of empty vesicles translated to the increased efflux values observed. With R_e/C_p^{aq}, the partition coefficient K was calculated for each efflux value (see Table 3.1). The values remain largely unchanged within error, at about 20 mM^{-1}.

Currently, much of the research on the mechanisms of CLP-membrane interactions involves biophysical characterization techniques such as the leakage assay. Since therapeutic application is a major goal of the research into CLPs, it is important to compare the performance of CLPs in artificial systems with that in cells. However, direct comparison or extrapolation of behaviour is difficult to establish as liposomal systems are easily manipulated compared to *in vitro* assays, which involve complex experimental conditions that involve solvent environment, membrane composition, and potential competitive binding. Here we attempted to correlate the partition behaviour of C6 between the two systems. A549 cancer cells were assayed to evaluate the cytotoxicity of C6 at three different seeding densities: 5000, 10000, and 20000 cells/well. The calculated IC_{50} values are 18.1±0.6 μM, 27.4±1.7 μM, and 43.9±5.2 μM respectively. By plotting the IC_{50} values against the cell numbers as shown in Figure 3.2.d, we see that IC_{50} values increased proportionally to cell densities in agreement with results from the leakage assay. Extrapolating to a cell number of 0, the aqueous concentration of C6 was calculated to be 10.5 μM. Given that cells double in number over the initial culturing period, the membrane-bound peptide to cell number ratio was found to be 0.75 nM/cell.

Table 3.1 Partition coefficient K, R_e and C_p^{aq} obtained from the calcein leakage assay with C6 and POPC LUVs.

Leakage values	8%	28%	36%	50%	58%	69%
C_p^{aq}(μM)	0±0.06	0.26±0.14	0.64±0.16	1.05±0.21	0.91±0.24	0.66±0.26
R_e (10^{-3})	7.4±0.4	14.2±0.8	15.3±0.9	17.8±1.1	21.5±1.3	25.6±1.5
K (mM^{-1})	N/A	54±29	24±6	17±4	24±6	39±16

3.3.4 Activity of C6 against cholesterol-rich membranes

The membrane selectivity of CLPs is of interest from a therapeutic perspective: the electrostatic attraction between cationic amino acids and negatively charged membranes is cited as the primary cause for the selectivity of CLPs against cancerous cells [12, 27]. However, bacteria also have negative surface charges which usually render them more susceptible to CLPs. Another reason for the susceptibility is the absence of cholesterol in bacteria; cholesterol orders the lipid tails in eukaryotic cell membranes, thus rendering them more resistant to CLPs [6, 191]. The absence of anionic lipids in our model liposome system allowed us to examine the influence of cholesterol on CLP-membrane interactions. Therefore we investigated the leakage induced by C6 in cholesterol-rich POPC LUVs in N buffer. As shown in Figure 3.3, C6 was less active on membranes composed of POPC and about 20 mol% cholesterol compared with membranes of only POPC, but the shift was small and of significance at higher efflux values. The presence of cholesterol increased membrane rigidity, which detered increased partitioning of C6 into the membrane beyond the initial uptake.

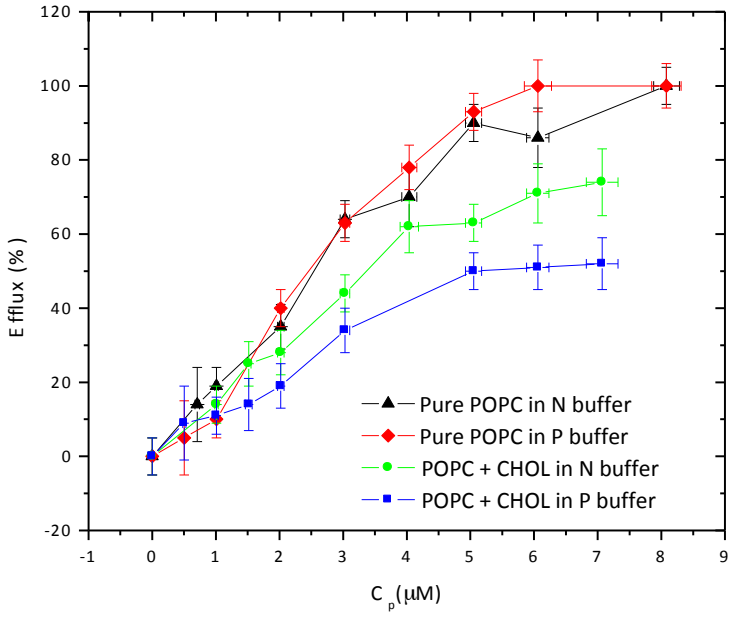

Figure 3.3 Efflux vs. C6 concentration profiles for POPC (100 μM) as well as for POPC and cholesterol liposomes in NaCl (N) and in phosphate (P) buffers. Vertical error bars are standard deviations obtained from at least three independent experiments. Horizontal error bars represent the instrumental error in the lipid concentration measurement.

3.3.5 Effect of phosphate ions on membrane activity of C6

With the demonstration of disruptive activity of C6 against both POPC and cholesterol-rich POPC membranes, it was of interest to understand the role of cholesterol in membrane permeabilization and the related interactions in the process.

Hydrogen bonding and electrostatic interaction are the two major forces believed to be involved in the initial contact between C6 peptides and exposed lipid head groups. Since the liposome leakage assay was performed at high ionic strength, the impact of electrostatics could be weak[29]. Moreover, molecular dynamics analysis performed by our collaborator found that the numbers of H-bonds between arginine residues and phosphate head groups of POPC were not uniformly distributed. As shown in Figure 3.4.a, arginine residues at position 1, 4, 11, 15 and 18 in C6 sequence were in the vicinity of cholesterol molecules, which was also evidenced by the

occurrence of H-bonds observed between those arginine residues and cholesterol molecules (Figure 3.4.b). These arginine residues formed more H-bonds with POPC molecules than the other arginine residues within the tested time of simulation (Figure 3.4.b). Taken together, it seems to suggest that the role of cholesterol involved providing higher chance for arginine to contact phosphate head groups, which could be due to the compact packing of POPC lipids around cholesterol. This observation might suggest that hydrogen bonding between C6 and membrane components plays a key role in the membrane activity of C6 on cholesterol-rich zwitterionic membranes.

To elucidate the role of hydrogen bonding in C6's effectiveness against cholesterol rich membranes, the calcein leakage assay was carried out in a buffer containing 50 mM NaH_2PO_4, 60 mM NaCl, 10 mM Tris and 0.5 mM EDTA at pH 7.4 (P buffer). The purpose of adding phosphates was to interfere with the hydrogen bonding between C6 and the membrane by occupying the "binding sites" on C6. As shown in Figure 3.3, the membrane disruptive activity of C6 decreased against cholesterol-rich membranes in P buffer when compared to that in N buffer. In the presence of POPC vesicles, the leakage profile of C6 showed no significant difference between N buffer and P buffer. In the case of cholesterol-rich POPC vesicles, higher order in the packing of lipid chains rendered the membrane less susceptible to peptide-induced membrane disorder and thus efflux was lower at a given peptide concentration. Comparing cholesterol-free and cholesterol-rich vesicles in N buffer, the profile was shifted to higher peptide concentrations for cholesterol-POPC vesicles (as shown Figure 3.3). The shift was small but not negligible. However, when comparing cholesterol-free and cholesterol-rich vesicles in P buffer, the difference was at least a two-fold increase in peptide concentration required to induce the same efflux from 50% upwards.

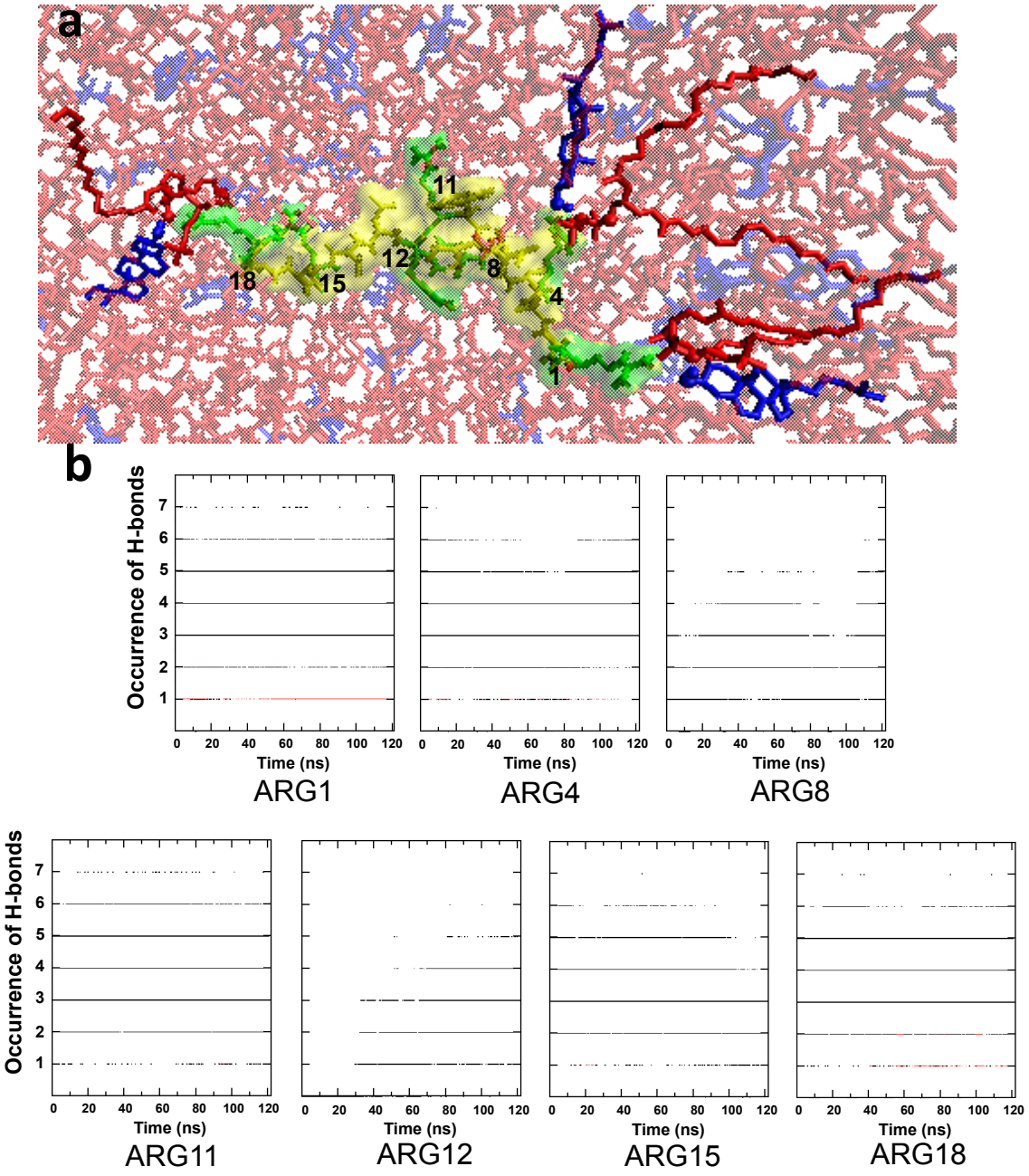

Figure 3.4 (a) A snapshot of simulation from above the membrane at 67 ns. The arginine residues in C6 peptide are shown in green with the rest residues shown in yellow, POPC molecules in red and cholesterol molecules in blue. The arginine residues are labeled with numbers to indicate the position of each arginine residue in C6 molecule. The N-terminus of C6 orients to right in the snapshot. (b) The occurrence of H-bonds between the guanidinium group of each arginine residue and POPC (black line) or CHOL (red line) molecules over time. The simulation shows that each guanidinium group can form a maximum of 7 H-bonds with neighbouring POPC molecules. All the arginine residues form H-bonds with neighbouring POPC molecules; while only arginine residues at position 1, 4, 11, 15 and 18 (refer to ARG1, ARG4, ARG11, ARG15, and ARG18)

form ~ 1 H-bond with neighbouring CHOL molecules, respectively. A neighbouring molecule is defined whenever POPC head groups or cholesterol hydroxyl groups are not farther than 0.35 nm of any atom of C6 peptide.

To investigate how the membrane selectivity of C6 in liposomes extrapolates to cells, we evaluated the cytotoxicity of C6 on two cancer cell lines, A549 and MCF-7. It was reported that MCF-7 cancer cells contained elevated levels of cholesterol-rich lipid rafts in their cell membranes [193]. We also confirmed that MCF-7 cells contain approximately two-fold higher cholesterol than that of A549 cells although the absolute mole-percentage could not be evaluated (Figure 3.5.a). As shown in Figure 3.5.b-c, C6 demonstrated comparable cytotoxicity against A549 cells and MCF-7 cells within error in N buffer, similar to leakage assay results where cholesterol only slightly inhibited C6 activity. Interestingly, the cytotoxicity of C6 against A549 cells increased significantly in P buffer compared to N buffer, but cytotoxicity against MCF-7 cells almost remained the same.

3.3.6 Hemolytic activity of C6

Clinical application of CLPs is expected to have many advantages over conventional chemotherapeutic agents, such as increased specificity and reduced hemolysis. The outer leaflet of red blood cell membranes contains zwitterionic phospholipids and cholesterol (~26%) [184]. According to our results, it would be possible to enhance the cytotoxicity of CLPs against cancer cells with lower cholesterol levels while limiting the hemolytic activity by inhibiting the hydrogen bonding between peptide and lipids. The hemolytic activities of C6 in both N and P buffers were tested using rabbit blood which showed similar hemolytic activity (Figure 3.5.c). Although there was no significant reduction in hemolytic activity with P buffer, the results still demonstrated potential in enhancing the specificity of CLPs towards cancerous cells by modulating their membrane selectivity.

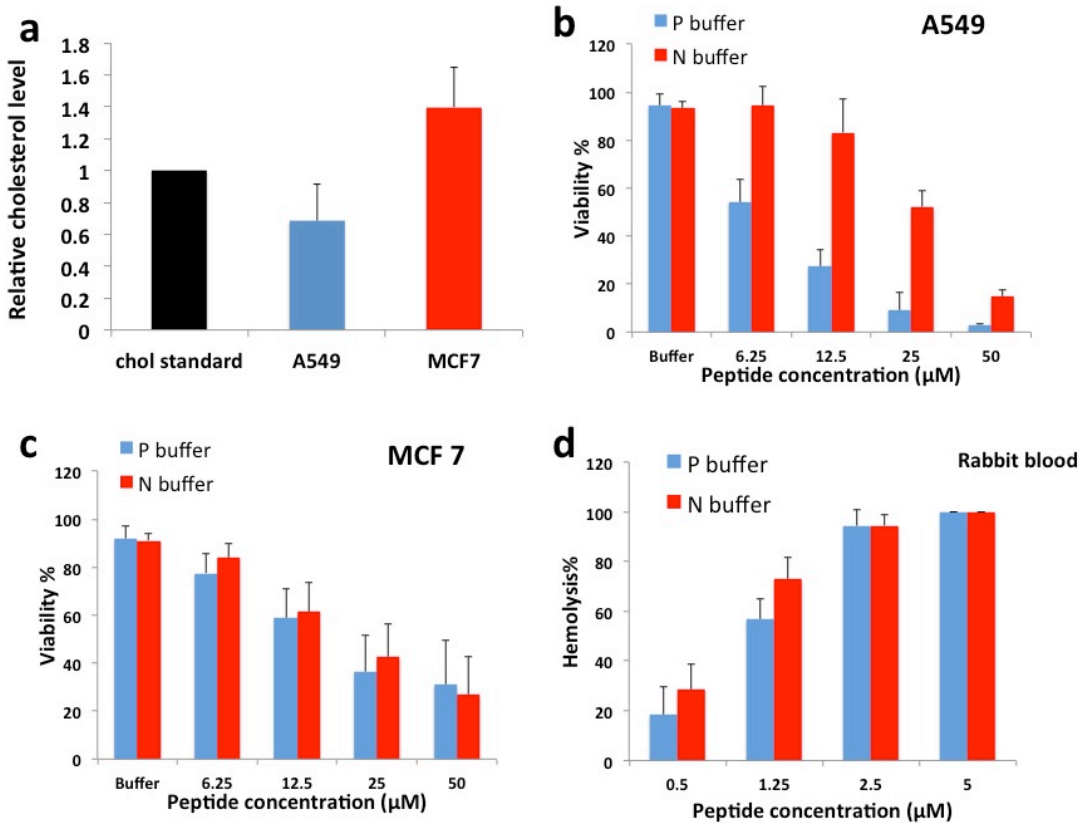

Figure 3.5 (a) Relative cholesterol levels of A549 cell line and MCF-7 cell line. *In vitro* cytotoxicity of C6 towards (b) A549 lung cancer cells, (c) MCF-7 breast cancer cells, and the hemolytic activity of C6 on (d) rabbit red blood cells. The results were averaged from at least three independent experiments. Error bars represent the standard deviation of multiple experiments.

3.4 Discussion

CD spectroscopy and steady state fluorescence results indicated that C6 interacted with the zwitterionic membrane but did not distinguish between association and insertion, although the secondary structure of the peptide changed from alpha-helical to more beta-sheet-like upon membrane-association. The mechanism of leakage as observed from the calcein leakage assay was all-or-none for both cholesterol-free and cholesterol-rich vesicles, which indicated that membrane permeabilization lasted long enough to equilibrate the vesicle contents with bulk

solution, likely on the order of milliseconds. If C6 did not initially have access to both leaflets, and translocated to the inner leaflet only after membrane permeabilization, then one would expect the partition coefficient to increase, as the inner leaflets of vesicles accommodated more peptide at higher efflux values. However, the partition coefficients in Table 3.2 did not increase with increasing peptide concentration within error, which suggested that that C6 penetrated the membrane and had access to both leaflets even at low peptide concentrations. Another possibility is that the inner leaflet of the bilayer did not influence partitioning behaviour. Given the large errors in the partition coefficient due to errors in extrapolated aqueous concentrations of the peptide, experimental limitations precluded a definite conclusion. The aforementioned results from various experiments indicated that C6 likely induced pore formation with a structure similar to the toroidal pore. However, the number of peptide molecules involved in the process is unknown.

In order to compare the leakage and *in vitro* assays, one could establish an empirical correlation between the activities of the peptide on model membranes and on cells, or an effective partition coefficient of C6 into cells based on results from the cell proliferation assays, or an effective C6 concentration per vesicle based on results from the leakage assays. Empirical correlations were unreliable and highly dependent on cell type, bilayer curvature (liposome/cell size), membrane composition and experimental details. The effective partition coefficient in cells and the effective C6 concentration per vesicle were estimated and discussed below.

To estimate an effective partition coefficient of C6 in cells, surface areas of cells were obtained by counting the pixels of cells occupied in microscopy images. The head group area of 0.65 nm^2 for POPC was divided from the surface area to roughly approximate the number of phospholipids on the cell surface [194]. The membrane-bound C6 to lipid ratio and the partition coefficient were then estimated to be about 14 and $1.4\times10^6\ M^{-1}$, respectively (see section 3.2.7 for details). The estimated effective partition coefficient was about five orders of magnitude greater than the values obtained from the leakage assay in Table 3.1.

To estimate the effective concentration of C6 per vesicle from leakage data, a surface area of 3.8×10^4 nm^2 was calculated for an average vesicle diameter of 110 nm, which corresponded to about $(1.17\pm 0.15)\times10^5$ lipids per vesicle. IC_{50} can be considered as akin to 50% leakage or efflux since the leakage mechanism for C6 was all-or-none. The C_{aq} value of 1.05 μM was a reasonable difference from the 11 μM aqueous concentration obtained from cell proliferation assays, given that higher aqueous concentrations were associated with higher peptide partitioning. However, R_e of 0.018 at 50% efflux corresponded to a C6 concentration of 3.5×10^{-21} M/vesicle or 3.3×10^{-12} nM/vesicle (± ~20% error); about eleven orders of magnitude less than the value obtained from the cell proliferation assays. If one takes into account that the surface area of a cell is much larger than that of a liposome (about 5 orders of magnitude higher), the difference in concentration of peptide per vesicle/cell between leakage and cell proliferation assays is reduced to about six orders of magnitude, which is similar to the difference obtained from the estimation of the effective partition coefficient in cells above.

A major factor that contributed to the great discrepancies in these effective partitioning estimates lay in the experimental setup: cells were seeded as sheets whereas leakage assays were done in solution. Therefore the interaction kinetics was different for the two experiments. Both estimation approaches indicated that cell membranes took up a greater amount of C6 at IC_{50} compared to the simple POPC liposome system at 50% efflux. Several considerations account for this observation: first and foremost, only having zwitterionic species in a model system neglected a major aspect of C6-cell interactions, as cancer cells have elevated levels of negatively charged components. As a consequence of the negative surface charge of cells, more C6 was able to bind to the cell membrane before electrostatic repulsion became prominent as compared with zwitterionic membranes. Also, the presence of proteins and other membrane components added complexity which interfered with C6 activity. Second, arginine-rich peptides have been proposed to disrupt the membrane by clustering anionic lipids [195]. Other groups have reported reduced activity of antimicrobial peptides in the absence of anionic lipids [180]. We did not observe the

effect of this added interaction in our leakage results with a POPC model system. Third, the overall C6 concentration required to disrupt the cell membrane was greater than that required for liposomes because of unspecific binding with other components in the culture media as well as repair mechanisms of the cell that counteract damages from C6. Overall, the efficacy of membrane-disruption of C6 can be expected to be much less in biological systems than in synthetic lipid systems.

In the membrane selectivity study, we intended to investigate the role of hydrogen bonding in C6 induced membrane leakage by inhibiting the hydrogen bonding between C6 and phospholipid membranes with phosphate ions. To find out whether there was any additional effect, other than hydrogen bonding with C6, induced by using P buffer, we also determined the secondary structures of C6 in P buffer with or without the presence of lipid vesicles. CD spectra showed that P buffer did not induce a conformational change of C6 (Figure 3.1.d). Furthermore, the conformation of membrane-associated C6 was similar in the two buffers (as shown Figure 3.7), which suggested that the process of membrane association remained the same. However, C6 was observed to be less stable in P buffer than in N buffer as the CD spectra show reduced signal intensity over the span of several hours with precipitation occurring within a day of dissolution (Figure 3.1.d). These observations indicated an enhanced hydrophobicity of C6 in P buffer. Hence, the changes in the membrane lytic activity of C6 in P buffer could mainly result from two factors: reduced hydrogen bonding opportunities between C6 and membranes, and enhanced hydrophobicity of C6. It has been reported that enhanced hydrophobicity of CLPs promotes their activity on both zwitterionic and cholesterol-rich membranes [92, 180]. Comparing the leakage profiles of C6 with POPC in the two buffers (Figure 3.3), the inhibited hydrogen bonding opportunities expected to cause a reduction in the activity of C6 in P buffer were likely compensated by the enhancement in the hydrophobicity of C6. On the other hand, the permeabilization of C6 was further inhibited in P buffer on cholesterol-rich membranes. This cannot be attributed to increased mechanical rigidity of the membrane alone, because the shift

caused by cholesterol inhibition of permeabilization in N buffer was less. The reduced hydrogen bonding opportunities between arginine, cholesterol and POPC as a result of C6's complexation with free phosphate ions was likely responsible for the enhanced inhibition.

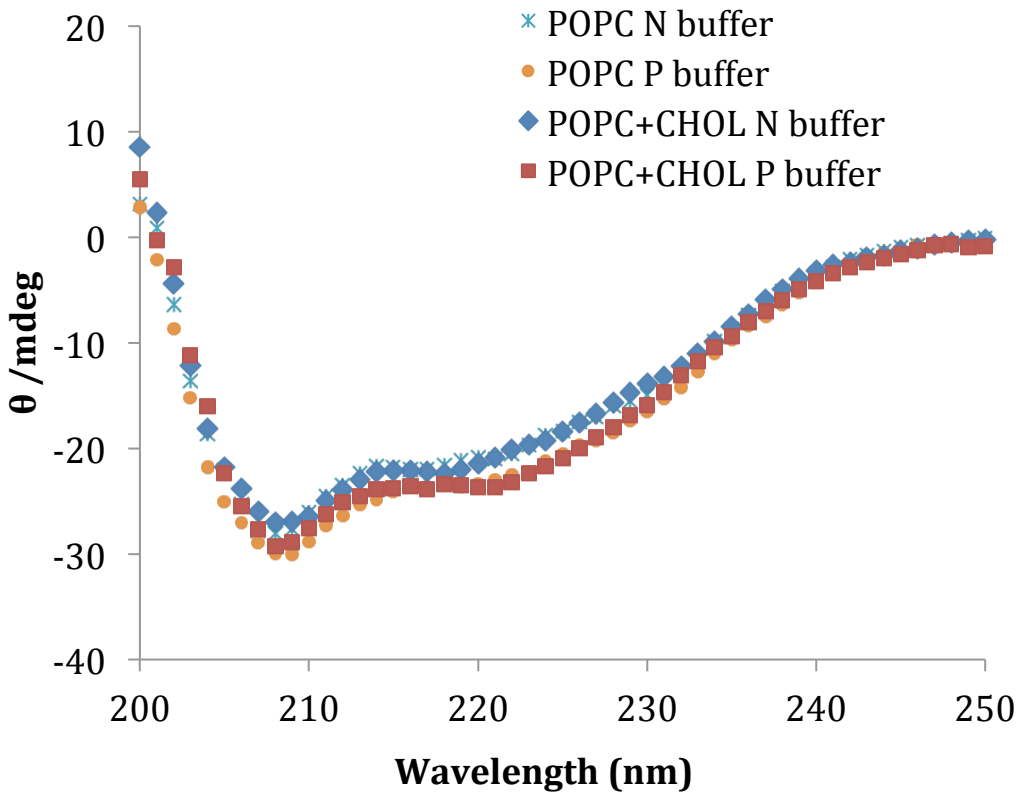

Figure 3.6 CD spectra of 80 μM C6 in N buffer solution (110 mM NaCl, 10 mM Tris, 0.5 mM EDTA at pH 7.4) or in P buffer solution (50 mM NaH_2PO_4, 60 mM NaCl, 10 mM Tris and 0.5 mM EDTA at pH7.4), with the presence of 2 mM POPC liposomes or 2 mM POPC/cholesterol (4:1) liposomes, after 1h incubation.

Although the cytotoxicity results were quite different from liposome leakage results, the same hydrogen bonding effect could still be seen: the enhanced activity of C6 against A549 cells could be attributed to the enhanced hydrophobicity of C6 in P buffer; however, the enhancement was compensated by phosphate induced inhibition of hydrogen bonding between C6 and MCF-7 membranes (higher cholesterol), resulting in the unchanged cytotoxicity against MCF-7 cells. We did not observe a significant enhancement in activity from increased peptide hydrophobicity in

leakage experiments—the inhibition of hydrogen bonding was likely more significant than increased hydrophobicity because it reduced peptide adsorption in the presence of phosphate which leaded to reduced leakage on cholesterol-rich membranes. However, the enhanced hydrophobicity seemed to be significant in cells, likely due to the complexity of their membrane composition and surface features, which could not be identified in this study. Except for zwitterionic lipids and cholesterol molecules, anionic lipids were another type of major cancerous cell membrane component that were related with the activity of CLPs via electrostatic interactions. However, the liposome leakage induced by C6 at high ionic strength suggested that electrostatics, in this particular case, was not playing a major role in the membrane adsorption/association of the peptide [29].

Arginine-rich peptides have been shown to cluster anionic lipids into domains [195]. The electrostatic interaction between C6 and anionic lipids was not the focus of the current study, although the CLPs that were previously investigated to cause much less damage to zwitterionic membranes compared to negatively charged membranes, as little leakage was observed. Since no anionic lipids were involved in our experiments, peptide-induced lipid clustering as a result of electrostatic attraction was largely eliminated. As CLPs were usually antimicrobial, we also assayed C6's activity on vesicles composed of *E. coli* polar lipid extracts (results not shown here). C6 caused the bacterial lipid extract vesicles to aggregate, which was likely due to the neutralization of the membrane surface charge by the peptide. The efflux values therefore could not be credited because decay profiles cannot be accurately measured for aggregated systems. The *E. coli* lipid extract was then supplemented with about 1 mol% PEG2000-DSPE to prevent vesicle aggregation. The leakage profile was greatly shifted to higher peptide concentrations, which seemed to be consistent with the insusceptibility of C6 to ionic strength. However, this lowered activity could either be a result of reduced permeabilizing efficacy against the bacterial membrane mimic, or reduced access of C6 to the membrane due to pegylated DSPE. Thus the effect of having a negative membrane charge could not be conclusively elucidated.

Similar to the case of MCF-7, the hemolytic activity of C6 against red blood cells maintained the same level due to the combined effects of inhibition of hydrogen bonding and enhanced hydrophobicity. As increased hydrophobicity of CLPs also promotes hemolysis [92], we could conclude that the activity of CLPs on cholesterol-rich membrane was related with their hemolytic activity. As we have shown that the hydrogen bonding had an important role in the efficacy of C6 against cholesterol-rich membranes, however, it may not solely due to simple "hydrogen bonding". It was suggested that the guanidinium group of arginine residue could form bidentate hydrogen bonds with the phosphate groups of POPC, which converted the bonded polar groups to lipophilic ion-pairs. This facilitated the entry of arginine residues into non-polar membrane cores once the peptide associated with the membrane [11, 196]. Furthermore, the ability of the guanidinium group to form multiple H-bonds could be the reason for the observation in Figure 3.4.b. In comparison, lysine may be less active against cholesterol-rich membranes as it is incapable of forming either bidentate H-bonds with phosphate or multiple H-bonds simultaneously. Consequently, lysine-rich CLPs are likely less hemolytic compared to arginine-rich CLPs. Here we summarized the hemolytic activities of several naturally occurring CLPs, as well as their arginine to lysine (R:K) ratios in Table 3.2. The peptides with higher arginine content were generally more hemolytic than the ones with higher lysine content, a trend uncorrelated with the overall proportion of cationic residues. The exception is melittin, whose hemolytic activity is partly attributed to hydrophobicity. Furthermore, synthetic lysine-rich CLPs also showed limited hemolytic activities [12, 27, 126]. The general trend of earlier studies indicates that arginine plays an important role in inducing hemolysis, albeit the ability of CLPs to form bidentate hydrogen bonds or multiple hydrogen bonds is not the sole determinant of hemolytic activity.

Table 3.2 Arginine-to-lysine ratio and hemolytic effect of selected naturally occurring CLPs.

Peptide	Primary amino acid sequence	R:K ratio	Hemolytic effect	Reference
BMAP-28	GGL**R**SLG**RK**IL**R**AW**KK**YGPIIVPII**R**I	4:3	++	[197]
Magainin 2	GIG**K**FLHSA**KK**FG**K**AFVGEIMNS	0:4	-	[92]
Ceropin B	**K**W**K**VF**KK**IE**K**MG**R**NI**R**NGIV**K**AGPAIAVLGEA**K**AL	2:7	-	[82]
Melittin	GIGAVL**K**VLTTGLPALISWI**KRKR**QQ	2:3	+++	[92]
LL-37	LLGDFF**RK**S**K**E**K**IG**K**EF**KR**IVQ**R**I**K**DFL**R**NLVP**R**TES	5:6	+	[82]
Gaegurin 5	FLGALF**K**VAS**K**VLPSV**K**CAIT**KK**C	0:5	-	[107]
Indolicindin	ILPW**K**WPWWPW**RR**	2:1	+	[198, 199]
Tachyplesin I	**K**WCF**R**VCY**R**GICY**RR**C**R**	5:1	+	[99]

Note: Bold letters indicate cationic amino acids. More "+" represents stronger hemolytic effect; "-" means no significant hemolysis at 100 μM.

Here, we demonstrated the roles of arginine and cholesterol in inducing leakage on cholesterol-rich membranes from a molecular basis. We also showed the potential of altering the specificity of CLPs towards cells with different surfaces by modulating the cholesterol-rich membrane selectivity of CLPs. Notwithstanding, the membrane selectivity of CLPs can also be altered by the length [200] and the residual volume [31] of peptides, adopting D-enantiomers of amino acids [27] and possibly the position of amino acids in the peptide sequence [201]. To manipulate the membrane selectivity of CLPs and to create CLPs with high specificity towards targeted cells, further studies are required to fully understand the interplay between the above factors, as well as targeted cell membrane compositions.

3.5 Conclusion

In this work, we have characterized an arginine-rich CLP, C6, and evaluated its membrane activity on pure and cholesterol-containing POPC membranes. The comparison between liposome and *in vitro* systems indicates that having only POPC in liposomes does not provide a comprehensive reference to predict the performance of CLPs in biological systems, especially when it comes to evaluating factors that affect membrane selectivity. The roles of arginine and cholesterol in the membrane disruption of cholesterol-rich POPC vesicles were investigated using molecular dynamics simulations. The guanidinium group of arginine can form bidentate hydrogen bonds with the phosphate of the lipid head group and the hydroxyl of cholesterol at the same time, likely facilitating the association of CLPs with the membrane. The disruptive activity of C6 on cholesterol-rich membranes was shown to decrease when hydrogen bonding between C6 and the membrane was inhibited by adding phosphate ions. The cytotoxicity of C6, with and without the presence of phosphate ions, was tested against cancer cells with low cholesterol (A549) and high cholesterol levels (MCF-7). Hemolytic activity was also assayed. Due to the complexity of cell membranes, changes in cytotoxicity with change in buffer are not correlated with results from the model membrane system: with phosphate buffer, the cytotoxicity of C6 is significantly enhanced against A549 cells but remains largely unchanged against MCF-7 cells and red blood cells. We attribute this discrepancy to enhanced hydrophobicity of C6 in P buffer and other unaccounted factors attributed to the complexity of cell membranes. However, there is great potential in enhancing the activity of CLPs towards specific cell types by modulating their membrane selectivity, with means beyond electrostatic intermolecular interactions. We hope to have provided valuable insight into the molecular mechanism of the interaction between arginine-rich CLPs and cholesterol-rich POPC membranes, as to benefit the future design of CLPs.

Chapter 4*

Antitumor Activity of an Amphiphilic Cationic Lytic Peptide and its Potential as Anticancer Drug Carrier for Enhanced and Selective Delivery

4.1 Introduction

With the progress of nanotechnology and materials science, nanoscaled drug delivery systems with various sizes, architectures and surface properties have been engineered for cancer therapy [39, 202]. The purpose of these nanocarrier systems aims to enhance the efficacy of delivered therapeutics in the aspects of controlling pharmacokinetics and pharmacodynamics, and targeted delivery. The size of the nanocarriers is essential for extended circulation time and accumulation in the tumor via the enhanced permeability and retention (EPR) effect [37]. Incorporating bioactive ligands provides specific interactions between nanocarriers and cancer cell surfaces, facilitating the localization and cellular uptake of therapeutics at the targeted site [170]. Moreover, the stimuli-responsive designs applied in drug delivery systems enable on-demand delivery. The stimuli-responsiveness allows drug delivery systems to recognize specific microenvironments, for instance, with a lower pH [44] or increased level of matrix

* This chapter is based on a manuscript "S. Lu, Y. Wu, Y. Ding, R. Wang, Z. Wan, R. Pan, Y. Yuan and P. Chen, Antitumor Activity of an Amphiphilic Cationic Lytic Peptide and its Potential as Anticancer Drug Carrier for Enhanced and Selective Delivery ". Y. Wu, R. Yang and Y. Yuan are collaborators from NO.3 people's hospital affiliated to Shanghai Jiao Tong University.
Author contribution: S.L. conceived idea and designed experiments; Y.W., R.W. and Y.Y. performed animal works; Y.D. performed AFM; S.L. performed *in vitro* characterization experiments; S.L., Z.W. and R.P. performed cytotoxicity studies; S.L., Y.D. and Y.W. analyzed data; S.L. wrote the manuscript; P.C. edited the manuscript.

metalloproteinases [49], and release the loaded drug in a tailored way. The sustained release of the loaded drug can also be triggered by exogenous stimuli, such as light [53, 156], heat [203, 204] or ultrasound [54, 55], at the disease sites. These rationally designed nanoparticle-base drug delivery systems offer numerous possibilities for therapeutic applications.

Peptides have shown great potential as drug carriers due to their favorable biocompatibility, non-toxic degradation products, as well as numerous design possibilities and bio-functionalities. The physicochemical properties of peptides vary with their sequences, and an amphiphilic structure is generally required to stabilize hydrophobic drugs in aqueous solution [69]. There is a special class of peptides called cationic lytic peptides (CLPs), which show anticancer activity by themselves [6]. These peptides are characterized by their overall positive charges and amphiphilicity, which enable them to insert into phospholipid bilayers, leading to the disruption of cell membranes. Many CLPs were found to selectively kill cancerous cells partly due to the interaction between the positive charges of CLPs and elevated negative charges on the surfaces of cancerous cells [12, 27]. Besides the lytic function, the amphiphilic structure of CLPs makes it also possible to use CLPs as a hydrophobic drug carrier. A similar idea has been carried out by Stephen et al. using a self-assembling peptide amphiphile (A CLP conjugated with a hydrophobic alky chain) to carry camptothecin *in vitro* and *in vivo* [66]. They claimed that the peptide amphiphile could enhance the cellular uptake of camptothecin. In our point of view, CLP-mediated drug delivery systems may have more advantages, such as selective delivery.

Previously, we reported on a cationic amphiphilic peptide, C6 (Ac-RLLRLLLRLWRRLLRL-LR-NH2), and its potential as a siRNA carrier [189]. In this work, a model hydrophobic anticancer drug, ellipticine (EPT), was chosen as the cargo to be delivered by C6. We evaluated the anticancer activity and selective killing of C6 *in vitro*, against A549 lung carcinoma cells, MCF-7 breast carcinoma cells and NIH-3T3 mouse fibroblast cells. Preliminary intratumoral administration of C6 on a xenograft A549 lung carcinoma model was also performed, showing that C6 was effective at inhibiting tumor growth. Furthermore, the ability of C6 to

stabilize EPT was demonstrated *in vitro*. Interestingly, the C6-EPT formulation showed enhanced anticancer efficacy (synergistic effect) and selective delivery. A membrane disruption-assisted mechanism was proposed to explain our observations.

4.2 Materials and methods

4.2.1 Sample preparation

Amphiphilic cationic peptide C6 was synthesized by Canpeptide Inc. (Montreal, Canada) with a purity above 95%. The procedure for peptide synthesis is briefly described in section 3.2.1. The anticancer drug ellipticine (EPT) was purchased from ENZO life science (Brockville, Canada). The peptide only samples were prepared by dissolving C6 powder in Milli-Q water. The C6-EPT complexes were prepared by adding freshly prepared 0.5 mg/ml C6 aqueous solution into a glass vial containing a thin film of EPT at the bottom [205]. The sample was stirred at 900 rpm by magnetic bar overnight before use. The neutral EPT control was prepared by dissolving EPT powder in DMSO (≥99.9%, Sigma, Oakville, Canada) at concentration of 1mg/ml; the EPT DMSO solution was diluted into culture media with a final content of 1% DMSO before treatment.

4.2.2 Cell culture

Mouse fibroblast cells (NIH-3T3), non-small lung carcinoma cells (A549) and breast carcinoma cells (MCF-7) were purchased from ATCC (Manassas, USA). All cell lines were cultured in ATCC recommended growth media: A549 cells were cultured in F-12 (Kaighn's modification) (F12K) media (HyClone Laboratories, Mississauga, Canada); MCF-7 cells were cultured in MEM Eagles with Earle's Ballanced Salts (HyClone Laboratories, Mississauga, Canada); NIH-3T3 cells were cultured in Dulbecco's Modified Eagle's Medium (DMEM)

(HyClone Laboratories, Mississauga, Canada). All the media contained 10% fetal bovine serum (FBS) (Invitrogen, Burlington, Canada) and 1% penicillin/streptomycin (MP Biomedicals, Montreal, Canada). The cells were cultured at 37 °C and 5% CO_2.

4.2.3 Cellular uptake of C6-EPT complexes

A549 cells were seeded into a 24-well plate at a density of 5×10^4 cells per well and cultured overnight. The cells were then treated with C6 or C6-EPT complexes and incubated for 10 min, 20 min, 30 min, 40 min and 1 h, respectively. The cells were washed with phosphate-buffered saline three times, and then incubated with Fluoroshield™ mounting solution with 4',6-diamidino-2-phenylindole (DAPI) (Sigma-Aldrich, Oakville, Canada) for 30 min. Afterwards, the cellular uptake of C6-EPT complexes was immediately imaged using an Axio Observer microscope (Carl Zeiss, Jena, Germany).

4.2.4 MTS assay

A549 cells were seed into a Falcon 96-well plate (Corning, USA) at the density of 10000 cells per well, while MCF-7 and NIH-3T3 cells were seeded at the density of 20000 cells per well. The seeded cells were incubated for 24 h before treatment. After the media was removed, 150 **μ**L fresh media was added with 50 **μ**L of treatment was added. Following 24 h incubation, MTS assays were performed using a CellTiter 96® AQueous Kit (Promega, Madison, USA) according to the manfacture's protocol. The absorbance was measured at 485 nm using a FLUOstar plate reader (BMG Labtech, Ortenberg, Germany). The untreated cells were used as the negative control. IC_{50} values were calculated by fitting to a sigmoid function.

4.2.5 Annexin V assay

Untreated or treated cells were labeled using FITC-Annexin V and 7-AAD (BD bioscience, Mississauga, Canada) after 18 h incubation. The staining procedure was following the manufacturer's instruction.

4.2.6 Lung carcinoma xenograft experiments

The xenograft tumor model was established using six-week-old male BALB/c nude mice. A549 lung carcinoma cells (5×10^6) were implanted subcutaneously into mice at the right armpit. The mice were then randomized into 3 groups (untreated, saline and C6 group, 5 mice in each group). The intratumoral administration was performed when the tumor volume reached 100-200 mm^3. C6 was injected at a dosage of 1mg/kg 3 times per week for 9 injections in total. The mice body weights and tumor sizes were recorded after each injection. Tumor volume was calculated as 0.5 × longest diameter × (shortest diameter)^2. The inhibition rate was calculated as (1- tumor weight of C6 group/ tumor weight of untreated group) ×100%.

4.2.7 Statistical analysis

Results were expressed as mean±SD. Statistical significance was determined by one-way analysis of variance (ANOVA). Differences were considered significant if $p<0.05$.

4.2.8 Ellipticine loading capacity

The amount of EPT stabilized by C6 in aqueous solution was determined by a UV-adsorption method described previously [205]. Briefly, a calibration curve of EPT UV-adsorption at concentrations ranging from 1×10^{-4}~ 5×10^{-4}mg/ml was made. The UV-adsorption of diluted C6-EPT complexes was measured, subtracting the UV-adsorption of C6, and substituted into the

calibration curve to obtain the EPT concentration. The value of EPT concentration in C6-EPT complexes was averaged from 3 measurements.

4.2.9 Dynamic laser scattering

The size distribution of C6 peptide and C6-EPT complexes were investigated on a Zetasizer Nano ZS (Malvern Instruments, Malvern, UK) with experimental parameters as previously described [205]. Disposable Solvent Resistant Micro Cuvettes (Malvern Instruments) were used to perform the measurements. Three measurements were performed to generate the intensity-based size distribution.

4.2.10 Surface tension measurement

The dynamic surface tensions of C6 aqueous solutions at various concentrations were measured using ADSA-P technique. The experimental set-up was described before [206]. The equilibrium surface tensions were estimated by averaging 10 data points at the end of each dynamic surface tension profile. The equilibrium surface tensions were plotted as a function of C6 concentration to determine the critical aggregation centration (CAC) of C6.

4.2.11 Atomic force microscopy

The nanostructures of C6 and C6-EPT complexes were imaged on a Dimension Icon AFM (Bruker, Santa Barbara, USA). The AFM samples were prepared by mounting 50 **µ**l of solution on a freshly cleaved mica surface (SPI, West Chester, USA). The mica was washed with 80 **µ**l Mili-Q water 5 times after the 15 min incubation. The air-dried AFM samples were scanned at room temperature using the peak force quantitative nanomechanical mapping (PF-QNM) mode. All images were acquired using a SCANASYST-AIR probe (Bruker, Santa Barbara, USA).

4.2.12 Fluorescence spectroscopy

The molecular states of EPT in C6-EPT complexes were identified using fluorescence spectroscopy. The samples were transferred into a square quartz cell and excited at 295 nm. The emission scans were performed on a QM4-SE spectra fluoremeter (PTI, London, Canada). The fluorescence emission of C6 aqueous solution was used as background. Detailed experimental settings have been described previously [205]. A standard (2 mM EPT in ethanol, sealed and degassed) sample was used in each run to correct the lamp intensity variations. The standard fluorescence intensity was obtained by taking an average of the fluorescence (I_s) from 424 to 432 nm (for the peak at 428 nm). The spectra of samples were normalized with I_s.

4.2.13 Circular dichroism spectroscopy

The secondary structure of C6 in aqueous solution or in C6-EPT complexes was determined using a J-715 circular dichroism spectrometer (Jasco Europe, Cremella, Italy). The samples were transferred into a 1 mm quartz cell (Hellma, Concord, Canada), and spectra were collected from 190 nm to 260 nm with a 1 nm bandwidth and data pitch, 2 s response time and 100 nm min^{-1} scanning speed. The reported spectra were averaged from two replicates, and solvent absorbance was subtracted from the data. The mean residue molar ellipticity of C8 peptide presented here was calculated following the formulas: Ellipticity (θ in deg cm^2 $dmol^{-1}$) = (millidegrees × mean residue weight)/(path length in millimetres × concentration of C8 peptide in mg ml^{-1}).

4.3 Results and discussion

4.3.1 *In vitro* cytotoxicity evaluation

To evaluate the cytotoxicity of C6, two cancerous cell lines, A549 and MCF-7, and a normal tissue cell line, NIH-3T3, were treated with varying concentrations of C6. The viability of the treated cells was determined using a MTS assay (Figure 4.1.a). The calculated IC_{50} values against A549 and MCF-7 cells were 27.2±2.8 μg/ml (11.1±1.1 μM) and 21.6±4.5 μg/ml (8.8±1.8 μM), respectively; while 55.6±4.5 μg/ml (22.6±1.8 μM) of C6 was needed to cause 50% death of NIH-3T3 cells, showing a moderate selectivity of C6 towards cancerous cells.

The cell death mechanism was investigated using Annexin V apoptosis detection kit. A549 cells were treated with water, or C6 solutions for 18 hours, and stained with FITC-Annexin V and 7-AAD. As shown in Figure 4.1.b, C6 induced both Annexin V and 7-AAD positive cells, suggesting a possible apoptotic mechanism of cell death [131].

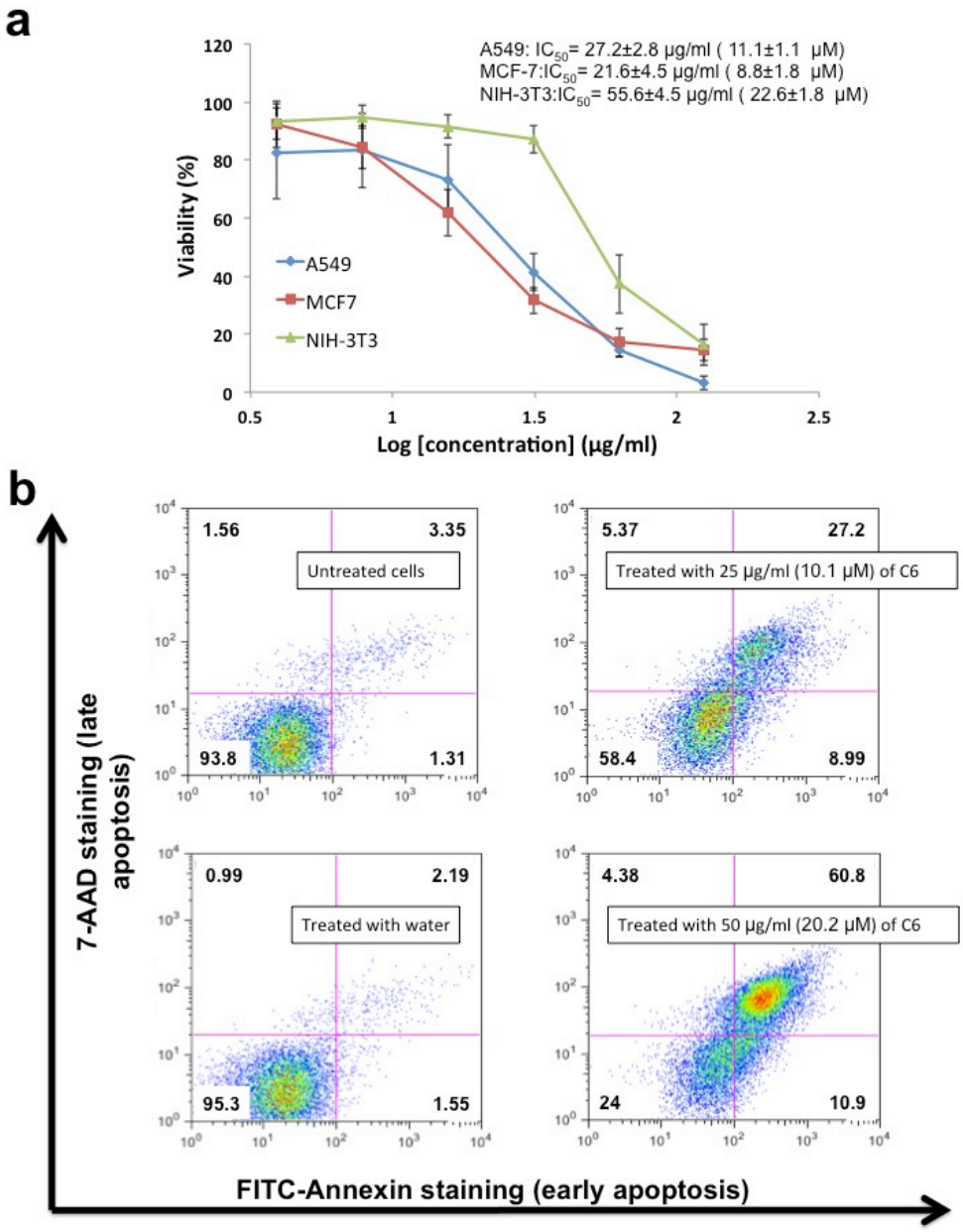

Figure 4.1 *In vitro* cytotoxicity evaluation. (a) Cytotoxicity of C6 against A549 (lung carcinoma), MCF-7 (breast carcinoma) and NIH-3T3 (mouse fibroblast). (b) A549 cells were treated with water or C6 peptide for 18 h. The apoptotic stage of cells was determined by FITC-Annexin V and 7-AAD staining.

4.3.2 Inhibition of tumor growth in xenografts

The lung cancer xenograft model was established by subcutaneous inoculation of A549 cells in BALB/c nude mice. C6 aqueous solution was injected intratumorally at a dosage of 1 mg/ml.

As shown in Figure 4.2.b-c, C6 inhibited the growth of tumor effectively with an inhibition rate of 42%. Furthermore, C6 did not show obvious toxicity to mice as the body weight of mice did not drop during the treatment (Figure 4.2.a).

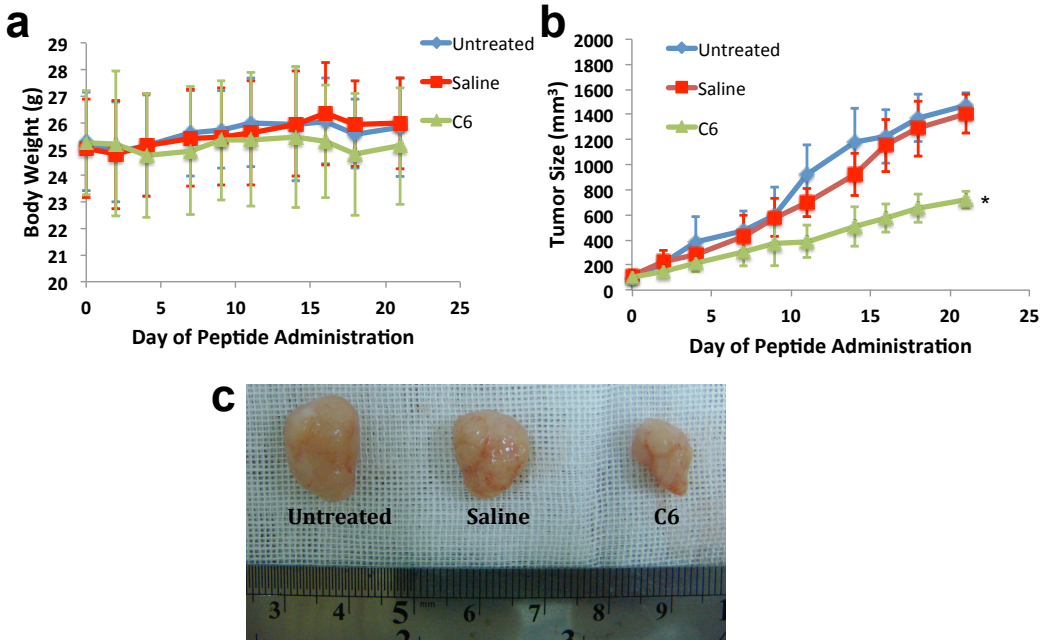

Figure 4.2 Intratumor administration of C6 in BALB/c nude mice. (a) The tumor sizes and (b) The body weights of mice in untreated, saline or C6 treated groups. (c) The representative images of A549 tumor in untreated, saline or C6 treated groups. *p<0.05 versus untreated group.

4.3.3 Drug delivery potential of C6

After demonstrating the anticancer activity of C6, we further investigated the potential use of the peptide-based drug as a hydrophobic drug delivery vector. Ellipticine (EPT) was used as the cargo for several reasons. First, EPT is a hydrophobic molecule. Second, the fluorescent properties of EPT has been fully studied [74], which makes it easy to characterize its molecular state. Third, an effective delivery system is required to reduce the adverse effects encountered during early clinical trials of its derivatives [75, 76].

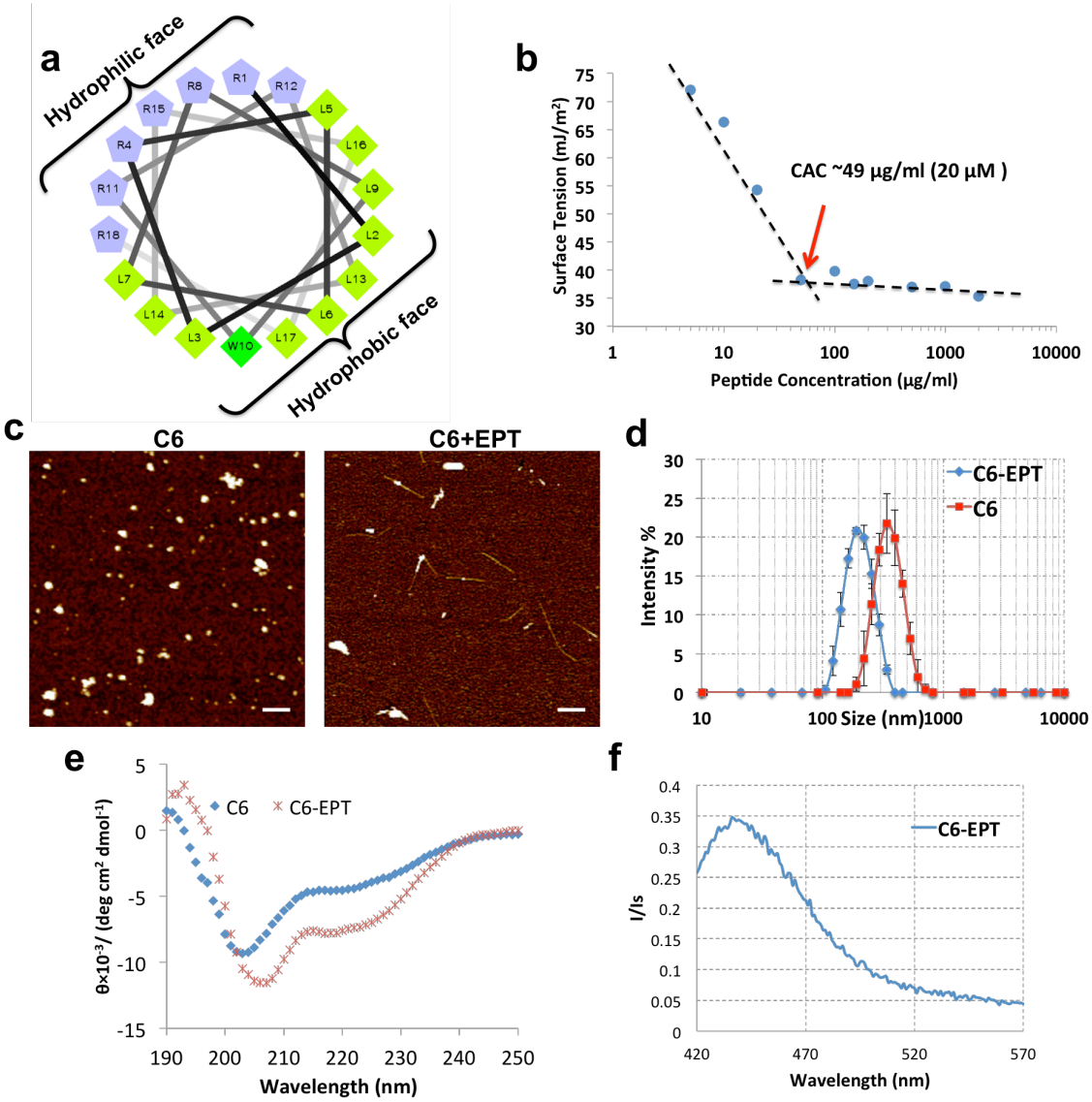

Figure 4.3 Physicochemical characterization of C6 and C6-EPT complexes. (a) Helical wheel of C6. (b) Critical aggregation concentration of C6 determined by equilibrium surface tension of C6. (c) Nanostructures of C6 or C6-EPT complexes determined by AFM. The scale bar is 200 nm. (d) Size distributions of C6 or C6-EPT complexes determined by DLS. (e) Secondary structures of C6 in aqueous solution or in C6-EPT complexes determined by CD. (f) Normalized fluorescence emission spectrum of C6-EPT complexes.

The helical wheel of C6 (Figure 4.3.a) illustrates that the C6 molecule possesses a hydrophilic side and a hydrophobic side when it is in a helical conformation. We hypothesized that the amphiphilic structure allows C6 to create a hydrophobic domain in aqueous solution, with

the hydrophobic sides facing inward to encapsulate hydrophobic EPT molecules; while the hydrophilic sides contact with aqueous environment, stabilizing the C6-EPT complex in water. The critical aggregation concentration (CAC) of C6 was determined to be ~49 μg/ml (20 μM) (Figure 4.3.b), indicating that the proposed formulation between C6 and EPT could happen above this concentration.

To test the proposed C6-EPT formulation, the stock solution of C6-EPT complexes was prepared by stirring 500 μg/ml (203. 3 μM) C6 solution in a vial containing a thin EPT film. The amount of EPT loaded by C6 was determined to be 14 ± 0.6 μg/ml (56.9 ± 0.2 μM) using a UV-based method [205]. The fluorescence emission spectrum of the loaded EPT had a maxima at ~430 nm (Figure 4.3.f), indicating neutral molecules [74]. As shown in the circular dichroism spectra (Figure 4.3.e), the spectrum of C6 had a negative peak at ~ 203 nm, with a negative shoulder centering at ~ 220 nm, indicating that C6 stayed as a mixture of random coil and α-helix in aqueous solution; the molar ellipticity $[\theta]_{222}$ (-4,400 deg cm^2 $dmol^{-1}$) at 222 nm corresponds to ~19% helical content [207]. In contrast, after formulating with EPT, the spectrum of C6-EPT complexes had a negative peak at ~208 nm with increased absorbance at ~222 nm when compared to C6 alone, indicating the α-helical content increased to ~27% with a $[\theta]_{222}$ value of -7,400 deg cm^2 $dmol^{-1}$; there was a small dip in the spectrum at ~218 nm, suggesting that a part of C6 adopted a β-sheet conformation. This observation is partially consistent with our hypothesis: the interaction between EPT molecules and hydrophobic residues stabilized the helical conformation, resulting in the increased content of α-helical conformation; the amphiphilic C6 helixes encapsulated EPT molecules into a hydrophobic interior to form nanoparticles. On the other hand, EPT molecules may also acted as bridges to connect extended C6 monomers, resulting in the β-sheet conformation. AFM images showed that C6 formed spherical aggregates by itself, and C6-EPT complexes became mixtures of filaments and irregular aggregates (Figure 4.3.c). The changes in nanostructure were in line with the changes in secondary structure. The particle sizes shown in AFM images were below 200 nm for both C6 and C6-EPT complexes,

and the width of fibrous C6-EPT particles was less than 30 nm. The hydrodynamic radius of C6 and C6-EPT complexes was also measured using dynamic laser scattering. The results showed that C6 particles have a major population at ~350 nm, and after formulating with EPT, the main sizes of the complexes shifted to ~190 nm (Figure 4.3.d). As C6 peptides were largely unstructured in aqueous solution, part of their arginine residues may be embedded in the core of the aggregates, resulting in loosen particles with large sizes; after formulating with EPT, with well ordered structure, the positively charged arginine residues oriented towards aqueous phase at particle surfaces, providing electrostatic repulsions, hence, leading to decreased particle sizes. The discrepancies in the size measurements by two techniques may be due to the different environments while the measurements were performed. Nevertheless, the particle sizes of C6-EPT complexes measured by either technique are ideal for passive targeting to tumor via the enhanced permeability and retention effect [208].

4.3.4 CLP-assisted delivery.

There are several potential advantages of using C6 as a drug carrier. First, the delivery vector is also an anticancer agent. Second, the lytic activity of C6 weakens the barrier function of cell membranes, resulting in enhanced cellular uptake of EPT. We refer to this mechanism as "CLP-assisted uptake", which is illustrated in Figure 4.4.a. Furthermore, the membrane disruptive ability of C6 varies depending on the type of cell membrane, which could cause selective delivery.

To investigate the potential of this CLP-mediated drug delivery system, the cellular uptake of EPT was monitored using fluorescence microscopy. In this study, A549 cells were treated with C6 or C6-EPT complexes at two different concentrations for 1 h and the fluorescence emission of EPT was observed via a green channel. The C6 treated cells were used as a control to indicate that the observed fluorescence was not from the peptide, and DAPI was used to locate the nucleus. As shown in Figure 4.4.b, in the case of high concentration of C6-EPT complexes, the green

fluorescence of EPT overlapped with DAPI. This suggested that EPT accumulated at the nuclei, where EPT is supposed to execute its function [72]. Also, from the merged image, we found that the cell membranes were broken, which resulted from membrane disruption induced by C6 [27, 131]. Due to the reduced concentration of C6, after treated with 4-time diluted C6-EPT complexes, there were cells that still maintained the integrity of their membranes. The green fluorescence of EPT shown on intact cells had a low intensity or distributed on the entire cell (indicated by solid arrows); in contrast, EPT again located at nuclei of the broken cells (indicated by dashed arrows) (Figure 4.4.b). This observation implies that EPT can easily penetrate the disrupted cell membranes to reach the nucleus, which supports "CLP-assisted uptake". This might be the reason for the observed synergistic effect between CLPs and anticancer agents [27, 87]. Based on this observation, we reasonably assume that cell membranes hinder the permeation of EPT, but still, the cellular uptake could happen through endocytosis. However, EPT may not be able to escape lysosomes, staying in cytoplasm [209]; on the other hand, EPT could directly penetrate the damaged cell membranes, easily reaching nucleus. This mechanism requires further detailed investigation.

A time-resolved study of cellular uptake of EPT was performed. Owing to the membrane disruption induced by C6, strong uptake of EPT was observed within 30 min incubation with most of the EPT localizing at the nucleus (Figure 4.4.c). Previous work from our group has studied the cellular uptake of EPT delivered by an ionic complementary peptide, EAK 16-II, which does not possess membrane lytic activity [72]. In that work, the concentration of EPT in EAK16-II-EPT complexes was 25 μg/ml, almost 7-fold higher than that in C6-EPT complexes. Higher concentration normally associates with stronger and faster uptake [210], however, it took more than 1 h to observe the accumulation of EPT in nuclei, which suggested the cellular uptake of C6-EPT complexes was faster and more efficient than EAK16-II-EPT complexes. This could also result from the "CLP-assisted uptake" mechanism.

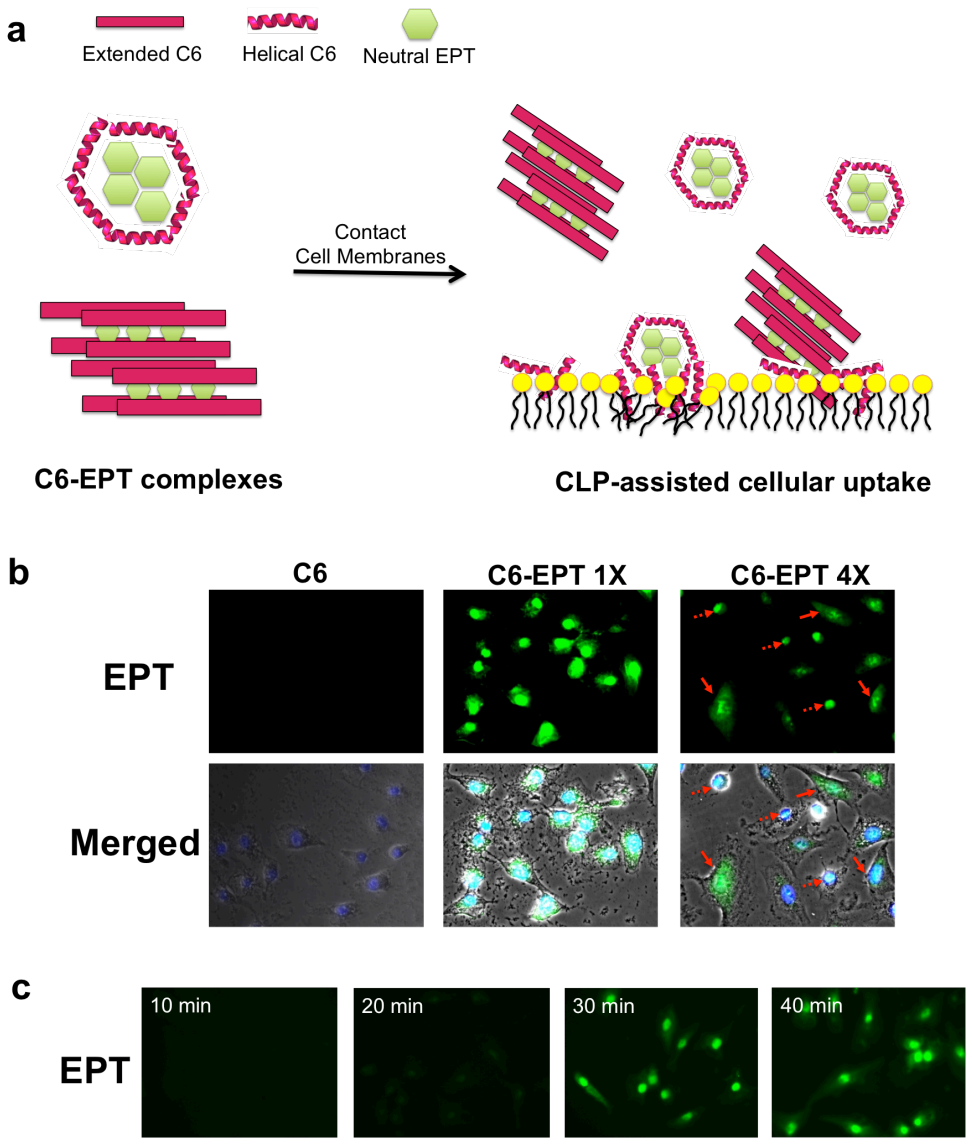

Figure 4.4 C6-mediated CLP-assisted cellular uptake of EPT. (a) Illustration for the CLP-assisted delivery mechanism. The formulation of C6-EPT complexes is based on the characterizations. (b) Cellular uptake of EPT delivered by C6 monitored using fluorescence microscope. EPT is shown in green, DAPI is shown in blue. 1X sample refers to complexes with with 125 μg/ml (53.6 μM) C6 and ~3.5 μg/ml (14.2 μM) EPT in the final culture media. The concentration of C6 sample was 125 μg/ml (53.6 μM). Cells with intact membranes are indicated by solid arrows, broken cells are indicated by dashed arrows. (c) Time study of cellular uptake of EPT from 1X C6-EPT complexes at 10 min, 20 min, 30 min and 40 min, respectively.

The *in vitro* cytotoxicity of EPT and C6-EPT complexes against lung cancer A549 cells and fibroblast NIH-3T3 cells was then evaluated. The cells were treated with C6-EPT complexes at

stock concentration or dilutions for 24 h incubation before performing a MTS assay. C6-EPT complexes exhibited significantly enhanced cytotoxicity compared with C6 or EPT control towards both A549 and NIH-3T3 cells (Figure 4.5 a,b,d). IC_{50} value of C6-EPT complexes was 12.2 μg/ml C6 with 0.34 μg/ml EPT on A549 cells and 40.7 μg/ml C6 with 1.14 μg/ml EPT on NIH-3T3 cells, which was much lower than that of EPT control (IC_{50} ~2.9 μg/ml on both A549 cells and NIH-3T3 cells) and C6 (IC_{50} 27.2 μg/ml on A549 cells and 55.6 μg/ml on NIH-3T3 cells), respectively. These results suggested an synergistic effect between C6 and EPT. The synergistic effect could result from our proposed enhanced cellular uptake of EPT, which may also be a general reason for the previously reported synergistic effect between other CLPs and anticancer agents [27, 87]. Furthermore, it was shown that the IC_{50} value of C6 on NIH-3T3 cells was 2-fold higher than that obtained for the A549 cells (Figure 4.1.a) and EPT was not selective toward the two cell lines. Although C6-EPT complexes presented enhanced cytotoxicity towards both cell lines, the enhancement on A549 cells was more significant than that on NIH-3T3 cells; IC_{50} value of C6-EPT complexes on NIH-3T3 cells became 3.4-fold higher than that obtained for the A549 cells, demonstrating an even greater selectivity compared to C6. This supported the proposed selective delivery. We postulated that, at the same concentration, C6 was less active against NIH-3T3 cells, hence, induced less permeability on NIH-3T3 cell membranes than A549 cell membranes; this difference may lead to different degrees of "CLP-assisted uptake" of EPT for the two types of cells. Consequently, EPT exerted different therapeutic efficacy on the two cell lines, which resulted in selective cytotoxicity of C6-EPT complexes.

The cytotoxicity results also showed that, at the concentrations where C6 could induce 30% to 60% cell death, C6-EPT complexes exhibited significantly enhanced cytotoxicity compared to C6, which could be contributed by EPT; with further decrease of C6 concentration, the enhanced cytotoxicity of C6-EPT complexes compared to C6 became less significant (Figure 4.5.b-d). The reason could be that the low concentration of C6 was no longer capable of inducing strong membrane disruption to assist cellular uptake of delivered EPT. To further investigate the potency

of “CLP-assisted uptake” and selective delivery, C6 aqueous solution at a concentration of 80 μg/ml (32.4 μM) was used to dilute C6-EPT complexes (referred to as C6-EPT+) instead of water for cytotoxicity test. The purpose was to keep C6 above a concentration that can activate the “CLP-assisted uptake”. C6 only samples diluted with the low concentration C6 solution (referred to as C6+) were used as controls to show the contribution of C6 on the cytotoxicity of C6-EPT complexes. Compared to C6+, C6-EPT+ killed 30% more A549 cells at the lowest test concentration, where the concentration of EPT was only 0.11 μg/ml (0.44 μM) (Figure 4.5.c). In contrast, the enhancement on the cytotoxicity of C6-EPT+ against NIH-3T3 cells was not remarkable compared to C6+; although the cytotoxicity of C6-EPT+ was stronger than the C6-EPT complexes, the elevated cytotoxicity was majorly contributed by the increased concentration of C6 (Figure 4.5.d,e). Taken together, it suggested that C6-EPT+ possessed an even greater selectivity. Since C6-EPT+ inhibited more than 50% of A549 cell proliferation within the tested range of concentrations, IC_{50} values were not estimated. .

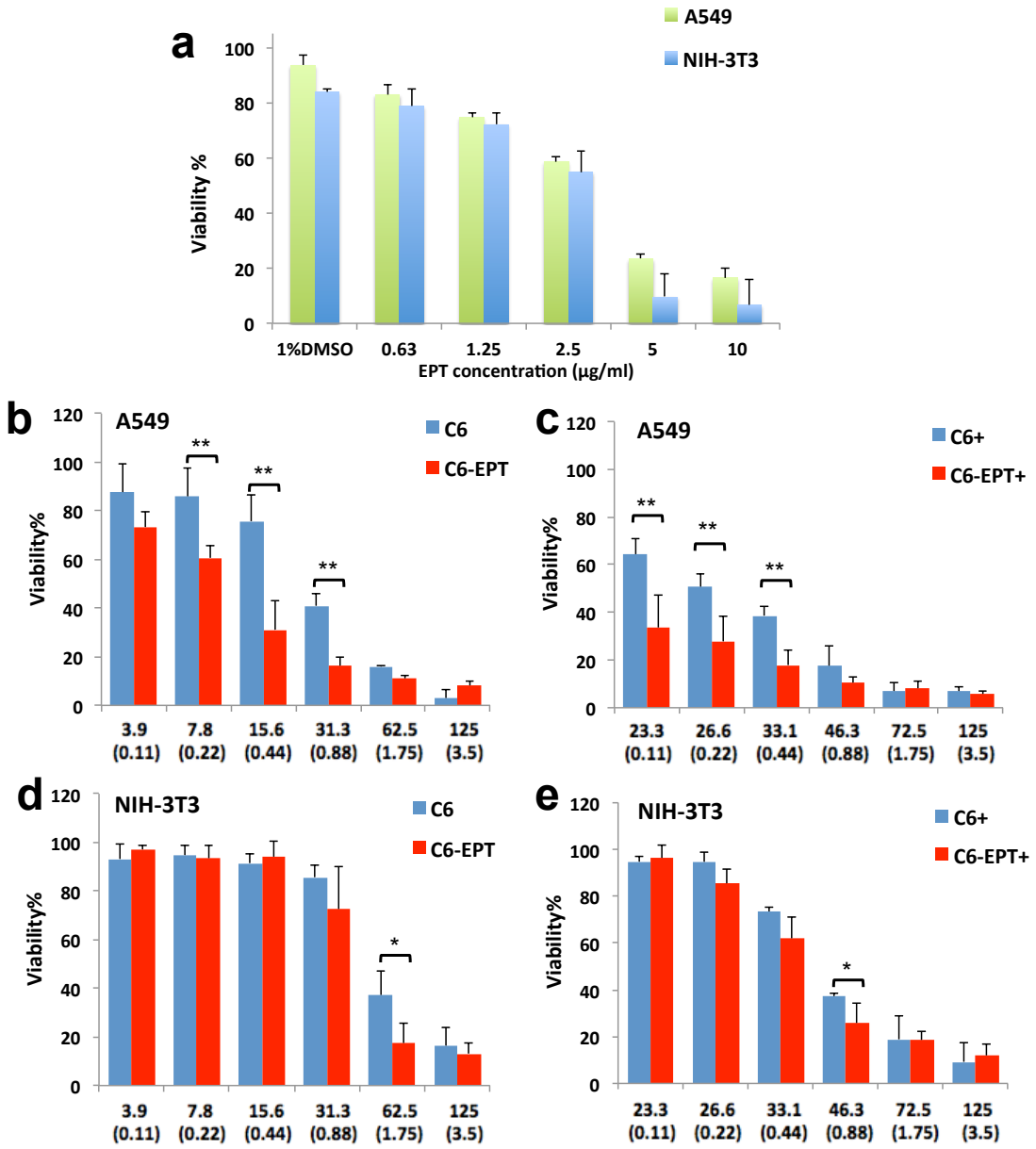

Figure 4.5 Evaluation of the cytotoxicity of (a) neutral EPT and C6-EPT complexes against (b,c) A549 (lung carcinoma) and (d,e) NIH-3T3 (mouse fibroblast). C6+ and C6-EPT+ refer to the samples diluted with 80 μg/ml (32.4 μM) C6 aqueous solution. X-axis represents the concentration of C6 in each sample, including C6 alone and C6-EPT complexes; the concentrations of EPT in C6-EPT complexes are shown in the brackets. The concentrations presented are mass concentrations (μg/ml) in the culture media. The viabilities were averaged from at least three independent experiments. Error bars are standard deviation (n>3). *p<0.05, **p<0.01 between the two compared samples.

In this work, we have demonstrated the potential use of C6 as a drug carrier empowered by a "CLP-assisted uptake" mechanism, which is the basis for the enhanced activity and selectivity of the CLP-mediated drug delivery system. This mechanism is also applicable for continued *in vivo* application. Different from *in vitro* studies, *in vivo* administration requires continuous injections of treatments to keep an effective concentration of therapeutic, allowing sufficient CLP to assist the uptake of the delivered anticancer agent. This would allow a lowered dosage of anticancer agent, reducing side effect. The selectivity of CLP-mediated systems could further limit the cytotoxicity towards normal tissues. Although the anticancer efficacy of C6-EPT is remarkable, an alternative encapsulation method might be considered for higher loading efficiencies and even higher anticancer efficacy. Selective delivery is a unique advantage of CLP-mediated drug delivery systems. To further improve the selectivity of the system, it is possible to design CLPs with high specificity towards cancerous cells for drug delivery purposes, which requires fully understanding the underlying mechanism for CLP-induced membrane lysis. Adopting cancer-specific drugs [211] as delivered cargo is another alternative to enhance the selectivity of the entire drug delivery system. Besides the functionalities mentioned above, we also postulate that CLP-mediated drug delivery systems may overcome the multidrug resistance (MDR) developed by cancer cells. It has been reported that many CLPs were active against multidrug resistant cancer cell lines [25, 83], possibly because CLPs attack cell membranes directly, which avoids general mechanisms of drug resistance [212]. The drug delivered by CLP may also not be affected by transmembrane protein pumps and transporters, which may be disabled disrupting the membrane. This should be further investigated with proper experiments.

4.4 Conclusion

In this study we have shown the anticancer activity of a cationic lytic peptide, C6, *in vitro* and *in vivo*. We also have demonstrated that the amphiphilic property allows C6 to encapsulate a

hydrophobic anticancer drug ellipticine in aqueous solution. The C6-EPT complexes exhibit high anticancer efficacy against A549 cells due to the enhanced cellular uptake of EPT. Selective delivery of EPT towards cancerous cells is also demonstrated. A "CLP-assisted uptake" mechanism is proposed to explain these observations. This C6-mediated drug delivery system presented provides a new concept to develop drug carriers: using CLPs (drug) work as drugs and vectors to deliver other drugs. The multifunctionalities of C6-EPT complexes demonstrated in this work suggest the great potential of CLP-mediated drug delivery systems.

Chapter 5*

Stimuli-responsive Self-assembling Cationic Lytic Peptide and its Potential for Self-guided Delivery

5.1 Introduction

Cationic lytic peptides (CLPs) are emerging as potential anticancer reagents with a new mode of action by inserting into cell membranes, disrupting their integrity, which leads to cell lysis [6]. The overall positive charge of CLPs suggests their preferential binding to negatively charged cell membrane surfaces. As a number of tumor cells possess negatively charged surfaces due to over-exposure of phosphatidylserine [19, 20] and high levels of aberrant O-glycosylated mucins [21, 22], CLPs could target this trait and lyse tumorous cells selectively [12, 23, 24]. CLPs can also overcome the drug resistance mechanisms occurring in tumor cells [25, 26], possibly because CLPs attack the cell membranes directly [6].

Despite these favorable features of CLPs, compared to conventional chemotherapeutic agents, there are issues such as hemolysis [82, 103, 213] and susceptibility to proteolytic degradation [178, 214], impeding the clinical usage of CLPs. To explore the potential of this class of peptides, synthetic diastereomeric lytic peptides consisting of D-amino acids were designed and showed to enhance selectivity towards cancerous cells *in vitro and in vivo* [27, 81],

* This chapter is based on a manuscript "S. Lu, L. Zhang, Y. Ding, D, Zhao, T. Zheng, P. Ouyang, J. Li, Z. Wan, D. Chu, W. Xu, Y. Yu, B. Chen, P. Chen, Stimuli-responsive Self-assembling Cationic Lytic Peptide and its Potential for Self-guided Delivery".
Author contribution: S.L. conceived idea and designed experiments; S.L. performed *in vitro* characterization experiments; S.L., L.Z. and Y.D. performed AFM; S.L., J.L., Z.W. and W.X. performed cytotoxicity studies; D.Z. performed hemolysis studies; Y.Y. and B.C. performed SEM; S.L., Y.D., T.Z., P.O. and D.C. analyzed data; S.L. wrote the manuscript; P.C. edited the manuscript.

minimized hemolytic effect [27] and increased resistance to proteolytic degradation [215]. Strategies for conjugating cationic lytic peptides to tumor targeting moieties, such as antibodies [33] or "tumor-homing" domains [32, 132], also represent improvements in targeted therapy.

The development of stimuli-responsive nanodevices is an active area of current drug delivery research because these systems can enhance biological specificity by releasing drugs at the pathological site in response to local stimuli [36, 42]. Self-assembling peptides that undergo a conformational change in response to applied environmental stimuli, leading to disassembly or transition of nanostructures, can also be achieved through rational sequence design [216-219]. Recently, our group has proposed an Amino Acid Pairing (AAP) strategy for constructing the sequence of self-assembling peptides [73]. This design strategy aims to achieve complementary intermolecular affinity by alternatively arranging amino acids, whose side chains provide different types of paring interactions (e.g., ionic, hydrophobic and hydrogen bonding), along the peptide sequence. This complementarity can lead to a variety of self-assemblies, including stable β -sheet-rich fibrous nanostructures Spontaneous Assembly [67, 73]. Inspired by the finding that the cytotoxicity of PI3-SH3 and HypF-N proteins can be eliminated by the formation of fibrillar structures [220], we come up with the idea of using stimuli-responsive nanostructures as a "swtich" to control the activity of CLPs, which could allow CLPs to navigate and target themselves with minimal side effect. Based on this idea, we herein propose a self-guided strategy which incorporates three elements: (i) self-assembled nanostructure of CLPs to improve their stability in physiological environments (and hence pharmacokinetics), (ii) nanostructure formation as a "switch" to turn off the lytic activity of CLPs when circulating in the normal tissue, and (iii) disassembly of the nanostructure in response to environmental stimuli, which allows the "release" of lytic activity at the targeted site. We postulate that a stable nanostructure formed by CLP is the key reason for the elimination of lytic activity: the CLP monomers with lytic activity are entrapped in the nanostructure, hence, unable to insert into and disrupt cell membranes. The

AAP principle could be suitable to design a self-guided CLP by incorporating controllable charge repulsion.

To prove the concept of self-guided, transformable peptide design, we devise and examine a stimuli-responsive CLP, C8, which is found to self-assemble into β-sheet rich nanofibers or disassemble into unstructured monomers in response to changes in pH, temperature and the presence of urea. The resulting stimuli-responsive self-assembly properties of C8 is shown to derive nanostructure-dependent cytotoxicity, along with selective cytotoxicity towards cancerous cells, demonstrating its self-guided navigation towards both environmental and molecular/cellular targets. This self-guided strategy integrates the advantages of stimuli-responsive nanodevices and inherent selective activity of CLPs, offering a new route to explore more sophisticated CLPs.

5.2 Materials and methods

5.2.1 Sample preparation

C8 peptide was purchased from company (Canpeptide Inc., Montreal, Canada) with a purity of 95%. The procedure for peptide synthesis is briefly described in section 3.2.1. The peptides were dissolved in Mili-Q water to give 80 μM stock. In the hemolysis study, C8 aqueous solutions (430 μM) at pH 7.4 or pH 4.0 were prepared as stock solution 3 or 5 days before use. The pH of the peptide solution was adjusted using hydrogen chloride solution or sodium hydroxide solution. The final pH was in the range of ±0.05 to the targeted value.

5.2.2 Fluorescence spectroscopy

The intrinsic tryptophan fluorescence of C8 peptides was monitored on a QM4-SE spectrafluoremeter (PTI, London, Canada). The emission spectra of C8 peptides (λ_{ex} 280 nm)

were collected from 310 nm to 400 nm. The slit widths of excitation and emission were set at 2 nm and 8 nm, respectively.

5.2.3 Circular dichroism spectroscopy

The secondary structure of C8 peptides in solution was monitored by circular dichroism on a J-715 circular dichroism spectrometer (Jasco Europe, Cremella, Italy) using 1 mm quartz cells (Hellma, Concord, Canada). Spectra were collected from 190 nm to 260 nm with a 1 nm bandwidth and data pitch, 1 s response time and 100 nm min^{-1} scanning speed. All the spectra were averaged from two replicates and solvent absorbance was subtracted from the data. The mean residue molar ellipticity of C8 peptide presented here was calculated following the formulas: Ellipticity (θ in deg cm^2 $dmol^{-1}$) = (millidegrees × mean residue weight)/(path length in millimetres × concentration of C8 peptide in mg ml^{-1}).

5.2.4 Microscopy

The morphologies of C8 peptides at different environments were imaged on a Dimension Icon AFM (Bruker, Santa Barbara, USA). A 50 **μ**l of sample solution was mounted on a freshly cleaved mica surface (SPI, West Chester, USA). Following 15 min incubation, the mica was washed with 80 **μ**l Mili-Q water for 5 times. After drying, AFM imaging was performed at room temperature using peak force quantitative nanomechanical mapping (PF-QNM) mode. All images were acquired using a SCANASYST-AIR probe (Bruker, Santa Barbara, USA).

To prepare the cell samples for AFM or SEM, A549 cells were seeded on coverslips, which were placed into a 6-well plate containing 150,000 cells. The cells were incubated for 24 h at 37°C and 5% CO_2. After removing media, 1.5 ml media and 500 **μ**L of sample were added into each to make a final concentration of 5 **μ**M for sample at pH 4.0 and 20 **μ**M for sample at pH 7.4. Following 3 h incubation under the same condition, peptide solutions were removed, and then

cells were washed with 1 mL of PBS for fixation. The cell fixation protocol was described previously [12]. For AFM, the morphology of A549 cells was imaged using a Dimension Icon AFM (Bruker, Santa Barbara, USA) at room temperature. The MLCT probes consisting of silicon nitride cantilevers (nominal spring constant of 0.01 N/m) with silicon nitride tips (tip radius of around 20 nm) were used. Topography was imaged by contact mode with low deflection set point and scan rate is 0.5 Hz to minimize the disturbance during the scan process. For SEM, the coverslips were mounted on metal stubs using double-sided sticky conductive tape. Then, the cells were sputter coated with 10 nm gold and imaged in a ULTRA plus SEM (Zeiss, Jena, Germany).

5.2.5 Cell culture

Human umbilical vein endothelial cells (HUVEC), mouse fibroblast cell lines (NIH-3T3) and adherent cancer cell lines (A549, non-small lung carcinoma; U87MG, glioblastoma; and MCF-7, breast carcinoma) were purchased from ATCC (Manassas, USA). A549 cells were cultured in F-12 (Kaighn's modification) (F12K) media (HyClone Laboratories, Mississauga, Canada); MCF-7 cells and U87MG cells were cultured in MEM Eagles with Earle's Ballanced Salts (HyClone Laboratories, Mississauga, Canada); NIH-3T3 cells were cultured in Dulbecco's Modified Eagle's Medium (DMEM) (HyClone Laboratories, Mississauga, Canada); HUVEC cells were cultured in EGM-2 media (Lonza, Allendale, USA). All the media contained 10% fetal bovine serum (FBS) (Invitrogen, Burlington, Canada). An incubator (Thermo Scientific, Ottawa, Canada) was used to keep cells maintained at 37 °C and 5% CO_2.

5.2.6 MTS assay

A549 and HUVEC cells were seeded onto a 96-well plate at a density of 5000 cells per well, and MCF-7, U87MG and NIH-3T3 cells were seeded at a density of 10000 cells per well. A549,

MCF-7, U87MG and NIH-3T3 cells were incubated for 24 h before treatment, and HUVEC cells were incubated for 48 h before treatment. After the media was removed, 150**μ**L fresh media was added with 50 **μ**L of C8 peptide solution at pH 4 or pH 7.4 to reach final concentrations of 5, 10 and 20 **μ**M. Mili-Q water at pH 4 or pH 7.4 was added as 0 **μ**M samples. The untreated cells were used as a control of 100% viability. Following 24 h incubation, MTS assays were performed using a CellTiter 96® AQueous Kit (Promega, Madison, USA) according to the manfacturer's protocol. The absorbance was measured at 485 nm using a FLUOstar plate reader (BMG Labtech, Ortenberg, Germany).

5.2.7 Hemolysis study

The hemolysis assay was performed by using fresh rabbit ear venous blood obtained from a 2-year old female New Zealand White rabbit (Central Animal Facility, Waterloo, Canada). The rabbit ear venous blood was collected in K2EDTA anticoagulant tube (BD medical, Mississauga, Canada). The blood sample was centrifuged at 1500 rpm for 15 min and washed three times by adding Phosphate Buffered Saline (PBS). After washing, the red blood cells (RBC) were isolated and suspended in PBS to make a 5% hematocrit solution. Test samples were diluted and mixed with RBC suspensions to create a final mixture (1 ml) containing 1%RBC and various concentrations of samples. The red blood cells mixed with 1% triton X-100 (Sigma, Oakville, Canada) and DPBS solution (HyClone Laboratories, Mississauga, Canada) were used as positive and negative controls to obtain 100% and 0% hemolysis, respectively. The mixture were incubated in water bath at 37 °C for 2 h. The samples were centrifuged at 3000 rpm for 5 min to separate RBC precipitation. The supernatants were collected in a 96-well plate. The released hemoglobin was monitored at 540 nm using a FLUOstar plate reader (BMG Labtech, Ortenberg, Germany). The percentage of hemolysis was calculated using the following equation:

$$Hemolysis\% = \frac{Abs(sample) - Abs(-)}{Abs(+) - Abs(-)} \times 100$$

Where Abs (sample), Abs (+) and Abs (-) represent the absorbance of C8 treated samples, 100% hemolysis sample and 0% hemolysis sample, respectively. The animal studies followed the protocols approved by the University of Waterloo Office of Research Ethics and the Animal Care Committee.

5.3 Results and discussion

5.3.1 Peptide design

The model peptide C8 consists of five types of amino acid residues, isoleucine (I), asparagine (N), arginine (R), histidine (H) and tryptophan (W). According to the properties of the amino acid side chains, isoleucine residues and asparagine residues provide attractive hydrophobic interactions and hydrogen bonding, respectively; while positively charged arginine residues provide electrostatic repulsion and hydrogen bonding [73]. Histidine residues, whose side chains have a pK_a ~6, could provide either hydrogen bonding or electrostatic repulsion depending on their protonation status. Tryptophan residues provide hydrophobic interactions, hydrogen bonding and work as internal fluorescent indicators; their aromatic rings could also stabilize the self-assembled nanostructures via π-π stacking [73].

The arrangement of the amino acids follows two criteria, which provide lytic activity and stimuli-responsively self-assembling properties, respectively. First, the peptide should possess separated hydrophobic and hydrophilic faces when adopting an α-helical conformation in associate with phospholipid membranes, resulting in membrane lytic ability (Scheme 5.1.a). Second, according to the AAP principle[73], the amino acids that provide different types of interactions are alternatively arranged in the sequence, leading to paired side chain interactions, facilitating the stacking of the β-sheets in aqueous solution (Scheme 5.1.b). Including the backbone hydrogen bonding, the competitions between repulsive and attractive forces governs the

assembly behavior of C8 molecules, whether to self-assemble into β-sheet rich nanofibers or disassemble into unstructured monomers (Scheme 5.1.b).

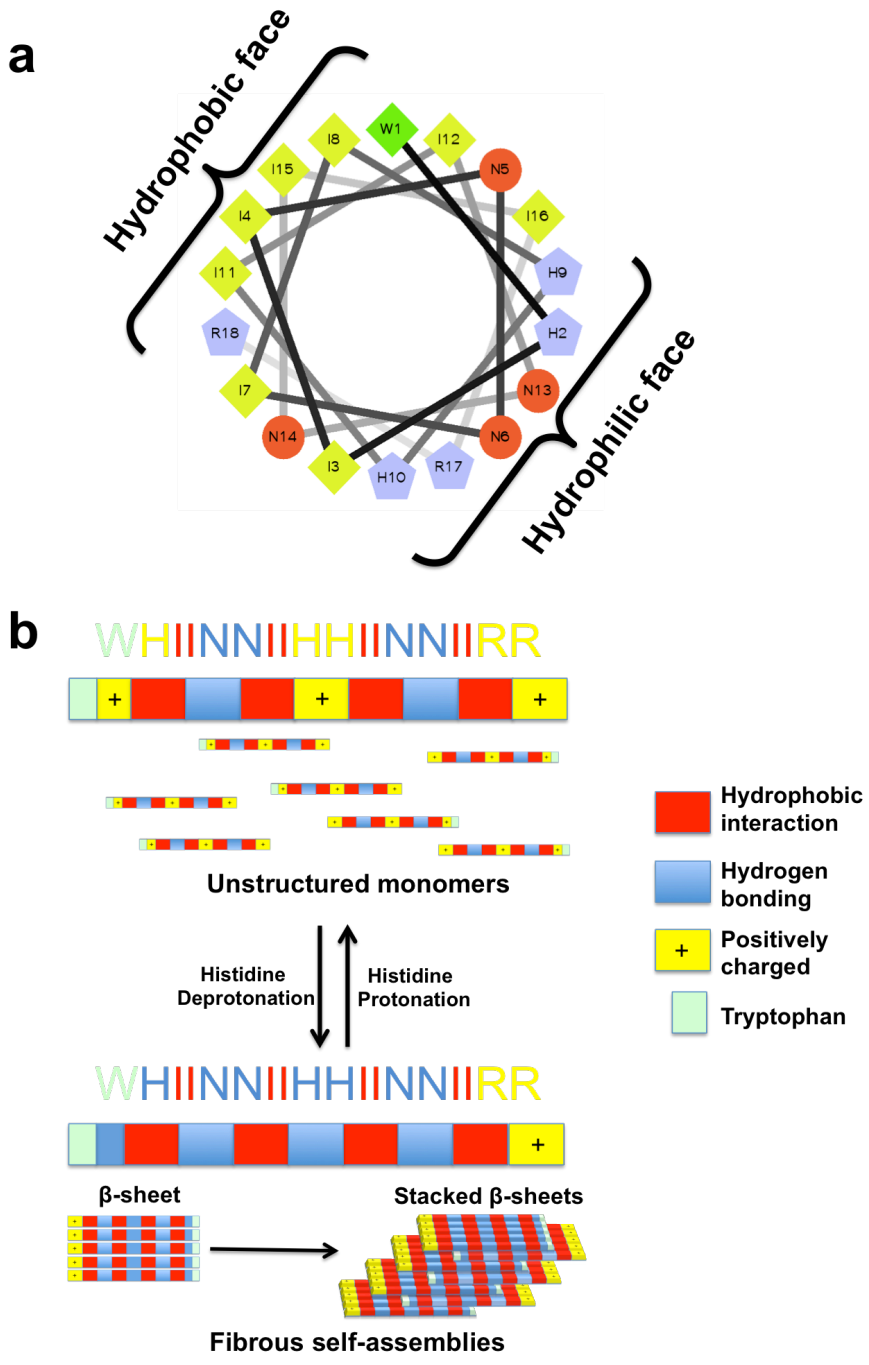

Scheme 5.1 Design of the model stimuli-responsive self-assembling CLP C8. (a) Helical wheel of C8. The charged amino acid residues are shown as light blue triangles, uncharged hydrophilic amino acid residues are shown as red circles, and hydrophobic amino acid residues are shown as

green diamonds. The amount of green decreases with the decreased hydrophobicity. (b) The mechanism of the intermolecular forces controlled self-assembly/disassembly of C8. The colors represent different types of forces provided by the side chains of amino acids. Depending on the protonation status of histidine residues, the overall intermolecular forces could become repulsive, leading to unstructured C8 monomers, or become attractive, leading to fibrous self-assemblies.

5.3.2 Self-assembly/disassembly of C8 in response to pH change

To verify the proposed self-assembling/disassembling behavior of C8, 80 μM C8 peptide was first prepared in aqueous solution at a pH of 8.0, where ~99% of histidine residues are supposed to be neutralized. The solution was incubated for 24 h at ambient temperature (22 ^{0}C). The secondary structure and morphology of the sample at pH 8.0 were determined by circular dichroism (CD) spectroscopy and atomic force microscopy (AFM). As shown in Figure 5.1.a, the spectrum had a negative peak at ~218 nm, indicating β-sheet conformation. The AFM image (Figure 5.1.c) confirmed the formation of fibrous networks [68]. Afterwards, the pH value of the sample was decreased to 4.0, where ~99% of the histidine residues were supposed to be protonated. The solution was incubated for another 24 h. The CD spectrum was recorded and showed that the C8 peptide at pH 4.0 became largely unstructured with a negative peak centered at ~200 nm. Furthermore, the AFM image (Figure 5.1.d) showed “melted” nanofiber networks with short and thin fibrils still existing. This self-assembling/disassembling process was reversible when the pH value was adjusted between 4.0 and 8.0.

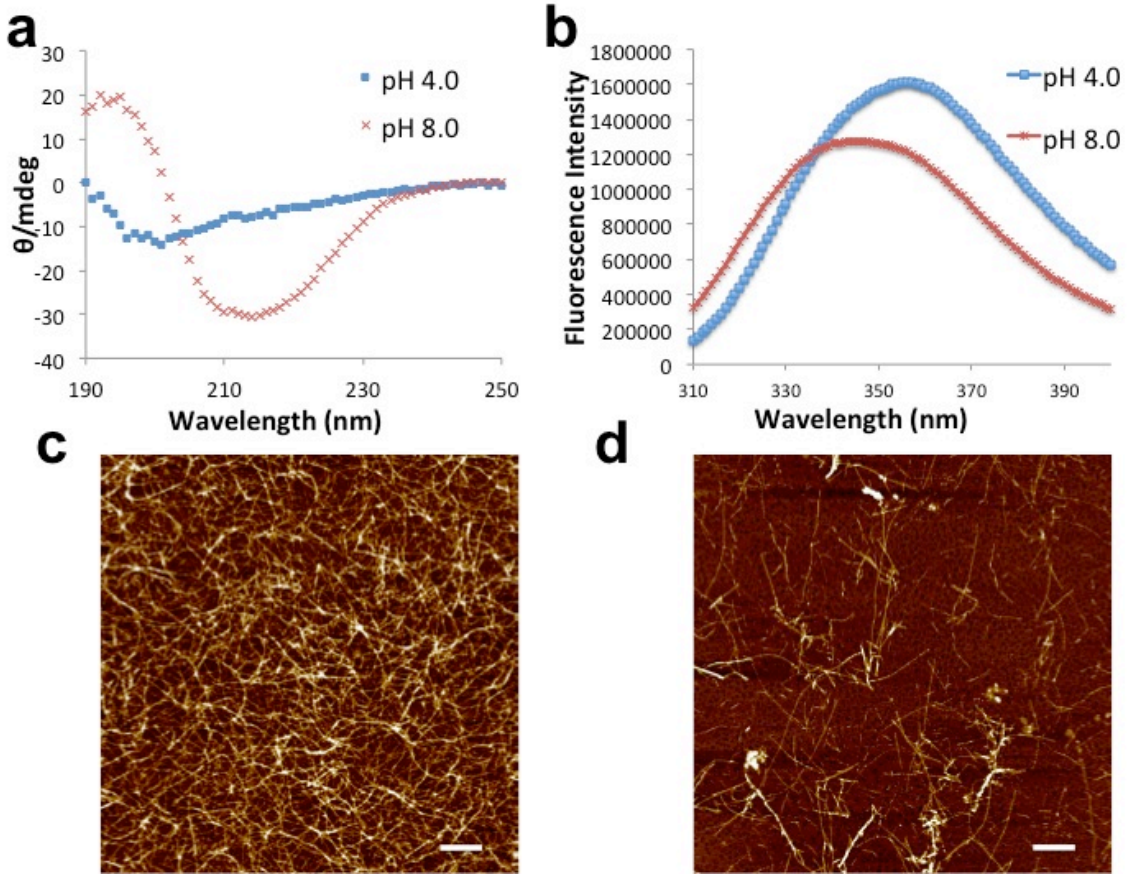

Figure 5.1 Characterization of the self-assembly and disassembly of C8. (a) circular dichroism spectra of C8 at pH 8.0 and at pH 4.0. (b) fluorescent emission of tryptophan residual of C8 at pH 8.0 and at pH 4.0. c-d, AFM images of C8 samples at pH 8.0 (c) and at pH 4.0 (d). The scale bar is 500 nm.

The intrinsic fluorescence emission of tryptophan in both samples at pH 4.0 and pH 8.0 were monitored. As shown in Figure 5.1.b, the fluorescent emission peak of tryptophan shifted from ~356 nm in sample at pH 4.0 to ~344 nm in sample at pH 8.0, indicating that tryptophan residues are located in a more hydrophobic environment when such peptides self-assembled into fibers [221]. This is consistent with our proposed mechanism of C8 self-assembly shown in Scheme 5.1.b, where the amino terminal tryptophan residues in C8 orient inside the hydrophobic core of the fibers while the C-terminal arginine residues remain exposed to water.

5.3.3 Temperature effect on reversible self-assembly/disassembly of C8

The reversible assembly of C8 was achieved through modulating intermolecular interactions,. To investigate further the effects of environmental stimuli on the intermolecular force balance, C8 peptide solutions (80 μM) were prepared at various pH values. These solutions were then either incubated at ambient temperature (22 ^{0}C) or at 0 ^{0}C on ice for 2 days, or heated at 37 ^{0}C for 6 h. The obtained secondary structure information showed that, at 0 ^{0}C, C8 peptides were unstructured when the environmental pH was lower than 5.4. When the pH increased to 5.8 and above, β-sheet became dominant conformation (Figure 5.2.a). In comparison, when the temperature increased to 22^{0}C, the CD spectrum of the C8 peptide started to gain β-sheet content (minima at 218 nm) at pH 5.2 and became dominant β-sheet at pH 5.4 (Figure 5.2.b). The heated C8 samples underwent a secondary structure transition at pH 5.0 (Figure 5.2.c). This tendency indicated that, with increased temperature, C8 molecules needed more charged histidine residues to compete the attractive forces. Hence, the overall effect of increasing temperature enhances the attractive forces.

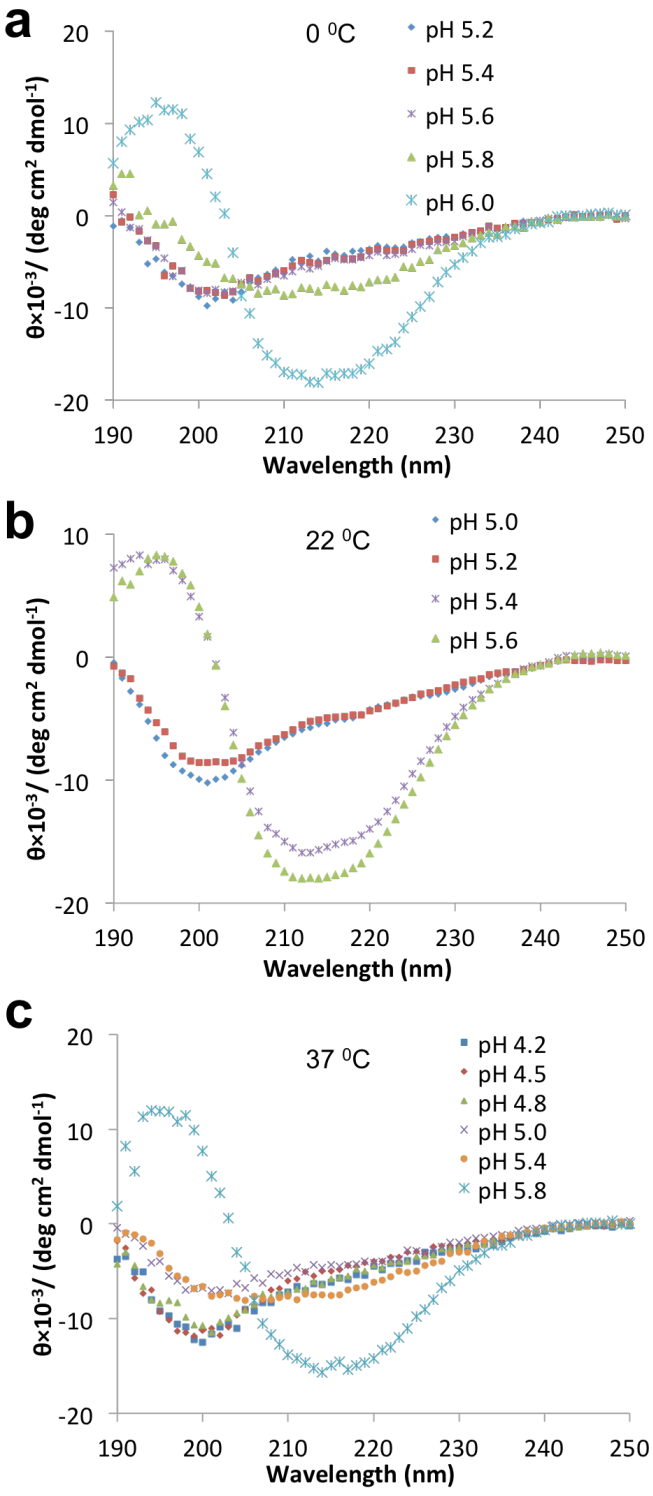

Figure 5.2 Secondary structures of C8 at various conditions. a-c, circular dichroism spectra of C8 at various pHs after incubation at 0 ^{0}C (a), 22 ^{0}C (b) and 37 ^{0}C (c), respectively.

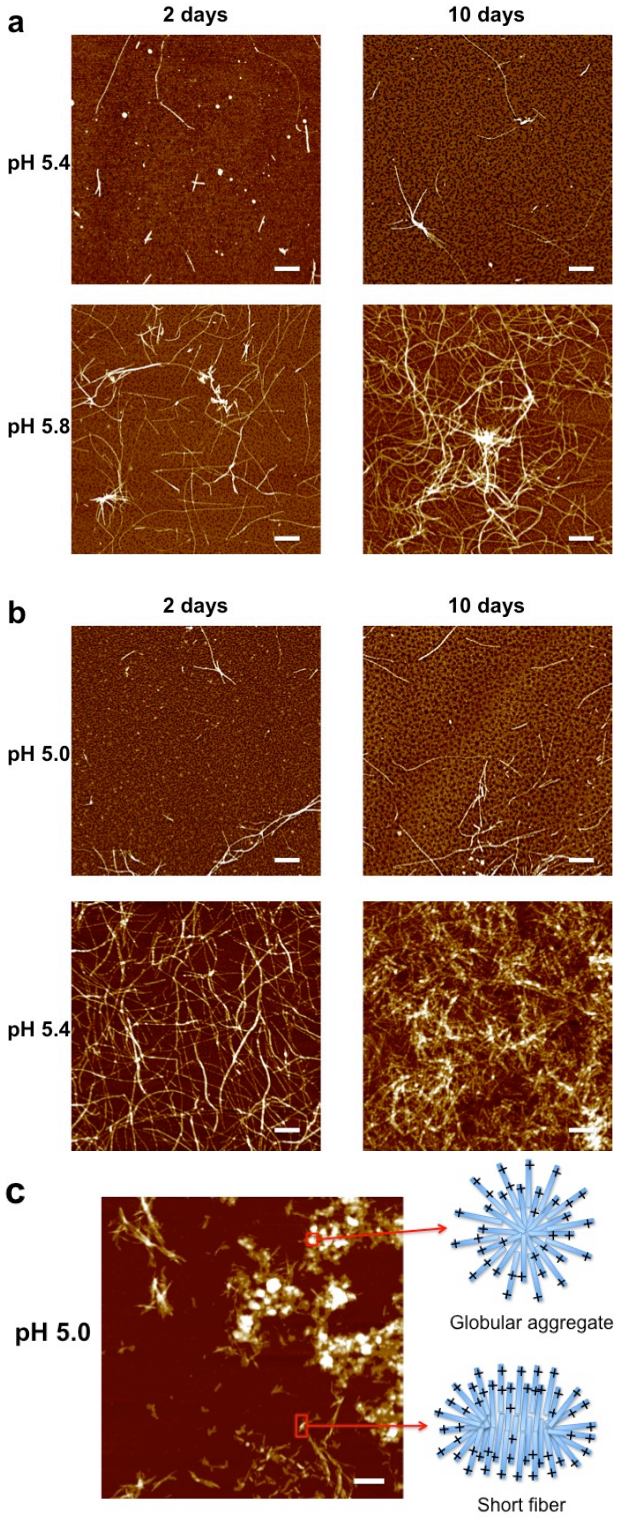

Figure 5.3 AFM images of C8 samples at various conditions. (a) C8 at pH 5.4 and at pH 5.8 incubated at 0 ^{0}C for 2 d and 10 d, respectively. (b) C8 at pH 5.0 and at pH 5.4 incubated at 22 ^{0}C for 2 d and 10 d, respectively. (c) C8 at pH 5.0 incubated at 37 ^{0}C for 6 h. The scale bar is 500 nm.

To match the secondary structure with their corresponding nanostructures, AFM images of samples at pH 5.4 and pH 5.8 at 0 ^{0}C, and samples at pH 5.0 and pH 5.4 at 22 ^{0}C were obtained after 2 d and 10 d incubation, respectively (Figure 5.3.a-b). For the dominantly unstructured samples, they seldom contained nanofibers even after 10 d incubation, while the samples showing β-sheet conformations formed abundant nanofibers after 2 d incubation. Interestingly, the heated C8 peptides at pH 5.0 appeared as short fibers and globular aggregates (Figure 5.3.c). Our explanation is that, as tryptophan is very hydrophobic, the enhanced hydrophobic interaction would make the tryptophan-terminus of C8 interact tightly, while due to the weakened hydrogen bonding and repulsions from protonated histidine residues, the peptide chains may stack in a less compact arrangement, resulting in the breakage of long fibers and the formation of spherical micelles, eventually growing into large aggregates (illustrated in Figure 5.3.c).

To investigate the temperature effect on the rate of self-assembly and disassembly of C8 peptides, we also performed dynamic studies using AFM. C8 samples at pH 8.0 were first prepared from the same C8 sample at pH 4.0, and then incubated at 0 ^{0}C, 22 ^{0}C or 37 ^{0}C. The process of the nanofiber formation was imaged over time. As shown in Figure 5.4, C8 peptides started to form mature fibers after 1 d at 0 ^{0}C, and required 4 d to grow into condensed fiber networks. With increased temperatures, only 1 d was needed to form the condensed fiber networks for 22 ^{0}C, and only 3 h for 37 ^{0}C, indicating that higher temperatures could promote the rate of self-assembly. Since the higher temperature enhances the overall attractive forces, it is essentially the intermolecular forces that control the self-assembly rate. This trend could also be seen from the self-assembly rates of the sample at pH 5.8 at 0 ^{0}C and the sample at pH 5.4 at 22 ^{0}C (Figure 5.3 a-b). Although they formed nanofibers, the required incubation time was quite long due to the low overall attractive intermolecular forces. Additionally, the long fibers formed in the sample at pH 8.0 at 37 ^{0}C become short after 9 h incubation, which may also result from the enhanced hydrophobic interaction and the weaken hydrogen bonding as discussed above.

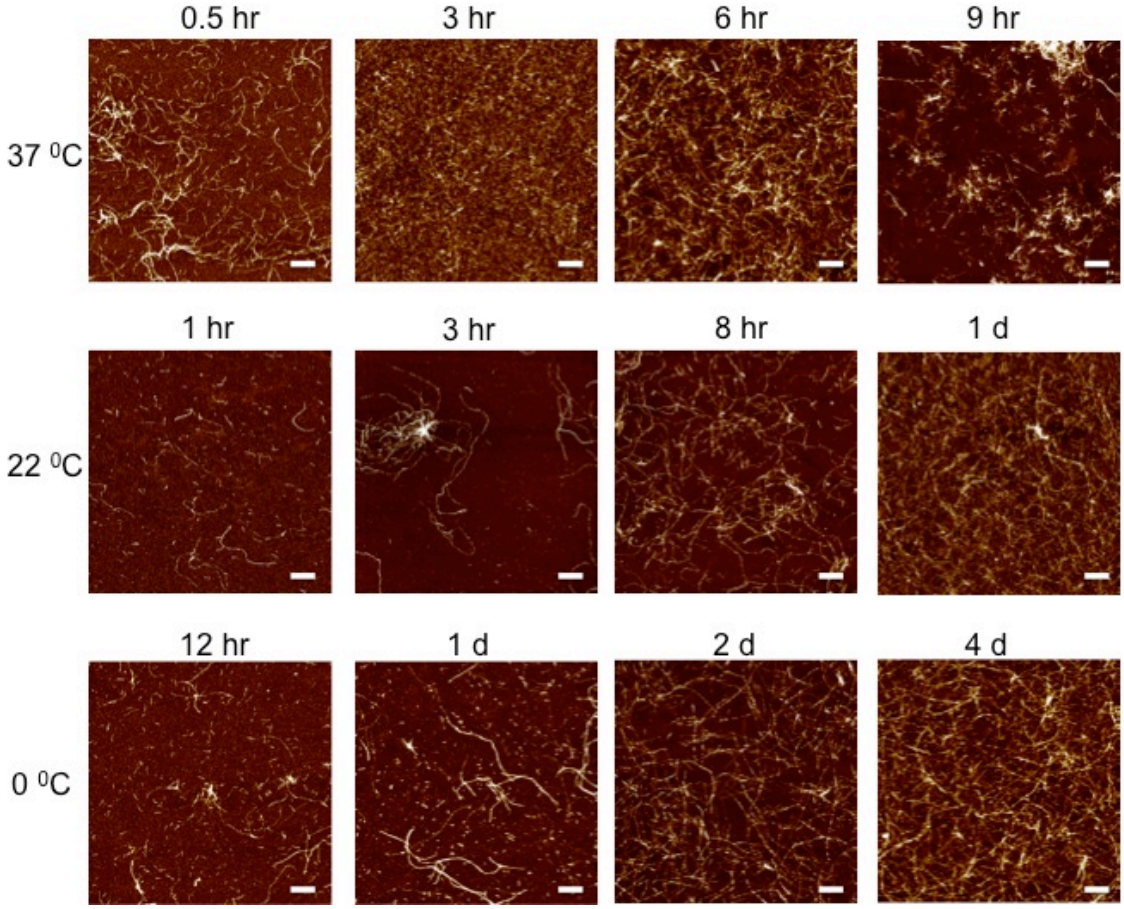

Figure 5.4 Imaging the self-assembling process of C8 by AFM.The sample at pH 8.0 incubated at 0 ^{0}C was imaged at 12 hours, 1day, 2 days and 4 days, respectively, after pH adjustment; 1 hour, 3 hours, 8 hours and 1day were chosen for the sample incubated at 22 ^{0}C; and 0.5 hour, 3 hours, 6 hours and 9 hours were chosen for the samples incubated at 37 ^{0}C. The scale bar is 500 nm.

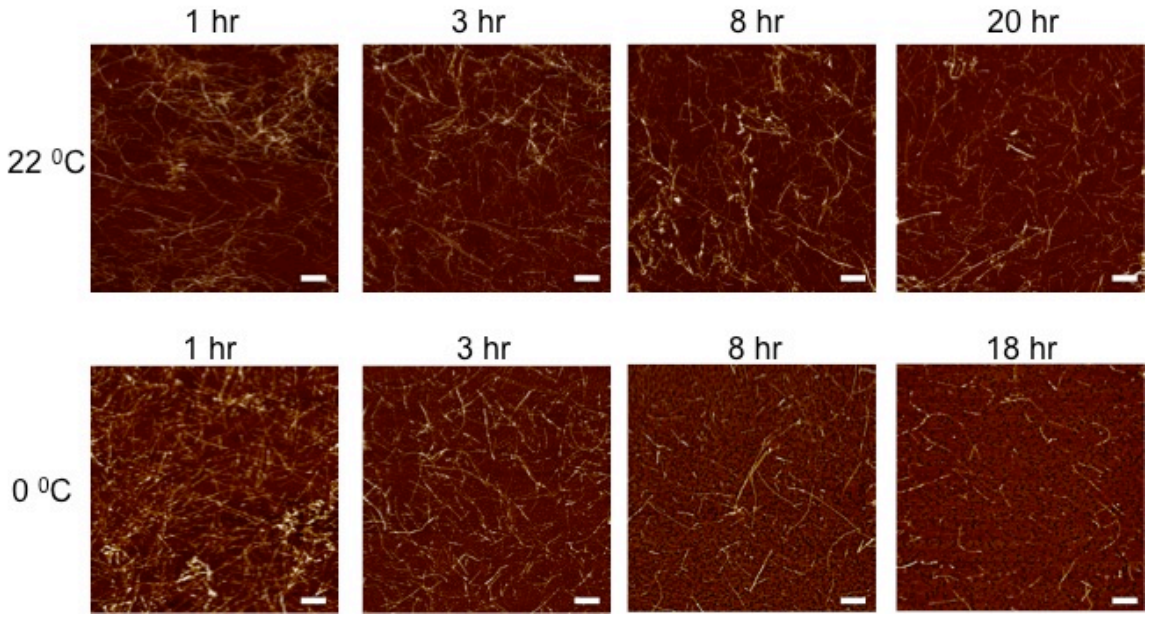

Figure 5.5 Imaging the disassembling process of C8 by AFM. The sample at pH 8.0 incubated at 0 ^{0}C was imaged at 1 hour, 3 hours, 8 hours and 18 hours, respectively, after pH adjustment to pH 4.0; 1 hour, 3 hours, 8 hours and 20 hours were chosen for the sample incubated at 22 ^{0}C. The scale bar is 500 nm.

In the disassembly process, the C8 samples at pH 8.0 with condensed fiber networks were acidified to pH 4.0 and imaged at 0 ^{0}C and 22 ^{0}C, respectively. As shown in Figure 5.5, the condensed fiber networks "melted" within 3 h at both temperatures. However, it seemed that a lower temperature could facilitate the melting of short fiber fragments from the fiber network, as the sample at 0 ^{0}C contained much less short fiber fragments when compared to the sample at 22 ^{0}C. We did not perform the dynamic study for 37 ^{0}C because high temperature also caused the breakage of long fibers, which made it hard to identify the degree of disassembly. The AFM image of the sample at 37 ^{0}C with 1 d incubation after the pH was adjusted to 4.0 was still taken, and showed that abundant short fibers still existed (Figure 5.6.a). This may also indicate that high temperature is not favorable to the disassembling process. Furthermore, another sample at 37 ^{0}C was further acidified to pH 3.0 and was found to disassemble more after 6 h incubation (Figure 5.6.b). Regarding this observation, we suggest two possible reasons: i) the formation of stable

nanofibers need overwhelming repulsive forces to diminish, and ii) the formation of the nanostructures may cause the pK_a of histidine residues shift to a lower value, hence the histdine residues are not fully protonated at pH 4.0, resulting in insufficient repulsive forces. These factors should be taken into account in designing stimuli-responsive peptides that disassemble at a specific pH value.

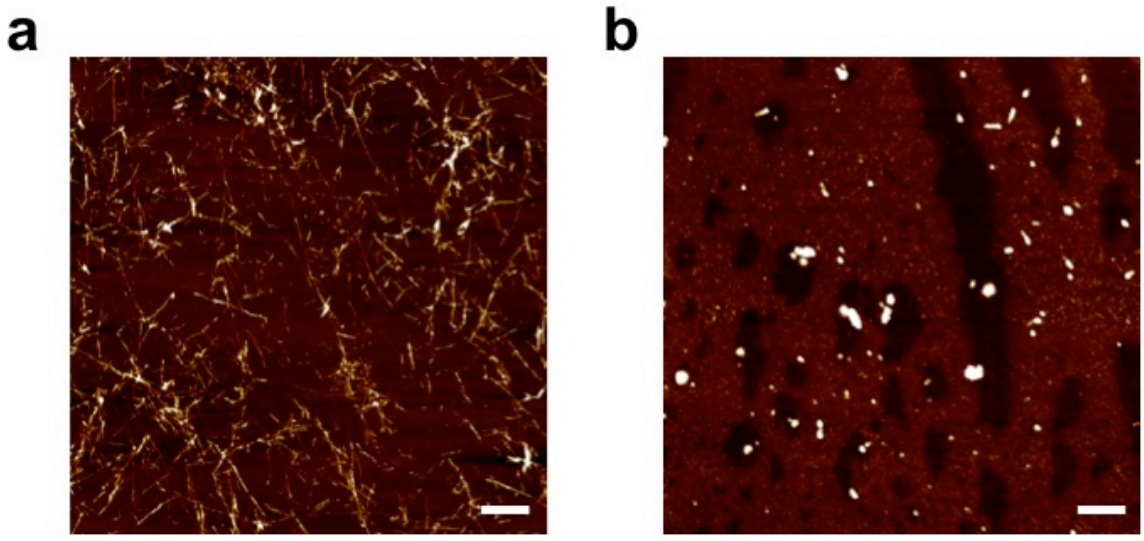

Figure 5.6 The morphology of C8 samples at pH 4.0 (a) after 1 d incubation at 37 ^{0}C and that at pH 3.0 (b) after 6 h incubation at 37 ^{0}C. Both samples are made from C8 sample at pH 8.0 with 1 d incubation at 37 ^{0}C. The scale bar is 500 nm.

5.3.4 Effect of urea on self-assembly of C8

As urea is known to unfold proteins by "breaking" hydrogen bonding, we added 20 mM urea into a C8 sample (80 μM) with a final pH of 6.0 and incubated it at 0 ^{0}C. After 2 d incubation, the sample showed a considerable content of β-sheet conformation, but not as high as that of the sample at the same conditions without urea (Figure 5.7.a). This may indicate a decreased self-assembly rate in the presence of urea. The AFM image confirmed the fiber formation of the urea added sample (2 d incubation); however, unlike the samples without urea, the fibers did not grow

to long fiber networks after 10 d incubation (shown in Figure 5.7.b), which may suggest that hydrogen bonds play an important role in the fiber growth and network formation.

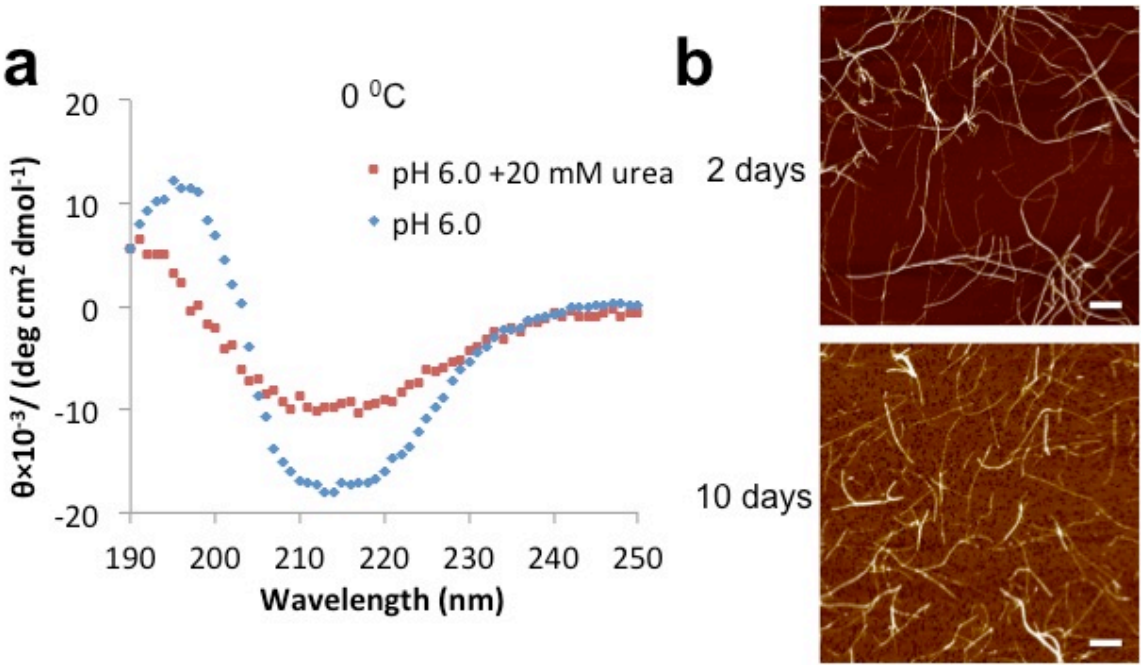

Figure 5.7 Characterization of C8 with the presence of urea. (a) Circular dichroism spectra of C8 at pH 6.0 with the presence of 20 mM urea after 2 d incubation. The CD spectra of C8 (pH 6.0) without urea was taken from Figure 5.2.a. (b) AFM images of the sample after 2 d o f incubation and 10 d incubation, respectively. The scale bar is 500 nm.

5.3.5 Estimation of force contributions

We have shown that increasing temperature enhanced the overall attractive forces in the case of C8 peptide. Knowing the significance of the enhancement induced by increased temperature could benefit the design of the next generation of self-guided CLPs with refined thermo-responsive properties. The secondary structure information shown in Figure 5.2 indicates that, with increased temperature, more protonated histidine residues are needed to counter the enhanced attractive forces to maintain C8 unstructured in solution. The percentage of protonated histidine residues at a specific pH can be estimated from Henderson-Hasselbalch equation.

Therefore, by knowing the pH values where the equilibrium of intermolecular forces composed of repulsive and attractive forces is reached at different temperatures, we may estimate the temperature-induced changes of forces relative to the side chain interactions provided by the amino acids. In our estimation, the highest pH value before a significant increase in the molar ellipticity at 200 nm occurs (Figure 5.2) was adopted as the point closest to the equilibrium of the repulsive forces and attractive forces: pH 5.6, pH 5.2 and pH 4.8 were selected for 0 ^{0}C, 22 ^{0}C and 37 ^{0}C, respectively. Substituting the concentrations of H^+, which correspond to each pH value, into Henderson-Hasselbalch equation: $pH = pK_a + log_{10}(\frac{[deprotonated\ histidine]}{[protonated\ histidine]})$ (a K_a of 10^{-6} was used in the calculation), we can obtain that ~72% histidine residues are protonated at pH 5.6, while ~86% and ~94% for pH 5.2 and pH 4.8, respectively. At these pHs, the repulsive forces provided by the side chains of arginine (E_R) and protonated histidine (E_H) are considered to be at the same level as the major attractive forces involving hydrogen bonding provided by the side chains of asparagine (HB_N), arginine (HB_R), tryptophan (HB_W) and deprotonated histidine (HB_H) (protonated histidine residue only serves as hydrogen donor [73], its contribution on hydrogen bonding is not counted in our estimation), along with hydrophobic interactions provided by the side chains of isoleusine (H_I) and tryptophan (H_W), as well as the peptide backbone hydrogen bonds (BHB). According to the ratio of each amino acid in C8, we obtain the balances between repulsive and attractive forces at each temperature as follow,

0 ^{0}C: $2E_R + (72\% \times 3\ or\ 2.16)E_H \approx 8H_I + H_W + 4HB_N + 2HB_R + HB_W + (28\% \times 3\ or\ 0.84)HB_H + BHB$ Eq. 5.1

22 ^{0}C: $2E_R + (86\% \times 3\ or\ 2.58)E_H \approx 8H_I + H_W + 4HB_N + 2HB_R + HB_W + (14\% \times 3\ or\ 0.42)HB_H + BHB + f_T$ Eq. 5.2

37 ^{0}C: $2E_R + (94\% \times 3\ or\ 2.82)E_H \approx 8H_I + H_W + 4HB_N + 2HB_R + HB_W + (6\% \times 3\ or\ 0.18)HB_H + BHB + f_T$ Eq. 5.3

In the balances, the symbols represent the strength of each type of force at 0 ^{0}C. The overall change in the strength of hydrogen bonding and hydrophobic interactions induced by increasing

temperature is denoted as f_T. The impact of temperature-induced force enhancement on individual C8 molecule from 0 ^{0}C to 22 ^{0}C could be estimated as $(0.42E_H + 0.42HB_H)$, or $0.019(E_H + HB_H)/^0$C, by subtracting balance (5.1) from balance (5.2). The estimation for the enhanced attractive interactions from 0 ^{0}C to 37 ^{0}C is obtained as $(0.66E_H + 0.66HB_H)$, or $0.018(E_H + HB_H)/^0$C, by subtracting balance (5.1) from balance (5.3). The two numbers are not significantly different from each other, which may suggest the impact of temperature changes linearly with the change in temperature. However, due to the low accuracy of the estimation, a solid, accurate conclusion cannot be made. The estimation also indicates that the impact of temperature is not strong. Since electrostatic interaction is normally stronger than hydrogen bonding, the enhancement on attractive forces induced by increased temperature (up to 37 ^{0}C) could be easily countered by adding one or two more positively charged amino acids in the C8 sequence.

According to the ratio of different amino acids in C8 sequence, it suggests that If we further approximate the same type of interaction from different amino acid residues as one identical force contribution (E denotes electrostatic force, H denotes hydrophobic interaction and HB denotes hydrogen bonding contributed by one amino acid side chain, respectively), from balance (5.1), it can be estimated that $4.16E \approx 9H + 7.84HB + BHB$ or $E \approx 2.16H + 1.88HB + 0.24BHB$. This information can be used to adjust the stimuli-responsive properties of self-guided CLP using C8 as design template. For example, we could expect that adding one more arginine residues and two more isoleucine residues in C8 sequence allow the peptide to self-assemble at higher pH when compare to C8, because extra repulsion is induced rather than attractive force.

5.3.6 Nanostructure-dependent lytic action of C8

In the process of CLP induced membrane disruption, the insertion of the peptide into lipids is a required step. According to our assumption, the stable β-sheet fiberous structure of C8 will

limit its building blocks to attack cell membranes (there are free monomers, but the concentration is not high enough to cause damage), resulting in limited or even zero toxicity. This safe nanostructured C8 is supposed to be the delivery vehicle, and when it reaches the target, the fibers could disassemble into monomeric membrane disruptors and execute the therapeutic function, achieving the targeted therapy. To prove the self-guided delivery strategy, the lytic action of C8 at both pH 7.4 and pH 4.0 (prepared by acidifying the sample at pH 7.4, 0 ^{0}C) was evaluated for low pH targeting. Although the unstructured C8 peptides would start to self-assemble when added into culture media (pH 7.4), the monomers could bind to cell membranes and lyse them before they form stable nanostructures. As expected, the proliferation of A549 (non-small cell lung carcinoma) cells was severely inhibited by the sample at pH 4.0 (unstructured); C8 at the concentration of 20 μM kills almost all the cells, and still reduced the number of cells by more than 60% at a low concentration of 5 μM. In contrast, C8 at pH 7.4 does not inhibit, but even slightly enhances the growth of the cells (Figure 5.8.a), which may be due to the formation of fiber networks [222, 223]. Besides the nanostructure formation, increasing pH also reduces the net positive charges on the C8 molecules, which may also be one possible reason for the "turn-off" of lytic action. To determine whether the lytic action of C8 is positive charge-dependent or nanostructure-dependent as we proposed, the lytic action of the sample at pH 5.4 prepared both at 0 ^{0}C and at 37 ^{0}C was tested. Supposedly, the two samples have the same net positive charge level, but one is unstructured at 0 ^{0}C and one forms β-sheet based nanostructures at 37 ^{0}C (Figure 5.2 a,c); and the results show that the 0 ^{0}C sample still maintained activity; in contrast, the 37 ^{0}C sample lost its lytic action (Figure 5.9), suggesting that the formation of nanostructure is the "switch" that controls the ability of membrane disruption of C8. We also observed that samples at pH 7.4 were still effective against the cancer cells before the condensed fiber networks formed (data is not shown), which could also support our hypothesis here.

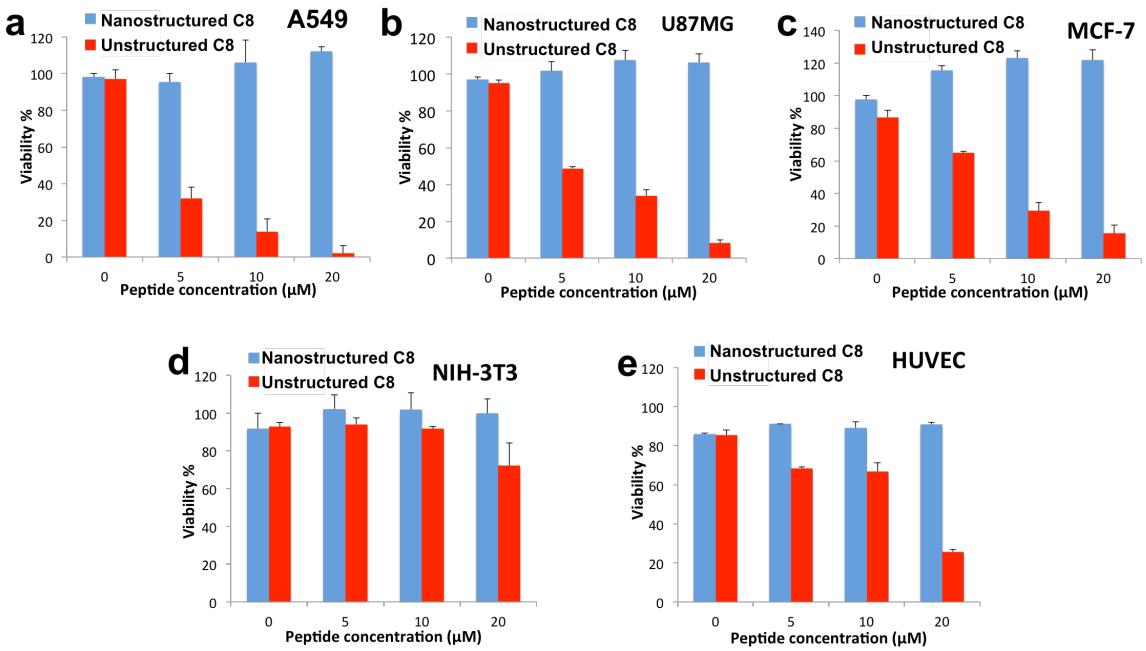

Figure 5.8 Evaluation of the cytotoxicity and hemolytic effect of nanostructured and unstructured C8 samples. a-e, viabilities of cancerous cell lines: A549 (a), U87MG (b), MCF-7 (c) and non-cancerous cell lines: NIH-3T3 (d), HUVEC (e) after 1 day treatment of C8 at pH 7.4 or C8 at pH 4.0. The data are averaged from at least three independent replicates. The standard deviations are shown as error bars.

Two other cancer cell lines, U87MG (glioblastoma) and MCF-7 (breast carcinoma), were also used to test the broad-spectrum anticancer activity of C8 peptide. Similar to the results on the A549 cell line, the C8 sample at pH 7.4 slightly promotes the growth of the cancer cells, and the C8 sample at pH 4.0 kills the cancer cells effectively (Figure 5.8.b-c). However, it seems that U87MG and MCF-7 are less sensitive to C8 than A549, evidenced by the higher viabilities after treatments with different concentrations of C8 samples at pH 4.0 than that of A549.

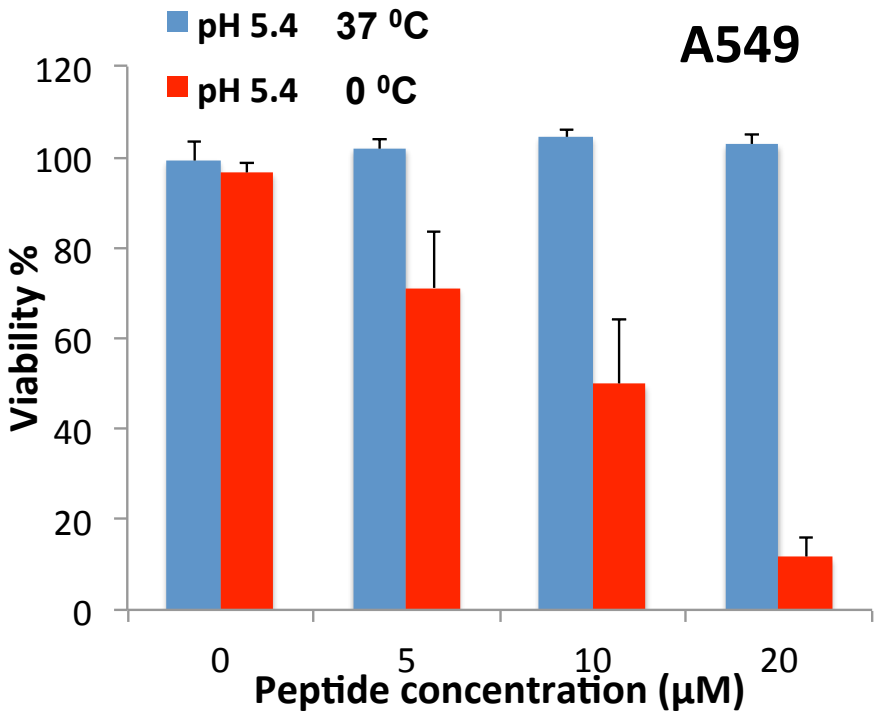

Figure 5.9 The viabilities of A549 cells treated with C8 pH 5.4 samples prepared by incubating the solutions at 0 ^{0}C or at 37 ^{0}C for 10 h. The data are averaged from three independent replicates. The standard deviations are shown as error bars.

The inherent selective lytic activity of C8 was investigated using two non-cancerous cell lines, NIH-3T3 (fibroblast) and HUVEC (Human Umbilical Vein Endothelial Cells). As shown in Figure 5.8.d, almost 70% of NIH-3T3 cells were still alive even when they were treated with 20 μM of C8 sample at pH 4.0, suggesting that NIH-3T3 was only slightly susceptible to the lytic action of C8. In the case of HUVEC cells, the viability was ~25% after treatment with C8 (20 μM) at pH 4.0, and the viabilities were ~70% for those treated with 10 μM and 5 μM of C8 samples at pH 4.0 (Figure 5.8.e), also showing that the activity of C8 pH 4.0 samples towards HUVEC cells was less than that towards cancerous cells. Probably due to the fragility of HUVEC cells, the cells treated with water at pH 4.0 only showed ~85% viability. Taking this into account, the lytic activity of C8 could be more limited towards HUVEC than it appeared in Figure 5.8.e. The C8 sample at pH 7.4 also did not show lytic action towards non-cancerous cells.

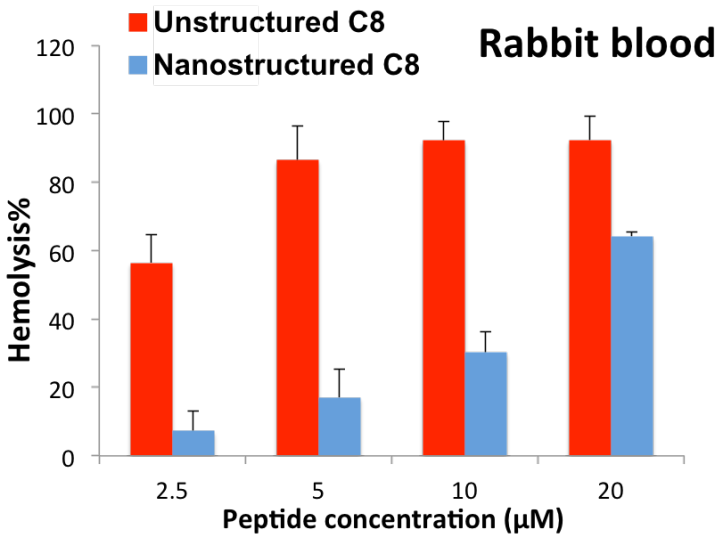

Figure 5.10 The hemolysis induced by C8 at pH 7.4 and C8 at pH 4.0 on rabbit red blood cells, respectively. The data are averaged from three independent replicates. The standard deviations are shown as error bars.

Except for "turning off" the lytic action of C8, the formation of nanostructures may also limit the hemolytic effect of CLPs [224]. To further investigate this potential, the hemolysis of rabbit red blood was evaluated after incubation with C8 samples at both pH 4.0 and pH 7.4. The results showed that the hemolytic effect of C8 has been significantly reduced at pH 7.4 (Figure 5.10). We also tested a 15 day-old pH 7.4 sample, which induced less than 10% hemolysis at the concentration of 20 μM (data is not shown). This suggests that the nanostructure formation could also control the hemolytic activity of C8 to a relatively low level, which requires peptide monomers to form mature nanofibers completely.

To visualize the membrane disruption, SEM and AFM were used to monitor the surface morphology changes of the A549 cells before and after peptide treatment. The representative SEM images of untreated cells, and cells treated with C8 samples at both of pH 7.4 and pH 4.0 (3 h incubation) were shown in Figure 5.10.a-c, respectively. The untreated cells and the cells treated with the sample at pH 7.4 exhibited an intact cell membrane with a smooth surface. On the other hand, the cells treated with the sample at pH 4.0 showed rough and porous cell

membrane surfaces, indicating that the cell membranes were disrupted. The AFM images showed the same observations (Figure 5.10.d-f).

Our study has shown the potential of controlling the lytic activity of C8 by the formation of nanostructures in a pH dependent way, which demonstrates the potential of targeting the acidic tumor microenvironment. Furthermore, the environmental stimuli-triggered lytic action combined with the inherent selectivity of CLPs could further enhance the specificity of lytic peptide-based drugs, along with a reduced hemolytic effect, resulting in minimal side effect. Additionally, since most of the CLPs are unstructured in aqueous solution, the formation of nanoparticles may also benefit from the enhanced permeability and retention (EPR) effect and elongated blood circulation time [39, 225]. The application is not just limited to cancer therapy, but could also be used to target acidophilic bacteria [226]. As shown previously, the self-assembling/disassembling behavior of C8 can be affected by various environmental stimuli. Therefore, other than pH, temperature and urea concentrations can also be the targeted stimuli, depending on applications. Our semi-quantitative estimates of the forces and temperature effect will help in designing CLP peptides for specific microenvironment targeting.

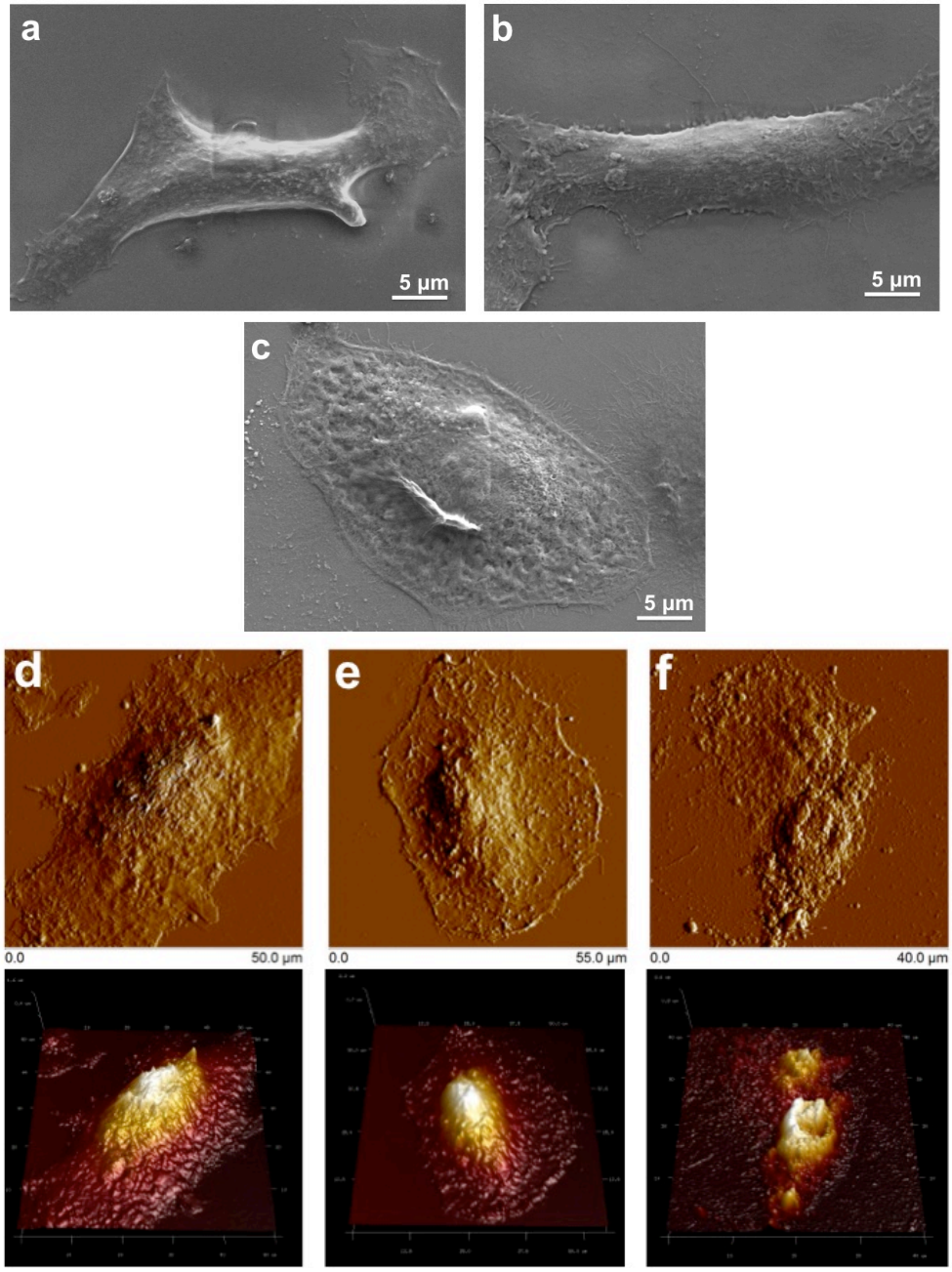

Figure 5.11 Visualization of morphologies of A549 cells before and after incubation with nanostructured or unstructured C8. a-f, SEM images (a-c) and deflection images associated with corresponding reconstructed 3-D images (d-f) of non-treated A549 cells (a,d) and A549 cells after incubation with 20 µM C8 at pH 7.4 (b,e) or with 5 µM C8 at pH 4.0 (c,f) for 3 hours, respectively.

In principle, our strategy is flexible enough to work with current strategies (adopting D-amino acids and conjugating with targeting moieties) for peptide design, which may add to the

potency of drugs in clinical usage. It is also possible for the stimuli-responsive CLPs to deliver and release chemotherapeutic agents at targeted sites. As CLPs could act synergistically with chemotherapeutic agents [27], in this delivery system, except for the roles of carrier and drug, the peptides may provide functionality in promoting the efficacy of the delivered chemotherapeutic agent.

5.4 Conclusions

We have successfully designed a stimuli-responsive cationic lytic peptide, C8, following our AAP principle. The model peptide can self-assemble into β-sheet rich nanofibers and disassemble into unstructured monomers, a transition that can be modulated by the equilibrium of intermolecular forces composed of repulsive electrostatic forces and attractive hydrogen bonding and hydrophobic interactions. The designed peptide shows triple-responsiveness towards pH, temperature and urea concentration, which influences the different types of intermolecular interactions seen for C8. The relative strength of repulsive forces and attractive forces, as well as the overall effect of temperature on the hydrophobic interaction and hydrogen bonding, was estimated, which could benefit the design of the next generation of stimuli-responsive peptides. The nanostructure-dependent lytic activity of C8 is tested *in vitro*, demonstrating the potential of self-guided delivery of stimuli-responsive, therapeutic CLPs. Along with the inherent selective toxicity of the cationic peptide itself, stimuli-responsive CLPs may further minimize side effects. We believe that our strategy opens a new path for developing CLP-based drugs with this study providing a basis for designing simuli-responsive CLPs that respond to targeted microenvironments.

Chapter 6*

pH-responsive Cationic Lytic Peptide for Synergistic, Selective and On-demand Delivery

6.1 Introduction

Nanotechnology offers tremendous possibilities for drug delivery systems to overcome the adverse side effects of conventional chemotherapeutics and enhance their anticancer activity[37]. Nanoscale drug delivery systems with size range of 10-100 nm can accumulate in tumor regions via the enhanced permeability and retention effect (EPR) [211, 227]. Except for the passive targeting, strategies using targeting ligands that aim at overexpressed receptors on cancer cell surfaces were reported to have promising results [41, 228, 229]. Stimuli-responsive systems provide another attractive alternative for on-demand delivery. Unlike ligands that target the surface traits of cancer cells, on-demand delivery systems react to external stimuli, such as temperature [154, 203], pH [163], or extracellular up-regulated enzymes [49] and release loaded drugs in a controlled manner.

Peptides are a promising class of molecules for bio-application owing to their bio-functionalities, potential biocompatibility, and design flexibilities. Peptides that self-assemble into micelles [230], vesicles [174] or fibrous structures [73] were designed and their potentials in

* This chapter is based on a manuscript "S. Lu, D. Bennett, H. Fan, Y. Ding, P. Long, M. Karttunen, P.Chen, pH-responsive Cationic Lytic Peptide for Synergistic, Selective and On-demand Delivery" H. Fan is collaborator from University of Toronto, D. Bennett and M. Karttunen are collaborators from University of Waterloo.
Author contribution: S.L. conceived idea and designed experiments; H.F. performed liposome leakage studies; D.B. performed MD simulations; S.L. performed *in vitro* characterization experiments; Y.D. performed AFM; S.L., P.L. performed cytotoxicity studies; S.L. and D.B. analyzed data; S.L. and D.B. wrote the manuscript; M.K. and P.C. edited the manuscript.

drug delivery has now been demonstrated. Aside from acting as drug carriers, peptides can also act as anti-cancer drugs themselves. Many natural antimicrobial peptides (AMPs) and synthetic cationic lytic peptides (CLPs) have shown activity against cancer cells by disrupting the integrity of cytoplasmic membranes (necrosis) or by depolarizing mitochondrial membranes (apoptosis) [6]. These peptides exhibit selective activity towards cancerous cells, which render them superior to conventional chemotherapeutics. This selective activity is generally attributed to the electrostatic interaction between the positive charges of the peptides and the negatively charged cancerous cell surfaces [6, 12]. However, the detailed mechanism of the selectivity is still not understood in detail. This knowledge is crucial to improve the selectivity of these peptides towards targeted cells or cell membranes.

We have reported a stimuli-responsive CLP, C8 (n-WHIINNIIHHIINNIIRR-c), which can self-assemble into β-sheet rich nanofibers or disassemble into unstructured monomers in response to changes in pH and temperature (reported in chapter 5). The formation of nanostructure works as the "switch" to control the lytic activity: the nanofibers are not toxic while the unstructured monomers or oligomers are membrane-active. According to the nanostructure-dependent membrane lytic activity, we proposed a "self-guided" strategy for CLPs. Here, we use C8 as a carrier for a model anticancer drug, ellipticine (EPT), to introduce a new method for drug delivery. This system holds several advantages when compared to conventional delivery systems. First, the drug carrier vehicle is also a drug, which participates in inhibiting the proliferation of cancer cells, enhancing the efficacy of the drug delivery system; furthermore, a synergistic effect is also found between active C8 and delivered EPT. Second, the stimuli-responsive property of C8 allows the drug delivery system to release the drug and activate the lytic activity of C8 in response to the change in pH (on-demand). Lastly, the drug delivery system also shows a selective cytotoxicity towards cancerous cells, which is consistent with the selectivity of C8. We attribute this to a proposed CLP-assisted uptake mechanism.

As the selective delivery of drugs originates from the different lytic activities of C8 on cell membranes with varying compositions, we investigated the lytic activities of C8 on model lipid membranes with different surface properties (zwitterionic, negatively charged and cholesterol-rich). Contrary to the traditional understanding, C8 shows better activity on cholesterol-rich membranes, but is less active on negatively charged membranes. Molecular dynamics (MD) simulations support this unusual membrane selectivity and provide an insight from the molecular level.

6.2 Materials and methods

6.2.1 Sample preparation

Cationic lytic peptide C8 was synthesized by Canpeptide Inc. (Montreal, Canada) with a purity above 95%. The procedure for peptide synthesis is briefly described in section 3.2.1. The anticancer drug ellipticine was purchased from ENZO life science (Brockville, Canada). The peptide only samples were prepared by dissolving C8 powder in Milli-Q water. The C8-EPT co-assemblies were prepared by adding EPT powder into C8 pH 4 aqueous solution. When EPT powder dissolved, the pH was then adjusted to 8 by adding sodium hydroxide solution. The sample was stirred using a magnetic bar at 900 rpm overnight. The pH 4 sample was prepared by adding hydrogen chloride solution into pH 8 samples and incubated for 2 days before usage. The final pH was in the range of ±0.2 to the targeted value.

6.2.2 Cell culture

Mouse fibroblast cells (NIH-3T3), non-small lung carcinoma cells (A549) and breast carcinoma cells (MCF-7) were purchased from ATCC (Manassas, USA). All cell lines were cultured in ATCC recommended growth media: A549 cells were cultured in F-12 (Kaighn's

modification) (F12K) media (HyClone Laboratories, Mississauga, Canada); MCF-7 cells were cultured in MEM Eagles with Earle's Ballanced Salts (HyClone Laboratories, Mississauga, Canada); NIH-3T3 cells were cultured in Dulbecco's Modified Eagle's Medium (DMEM) (HyClone Laboratories, Mississauga, Canada). All the media contained 10% fetal bovine serum (FBS) (Invitrogen, Burlington, Canada) and 1% penicillin/streptomycin (MP Biomedicals, Montreal, Canada). The cells were cultured at 37 °C and 5% CO_2.

6.2.3 MTS assay

A549 cells were seeded into wells of 96-well plates at the density of 10000 cells per well, while MCF-7 and NIH-3T3 cells were seeded at the density of 20000 cells per well. The seeded cells were incubated for 24 h before treatment. After the media was removed, 150**µ**L of fresh media was added with 50 **µ**L of the treatment solution. Following a 24 h incubation period, MTS assays were performed using a CellTiter 96® AQueous Kit (Promega, Madison, USA) according to the manfacturer's protocol. The absorbance was measured at 485 nm using a FLUOstar plate reader (BMG Labtech, Ortenberg, Germany). Untreated cells were used as the negative control. IC_{50} values were calculated .

6.2.4 Statistical analysis

Results were expressed as mean±SD. Statistical significance was determined by one-way analysis of variance (ANOVA). Differences were considered significant if $p<0.05$.

6.2.5 Annexin V assay

Untreated or treated cells were labeled using FITC-Annexin V and 7-AAD (BD bioscience, Mississauga, Canada) after an 18 h incubation period. The staining procedure was performed as described by the manufacturer.

6.2.6 Atomic force microscopy

The nanostructures of the C8 peptide aqueous solution (pH 8), C8-EPT co-assemblies at both pH 8 and pH 4 were imaged on a Dimension Icon AFM (Bruker, Santa Barbara, USA). The AFM samples were prepared by mounting 50 **µ**l of sample solution on a freshly cleaved mica surface (SPI, West Chester, USA). The mica was washed with 80 **µ**l Mili-Q water for 5 times after 10 min incubation. The air-dried AFM samples were scanned at room temperature using peak force quantitative nanomechanical mapping (PF-QNM) mode. All images were acquired using a SCANASYST-AIR probe (Bruker, Santa Barbara, USA).

6.2.7 Fluorescence spectroscopy

The molecular states of EPT in C8-EPT co-assemblies were identified using fluorescence spectroscopy. The samples were transferred into a square quartz cell and excited at 295 nm. The emission scans were performed on a QM4-SE spectra fluoremeter (PTI, London, Canada). Detailed experimental settings have been described previously [205].

6.2.8 Circular dichroism spectroscopy

The secondary structures of C8-EPT co-assemblies were determined using a J-715 circular dichroism spectrometer (Jasco Europe, Cremella, Italy). The samples were transferred into a 1 mm quartz cell, and spectra were collected from 190 nm to 260 nm with a 1 nm bandwidth and

data pitch, 2 s response time and 100 nm min^{-1} scanning speed. The presented spectra were averaged from two replicates, and solvent absorbance was subtracted from the data. The mean residue molar ellipticity of C8 peptide presented here was calculated following the formulas: Ellipticity (θ in deg cm^2 $dmol^{-1}$) = (millidegrees × mean residue weight)/(path length in millimetres × concentration of C8 peptide in mg ml^{-1}).

6.2.9 Membrane leakage assay

Large unilamellar vesicles (LUVs) of pure POPC, POPC/cholesterol (20 mol%) and *E. coli* polar extract lipids (PE/PG/CA 67/23.2/9.8 wt%) (Avanti Polar Lipids) were prepared by extrusion. The lipids were first dissolved in chloroform (≥99.5%, Sigma, Oakville, Canada), then dried under a gentle stream of nitrogen (prepurified) and placed under vacuum to remove trace amount of solvent. The lipid film was re-dissolved in a calcein buffer containing 70 mM calcein, 10 mM Tris and 0.5 mM EDTA at pH 7.4, then freezed in dry ice and thawed in warm water for 7 cycles. The lipid solutions were extruded using 100-nm pore size filters to obtain LUVs. Free calcein was then removed by exchanging the external buffer for a Tris buffer (110 mM NaCl, 10 mM Tris and 0.5 mM EDTA at pH7.4) on a PD-10 De-salting Column (GE healthcare, New Jersey, USA). The lipid concentration was then determined by a phosphate colorimetric assay kit (BioVision, Milpitas, USA). The calcein-loaded vesicles (CLVs) were added to varying concentrations of freshly prepared C8 Tris buffer solutions. After one hour of incubation on a rotatory shaker, the samples were placed in a Horiba JobinYvon Fluorolog 3 (Edison, NJ, USA) for fluorescence lifetime measurements. The excitation source was a 467 nm 1MHz laser diode and emission was measured for 180 seconds at 515 nm using time-correlated single photon counting. The resulting decay curves were then saved with the instrument response function for further analysis. The detailed analysis for efflux value was previously described [190].

6.2.10 Molecular dynamics simulations

We ran 6 sets of MARTINI CG [231] simulations using GROMACS 4 [232]. Nine C8 monomers were restrained to remain within the bilayer core, and self-assembled into aggregates within 1 μs of simulation. The simulations were run with the standard run parameters [231]. Each bead represents 3-4 heavy atoms that interact with a standard Lennard-Jones potential (1.2 nm cut-off) and shifted Coulomb potential (0-1.2 nm shift with no long-range electrostatics). The CG simulations were then converted to atomistic resolution using the Backwards method [233]. The simulations were then continued using the atomistic GROMOS peptide force field [234] and the GROMOS lipid parameters [235, 236].

6.3 Results

6.3.1 Selective cytotoxicity

The cytotoxicity of the unstructured peptide C8 (at pH 4) towards A549 (lung carcinoma), MCF-7 (breast carcinoma) and NIH-3T3 (mouse fibroblast) was evaluated using an MTS cell viability assay. Figure 6.1 shows that cytotoxicity of peptide was dose-dependent. The IC_{50} value for unstructured C8 against A549 was calculated to be 20.9±6.6 μg/ml (9.0±2.8 μM), and 21.7±4.5 μg/ml (9.3±1.9 μM) for MCF-7 cells. These values are comparable to IC_{50} values reported for synthetic anticancer peptides in the literature [12, 27, 130, 131]. Meanwhile, the IC_{50} value for unstructured C8 against the noncancerous cell line NIH-3T3 was 40.5±2.3 μg/ml (17.4±1.0 μM), showing a moderate selectivity of about two-fold greater against cancerous cells.

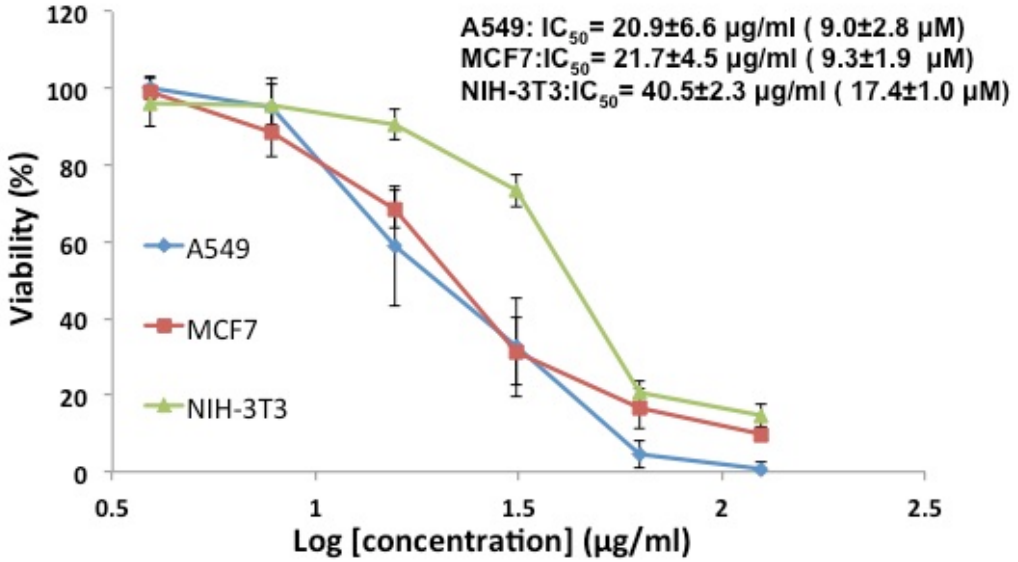

Figure 6.1 Cytotoxicity of C8 against A549 (lung carcinoma), MCF-7 (breast carcinoma) and NIH-3T3 (mouse fibroblast). The cells were incubated with C8 for 24 h. The data are averaged from at least three independent replicates. The error bars represent standard deviations.

6.3.2 Mechanism of cell death induced by C8

To investigate the mechanism of cell death induced by unstructured C8, A549 cells were treated with 25 µg/ml (10.7 µM) or 50 µg/ml (21.4 µM) of C8. After 18 h of incubation, we observed numerous floating dead cells and debris from lysed cells in wells containing treated cells. Washing the cells three times to remove the floating cells and cell debris, the remaining cells were stained with FITC-Annexin V and 7-AAD. As shown in Figure 6.2.a, most of them were still intact or at the early apoptosis stage. The optical microscopy image (Figure 6.2.b) shows that A549 cells were lysed with their nuclei remaining intact after a treatment of 53.6 µM C8 for 2 min. Both of these observations suggest that C8 kills cells mainly through a necrotic mechanism [27, 131].

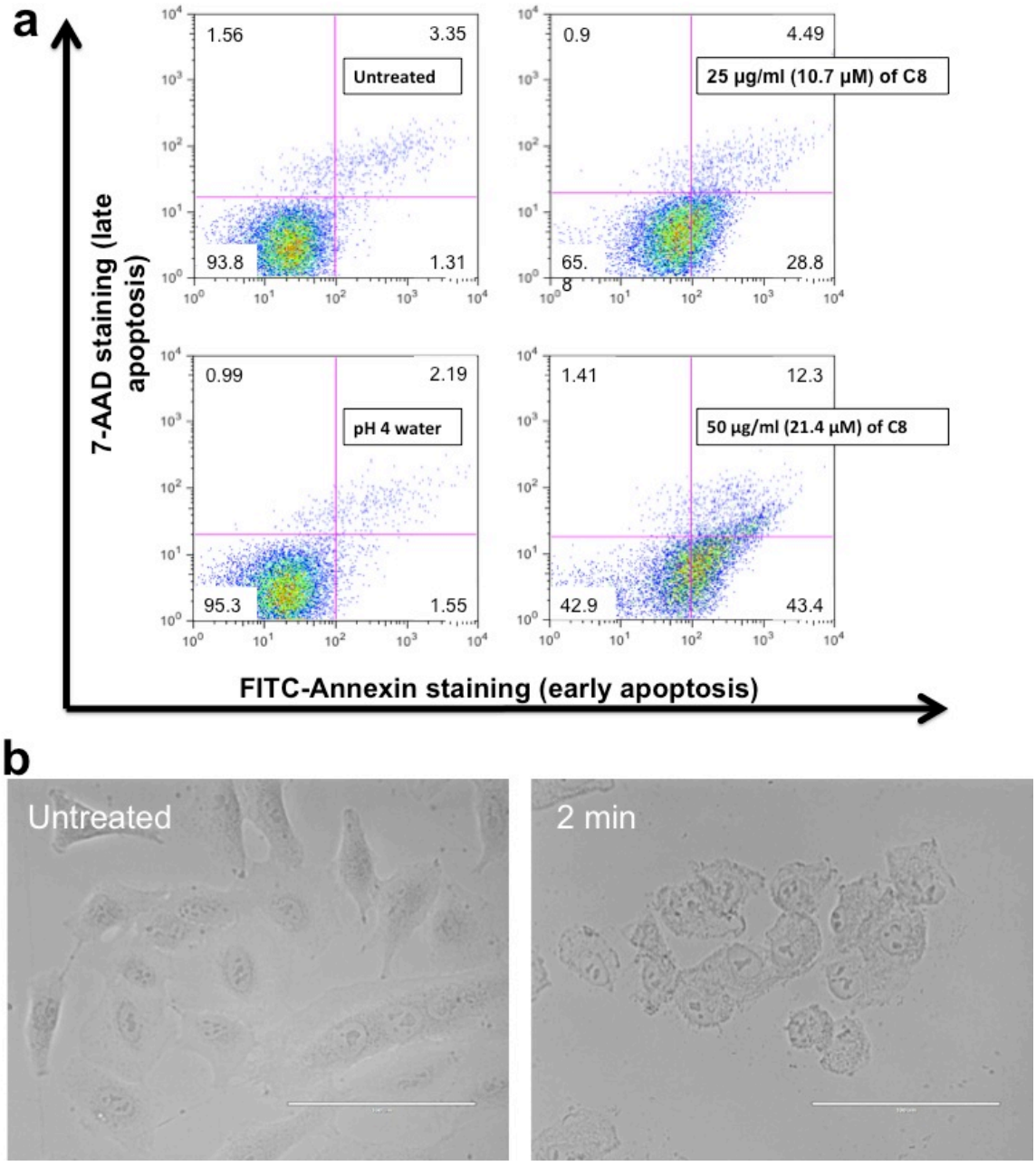

Figure 6.2 The mechanism of cell death induced by C8. (a) The apoptotic stage of A549 cells treated with unstructured C8 determined by FITC-Annexin and 7-AAD labeling. (b) The morphology of A549 cells treated with unstructured C8. The images were produced using a EVOS ® FL Cell imaging system (AMG, Mill Creek, USA).

6.3.3 Selective and on-demand drug delivery

Based on our knowledge of peptide-based EPT delivery systems [71, 73], we proposed a mechanism for the co-assembly of C8 and EPT at pH 8. At pH 8, the histidine residues are deprotonated while arginine residues remain positively charged. Hence, the C8 peptides stack together via hydrogen bonding between histidine, asparagine, tryptophan and the peptide backbone, and hydrophobic interactions between isoleucine and tryptophan to form β-sheets (π-π stacking provided by tryptophan may also be involved), leading to the formation of nanofibers. In the context of β-sheets, the positively charged arginine residues are orientated toward the aqueous environment, while the rest of the residues in C8 form the hydrophobic core of the nanofibers. Ellipticine molecules can interact with C8 peptide via hydrogen bonding and hydrophobic interaction, and localize in the core of the nanofibers (Figure 6.3.d).

To confirm the proposed mechanism, AFM images of C8 and C8-EPT co-assemblies were obtained at pH 8 (Figure 6.3.a). Similar to the case of EAK16-II and EPT [205], C8 formed thin nanofibers by itself, while thick nanofibers and large nodes were present in C8-EPT co-assemblies. This indicates that EPT participated in the self-assembly process. The fluorescence spectrum of EPT in C8-EPT co-assemblies at pH 8 indicates that EPT remained mostly as neutral molecules (fluorescence emission peak centered at ~430 nm) [74] (Figure 6.3.b), which should be encapsulated in the hydrophobic core of the nanofibers, supporting our proposed mechanism.

The AFM images showed that the condensed nanofiber network and nodes formed by C8 and EPT "melted" to short fragments after the pH was reduced to 4 (Figure 6.3.a). The secondary structure of C8 in the co-assemblies as probed by CD had a significant reduction in β-sheet content when the pH was reduced to 4 (Figure 6.3.c), indicating disassembly. Protonated EPT (fluorescence emission peak centered at 530 nm) dominated at low pH [205], which could further destabilize the aggregate (Figure 6.3.b).

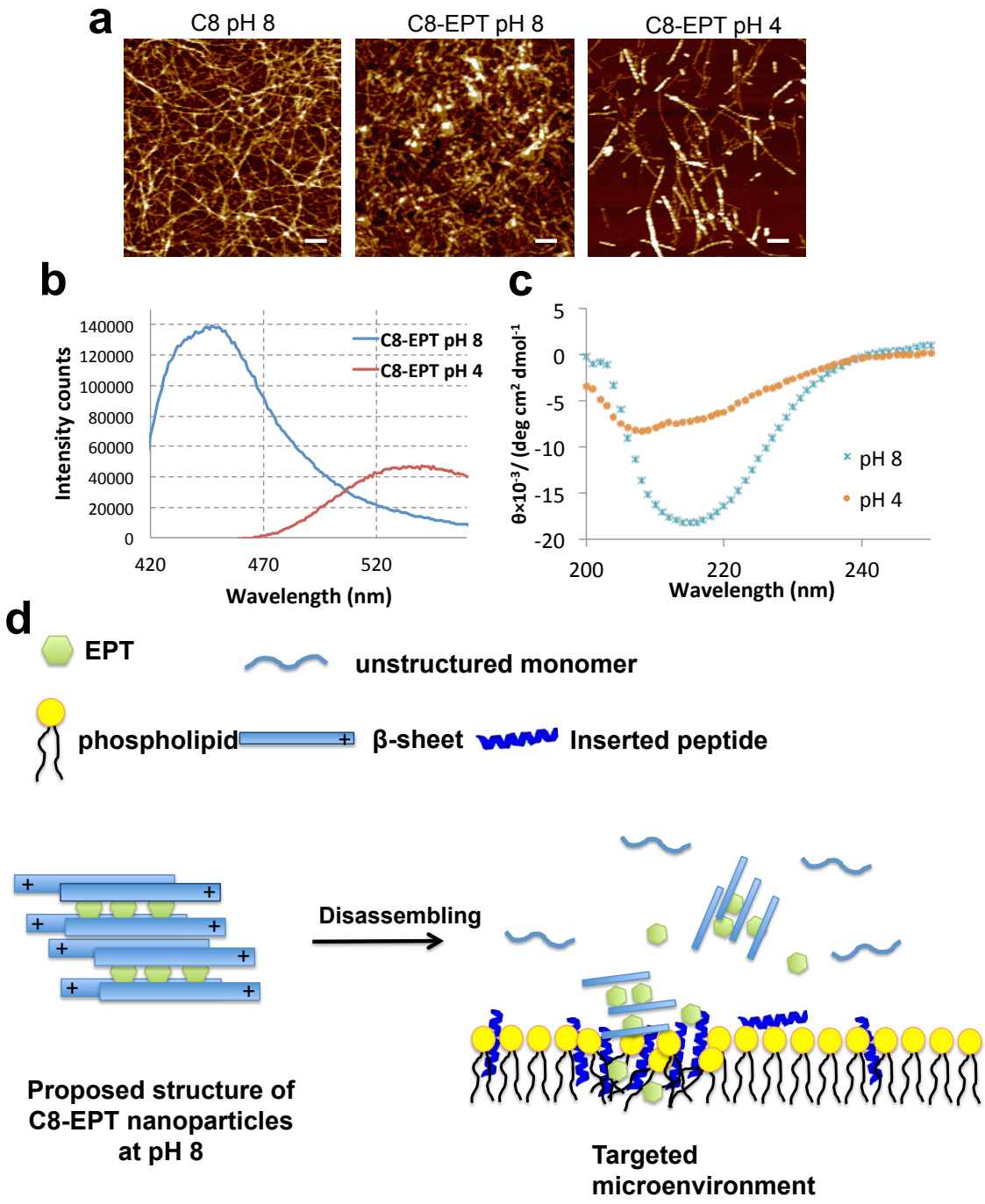

Figure 6.3 Characterization of C8-EPT co-assemblies and proposed co-assembly and delivery mechanism. a-c. the characterization of physicochemical properties of C8-EPT co-assemblies at pH 4 or pH 8 using AFM (a), fluorescence microscopy (b) and circular dichroism (c). The C8-EPT co-assemblies contain 500 μg/ml (214.6 μM) C8 and 50 μg/ml (203.3 μM) EPT, the C8 pH 8 sample is at the concentration of 500 μg/ml (214.6 μM). d) Schematic of the co-assembly of C8-EPT and the on-demand CLP-assisted delivery mechanism.

The *in vitro* cytotoxicity of C8-EPT samples at pH 8 (referred to as C8-EPT (pH 8)) and pH 4 (referred to as C8-EPT (pH 4)) was evaluated on A549 and NIH-3T3 cell lines. We postulated that the membrane damage induced by active C8 monomers could facilitate cellular uptake of the delivered EPT (as illustrated in Figure 6.3.d), which we term "CLP-assisted uptake" mechanism. As shown in Figure 6.5.b-d, the C8-EPT (pH 8) co-assemblies exhibited almost no toxicity towards either cell line. Our previous work has reported that neutral EPT and EPT crystalline delivered by EFK16-II are active in inhibiting the proliferation of A549 cells [69]. Therefore, the minimized cytotoxicity of C8-EPT (pH 8) could be attributed to the inactive nanostructured C8, which is in line with our hypothesis. In contrast, the disassembled C8-EPT (pH 4) co-assemblies were active in inhibiting the growth of both types of cells (Figure 6.5.b). The C8-EPT (pH 4) could still kill ~95% of A549 cells after a 4-fold dilution. In comparison, when treated with the same concentration of C8, the A549 cells still showed ~30% viability. Water at pH 4 or pH 8 did not affect the growth of cell significantly (viability of both A549 and NIH-3T3 cells treated with water control at either pH was above 90%). EPT aqueous solution at pH 4 was used as the protonated EPT control. It was also less active than C8-EPT (pH 4) (Figure 6.5.a). Taken together, these results suggest that the combination of C8 and EPT is more effective than either C8 or EPT alone. We also performed a one-hour treatment with C8-EPT (pH 4) and EAK16-II-EPT drug delivery system (EAK16-II only acts as the drug carrier) [205]. C8-EPT (pH 4) showed strong cytotoxicity and the morphologies of the treated cells also changed in 2 min (Figure 6.4.b), while one hour is too short for EPT to induce apoptotic cell death (Figure 6.4.a). These results strongly suggest that C8 can still exert its lytic action in the C8-EPT (pH 4) system.

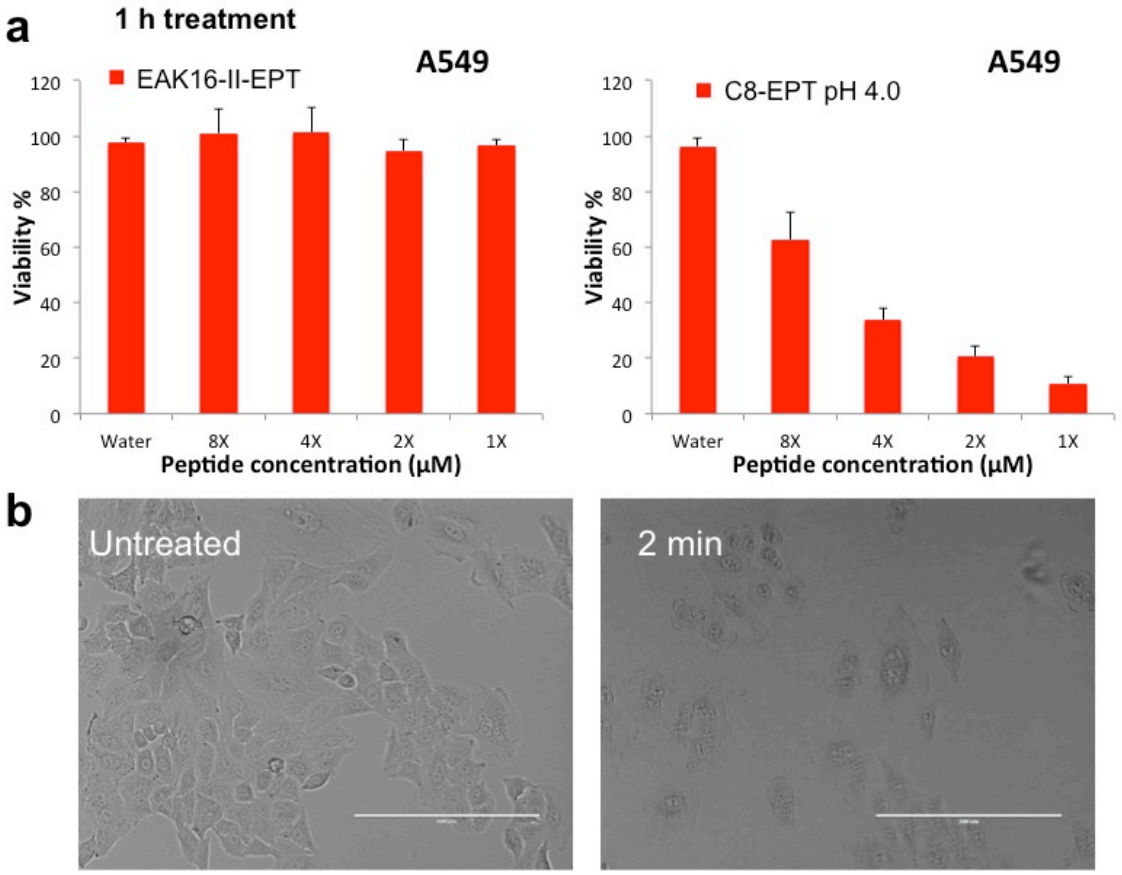

Figure 6.4 (a) Cytotoxicity of (left) EAK16-II-EPT co-assemblies (1X refers to 125 μg/ml EAK16-II (77.4 μM) and 25 μg/ml (51.8 μM) EPT) or (right) C8-EPT (pH 4) sample (1X refers to 125 μg/ml (53.6 μM) C8 and 12.5 μg/ml (50.8 μM) EPT) against A549 cells with 1h of incubation. The viabilities were averaged from at least three independent experiments, error bars are standard deviations. (b) Optical microscopy images of untreated A549 cells and A549 cells treated with C8-EPT (pH 4) sample for 2 min.

Beyond the pH-responsive (on-demand) delivery, the differential membrane activity of C8 may also be utilized to achieve a selective delivery of EPT and synergistic effect between C8 and EPT. The cytotoxicity of protonated EPT against A549 and NIH-3T3 cell lines was evaluated, and found to be not particularly selective (Figure 6.5.a). As shown above, the delivery of drug depends on the membrane activity of C8. Since C8 was less active against NIH-3T3 cell lines than A549 (Figure 6.1), the unstructured C8 was expected to cause less damage to NIH-3T3 cells when treating both cell lines with the same concentrations of C8-EPT (pH 4), leading to less

efficient cellular uptake of EPT. Comparing the cytotoxicity of C8-EPT (pH 4) against A549 and NIH-3T3 cell lines (Figure 6.5.b-d), we found that C8-EPT (pH 4) was more active, although not significantly, against A549 cells. For example, after 8-fold dilution, C8-EPT (pH 4) kills ~65% of A549 cells, but kills ~30% less of NIH-3T3 cells. Moreover, the cytotoxicity of C8-EPT complexes against NIH-3T3 cells was comparable to that of EPT, implying that the C8 induced enhancement in cellular uptake of EPT weakens due to less activity of C8 against NIH-3T3 cells. With further dilution, C8 is incapable of disrupting the cell membrane of both cell lines; C8-EPT (pH 4) became less active and selective against both cell lines.

To further investigate the potential of selective delivery, we used 60 μg/ml (25.2 μM) C8 aqueous solution at pH 4 to dilute C8-EPT (pH 4) (referred to as C8-EPT+), instead of water. The motivation is to maintain the concentration of C8 at a level that is capable of disrupting the membrane of A549 cells but not the NIH-3T3 cells. C8 samples at corresponding concentrations were used as controls to show the contribution of C8 to the cytotoxicity of C8-EPT+. As shown in Figure 6.5.c,e, the C8-EPT+ samples presented a significant enhancement on its cytotoxicity against A549 cells. Even diluted by 32-fold, C8-EPT+ sample still showed enhancement on cytotoxicity when compared to C8 alone, inhibiting ~20% more of cell growth (Figure 6.5.c). At the same concentration as in 32-fold diluted C8-EPT+, EPT was non-toxic, which demonstrated the synergistic effect resulting from the "CLP-assisted uptake" mechanism. In contrast, no significant enhancement was observed on the cytotoxicity against NIH-3T3 cells (Figure 6.5.e), because NIH-3T3 cells were less susceptible to the increased amount of C8. As a consequence, the selectivity of C8-mediated EPT delivery system towards A549 cells has been enhanced.

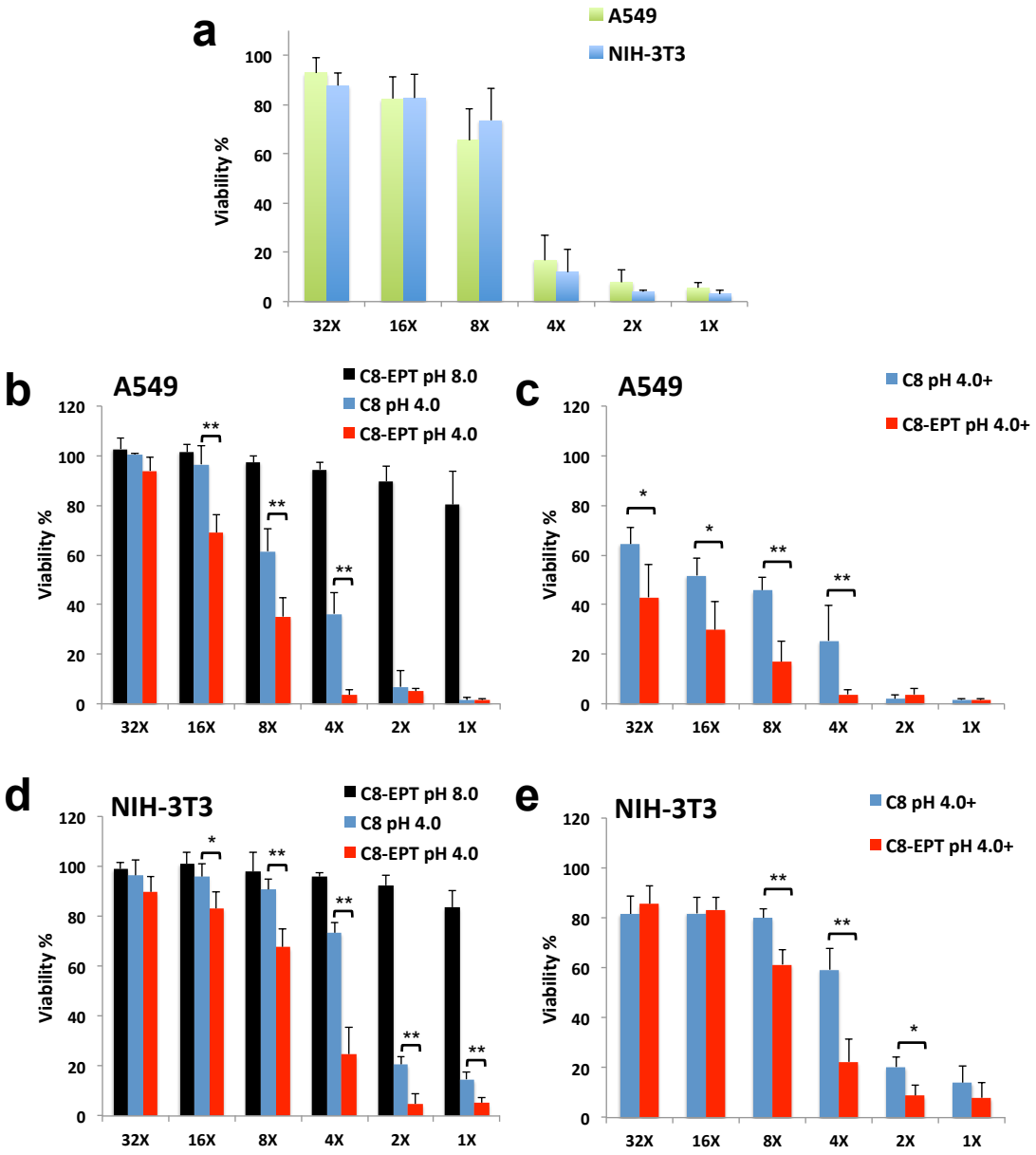

Figure 6.5 Evaluation of the cytotoxicity of EPT and C8-EPT co-assemblies against A549 (lung carcinoma) and NIH-3T3 (mouse fibroblast). Cytotoxicity of protonated EPT (a) and C8-EPT co-assemblies diluted with water (b,d) and unstructured C8 aqueous solution at concentration of 60 μg/ml (25.2 μM) (c,e). The samples with "+" represent that they are diluted with unstructured C8 aqueous solution. 1X refers to 12.5 μg/ml (50.8 μM) EPT, or 125 μg/ml (53.6 μM) C8, or the C8-EPT co-assemblies with 125 μg/ml (53.6 μM) C8 and 12.5 μg/ml (50.8 μM) EPT in the final culture media. The viabilities were averaged from at least three independent experiments, Error bars are standard deviation. *$p<0.05$, **$p<0.01$ between the two samples.

6.3.4 Membrane selectivity and lysis

The leakage of calcein from large lamellar vesicles was measured to address the mechanism of C8 selectivity and cell lysis. At low concentrations (sub micromolar), C8 induced leakage from both a pure POPC liposome and a POPC liposome containing 20 mol% cholesterol (Figure 6.6.a). A model bacterial membrane with polar lipid extracts of *E.coli* required roughly 10 times higher concentration of C8 to induce leakage. An antimicrobial ring test was also performed on *E.coli*, showing that C8 did not have antimicrobial activity (data not shown), which supports this unusual membrane selectivity. The mechanism of leakage in all 3 model membranes was found to be graded [190] (data not shown).

Figure 6.6.b showed atomistic stimulations for C8 aggregates, in 3 model membranes: pure POPC, 20 mol% cholesterol/POPC, and 1:3 POPG: POPE mixtures. When all three histidines were neutral, no large pores were observed in any of the model membranes. Relatively large dynamic disordered toroidal pores were observed in POPC and 20 mol% cholesterol membranes when the histidines were charged, while no pores are observed for the POPE/POPG mixture. These pores were sufficiently large to allow calcein molecules to diffuse through them (Figure 6.7.a). For the POPE/POPG mixture C8 preferred to interact with the interface, likely due to the strong electrostatic interactions between the peptide and the PG head group, as well as the increased hydrogen bonding capacity of PE compared to PC. Free energy profiles for single C8 molecules to move from water to the center of the 3 model membranes are shown in Figure 6.7.b. The deep free energy minima at the interface of the PE/PG mixture supports our hypothesis that the negatively charged PG attracted C8 to the interface, which reduced pore formation.

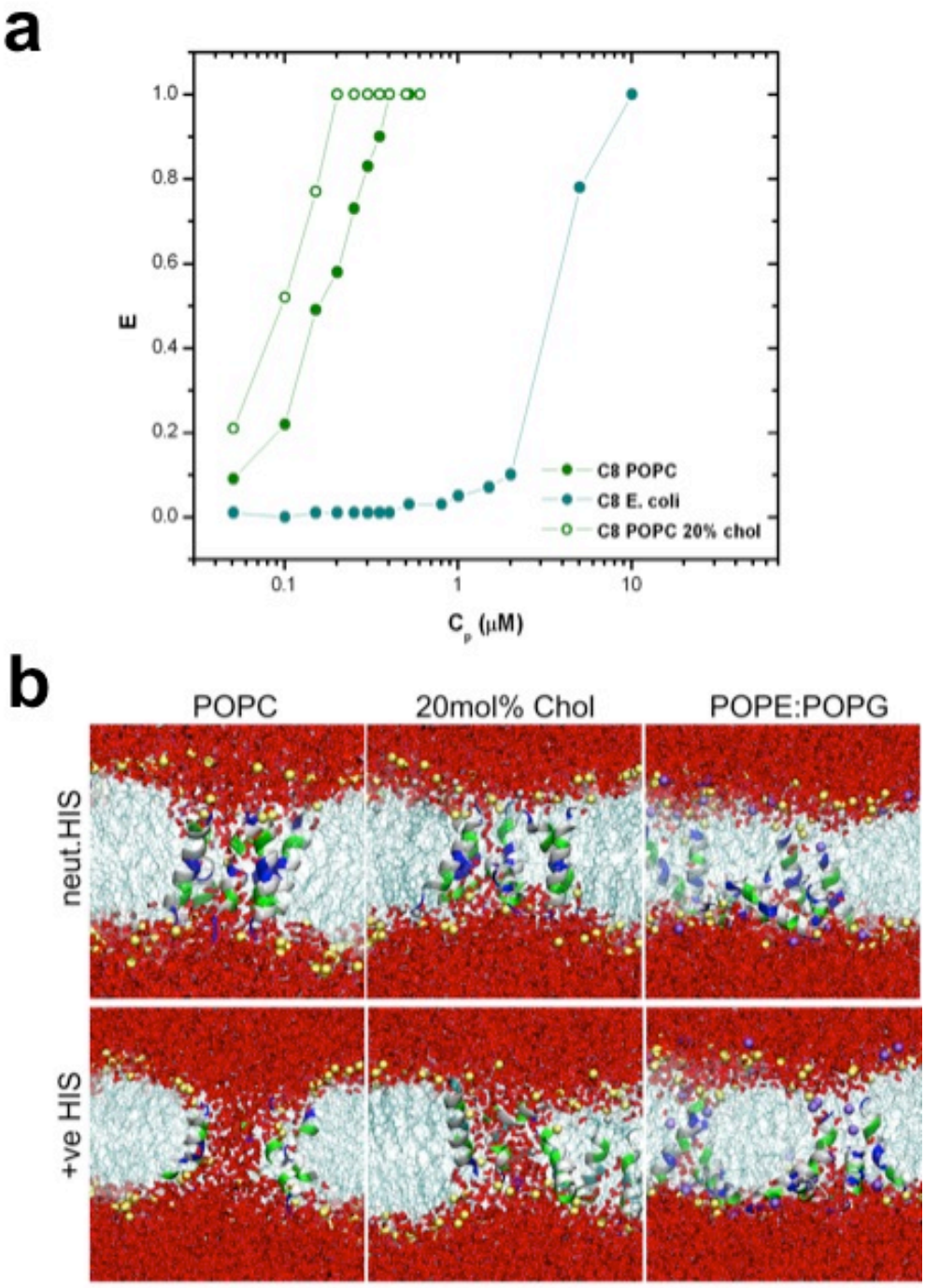

Figure 6.6 Membrane leakage induced by C8. (a) Leakage induced by C8 on pure POPC, POPC+20% cholesterol and *E. coli* extract lipid membranes**.** (b)Atomistic molecular dynamics simulations of C8 aggregation within different model membranes. Representations are: water, red; lipid tails, thin cyan; POPC phosphorous, yellow; POPG phosphorous, blue; cholesterol oxygen, white; the peptides are in cartoon representation colored by residue type (charged and histidine, blue; hydrophobic white; polar, green).

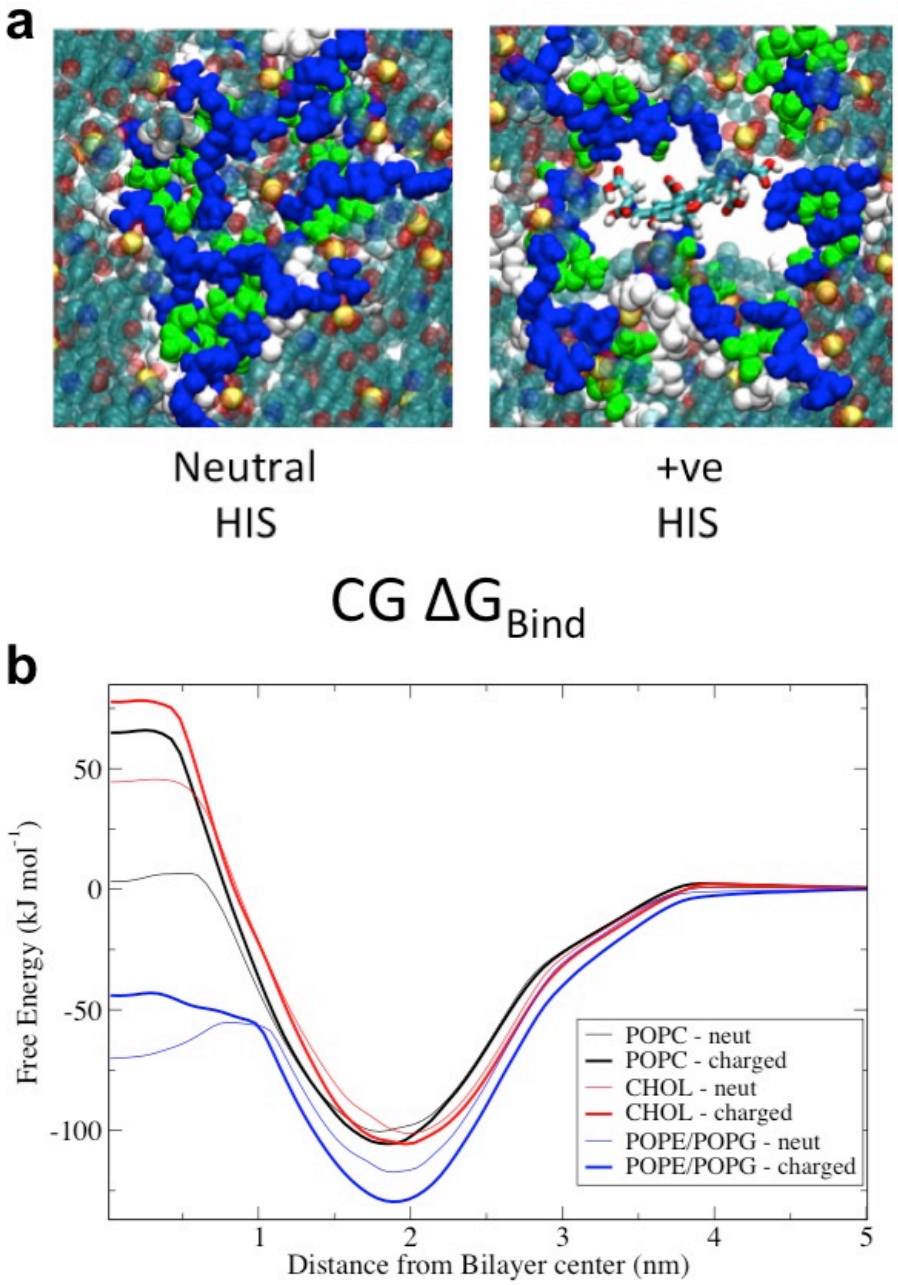

Figure 6.7 (a) The top view of a pore in the POPC bilayer with neutral (left) and charged (right) C8 peptides. Water is not shown for clarity, and the peptide and lipids are in Van der Waals representation. The peptide is coloured white for hydrophobic residues, green for polar and blue for histidine and arginine. A calcein molecule in licorice representation is over laid on the pore to illustrate that the pore is large enough to leak calcein when C8's histidines are charged, but not when neutral. (b) Free energy profiles for moving a single C8 peptide from water to the center of the different membranes. These calculations were performed with the MARTINI coarse-grained model. The free energy troughs at the water-membrane interface show that monomers would bind to the lipid environment.

6.4 Discussion

We presented C8, a novel anticancer peptide and pH-triggered drug delivery vector. Based on our in-depth characterization, Figure 6.3.d presents a schematic for our hypothesized mechanism of enhanced (synergistic) and selective delivery of EPT. This peptide illustrates 3 main design features: pH responsive co-assembly with an effective anticancer drug (EPT), low toxicity in the high pH co-assembled form and high toxicity in the low pH disassembled state, and membrane selectivity.

The unique advantage of using a CLP to deliver an anticancer drug is that both the delivered drug and delivery vector can execute a therapeutic function. We have shown that C8 has the potential for on-demand delivery, which likely originates from its membrane lytic action: it is possible that C8 permeabilizes the cell membrane, weakening its barrier to the anticancer drug, which leads to enhanced uptake and efficacy. We postulate that the EPT is encapsulated in the non-toxic C8 nanofibers, at pH 8, which limits its toxicity. When the co-assemblies reach the targeted environment (in our case low pH), the peptide nanofibers disassemble to release active monomers and the encapsulated EPT which work synergistically via the proposed "CLP-assisted uptake" mechanism. This mechanism may also explain the synergistic effects observed in other combinations of CLPs and chemotherapeutic drugs [27, 87]. As "CLP-assisted uptake" mechanism is largely dependent on the membrane activity of CLPs, we utilized the discrepancy on the activity of C8 against A549 cells and NIH-3T3 cells to achieve selective delivery of EPT. The synergistic effect between C8 and EPT allows a reduced dosage, limiting the adverse side effects; the selectivity rendered by C8 could improve the safety issue further. This "CLP-assisted uptake" mechanism mediated synergistic effect could be quite applicable in *in vivo* application. *In vivo* administration requires continuous injections of treatments to maintain an effective concentration in the body, which allows the CLP to possess sufficient membrane activity to

enhance cellular uptake of delivered drug. Furthermore, the choice of dosage would be important, utilizing the selectivity, to minimize the side effects but still maintain a good antitumor efficacy.

CLPs can selectively bind and lyse specific cell membranes, which is a promising property, given that cancer cells and microbes have different lipid compositions from healthy mammalian cell membranes [6]. C8 has unusual membrane selectivity in contrast to many traditional CLPs. Many CLPs have anticancer and antimicrobial activity that has been attributed to the negatively charged surfaces of both types of cell membranes and lower cholesterol concentrations [6]. C8 does not have antimicrobial activity but does selectively kill cancer cells. The model membrane vesicle leakage assays showed that 20 mol% cholesterol did not reduce the effectiveness of C8, but a *E.coli* lipid extract membrane was markedly more resistant to C8 induced leakage. These studies support the finding that C8 is not particularly antimicrobial, but do not explain its selectivity for cancer cells. This suggests that the traditional view that the membrane selectivity of CLP's is due to the negatively charged lipids or cholesterol content is incomplete. Future studies into the specific structure and composition of different cell membranes would enable more comprehensive model membrane studies and drug delivery targets.

The mechanism for C8 permeabilization of the membrane on a molecular level involves the amphiphilic helices aggregating within the bilayer core, forming a disordered torroidal pore which agrees with many previous MD simulations of CLPs [237, 238]. The protonation state of histidine is crucial for pores to form, with relatively large pores when protonated and charged. This suggests the interesting possibility of tuning activities based on the local pH. The simulations agree qualitatively with the leakage results, with pore formation in zwitterionic bilayers with and without cholesterol, but not the bacterial mimic (largely PE and PG). C8 has a stronger affinity or lower free energy for the interface of the bacterial bilayer compared to the POPC and POPC/CHOL bilayers, which cause them to bind to the interface and not aggregate into toroidal pores.

The potential for peptide-based nano-drug carriers is promising. C8 provides a solid basis for future peptide designs. Our characterization and design features, including pH responsive co-assembly, drug delivery, and membrane selectivity and lysis, will expand a new and important area of research—CLP-mediated multi-functional drug delivery system. Due to the flexibility in the choice of amino acids, many possible substitutions may improve the design of C8 to enhance the effectiveness for cancer treatment. Mutations in peptide sequence to shift the pH responsive disassembly from around 4 to 6.2-7.2, close to the extracellular environment of solid tumor [42, 165], would make C8 more effective. Decreasing the hydrophobic content, or increasing the number of charged or polar residues, may destabilize the beta sheets in higher pH conditions. Increasing the selectivity towards cancer cells is also crucial, but is much more difficult to accomplish. Similar multi-disciplinary approaches with libraries of peptides and more model membranes will allow for a more thorough basis for understanding the membrane selectivity. Incorporating multiple histidines into the design of C8 with two additional arginine residues may explain the unique properties of the peptide. We expect that variants of C8 have the potential for effective drug delivery and therapeutic applications.

Chapter 7

Conclusions and Recommendations

8.1 Original contributions to research

This thesis represents new findings in the application of CLPs for anticancer treatment from three aspects: 1) the molecular mechanism of membrane selectivity of CLPs; 2) development of stimuli-responsive CLPs; 3) the potential use of CLPs as hydrophobic drug carriers. The thesis includes the following parts: (i) studies on the membrane activity and selectivity of an arginine-rich amphiphilic peptide using liposomes and mammalian cells; (ii) investigation of anticancer activity of an arginine-rich peptide *in vitro* and *in vivo*, and the therapeutic effect of peptide-ellipticine complex against cancerous or healthy cells; (iii) characterization of a stimuli-responsive CLP and its nanostructure-dependent cytotoxicity; and (iv) investigation of the potential use of stimuli-responsive CLP as ellipticine nanocarrier for synergistic, selective and/or on-demand delivery. The original contributions to research of each part are summarized in the following sections.

8.1.1 Tuning the membrane selectivity of C6 by hydrogen bonding.

An arginine-rich amphiphlic peptide C6 was found to show comparable membrane lytic activity against pure POPC membranes or cholesterol-rich (20 mol%) POPC membranes based on liposome leakage assay. After inhibiting the hydrogen bonding between C6 and membrane

components by adding phosphate salt, the membrane lytic activity of C6 against cholesterol-rich membrane reduced significantly while did not change much against pure POPC membranes. This demonstrates that hydrogen bonding plays an important role in the activity of CLP against cholesterol-rich membranes, which is reported for the first time.

The effect of hydrogen bonding was also shown in cytotoxicity studies of C6 on A549 cells, MCF-7 cells and red blood cells with various membrane-cholesterol contents. Although the outcomes were consequences of a combinatial factors due to the complexity of the cellular system, the results still could demonstrate the potential of tuning the activity of CLPs against specific cell types by modulating their membrane selectivity. This study adds new molecular insights into the mechanism of membrane selectivity of CLPs.

8.1.2 *In vitro* and *in vivo* anticancer activity of C6 and *in vitro* delivery of C6-EPT complexes.

The cytotoxicity of C6 was evaluated *in vitro,* and found to be selective towards cancerous cells. Its anticancer activity was demonstrated in the context of an A549 nude mice tumor model. A subsequent study found that C6 could stabilize neutral ellipticine in aqueous solution. C6 was prone to become unstructured in aqueous solution, but maintained a helical conformation and a β-sheet component after forming complexes with ellipticine.

The C6-EPT complexes exhibited enhanced cytotoxicity towards A549 cells when compared to C6 or neutral EPT alone. The membrane permeability induced by C6 was suggested to be the reason for the enhancement in cytotoxicity. Such an enhancement became more pronounced when the C6-EPT complexes were diluted with a low concentration C6 aqueous solution, which maintained the concentration of C6 constant in complexes that disrupted cell membranes. In contrast, the enhancement was not significant for NIH-3T3 cells, in both cases of dilution with water or C6 aqueous solution. This could be due to that C6 may be less active against NIH-3T3, hence induced less permeability on NIH-3T3 cell membranes than on A549 cell membranes at the

same concentration. We term this "CLP-assisted uptake" mechanism. This mechanism results in different degrees of enhancement, leading to the selectivity of C6-EPT complexes. This study demonstrates the capability of amphiphilic CLPs as hydrophobic anticancer drug carriers for enhanced and selective delivery.

8.1.3 Stimuli-responsiveness and nanostructure-dependent cytotoxicity of C8.

A stimuli-responsive peptide, C8, was designed based on our amino acid pairing principle. Controlled by the balance of intermolecular forces between repulsive electrostatic forces and attractive hydrogen bonding and hydrophobic interactions, the designed peptide can self-assemble into β-sheet rich nanofibers or disassemble into unstructured monomers. As the pH controls protonation status of histidine residues, temperature affects hydrogen bonding and hydrophobic interactions and urea interferes with the formation of hydrogen bonds, C8 was shown to be a triple-responsive self-assembling peptide.

We also proposed the balance equations for the repulsive and attractive forces at different temperatures using the critical pH, at which the peptide starts to assume a β-sheet conformation. With these equations, we can estimate the relative strength of different types of intermolecular forces, as well as the overall effect of temperature on the hydrophobic interaction and hydrogen bonding. This knowledge will provide a basis to modulate the intermolecular interactions of the stimuli-responsive peptides, to respond to specific environmental conditions.

The nanostructure formation was found to work as the "switch" to control the lytic activity of the therapeutic peptide: the non-toxic nanostructured peptide is a carrier, and it disassembles into active monomers in response to the target microenvironment. We showed the nanostructure-dependent lytic action of C8 *in vitro*, demonstrating the potential of this "self-guided delivery" strategy. Furthermore, the hemolytic activity of the nanostructured peptide was significantly reduced. Along with the inherent selective killing of cancerous cells, the results extend the usage

of cationic lytic peptides as "self-guided" therapeutic agents. The approach proposed here has never been reported in the literature.

8.1.4 Co-assembly of ellipticine with C8 and pH-responsive, synergistic and selective delivery of C8-EPT complexes.

C8 was found to co-assemble with neutral EPT, forming thicker nanofibers and globular aggregates at pH 8 when compare to the thin nanofiber networks formed by C8 alone at the same condition. The C8-EPT co-assemblies disassemble at pH 4.0, releasing protonated ellipticine.

The formation of nanostructure of co-assemblies of C8-EPT was found to greatly affect their cytotoxicity. The C8-EPT co-assemblies at pH 8 showed minimal cytotoxicity against both A549 cells and NIH-3T3 cells. In contrast, the disassembled C8-EPT samples were active in inhibiting cell growth. This could be due to the inactivation of membrane lytic activity of C8 by the formation of nanostructures. The enhanced efficacy and selectivity found in C6-mediated system were also shown in this C8-mediated system, along with the pH-responsive cytotoxicity, which may suggest the "CLP-assisted uptake" mechanism represents a general behavior of CLP-mediated drug delivery system. This study further shows the possibility to involve stimuli-responsiveness into CLP-mediated drug delivery system.

8.2 Recommendation

Based on the outcomes of this thesis, the following recommendations are suggested for the future development of CLP-related therapeutics:

1. To investigate the effect of hydrogen bonding on the membrane activity and selectivity of CLPs further, peptides with lysine residues (positively charged, less capable of forming hydrogen bonding than arginine), or peptides contain asparagine,

glutamine residues (neutral, provide hydrogen bonding) may be studied . The positions of the amino acids in the peptide sequences may also affect membrane activity and selectivity. This should also be studied. Furthermore, evaluation of membrane lytic activity on various types of model membranes maybe considered. This information could provide criteria to target a specific type of cell membranes with complicate compositions.

2. To optimize CLPs with desired stimuli-responsive properties, the designs can benefit from our study in chapter 5. For instance, using C8 peptide as a template, new peptides can have more arginine or histidine residues to target higher pH; more hydrogen bonding and less hydrophobic interaction between peptides could facilitate disassembly at increased temperature and/or an environment with high urea content. The peptides also need to maintain an amphiphilicity to preserve membrane lytic activity.
3. To minimize hemolytic effect of CLPs, new peptide design may involve D-amino acid or tumor-targeting sequence (such as an iRGD sequence [239], which is short, and contains positively charged R and negatively charged D that facilitate self-assembly). Partial substitution of arginine residues with lysine residues may also help.
4. For CLP-mediated drug delivery systems, there are three approaches can be used to enhance their tumor-specificity: (i) using CLPs with high selectivity towards cancerous cells; (ii) adopting cancer cell-specific therapeutic agents, such as alpha-tocopheryl succinate, as the delivered cargo; (iii) incorporating exogenous stimuli-responsive moieties to achieve multi-responsiveness.
5. It will be necessary to adopt an efficient method to encapsulate hydrophobic drug with amphiphilic CLP, such as solvent evaporation technique [66]. There is also a need to develop a robust method to evaluate the encapsulation efficiency of the CLP-mediated delivery systems.

6. To further understand the “CLP-assisted uptake” mechanism, the cellular uptake pathway and the subcellular distribution of the delivered drug should be investigated.

References

[1] W.B. Pratt, Ruddon, R. W., Ensminger, W. D., and Maybaum, J., The Anticancer Drugs, Oxford University Press, Inc., New York, 1994.

[2] E. Espinosa, P. Zamora, J. Feliu, M. Gonzalez Baron, Classification of anticancer drugs--a new system based on therapeutic targets, Cancer treatment reviews, 29 (2003) 515-523.

[3] J. Cassidy, J.L. Misset, Oxaliplatin-related side effects: characteristics and management, Seminars in oncology, 29 (2002) 11-20.

[4] B. Kalyanaraman, J. Joseph, S. Kalivendi, S. Wang, E. Konorev, S. Kotamraju, Doxorubicin-induced apoptosis: implications in cardiotoxicity, Molecular and cellular biochemistry, 234-235 (2002) 119-124.

[5] L. Gatti, F. Zunino, Overview of tumor cell chemoresistance mechanisms, Methods in molecular medicine, 111 (2005) 127-148.

[6] D.W. Hoskin, A. Ramamoorthy, Studies on anticancer activities of antimicrobial peptides, Biochimica et biophysica acta, 1778 (2008) 357-375.

[7] J.S. Mader, D.W. Hoskin, Cationic antimicrobial peptides as novel cytotoxic agents for cancer treatment, Expert Opin Inv Drug, 15 (2006) 933-946.

[8] H.G. Boman, Peptide Antibiotics and Their Role in Innate Immunity, Annu Rev Immunol, 13 (1995) 61-92.

[9] M. Zasloff, Antimicrobial peptides of multicellular organisms, Nature, 415 (2002) 389-395.

[10] K.A. Henzler Wildman, D.K. Lee, A. Ramamoorthy, Mechanism of lipid bilayer disruption by the human antimicrobial peptide, LL-37, Biochemistry, 42 (2003) 6545-6558.

[11] M. Tang, A.J. Waring, M. Hong, Phosphate-mediated arginine insertion into lipid membranes and pore formation by a cationic membrane peptide from solid-state NMR, Journal of the American Chemical Society, 129 (2007) 11438-11446.

[12] C. Sinthuvanich, A.S. Veiga, K. Gupta, D. Gaspar, R. Blumenthal, J.P. Schneider, Anticancer beta-hairpin peptides: membrane-induced folding triggers activity, Journal of the American Chemical Society, 134 (2012) 6210-6217.

[13] C.T. Taylor, G.T. Furuta, K. Synnestvedt, S.P. Colgan, Phosphorylation-dependent targeting of cAMP response element binding protein to the ubiquitin/proteasome pathway in hypoxia, Proceedings of the National Academy of Sciences of the United States of America, 97 (2000) 12091-12096.

[14] Z. Oren, Y. Shai, Mode of action of linear amphipathic alpha-helical antimicrobial peptides, Biopolymers, 47 (1998) 451-463.

[15] Y. Shai, Mechanism of the binding, insertion and destabilization of phospholipid bilayer membranes by alpha-helical antimicrobial and cell non-selective membrane-lytic peptides, Biochimica et biophysica acta, 1462 (1999) 55-70.

[16] G. Ehrenstein, H. Lecar, Electrically Gated Ionic Channels in Lipid Bilayers, Q Rev Biophys, 10 (1977) 1-34.

[17] K. Matsuzaki, O. Murase, N. Fujii, K. Miyajima, An antimicrobial peptide, magainin 2, induced rapid flip-flop of phospholipids coupled with pore formation and peptide translocation, Biochemistry, 35 (1996) 11361-11368.

[18] B. Bechinger, K. Lohner, Detergent-like actions of linear amphipathic cationic antimicrobial peptides, Biochimica et biophysica acta, 1758 (2006) 1529-1539.

[19] S. Riedl, B. Rinner, M. Asslaber, H. Schaider, S. Walzer, A. Novak, K. Lohner, D. Zweytick, In search of a novel target - phosphatidylserine exposed by non-apoptotic tumor cells and metastases of malignancies with poor treatment efficacy, Biochimica et biophysica acta, 1808 (2011) 2638-2645.

[20] T. Utsugi, A.J. Schroit, J. Connor, C.D. Bucana, I.J. Fidler, Elevated expression of phosphatidylserine in the outer membrane leaflet of human tumor cells and recognition by activated human blood monocytes, Cancer research, 51 (1991) 3062-3066.

[21] M.D. Burdick, A. Harris, C.J. Reid, T. Iwamura, M.A. Hollingsworth, Oligosaccharides expressed on MUC1 produced by pancreatic and colon tumor cell lines, The Journal of biological chemistry, 272 (1997) 24198-24202.

[22] C.A. Reis, H. Osorio, L. Silva, C. Gomes, L. David, Alterations in glycosylation as biomarkers for cancer detection, Journal of Clinical Pathology, 63 (2010) 322-329.

[23] K. Okumura, A. Itoh, E. Isogai, K. Hirose, Y. Hosokawa, Y. Abiko, T. Shibata, M. Hirata, H. Isogai, C-terminal domain of human CAP18 antimicrobial peptide induces apoptosis in oral squamous cell carcinoma SAS-H1 cells, Cancer letters, 212 (2004) 185-194.

[24] J.S. Mader, J. Salsman, D.M. Conrad, D.W. Hoskin, Bovine lactoferricin selectively induces apoptosis in human leukemia and carcinoma cell lines, Molecular cancer therapeutics, 4 (2005) 612-624.

[25] S. Kim, S.S. Kim, Y.J. Bang, S.J. Kim, B.J. Lee, In vitro activities of native and designed peptide antibiotics against drug sensitive and resistant tumor cell lines, Peptides, 24 (2003) 945-953.

[26] Y. Ohsaki, A.F. Gazdar, H.C. Chen, B.E. Johnson, Antitumor activity of magainin analogues against human lung cancer cell lines, Cancer research, 52 (1992) 3534-3538.

[27] N. Papo, A. Braunstein, Z. Eshhar, Y. Shai, Suppression of human prostate tumor growth in mice by a cytolytic D-, L-amino Acid Peptide: membrane lysis, increased necrosis, and inhibition of prostate-specific antigen secretion, Cancer research, 64 (2004) 5779-5786.

[28] M.A. Baker, W.L. Maloy, M. Zasloff, L.S. Jacob, Anticancer efficacy of Magainin2 and analogue peptides, Cancer research, 53 (1993) 3052-3057.

[29] L. Ringstad, A. Schmidtchen, M. Malmsten, Effect of peptide length on the interaction between consensus peptides and DOPC/DOPA bilayers, Langmuir, 22 (2006) 5042-5050.

[30] L. Ringstad, E. Andersson Nordahl, A. Schmidtchen, M. Malmsten, Composition effect on peptide interaction with lipids and bacteria: variants of C3a peptide CNY21, Biophysical journal, 92 (2007) 87-98.

[31] A. Schmidtchen, M. Pasupuleti, M. Morgelin, M. Davoudi, J. Alenfall, A. Chalupka, M. Malmsten, Boosting Antimicrobial Peptides by Hydrophobic Oligopeptide End Tags, Journal of Biological Chemistry, 284 (2009) 17584-17594.

[32] H.M. Ellerby, W. Arap, L.M. Ellerby, R. Kain, R. Andrusiak, G.D. Rio, S. Krajewski, C.R. Lombardo, R. Rao, E. Ruoslahti, D.E. Bredesen, R. Pasqualini, Anti-cancer activity of targeted pro-apoptotic peptides, Nature medicine, 5 (1999) 1032-1038.

[33] A.J. Marks, M.S. Cooper, R.J. Anderson, K.H. Orchard, G. Hale, J.M. North, K. Ganeshaguru, A.J. Steele, A.B. Mehta, M.W. Lowdell, R.G. Wickremasinghe, Selective apoptotic killing of malignant hemopoietic cells by anti body-targeted delivery of an amphipathic peptide, Cancer research, 65 (2005) 2373-2377.

[34] D.J. Toft, T.J. Moyer, S.M. Standley, Y. Ruff, A. Ugolkov, S.I. Stupp, V.L. Cryns, Coassembled cytotoxic and pegylated peptide amphiphiles form filamentous nanostructures with potent antitumor activity in models of breast cancer, ACS nano, 6 (2012) 7956-7965.

[35] B.R. Lee, K.T. Oh, Y.T. Oh, H.J. Baik, S.Y. Park, Y.S. Youn, E.S. Lee, A novel pH-responsive polysaccharidic ionic complex for proapoptotic D-(KLAKLAK)(2) peptide delivery, Chemical communications, 47 (2011) 3852-3854.

[36] V.P. Torchilin, Multifunctional, stimuli-sensitive nanoparticulate systems for drug delivery, Nature reviews. Drug discovery, 13 (2014) 813-827.

[37] R.A. Petros, J.M. DeSimone, Strategies in the design of nanoparticles for therapeutic applications, Nature reviews. Drug discovery, 9 (2010) 615-627.

[38] H. Maeda, Macromolecular therapeutics in cancer treatment: the EPR effect and beyond, Journal of controlled release : official journal of the Controlled Release Society, 164 (2012) 138-144.

[39] M.E. Davis, Z. Chen, D.M. Shin, Nanoparticle therapeutics: an emerging treatment modality for cancer, Nature Reviews Drug Discovery, 7 (2008) 771-782.

[40] Y. Zhang, H.F. Chan, K.W. Leong, Advanced materials and processing for drug delivery: the past and the future, Adv Drug Deliv Rev, 65 (2013) 104-120.

[41] T.M. Allen, Ligand-targeted therapeutics in anticancer therapy, Nature reviews. Cancer, 2 (2002) 750-763.

[42] S. Mura, J. Nicolas, P. Couvreur, Stimuli-responsive nanocarriers for drug delivery, Nat Mater, 12 (2013) 991-1003.

[43] W. Chen, F. Meng, R. Cheng, Z. Zhong, pH-Sensitive degradable polymersomes for triggered release of anticancer drugs: a comparative study with micelles, Journal of controlled release : official journal of the Controlled Release Society, 142 (2010) 40-46.

[44] K.H. Min, J.H. Kim, S.M. Bae, H. Shin, M.S. Kim, S. Park, H. Lee, R.W. Park, I.S. Kim, K. Kim, I.C. Kwon, S.Y. Jeong, D.S. Lee, Tumoral acidic pH-responsive MPEG-poly(beta-amino ester) polymeric micelles for cancer targeting therapy, Journal of controlled release : official journal of the Controlled Release Society, 144 (2010) 259-266.

[45] J. Li, M. Huo, J. Wang, J. Zhou, J.M. Mohammad, Y. Zhang, Q. Zhu, A.Y. Waddad, Q. Zhang, Redox-sensitive micelles self-assembled from amphiphilic hyaluronic acid-deoxycholic acid conjugates for targeted intracellular delivery of paclitaxel, Biomaterials, 33 (2012) 2310-2320.

[46] P. Yang, D. Li, S. Jin, J. Ding, J. Guo, W. Shi, C. Wang, Stimuli-responsive biodegradable poly(methacrylic acid) based nanocapsules for ultrasound traced and triggered drug delivery system, Biomaterials, 35 (2014) 2079-2088.

[47] J.S. Lee, T. Groothuis, C. Cusan, D. Mink, J. Feijen, Lysosomally cleavable peptide-containing polymersomes modified with anti-EGFR antibody for systemic cancer chemotherapy, Biomaterials, 32 (2011) 9144-9153.

[48] L. Zhu, P. Kate, V.P. Torchilin, Matrix metalloprotease 2-responsive multifunctional liposomal nanocarrier for enhanced tumor targeting, ACS nano, 6 (2012) 3491-3498.

[49] L. Zhu, T. Wang, F. Perche, A. Taigind, V.P. Torchilin, Enhanced anticancer activity of nanopreparation containing an MMP2-sensitive PEG-drug conjugate and cell-penetrating moiety, Proceedings of the National Academy of Sciences of the United States of America, 110 (2013) 17047-17052.

[50] R. Cheng, F. Meng, C. Deng, H.A. Klok, Z. Zhong, Dual and multi-stimuli responsive polymeric nanoparticles for programmed site-specific drug delivery, Biomaterials, 34 (2013) 3647-3657.

[51] Z. Xiao, C. Ji, J. Shi, E.M. Pridgen, J. Frieder, J. Wu, O.C. Farokhzad, DNA self-assembly of targeted near-infrared-responsive gold nanoparticles for cancer thermo-chemotherapy, Angewandte Chemie, 51 (2012) 11853-11857.

[52] J. Yang, J. Lee, J. Kang, S.J. Oh, H.J. Ko, J.H. Son, K. Lee, J.S. Suh, Y.M. Huh, S. Haam, Smart Drug-Loaded Polymer Gold Nanoshells for Systemic and Localized Therapy of Human Epithelial Cancer, Adv Mater, 21 (2009) 4339-+.

[53] K.A. Carter, S. Shao, M.I. Hoopes, D. Luo, B. Ahsan, V.M. Grigoryants, W. Song, H. Huang, G. Zhang, R.K. Pandey, J. Geng, B.A. Pfeifer, C.P. Scholes, J. Ortega, M. Karttunen, J.F. Lovell, Porphyrin-phospholipid liposomes permeabilized by near-infrared light, Nature communications, 5 (2014) 3546.

[54] A. Schroeder, R. Honen, K. Turjeman, A. Gabizon, J. Kost, Y. Barenholz, Ultrasound triggered release of cisplatin from liposomes in murine tumors, Journal of controlled release : official journal of the Controlled Release Society, 137 (2009) 63-68.

[55] N.Y. Rapoport, A.M. Kennedy, J.E. Shea, C.L. Scaife, K.H. Nam, Controlled and targeted tumor chemotherapy by ultrasound-activated nanoemulsions/microbubbles, Journal of controlled release : official journal of the Controlled Release Society, 138 (2009) 268-276.

[56] T. Yin, P. Wang, J. Li, Y. Wang, B. Zheng, R. Zheng, D. Cheng, X. Shuai, Tumor-penetrating codelivery of siRNA and paclitaxel with ultrasound-responsive nanobubbles hetero-assembled from polymeric micelles and liposomes, Biomaterials, 35 (2014) 5932-5943.

[57] Z.S. Al-Ahmady, W.T. Al-Jamal, J.V. Bossche, T.T. Bui, A.F. Drake, A.J. Mason, K. Kostarelos, Lipid-peptide vesicle nanoscale hybrids for triggered drug release by mild hyperthermia in vitro and in vivo, ACS nano, 6 (2012) 9335-9346.

[58] S.-H. Hu, R.-H. Fang, Y.-W. Chen, B.-J. Liao, I.W. Chen, S.-Y. Chen, Photoresponsive Protein–Graphene–Protein Hybrid Capsules with Dual Targeted Heat-Triggered Drug Delivery Approach for Enhanced Tumor Therapy, Advanced Functional Materials, (2014) n/a-n/a.

[59] L. Zhang, T. Wang, L. Yang, C. Liu, C. Wang, H. Liu, Y.A. Wang, Z. Su, General route to multifunctional uniform yolk/mesoporous silica shell nanocapsules: a platform for simultaneous cancer-targeted imaging and magnetically guided drug delivery, Chemistry, 18 (2012) 12512-12521.

[60] V. Plassat, C. Wilhelm, V. Marsaud, C. Menager, F. Gazeau, J.M. Renoir, S. Lesieur, Anti-Estrogen-Loaded Superparamagnetic Liposomes for Intracellular Magnetic Targeting and Treatment of Breast Cancer Tumors, Advanced Functional Materials, 21 (2011) 83-92.

[61] H. Shao, J.R. Parquette, Controllable peptide-dendron self-assembly: interconversion of nanotubes and fibrillar nanostructures, Angewandte Chemie, 48 (2009) 2525-2528.

[62] E.P. Holowka, D.J. Pochan, T.J. Deming, Charged polypeptide vesicles with controllable diameter, Journal of the American Chemical Society, 127 (2005) 12423-12428.

[63] D. Haldar, A. Banerjee, M.G. Drew, A.K. Das, A. Banerjee, First crystallographic signature of an acyclic peptide nanorod: molecular mechanism of nanorod formation by a self-assembled tetrapeptide, Chemical communications, (2003) 1406-1407.

[64] S. Santoso, W. Hwang, H. Hartman, S. Zhang, Self-assembly of Surfactant-like Peptides with Variable Glycine Tails to Form Nanotubes and Nanovesicles, Nano Letters, 2 (2002) 687-691.

[65] Y. Hong, R.L. Legge, S. Zhang, P. Chen, Effect of amino acid sequence and pH on nanofiber formation of self-assembling peptides EAK16-II and EAK16-IV, Biomacromolecules, 4 (2003) 1433-1442.

[66] S. Soukasene, D.J. Toft, T.J. Moyer, H. Lu, H.K. Lee, S.M. Standley, V.L. Cryns, S.I. Stupp, Antitumor activity of peptide amphiphile nanofiber-encapsulated camptothecin, ACS nano, 5 (2011) 9113-9121.

[67] S.G. Zhang, T. Holmes, C. Lockshin, A. Rich, Spontaneous Assembly of a Self-Complementary Oligopeptide to Form a Stable Macroscopic Membrane, Proceedings of the National Academy of Sciences of the United States of America, 90 (1993) 3334-3338.

[68] P. Chen, Self-assembly of ionic-complementary peptides: a physicochemical viewpoint, Colloid Surface A, 261 (2005) 3-24.

[69] S.Y. Fung, H. Yang, P. Chen, Sequence effect of self-assembling peptides on the complexation and in vitro delivery of the hydrophobic anticancer drug ellipticine, Plos One, 3 (2008) e1956.

[70] C. Keyes-Baig, J. Duhamel, S.Y. Fung, J. Bezaire, P. Chen, Self-assembling peptide as a potential carrier of hydrophobic compounds, Journal of the American Chemical Society, 126 (2004) 7522-7532.

[71] S.Y. Fung, H. Yang, P.T. Bhola, P. Sadatmousavi, E. Muzar, M.Y. Liu, P. Chen, Self-Assembling Peptide as a Potential Carrier for Hydrophobic Anticancer Drug Ellipticine: Complexation, Release and In Vitro Delivery, Advanced Functional Materials, 19 (2009) 74-83.

[72] Y. Wu, P. Sadatmousavi, R. Wang, S. Lu, Y.F. Yuan, P. Chen, Self-assembling peptide-based nanoparticles enhance anticancer effect of ellipticine in vitro and in vivo, International journal of nanomedicine, 7 (2012) 3221-3233.

[73] S.Y. Fung, H. Yang, P. Sadatmousavi, Y. Sheng, T. Mamo, R. Nazarian, P. Chen, Amino Acid Pairing for De Novo Design of Self-Assembling Peptides and Their Drug Delivery Potential, Advanced Functional Materials, 21 (2011) 2456-2464.

[74] S.Y. Fung, J. Duhamel, P. Chen, Solvent effect on the photophysical properties of the anticancer agent ellipticine, The journal of physical chemistry. A, 110 (2006) 11446-11454.

[75] A. Clarysse, A. Brugarolas, P. Siegenthaler, R. Abele, F. Cavalli, R. de Jager, G. Renard, M. Rozencweig, H.H. Hansen, Phase II study of 9-hydroxy-2N-methylellipticinium acetate, European journal of cancer & clinical oncology, 20 (1984) 243-247.

[76] P. Dodion, M. Rozencweig, C. Nicaise, M. Piccart, E. Cumps, N. Crespeigne, D. Kisner, Y. Kenis, Phase I clinical study of 9-hydroxy-2N-methyl-ellipticinium acetate (NSC-264137) administered on a 5-day i.v. schedule, European journal of cancer & clinical oncology, 18 (1982) 519-522.

[77] K.A. Brogden, Antimicrobial peptides: pore formers or metabolic inhibitors in bacteria?, Nature reviews. Microbiology, 3 (2005) 238-250.

[78] R.C. Skarnes, D.W. Watson, Antimicrobial factors of normal tissues and fluids, Bacteriological reviews, 21 (1957) 273-294.

[79] R.E.W. Hancock, H.G. Sahl, Antimicrobial and host-defense peptides as new anti-infective therapeutic strategies, Nat Biotechnol, 24 (2006) 1551-1557.

[80] L.T. Eliassen, G. Berge, A. Leknessund, M. Wikman, I. Lindin, C. Lokke, F. Ponthan, J.I. Johnsen, B. Sveinbjornsson, P. Kogner, T. Flaegstad, O. Rekdal, The antimicrobial peptide, Lactoferricin B, is cytotoxic to neuroblastoma cells in vitro and inhibits xenograft growth in vivo, Int J Cancer, 119 (2006) 493-500.

[81] N. Papo, D. Seger, A. Makovitzki, V. Kalchenko, Z. Eshhar, H. Degani, Y. Shai, Inhibition of tumor growth and elimination of multiple metastases in human prostate and breast xenografts

by systemic inoculation of a host defense-like lytic peptide, Cancer research, 66 (2006) 5371-5378.

[82] Z. Oren, J.C. Lerman, G.H. Gudmundsson, B. Agerberth, Y. Shai, Structure and organization of the human antimicrobial peptide LL-37 in phospholipid membranes: relevance to the molecular basis for its non-cell-selective activity, The Biochemical journal, 341 (Pt 3) (1999) 501-513.

[83] A.J. Moore, D.A. Devine, M.C. Bibby, Preliminary experimental anticancer activity of cecropins, Peptide research, 7 (1994) 265-269.

[84] T.A. Holak, A. Engstrom, P.J. Kraulis, G. Lindeberg, H. Bennich, T.A. Jones, A.M. Gronenborn, G.M. Clore, The solution conformation of the antibacterial peptide cecropin A: a nuclear magnetic resonance and dynamical simulated annealing study, Biochemistry, 27 (1988) 7620-7629.

[85] S.C. Hung, W. Wang, S.I. Chan, H.M. Chen, Membrane lysis by the antibacterial peptides cecropins B1 and B3: A spin-label electron spin resonance study on phospholipid bilayers, Biophysical journal, 77 (1999) 3120-3133.

[86] H.M. Chen, W. Wang, D. Smith, S.C. Chan, Effects of the anti-bacterial peptide cecropin B and its analogs, cecropins B-1 and B-2, on liposomes, bacteria, and cancer cells, Biochimica et biophysica acta, 1336 (1997) 171-179.

[87] L. Hui, K. Leung, H.M. Chen, The combined effects of antibacterial peptide cecropin A and anti-cancer agents on leukemia cells, Anticancer research, 22 (2002) 2811-2816.

[88] S. Srisailam, T.K. Kumar, A.I. Arunkumar, K.W. Leung, C. Yu, H.M. Chen, Crumpled structure of the custom hydrophobic lytic peptide cecropin B3, European journal of biochemistry / FEBS, 268 (2001) 4278-4284.

[89] K. Hristova, C.E. Dempsey, S.H. White, Structure, location, and lipid perturbations of melittin at the membrane interface, Biophysical journal, 80 (2001) 801-811.

[90] S.F. Sui, H. Wu, Y. Guo, K.S. Chen, Conformational changes of melittin upon insertion into phospholipid monolayer and vesicle, Journal of biochemistry, 116 (1994) 482-487.

[91] S.S. Saini, A.K. Chopra, J.W. Peterson, Melittin activates endogenous phospholipase D during cytolysis of human monocytic leukemia cells, Toxicon : official journal of the International Society on Toxinology, 37 (1999) 1605-1619.

[92] K. Matsuzaki, K. Sugishita, N. Fujii, K. Miyajima, Molecular-Basis for Membrane Selectivity of an Antimicrobial Peptide, Magainin-2, Biochemistry, 34 (1995) 3423-3429.

[93] M.T. Tosteson, D.C. Tosteson, The sting. Melittin forms channels in lipid bilayers, Biophysical journal, 36 (1981) 109-116.

[94] M.T. Tosteson, S.J. Holmes, M. Razin, D.C. Tosteson, Melittin lysis of red cells, The Journal of membrane biology, 87 (1985) 35-44.

[95] P. Vihinen, V.M. Kahari, Matrix metalloproteinases in cancer: prognostic markers and therapeutic targets, Int J Cancer, 99 (2002) 157-166.

[96] L. Holle, W. Song, E. Holle, Y. Wei, T. Wagner, X. Yu, A matrix metalloproteinase 2 cleavable melittin/avidin conjugate specifically targets tumor cells in vitro and in vivo, International journal of oncology, 22 (2003) 93-98.

[97] P.J. Russell, D. Hewish, T. Carter, K. Sterling-Levis, K. Ow, M. Hattarki, L. Doughty, R. Guthrie, D. Shapira, P.L. Molloy, J.A. Werkmeister, A.A. Kortt, Cytotoxic properties of immunoconjugates containing melittin-like peptide 101 against prostate cancer: in vitro and in vivo studies, Cancer immunology, immunotherapy : CII, 53 (2004) 411-421.

[98] A.G. Rao, Conformation and antimicrobial activity of linear derivatives of tachyplesin lacking disulfide bonds, Archives of biochemistry and biophysics, 361 (1999) 127-134.

[99] A. Ramamoorthy, S. Thennarasu, A. Tan, K. Gottipati, S. Sreekumar, D.L. Heyl, F.Y. An, C.E. Shelburne, Deletion of all cysteines in tachyplesin I abolishes hemolytic activity and retains antimicrobial activity and lipopolysaccharide selective binding, Biochemistry, 45 (2006) 6529-6540.

[100] J. Chen, X.M. Xu, C.B. Underhill, S. Yang, L. Wang, Y. Chen, S. Hong, K. Creswell, L. Zhang, Tachyplesin activates the classic complement pathway to kill tumor cells, Cancer research, 65 (2005) 4614-4622.

[101] P. Rooney, S. Kumar, J. Ponting, M. Wang, The role of hyaluronan in tumour neovascularization (review), Int J Cancer, 60 (1995) 632-636.

[102] Y. Chen, X. Xu, S. Hong, J. Chen, N. Liu, C.B. Underhill, K. Creswell, L. Zhang, RGD-Tachyplesin inhibits tumor growth, Cancer research, 61 (2001) 2434-2438.

[103] C. Hetru, L. Letellier, Z. Oren, J.A. Hoffmann, Y. Shai, Androctonin, a hydrophilic disulphide-bridged non-haemolytic anti-microbial peptide: a plausible mode of action, The Biochemical journal, 345 Pt 3 (2000) 653-664.

[104] G.L. Ouyang, Q.F. Li, X.X. Peng, Q.R. Liu, S.G. Hong, Effects of tachyplesin on proliferation and differentiation of human hepatocellular carcinoma SMMC-7721 cells, World journal of gastroenterology : WJG, 8 (2002) 1053-1058.

[105] M. Zasloff, Magainins, a class of antimicrobial peptides from Xenopus skin: isolation, characterization of two active forms, and partial cDNA sequence of a precursor, Proceedings of the National Academy of Sciences of the United States of America, 84 (1987) 5449-5453.

[106] J. Lehmann, M. Retz, S.S. Sidhu, H. Suttmann, M. Sell, F. Paulsen, J. Harder, G. Unteregger, M. Stockle, Antitumor activity of the antimicrobial peptide magainin II against bladder cancer cell lines, European urology, 50 (2006) 141-147.

[107] H.S. Won, M.D. Seo, S.J. Jung, S.J. Lee, S.J. Kang, W.S. Son, H.J. Kim, T.K. Park, S.J. Park, B.J. Lee, Structural determinants for the membrane interaction of novel bioactive undecapeptides derived from gaegurin 5, Journal of medicinal chemistry, 49 (2006) 4886-4895.

[108] M. Tomita, W. Bellamy, M. Takase, K. Yamauchi, H. Wakabayashi, K. Kawase, Potent antibacterial peptides generated by pepsin digestion of bovine lactoferrin, Journal of dairy science, 74 (1991) 4137-4142.

[109] W. Bellamy, M. Takase, K. Yamauchi, H. Wakabayashi, K. Kawase, M. Tomita, Identification of the bactericidal domain of lactoferrin, Biochimica et biophysica acta, 1121 (1992) 130-136.

[110] P.M. Hwang, N. Zhou, X. Shan, C.H. Arrowsmith, H.J. Vogel, Three-dimensional solution structure of lactoferricin B, an antimicrobial peptide derived from bovine lactoferrin, Biochemistry, 37 (1998) 4288-4298.

[111] Y.C. Yoo, R. Watanabe, Y. Koike, M. Mitobe, K. Shimazaki, S. Watanabe, I. Azuma, Apoptosis in human leukemic cells induced by lactoferricin, a bovine milk protein-derived peptide: involvement of reactive oxygen species, Biochemical and biophysical research communications, 237 (1997) 624-628.

[112] L.T. Eliassen, G. Berge, B. Sveinbjornsson, J.S. Svendsen, L.H. Vorland, O. Rekdal, Evidence for a direct antitumor mechanism of action of bovine lactoferricin, Anticancer research, 22 (2002) 2703-2710.

[113] S.J. Furlong, J.S. Mader, D.W. Hoskin, Lactoferricin-induced apoptosis in estrogen-nonresponsive MDA-MB-435 breast cancer cells is enhanced by C6 ceramide or tamoxifen, Oncology reports, 15 (2006) 1385-1390.

[114] J.S. Mader, A. Richardson, J. Salsman, D. Top, R. de Antueno, R. Duncan, D.W. Hoskin, Bovine lactoferricin causes apoptosis in Jurkat T-leukemia cells by sequential permeabilization of the cell membrane and targeting of mitochondria, Experimental cell research, 313 (2007) 2634-2650.

[115] Y.C. Yoo, S. Watanabe, R. Watanabe, K. Hata, K. Shimazaki, I. Azuma, Bovine lactoferrin and lactoferricin, a peptide derived from bovine lactoferrin, inhibit tumor metastasis in mice, Japanese journal of cancer research : Gann, 88 (1997) 184-190.

[116] M. Iigo, T. Kuhara, Y. Ushida, K. Sekine, M.A. Moore, H. Tsuda, Inhibitory effects of bovine lactoferrin on colon carcinoma 26 lung metastasis in mice, Clinical & experimental metastasis, 17 (1999) 35-40.

[117] J.S. Mader, D. Smyth, J. Marshall, D.W. Hoskin, Bovine lactoferricin inhibits basic fibroblast growth factor- and vascular endothelial growth factor165-induced angiogenesis by competing for heparin-like binding sites on endothelial cells, The American journal of pathology, 169 (2006) 1753-1766.

[118] W.K. Wu, J.J. Sung, K.F. To, L. Yu, H.T. Li, Z.J. Li, K.M. Chu, J. Yu, C.H. Cho, The host defense peptide LL-37 activates the tumor-suppressing bone morphogenetic protein signaling via inhibition of proteasome in gastric cancer cells, Journal of cellular physiology, 223 (2010) 178-186.

[119] J. Johansson, G.H. Gudmundsson, M.E. Rottenberg, K.D. Berndt, B. Agerberth, Conformation-dependent antibacterial activity of the naturally occurring human peptide LL-37, The Journal of biological chemistry, 273 (1998) 3718-3724.

[120] J.E. Kim, H.J. Kim, J.M. Choi, K.H. Lee, T.Y. Kim, B.K. Cho, J.Y. Jung, K.Y. Chung, D. Cho, H.J. Park, The antimicrobial peptide human cationic antimicrobial protein-18/cathelicidin LL-37 as a putative growth factor for malignant melanoma, The British journal of dermatology, 163 (2010) 959-967.

[121] A. Risso, M. Zanetti, R. Gennaro, Cytotoxicity and apoptosis mediated by two peptides of innate immunity, Cellular immunology, 189 (1998) 107-115.

[122] A. Risso, E. Braidot, M.C. Sordano, A. Vianello, F. Macri, B. Skerlavaj, M. Zanetti, R. Gennaro, P. Bernardi, BMAP-28, an antibiotic peptide of innate immunity, induces cell death through opening of the mitochondrial permeability transition pore, Molecular and cellular biology, 22 (2002) 1926-1935.

[123] B. Skerlavaj, R. Gennaro, L. Bagella, L. Merluzzi, A. Risso, M. Zanetti, Biological characterization of two novel cathelicidin-derived peptides and identification of structural requirements for their antimicrobial and cell lytic activities, The Journal of biological chemistry, 271 (1996) 28375-28381.

[124] W.L. Maloy, U.P. Kari, Structure-activity studies on magainins and other host defense peptides, Biopolymers, 37 (1995) 105-122.

[125] S.E. Blondelle, R.A. Houghten, Design of model amphipathic peptides having potent antimicrobial activities, Biochemistry, 31 (1992) 12688-12694.

[126] M.M. Javadpour, M.M. Juban, W.C. Lo, S.M. Bishop, J.B. Alberty, S.M. Cowell, C.L. Becker, M.L. McLaughlin, De novo antimicrobial peptides with low mammalian cell toxicity, Journal of medicinal chemistry, 39 (1996) 3107-3113.

[127] N. Papo, Y. Shai, New lytic peptides based on the D,L-amphipathic helix motif preferentially kill tumor cells compared to normal cells, Biochemistry, 42 (2003) 9346-9354.

[128] R. Bessalle, A. Kapitkovsky, A. Gorea, I. Shalit, M. Fridkin, All-D-magainin: chirality, antimicrobial activity and proteolytic resistance, FEBS letters, 274 (1990) 151-155.

[129] J.C. Mai, Z. Mi, S.H. Kim, B. Ng, P.D. Robbins, A proapoptotic peptide for the treatment of solid tumors, Cancer research, 61 (2001) 7709-7712.

[130] J. Zhong, Y. Chau, Antitumor activity of a membrane lytic peptide cyclized with a linker sensitive to membrane type 1-matrix metalloproteinase, Molecular cancer therapeutics, 7 (2008) 2933-2940.

[131] S.M. Standley, D.J. Toft, H. Cheng, S. Soukasene, J. Chen, S.M. Raja, V. Band, H. Band, V.L. Cryns, S.I. Stupp, Induction of cancer cell death by self-assembling nanostructures incorporating a cytotoxic peptide, Cancer research, 70 (2010) 3020-3026.

[132] L. Agemy, D. Friedmann-Morvinski, V.R. Kotamraju, L. Roth, K.N. Sugahara, O.M. Girard, R.F. Mattrey, I.M. Verma, E. Ruoslahti, Targeted nanoparticle enhanced proapoptotic peptide as potential therapy for glioblastoma, Proceedings of the National Academy of Sciences of the United States of America, 108 (2011) 17450-17455.

[133] E.J.J. Lugtenberg, R. Peters, Distribution of Lipids in Cytoplasmic and Outer Membranes of Escherichia-Coli-K12, Biochimica et biophysica acta, 441 (1976) 38-47.

[134] J. Henriksen, A.C. Rowat, E. Brief, Y.W. Hsueh, J.L. Thewalt, M.J. Zuckermann, J.H. Ipsen, Universal behavior of membranes with sterols, Biophysical journal, 90 (2006) 1639-1649.

[135] A.J. Krauson, J. He, W.C. Wimley, Gain-of-Function Analogues of the Pore-Forming Peptide Melittin Selected by Orthogonal High-Throughput Screening, Journal of the American Chemical Society, 134 (2012) 12732-12741.

[136] L. Ringstad, L. Kacprzyk, A. Schmidtchen, M. Malmsten, Effects of topology, length, and charge on the activity of a kininogen-derived peptide on lipid membranes and bacteria, Biochimica et biophysica acta, 1768 (2007) 715-727.

[137] A. Giangaspero, L. Sandri, A. Tossi, Amphipathic alpha helical antimicrobial peptides, European journal of biochemistry / FEBS, 268 (2001) 5589-5600.

[138] A.A. Stromstedt, P. Wessman, L. Ringstad, K. Edwards, M. Malmsten, Effect of lipid headgroup composition on the interaction between melittin and lipid bilayers, J Colloid Interf Sci, 311 (2007) 59-69.

[139] W. Baranska-Rybak, A. Sonesson, R. Nowicki, A. Schmidtchen, Glycosaminoglycans inhibit the antibacterial activity of LL-37 in biological fluids, The Journal of antimicrobial chemotherapy, 57 (2006) 260-265.

[140] B. Fadnes, O. Rekdal, L. Uhlin-Hansen, The anticancer activity of lytic peptides is inhibited by heparan sulfate on the surface of the tumor cells, Bmc Cancer, 9 (2009).

[141] I. Cornut, K. Buttner, J.L. Dasseux, J. Dufourcq, The amphipathic alpha-helix concept. Application to the de novo design of ideally amphipathic Leu, Lys peptides with hemolytic activity higher than that of melittin, FEBS letters, 349 (1994) 29-33.

[142] J.B. Rothbard, T.C. Jessop, P.A. Wender, Adaptive translocation: the role of hydrogen bonding and membrane potential in the uptake of guanidinium-rich transporters into cells, Adv Drug Deliver Rev, 57 (2005) 495-504.

[143] M. Tang, A.J. Waring, R.I. Lehrer, M. Hong, Effects of guanidinium-phosphate hydrogen bonding on the membrane-bound structure and activity of an arginine-rich membrane peptide from solid-state NMR spectroscopy, Angewandte Chemie, 47 (2008) 3202-3205.

[144] D. Sarker, P. Workman, Pharmacodynamic biomarkers for molecular cancer therapeutics, Adv Cancer Res, 96 (2007) 213-268.

[145] T.M. Allen, P.R. Cullis, Drug delivery systems: entering the mainstream, Science, 303 (2004) 1818-1822.

[146] S.V. Vinogradov, T.K. Bronich, A.V. Kabanov, Nanosized cationic hydrogels for drug delivery: preparation, properties and interactions with cells, Adv Drug Deliv Rev, 54 (2002) 135-147.

[147] M.D. Howard, M. Jay, T.D. Dziublal, X.L. Lu, PEGylation of nanocarrier drug delivery systems: State of the art, J Biomed Nanotechnol, 4 (2008) 133-148.

[148] X.J. Zhao, S.G. Zhang, Fabrication of molecular materials using peptide construction motifs, Trends Biotechnol, 22 (2004) 470-476.

[149] M.B. Yatvin, J.N. Weinstein, W.H. Dennis, R. Blumenthal, Design of liposomes for enhanced local release of drugs by hyperthermia, Science, 202 (1978) 1290-1293.

[150] J.N. Weinstein, R.L. Magin, M.B. Yatvin, D.S. Zaharko, Liposomes and Local Hyperthermia - Selective Delivery of Methotrexate to Heated Tumors, Science, 204 (1979) 188-191.

[151] G. Kong, M.W. Dewhirst, Hyperthermia and liposomes, Int J Hyperther, 15 (1999) 345-370.

[152] M.B. Yatvin, H. Muhlensiepen, W. Porschen, J.N. Weinstein, L.E. Feinendegen, Selective Delivery of Liposome-Associated Cis-Dichlorodiammineplatinum(Ii)by Heat and Its Influence on Tumor Drug Uptake and Growth, Cancer research, 41 (1981) 1602-1607.

[153] B.M. Dicheva, G.A. Koning, Targeted thermosensitive liposomes: an attractive novel approach for increased drug delivery to solid tumors, Expert Opin Drug Del, 11 (2014) 83-100.

[154] K.J. Chen, H.F. Liang, H.L. Chen, Y.C. Wang, P.Y. Cheng, H.L. Liu, Y.N. Xia, H.W. Sung, A Thermoresponsive Bubble-Generating Liposomal System for Triggering Localized Extracellular Drug Delivery, ACS nano, 7 (2013) 438-446.

[155] Q. Yuan, Y. Zhang, T. Chen, D. Lu, Z. Zhao, X. Zhang, Z. Li, C.H. Yan, W. Tan, Photon-manipulated drug release from a mesoporous nanocontainer controlled by azobenzene-modified nucleic acid, ACS nano, 6 (2012) 6337-6344.

[156] J. Lu, E. Choi, F. Tamanoi, J.I. Zink, Light-activated nanoimpeller-controlled drug release in cancer cells, Small, 4 (2008) 421-426.

[157] R. Tong, H.D. Hemmati, R. Langer, D.S. Kohane, Photoswitchable nanoparticles for triggered tissue penetration and drug delivery, Journal of the American Chemical Society, 134 (2012) 8848-8855.

[158] R. Tong, H.H. Chiang, D.S. Kohane, Photoswitchable nanoparticles for in vivo cancer chemotherapy, Proceedings of the National Academy of Sciences of the United States of America, 110 (2013) 19048-19053.

[159] D. He, X. He, K. Wang, J. Cao, Y. Zhao, A light-responsive reversible molecule-gated system using thymine-modified mesoporous silica nanoparticles, Langmuir, 28 (2012) 4003-4008.

[160] W.G. Pitt, G.A. Husseini, B.J. Staples, Ultrasonic drug delivery--a general review, Expert Opin Drug Deliv, 1 (2004) 37-56.

[161] M.Y. Hua, H.L. Liu, H.W. Yang, P.Y. Chen, R.Y. Tsai, C.Y. Huang, I.C. Tseng, L.A. Lyu, C.C. Ma, H.J. Tang, T.C. Yen, K.C. Wei, The effectiveness of a magnetic nanoparticle-based delivery system for BCNU in the treatment of gliomas, Biomaterials, 32 (2011) 516-527.

[162] K.T. Oh, H.Q. Yin, E.S. Lee, Y.H. Bae, Polymeric nanovehicles for anticancer drugs with triggering release mechanisms, J Mater Chem, 17 (2007) 3987-4001.

[163] E. Koren, A. Apte, A. Jani, V.P. Torchilin, Multifunctional PEGylated 2C5-immunoliposomes containing pH-sensitive bonds and TAT peptide for enhanced tumor cell internalization and cytotoxicity, Journal of Controlled Release, 160 (2012) 264-273.

[164] E.S. Lee, Z. Gao, D. Kim, K. Park, I.C. Kwon, Y.H. Bae, Super pH-sensitive multifunctional polymeric micelle for tumor pH(e) specific TAT exposure and multidrug resistance, Journal of controlled release : official journal of the Controlled Release Society, 129 (2008) 228-236.

[165] M. An, D. Wijesinghe, O.A. Andreev, Y.K. Reshetnyak, D.M. Engelman, pH-(low)-insertion-peptide (pHLIP) translocation of membrane impermeable phalloidin toxin inhibits cancer cell proliferation, Proceedings of the National Academy of Sciences of the United States of America, 107 (2010) 20246-20250.

[166] D.P. Jones, J.L. Carlson, P.S. Samiec, P. Sternberg, Jr., V.C. Mody, Jr., R.L. Reed, L.A. Brown, Glutathione measurement in human plasma. Evaluation of sample collection, storage and derivatization conditions for analysis of dansyl derivatives by HPLC, Clinica chimica acta; international journal of clinical chemistry, 275 (1998) 175-184.

[167] Y.C. Wang, F. Wang, T.M. Sun, J. Wang, Redox-responsive nanoparticles from the single disulfide bond-bridged block copolymer as drug carriers for overcoming multidrug resistance in cancer cells, Bioconjugate chemistry, 22 (2011) 1939-1945.

[168] Y. Li, K. Xiao, J. Luo, W. Xiao, J.S. Lee, A.M. Gonik, J. Kato, T.A. Dong, K.S. Lam, Well-defined, reversible disulfide cross-linked micelles for on-demand paclitaxel delivery, Biomaterials, 32 (2011) 6633-6645.

[169] J. Dai, S. Lin, D. Cheng, S. Zou, X. Shuai, Interlayer-crosslinked micelle with partially hydrated core showing reduction and pH dual sensitivity for pinpointed intracellular drug release, Angewandte Chemie, 50 (2011) 9404-9408.

[170] O.H. Aina, T.C. Sroka, M.L. Chen, K.S. Lam, Therapeutic cancer targeting peptides, Biopolymers, 66 (2002) 184-199.

[171] J.J. Schwartz, S. Zhang, Peptide-mediated cellular delivery, Current opinion in molecular therapeutics, 2 (2000) 162-167.

[172] Y.B. Lim, E. Lee, M. Lee, Cell-penetrating-peptide-coated nanoribbons for intracellular nanocarriers, Angewandte Chemie, 46 (2007) 3475-3478.

[173] E.G. Bellomo, M.D. Wyrsta, L. Pakstis, D.J. Pochan, T.J. Deming, Stimuli-responsive polypeptide vesicles by conformation-specific assembly, Nat Mater, 3 (2004) 244-248.

[174] E.P. Holowka, V.Z. Sun, D.T. Kamei, T.J. Deming, Polyarginine segments in block copolypeptides drive both vesicular assembly and intracellular delivery, Nat Mater, 6 (2007) 52-57.

[175] S. Zhang, C. Lockshin, A. Herbert, E. Winter, A. Rich, Zuotin, a putative Z-DNA binding protein in Saccharomyces cerevisiae, The EMBO journal, 11 (1992) 3787-3796.

[176] S. Zhang, T.C. Holmes, C.M. DiPersio, R.O. Hynes, X. Su, A. Rich, Self-complementary oligopeptide matrices support mammalian cell attachment, Biomaterials, 16 (1995) 1385-1393.

[177] S. Adamia, C.A. Maxwell, L.M. Pilarski, Hyaluronan and hyaluronan synthases: potential therapeutic targets in cancer, Current drug targets. Cardiovascular & haematological disorders, 5 (2005) 3-14.

[178] A. Giuliani, G. Pirri, S.F. Nicoletto, Antimicrobial peptides: an overview of a promising class of therapeutics, Cent Eur J Biol, 2 (2007) 1-33.

[179] M. Miteva, M. Andersson, A. Karshikoff, G. Otting, Molecular electroporation: a unifying concept for the description of membrane pore formation by antibacterial peptides, exemplified with NK-lysin, FEBS letters, 462 (1999) 155-158.

[180] A.A. Stromstedt, L. Ringstad, A. Schmidtchen, M. Malmsten, Interaction between amphiphilic peptides and phospholipid membranes, Curr Opin Colloid In, 15 (2010) 467-478.

[181] L.T. Nguyen, E.F. Haney, H.J. Vogel, The expanding scope of antimicrobial peptide structures and their modes of action, Trends Biotechnol, 29 (2011) 464-472.

[182] I. Dobrzynska, B. Szachowicz-Petelska, S. Sulkowski, Z. Figaszewski, Changes in electric charge and phospholipids composition in human colorectal cancer cells, Molecular and cellular biochemistry, 276 (2005) 113-119.

[183] K. Simons, E. Ikonen, Cell biology - How cells handle cholesterol, Science, 290 (2000) 1721-1726.

[184] G.J. Nelson, Lipid Composition of Erythrocytes in Various Mammalian Species, Biochimica et biophysica acta, 144 (1967) 221-&.

[185] T. Rog, M. Pasenkiewicz-Gierula, I. Vattulainen, M. Karttunen, Ordering effects of cholesterol and its analogues, Biochimica et biophysica acta, 1788 (2009) 97-121.

[186] L. Silvestro, K. Gupta, J.N. Weiser, P.H. Axelsen, The concentration-dependent membrane activity of cecropin A, Biochemistry, 36 (1997) 11452-11460.

[187] R.M. Verly, M.A. Rodrigues, K.R. Daghastanli, A.M. Denadai, I.M. Cuccovia, C. Bloch, Jr., F. Frezard, M.M. Santoro, D. Pilo-Veloso, M.P. Bemquerer, Effect of cholesterol on the interaction of the amphibian antimicrobial peptide DD K with liposomes, Peptides, 29 (2008) 15-24.

[188] E. Glukhov, M. Stark, L.L. Burrows, C.M. Deber, Basis for selectivity of cationic antimicrobial peptides for bacterial versus mammalian membranes, The Journal of biological chemistry, 280 (2005) 33960-33967.

[189] M. Jafari, W. Xu, S. Naahidi, B. Chen, P. Chen, A new amphipathic, amino-acid-pairing (AAP) peptide as siRNA delivery carrier: physicochemical characterization and in vitro uptake, The journal of physical chemistry. B, 116 (2012) 13183-13191.

[190] H. Patel, C. Tscheka, H. Heerklotz, Characterizing vesicle leakage by fluorescence lifetime measurements, Soft Matter, 5 (2009) 2849-2851.

[191] E.J. Prenner, R.N. Lewis, M. Jelokhani-Niaraki, R.S. Hodges, R.N. McElhaney, Cholesterol attenuates the interaction of the antimicrobial peptide gramicidin S with phospholipid bilayer membranes, Biochimica et biophysica acta, 1510 (2001) 83-92.

[192] J.T. Vivian, P.R. Callis, Mechanisms of tryptophan fluorescence shifts in proteins, Biophysical journal, 80 (2001) 2093-2109.

[193] Y.C. Li, M.J. Park, S.K. Ye, C.W. Kim, Y.N. Kim, Elevated levels of cholesterol-rich lipid rafts in cancer cells are correlated with apoptosis sensitivity induced by cholesterol-depleting agents, The American journal of pathology, 168 (2006) 1107-1118; quiz 1404-1105.

[194] H. Heller, M. Schaefer, K. Schulten, Molecular-Dynamics Simulation of a Bilayer of 200 Lipids in the Gel and in the Liquid-Crystal Phases, J Phys Chem-Us, 97 (1993) 8343-8360.

[195] R.M. Epand, R.F. Epand, Bacterial membrane lipids in the action of antimicrobial agents, Journal of peptide science : an official publication of the European Peptide Society, 17 (2011) 298-305.

[196] M. Onda, K. Yoshihara, H. Koyano, K. Ariga, T. Kunitake, Molecular recognition of nucleotides by the guanidinium unit at the surface of aqueous micelles and bilayers. A comparison of microscopic and macroscopic interfaces, Journal of the American Chemical Society, 118 (1996) 8524-8530.

[197] J. Kindrachuk, E. Scruten, S. Attah-Poku, K. Bell, A. Potter, L.A. Babiuk, P.J. Griebel, S. Napper, Stability, Toxicity, and Biological Activity of Host Defense Peptide BMAP28 and Its Inversed and Retro-Inversed Isomers, Biopolymers, 96 (2011) 14-24.

[198] I. Ahmad, W.R. Perkins, D.M. Lupan, M.E. Selsted, A.S. Janoff, Liposomal Entrapment of the Neutrophil-Derived Peptide Indolicidin Endows It with in-Vivo Antifungal Activity, Bba-Biomembranes, 1237 (1995) 109-114.

[199] C. Subbalakshmi, V. Krishnakumari, R. Nagaraj, N. Sitaram, Requirements for antibacterial and hemolytic activities in the bovine neutrophil derived 13-residue peptide indolicidin, FEBS letters, 395 (1996) 48-52.

[200] N. Sal-Man, Z. Oren, Y. Shai, Preassembly of membrane-active peptides is an important factor in their selectivity toward target cells, Biochemistry, 41 (2002) 11921-11930.

[201] R. Halevy, A. Rozek, S. Kolusheva, R.E. Hancock, R. Jelinek, Membrane binding and permeation by indolicidin analogs studied by a biomimetic lipid/polydiacetylene vesicle assay, Peptides, 24 (2003) 1753-1761.

[202] J. Kopecek, Smart and genetically engineered biomaterials and drug delivery systems, European journal of pharmaceutical sciences : official journal of the European Federation for Pharmaceutical Sciences, 20 (2003) 1-16.

[203] T. Tagami, W.D. Foltz, M.J. Ernsting, C.M. Lee, I.F. Tannock, J.P. May, S.D. Li, MRI monitoring of intratumoral drug delivery and prediction of the therapeutic effect with a multifunctional thermosensitive liposome, Biomaterials, 32 (2011) 6570-6578.

[204] K. Katagiri, Y. Imai, K. Koumoto, T. Kaiden, K. Kono, S. Aoshima, Magnetoresponsive on-demand release of hybrid liposomes formed from Fe3 O4 nanoparticles and thermosensitive block copolymers, Small, 7 (2011) 1683-1689.

[205] S. Lu, H. Wang, Y.B. Sheng, M.Y. Liu, P. Chen, Molecular binding of self-assembling peptide EAK16-II with anticancer agent EPT and its implication in cancer cell inhibition, Journal of Controlled Release, 160 (2012) 33-40.

[206] S.Y. Fung, C. Keyes, J. Duhamel, P. Chen, Concentration effect on the aggregation of a self-assembling oligopeptide, Biophysical journal, 85 (2003) 537-548.

[207] J.A. Morrow, M.L. Segall, S. Lund-Katz, M.C. Phillips, M. Knapp, B. Rupp, K.H. Weisgraber, Differences in Stability among the Human Apolipoprotein E Isoforms Determined by the Amino-Terminal Domain†, Biochemistry, 39 (2000) 11657-11666.

[208] Y.H. Bae, K. Park, Targeted drug delivery to tumors: myths, reality and possibility, Journal of controlled release : official journal of the Controlled Release Society, 153 (2011) 198-205.

[209] R. Bawa, S.Y. Fung, A. Shiozaki, H. Yang, G. Zheng, S. Keshavjee, M. Liu, Self-assembling peptide-based nanoparticles enhance cellular delivery of the hydrophobic anticancer drug ellipticine through caveolae-dependent endocytosis, Nanomedicine : nanotechnology, biology, and medicine, 8 (2012) 647-654.

[210] D.P. Gately, S.B. Howell, Cellular accumulation of the anticancer agent cisplatin: a review, British journal of cancer, 67 (1993) 1171-1176.

[211] Y.W. Won, S.M. Yoon, K.S. Lim, Y.H. Kim, Self-Assembled Nanoparticles with Dual Effects of Passive Tumor Targeting and Cancer-Selective Anticancer Effects, Advanced Functional Materials, 22 (2012) 1199-1208.

[212] Cancer multidrug resistance, Nat Biotechnol, 18 Suppl (2000) IT18-20.

[213] S.E. Blondelle, R.A. Houghten, Hemolytic and antimicrobial activities of the twenty-four individual omission analogues of melittin, Biochemistry, 30 (1991) 4671-4678.

[214] M. Werle, A. Bernkop-Schnurch, Strategies to improve plasma half life time of peptide and protein drugs, Amino Acids, 30 (2006) 351-367.

[215] Z. Oren, J. Hong, Y. Shai, A repertoire of novel antibacterial diastereomeric peptides with selective cytolytic activity, Journal of Biological Chemistry, 272 (1997) 14643-14649.

[216] J.P. Schneider, D.J. Pochan, B. Ozbas, K. Rajagopal, L. Pakstis, J. Kretsinger, Responsive hydrogels from the intramolecular folding and self-assembly of a designed peptide, Journal of the American Chemical Society, 124 (2002) 15030-15037.

[217] D.J. Pochan, J.P. Schneider, J. Kretsinger, B. Ozbas, K. Rajagopal, L. Haines, Thermally reversible hydrogels via intramolecular folding and consequent self-assembly of a de novo designed peptide, Journal of the American Chemical Society, 125 (2003) 11802-11803.

[218] D.M. Ke, C.L. Zhan, A.D.Q. Li, J.N. Yao, Morphological Transformation between Nanofibers and Vesicles in a Controllable Bipyridine-Tripeptide Self-Assembly, Angew Chem Int Edit, 50 (2011) 3715-3719.

[219] I.W. Hamley, A. Dehsorkhi, V. Castelletto, S. Furzeland, D. Atkins, J. Seitsonen, J. Ruokolainen, Reversible helical unwinding transition of a self-assembling peptide amphiphile, Soft Matter, 9 (2013) 9290-9293.

[220] M. Bucciantini, E. Giannoni, F. Chiti, F. Baroni, L. Formigli, J.S. Zurdo, N. Taddei, G. Ramponi, C.M. Dobson, M. Stefani, Inherent toxicity of aggregates implies a common mechanism for protein misfolding diseases, Nature, 416 (2002) 507-511.

[221] K. Konate, L. Crombez, S. Deshayes, M. Decaffmeyer, A. Thomas, R. Brasseur, G. Aldrian, F. Heitz, G. Divita, Insight into the Cellular Uptake Mechanism of a Secondary Amphipathic Cell-Penetrating Peptide for siRNA Delivery, Biochemistry, 49 (2010) 3393-3402.

[222] E.F. Banwell, E.S. Abelardo, D.J. Adams, M.A. Birchall, A. Corrigan, A.M. Donald, M. Kirkland, L.C. Serpell, M.F. Butler, D.N. Woolfson, Rational design and application of responsive alpha-helical peptide hydrogels, Nat Mater, 8 (2009) 596-600.

[223] M.W. Tibbitt, K.S. Anseth, Hydrogels as Extracellular Matrix Mimics for 3D Cell Culture, Biotechnol Bioeng, 103 (2009) 655-663.

[224] L.H. Liu, K.J. Xu, H.Y. Wang, P.K.J. Tan, W.M. Fan, S.S. Venkatraman, L.J. Li, Y.Y. Yang, Self-assembled cationic peptide nanoparticles as an efficient antimicrobial agent, Nat Nanotechnol, 4 (2009) 457-463.

[225] H. Maeda, Macromolecular therapeutics in cancer treatment: The EPR effect and beyond, J Control Release, 164 (2012) 138-144.

[226] A.F. Radovic-Moreno, T.K. Lu, V.A. Puscasu, C.J. Yoon, R. Langer, O.C. Farokhzad, Surface Charge-Switching Polymeric Nanoparticles for Bacterial Cell Wall-Targeted Delivery of Antibiotics, ACS nano, 6 (2012) 4279-4287.

[227] C.C. Lee, J.A. MacKay, J.M.J. Frechet, F.C. Szoka, Designing dendrimers for biological applications, Nat Biotechnol, 23 (2005) 1517-1526.

[228] M. Shi, K. Ho, A. Keating, M.S. Shoichet, Doxorubicin-Conjugated lmmuno-Nanoparticles for Intracellular Anticancer Drug Delivery, Advanced Functional Materials, 19 (2009) 1689-1696.

[229] H. Chen, R. Ahn, J. Van den Bossche, D.H. Thompson, T.V. O'Halloran, Folate-mediated intracellular drug delivery increases the anticancer efficacy of nanoparticulate formulation of arsenic trioxide, Molecular cancer therapeutics, 8 (2009) 1955-1963.

[230] A. Chilkoti, Self-assembling chimeric polypeptide-doxorubicin conjugate nanoparticles that abolish tumors after a single injection, Abstr Pap Am Chem S, 239 (2010).

[231] S.J. Marrink, H.J. Risselada, S. Yefimov, D.P. Tieleman, A.H. de Vries, The MARTINI force field: Coarse grained model for biomolecular simulations, Journal of Physical Chemistry B, 111 (2007) 7812-7824.

[232] B. Hess, C. Kutzner, D. van der Spoel, E. Lindahl, GROMACS 4: Algorithms for highly efficient, load-balanced, and scalable molecular simulation, J Chem Theory Comput, 4 (2008) 435-447.

[233] T.A. Wassenaar, K. Pluhackova, R.A. Bockmann, S.J. Marrink, D.P. Tieleman, Going Backward: A Flexible Geometric Approach to Reverse Transformation from Coarse Grained to Atomistic Models, J Chem Theory Comput, 10 (2014) 676-690.

[234] N. Schmid, A.P. Eichenberger, A. Choutko, S. Riniker, M. Winger, A.E. Mark, W.F. van Gunsteren, Definition and testing of the GROMOS force-field versions 54A7 and 54B7, Eur Biophys J Biophy, 40 (2011) 843-856.

[235] D. Poger, W.F. Van Gunsteren, A.E. Mark, A New Force Field for Simulating Phosphatidylcholine Bilayers, J Comput Chem, 31 (2010) 1117-1125.

[236] A. Kukol, Lipid Models for United-Atom Molecular Dynamics Simulations of Proteins, J Chem Theory Comput, 5 (2009) 615-626.

[237] M. Mihajlovic, T. Lazaridis, Antimicrobial peptides in toroidal and cylindrical pores, Bba-Biomembranes, 1798 (2010) 1485-1493.

[238] D. Sengupta, H. Leontiadou, A.E. Mark, S.J. Marrink, Toroidal pores formed by antimicrobial peptides show significant disorder, Bba-Biomembranes, 1778 (2008) 2308-2317.

[239] K.N. Sugahara, T. Teesalu, P.P. Karmali, V.R. Kotamraju, L. Agemy, D.R. Greenwald, E. Ruoslahti, Coadministration of a tumor-penetrating peptide enhances the efficacy of cancer drugs, Science, 328 (2010) 1031-1035.